From coastlines to the deep sea: modeling plastic transport in the global ocean

Inauguraldissertation

der Philosophisch–naturwissenschaftlichen Fakultät
der Universität Bern

vorgelegt von

Victor Onink

aus Leiden, Niederlande

Leiter der Arbeit:
Dr. Charlotte Laufkötter

Abteilung für Klima– und Umweltphysik
Physikalisches Institut der Universität Bern

From coastlines to the deep sea: modeling plastic transport in the global ocean

Inauguraldissertation

der Philosophisch–naturwissenschaftlichen Fakultät
der Universität Bern

vorgelegt von

Victor Onink

aus Leiden, Niederlande

Leiter der Arbeit:

Dr. Charlotte Laufkötter

Abteilung für Klima– und Umweltphysik
Physikalisches Institut der Universität Bern

Von der Philosophisch–naturwissenschaftlichen Fakultät angenommen.

Bern, 27.06.2022

Der Dekan
Prof. Dr. Zoltan Balogh

Thesis summary

Plastic is one of the most commonly used materials in the world today, with polymers such as polypropylene and polyethylene used for applications such as packaging, textiles and commercial fishery. However, not all plastic objects are properly disposed of at the end of their useful lives, and today plastic pollution is ubiquitous throughout the environment and particularly in the ocean. Here plastic pollution can cause harm in a variety of ways, such as entangling marine wildlife, leaching chemical compounds into the water and causing economic damage by deterring tourism at commercial beaches. However, it is difficult to understand the full scope of these threats, in part because the fate of plastic once it enters the ocean is poorly understood. Plastic debris has been found everywhere from on coastlines to the open ocean, and from the ocean surface down to the deep ocean on the seafloor, but it is not always clear what physical processes contribute to the observed distribution of plastic objects. Numerical models can provide insight into plastic debris transport by modeling various transport scenarios, but physical processes such as plastic beaching and resuspension, vertical transport and fragmentation are not always completely represented or even included at all.

This thesis investigates the transport of plastic debris in the global ocean by means of Lagrangian particle transport scenarios, where plastic debris is represented by virtual particles. Using circulation and other oceanographic data from oceanic general circulation model (OGCM) reanalysis products, particles trajectories are calculated that provide insight into the distribution and pathways of plastic debris in marine environments. By modifying the model setup in the various scenarios, the influence of different physical processes on plastic transport is investigated.

Chapter 1 provides a general overview of marine plastic pollution, where this is broadly split into insights gained from the observational record and from modeling studies. The current understanding of the relative distribution of plastic debris on a global scale is described, as well as the current knowledge of how this is influenced by various physical processes. This also highlights current knowledge gaps such as the role of coastal and vertical transport processes, which are investigated in later chapters of this thesis.

While the specific model frameworks are described in each subsequent chapter in this thesis, chapter 2 provides a general overview of Lagrangian ocean modeling and particularly the Parcels modeling framework. In addition, while all the details of OGCMs and ocean reanalysis products are beyond the scope of this thesis, a general overview is given of various OGCM features that are relevant to the work described in the following chapters.

Chapter 3 investigates plastic debris beaching and resuspension on a global scale. The spatial and temporal resolutions of OGCMs are insufficient to resolve the physical processes that contribute to debris beaching and resuspension, and stochastic parametrizations are introduced to represent plastic beaching and resuspension within a large-scale modeling framework. Coastlines and coastal waters are globally shown to hold at least 77% of all positively buoyant plastic debris, with the spatial distribution of beached plastic being strongly influenced by the model input

scenario. As such, coastal dynamics are shown to play a more prominent role in global-scale plastic transport than previously thought.

Chapter 4 describes various parametrizations for modelling the wind-driven vertical turbulent mixing of buoyant particles within the surface mixed layer. Ocean reanalysis products generally do not provide turbulence data fields, but turbulent vertical transport is an important driving process in the full three-dimensional distribution of plastic in the ocean. The modeled vertical microplastic concentration profiles correspond reasonably well with field observations, and the parametrizations are numerically stable with an integration timestep $\Delta t = 30$ seconds. This makes it computationally feasible to apply the paramatrizations in large-scale three-dimensional modeling frameworks.

Chapter 5 examines the influence of particle size on the three-dimensional transport of microplastic debris in the Mediterranean Sea. The distribution of plastic in beached, coastal waters and open waters reservoirs is strongly affected by the particle size, with smaller particles being more likely to reach open water. Smaller particles are also mixed farther below the ocean surface up to depths of 3000 m. Fragmentation is shown to be a slow process over timescales of years to decades, with ocean-based fragmentation likely being negligible compared with beach-based fragmentation processes. Therefore, while fragmentation was not shown to strongly influence the particle size distribution over the course of 3 years, over longer timescales it can play an important in the gradual plastic mass transfer to offshore and subsurface waters.

Finally, chapter 6 provides a general overview and discussion of the main results described in chapters 3 - 5, and outlines future possible research directions.

Contents

Chapter 1

Introduction

Oceanic pollution has been an ever-present issue since the Industrial Revolution, but plastics are perhaps the most clearly visible example of how human behavior can affect marine ecosystems. Plastics are ubiquitous throughout the global ocean, from on coastlines (Browne et al., 2015; Pieper et al., 2019a) to the open ocean (Law et al., 2010; Van Sebille et al., 2015), to down on the sea floor (Van Cauwenberghe et al., 2013; Brignac et al., 2019). Research has shown that plastic pollution can cause harm in various ways. On the individual level, plastic debris can cause physical harm to marine organisms. Discarded fishing nets can persist for years at or just below the ocean surface, and result in marine wildlife such as birds, fish and marine mammals getting entangled in the netting (Gregory, 2009; Votier et al., 2011; Ryan, 2018). Smaller plastic debris such as microplastic (< 5 mm in size) can also be ingested by marine organisms (Mascarenhas et al., 2004; Gregory, 2009; Dawson et al., 2018), which can result in supressed appetite, damage to the gastrointestinal tract and heightened exposure to toxic compounds leaching from the plastic fragments (Brandão et al., 2011; Bond et al., 2013; Lavers et al., 2014; Attademo et al., 2015; Puskic et al., 2020). Ingestion also occurs with commercially fished species such as sea bass and flounder (Bessa et al., 2018), and this can result in microplastic fragments entering the human food chain (Mercogliano et al., 2020). Plastic debris further causes harm to ecosystems, as plastic debris can be colonized by marine organisms and increase the likelihood of a species being transported across large distances and being introduced in new environments (Barnes, 2002; Audrézet et al., 2021). Finally, plastic pollution can result in economic damage, as large quantities of plastic debris can deter tourism at commercial beaches (Ballance et al., 2000).

However, it remains difficult to establish exactly *how much* harm plastic pollution causes in marine ecosystems as a whole. This would require a more complete understanding of what exactly happens to a plastic object when it enters a marine environment and what interactions occur with marine wildlife on a species level. The physical, chemical and biological surroundings can affect the ultimate fate of a plastic object in the ocean, and it is of vital importance to understand how marine debris undergoes processes such as beaching, transport by ocean currents and fragmentation into gradually smaller pieces in order to evaluate the impact it might have on marine ecosystems.

This thesis investigates the impact various physical processes have on the transport and fate of plastic debris in the global ocean. First, this chapter will provide an overview of the necessary background knowledge to set a baseline for the subsequent chapters, by giving an overview of the insights that field observations provide regarding the distribution and impact of plastic debris in the ocean (section 1.1). This is followed by the benefits and challenges of using computational models to simulate plastic transport (section 1.2), before defining the exact scope of this thesis (section 1.3).

1.1 The observational record of marine plastics

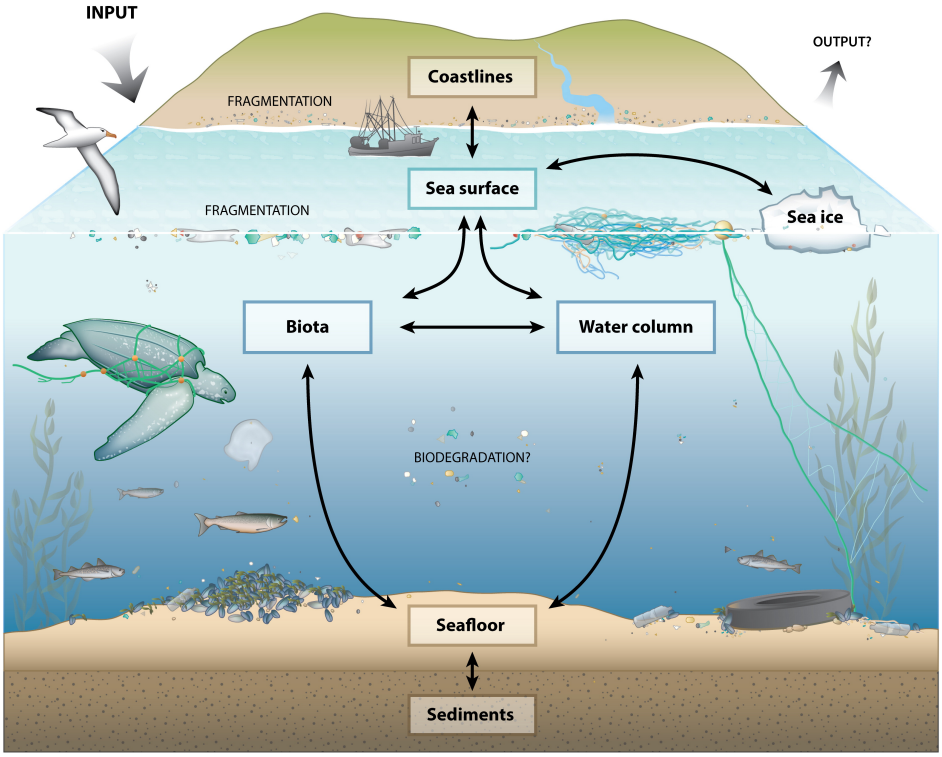

AR Law KL. 2017.
Annu. Rev. Mar. Sci. 9:205–29

Figure 1.1: Reservoirs of plastic in marine environments, where the arrows indicate potential fluxes of plastic mass between reservoirs. Figure retrieved from Law (2017).

Plastic pollution comes in a wide range of types and sizes. Although polyethylene and polypropylene are generally the most common polymers found at the ocean surface (Cózar et al., 2014; Enders et al., 2015; Brignac et al., 2019), a wide variety of polymers are reported in the literature such as polystyrene, PET, and PLA. Meanwhile, the sizes of plastic objects can span multiple orders of magnitude (Cózar et al., 2014, 2015; Enders et al., 2015), from meters down to micro- or nanometer scales (Morét-Ferguson et al., 2010; Lebreton et al., 2018; Piccardo et al., 2020). While sampling plastics in ocean environments comes with a variety of operational and procedural challenges, observational records are a vital component of understanding the degree of plastic pollution in the ocean. While the mass balance of marine plastic in the ocean is highly uncertain and largely incomplete, Figure 1.1 shows the main reservoirs and interactions between them.

Given that plastic is not a naturally occurring material, it has to enter the ocean as a result of anthropogenic activities. These sources can be split into two broad categories, land-based and ocean-based sources, where land-based sources are estimated to account for the majority of the total inputs (Faris & Hart, 1994; Derraik, 2002; Li et al., 2016). Rivers are considered to be major contributors of land-based plastic inputs (Schmidt et al., 2017; Lebreton et al., 2017; Meijer et al., 2021), with between $0.8 - 2.7$ million tons of plastic estimated to enter the ocean per year (Meijer et al., 2021). Other contributors of land-based plastic pollution include coastal recreational activities (Lee et al., 2013), accidental spillages (Redford et al., 1997; Karlsson et al., 2018) and natural disasters such as hurricanes and tsunamis (Barnes et al., 2009; Lebreton et al., 2018).

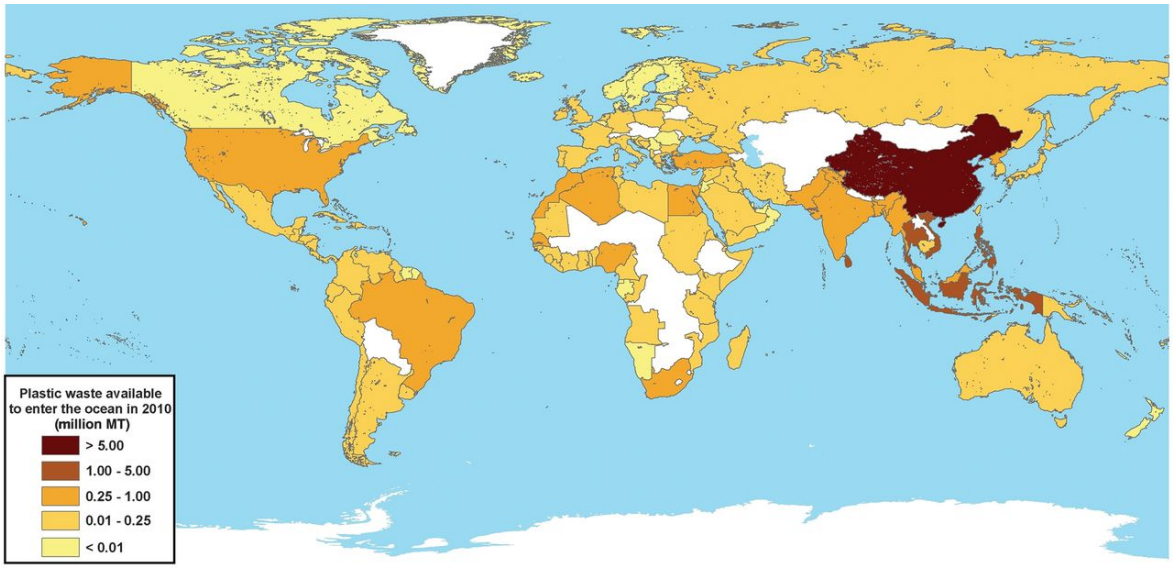

Figure 1.2: The estimated mass of mismanaged plastic waste generated in 2010 by populations within 50 km of coastlines. Figure retrieved from Jambeck et al. (2015).

Given the wide range of contributing factors, estimates of the amount of plastic that enters the ocean each year are uncertain. The Jambeck et al. (2015) estimate of $4.8 - 12.7$ million tons entering the ocean globally in 2010 alone is the most commonly cited estimate (Figure 1.2), but more localized field studies suggest that input estimates following the Jambeck approach are too high (Tramoy et al., 2019; Van Emmerik et al., 2019). For certain estimates Jambeck et al. (2015) had to rely on expert judgement rather than observation studies given that direct measurements were not available. As such, while Jambeck et al. (2015) estimated 15 - 40% of all Indonesian plastic waste ended up in the ocean, Van Emmerik et al. (2019) found that in Jakarta this fraction is only around 3%. Lebreton et al. (2017) and Schmidt et al. (2017) estimate $0.41 - 4$ million tons enter the ocean from river sources, but this similarly might be an overestimate given that these estimates are in part based on the mismanaged plastic waste estimates from Jambeck et al. (2015). Given the difficulties in quantifying plastic mismanagement and the transport of mismanagement plastic into marine systems, further refining estimates of land-based plastic inputs remains an ongoing challenge.

While ocean-based sources are thought to make a smaller contribution to marine plastic inputs in comparison to land-based sources (Faris & Hart, 1994; Lebreton et al., 2012), discarded fishing gear alone is estimated to add 640 000 tons of marine debris each year (Good et al., 2010; Li et al., 2016). In addition, fishing gear in the form of ghost nets can cause considerable harm to marine wildlife, as sea creatures can get entangled in drifting nets and drown (Gunn et al., 2010). Ghost nets can also release toxic chemical compounds (Dabrowska et al., 2021). Finally, plastic can enter the ocean via waste dumping from shipping (Ryan et al., 2019; Eo et al., 2022), despite MARPOL Annex V prohibiting this practice since 1989 (Henderson, 2001). Given that ocean-based inputs are widely distributed and the types of fishing materials vary widely geographically (Richardson et al., 2019), estimates of ocean-based plastic inputs remain highly unreliable. However, given that 5.7% of all fishing nets and up to 29% of all lines used globally are lost per year (Richardson et al., 2019), ocean-based plastic inputs are likely a significant contributor to the total amount of marine plastic. Additional research is required to further quantify the input from these sources.

Field measurements show that plastic debris, particularly microplastic particles, can be found almost anywhere in the ocean. The majority of the field measurements have been collected

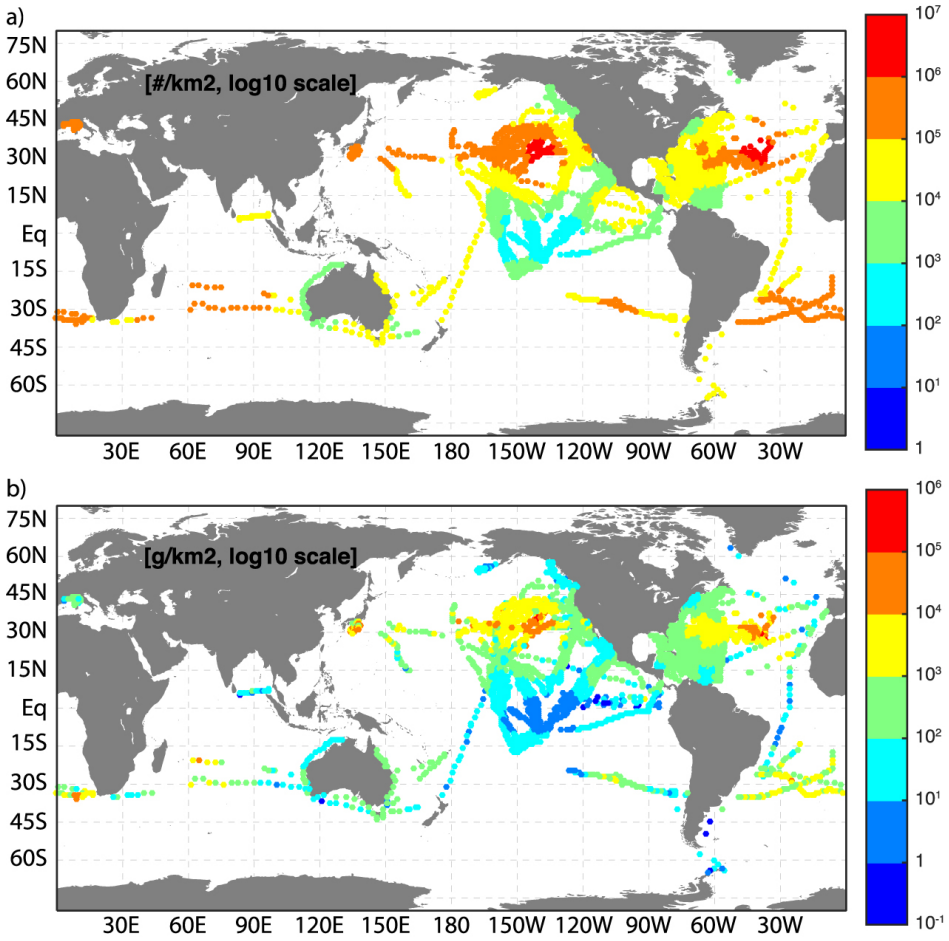

Figure 1.3: Standardized microplastic (a) count and (b) mass measurements collected with surface trawls, where standardization was done relative to the year of study, geographic location and the wind speed. Figure retrieved from Van Sebille et al. (2015).

at the ocean surface using neuston nets, which are nets dragged behind a vessel that float at the ocean surface. These nets generally have a mesh size of around 0.33 mm, and therefore do not effectively sample particles smaller than 0.33 mm. At the same time the small ocean surface area they sample makes it unlikely they sample particles much larger than 10 mm as these are less numerous at the ocean surface (Van Sebille et al., 2015). The highest surface ocean concentrations are typically found in the ocean gyres (Figure 1.3), with concentrations of over 10^7 particles per square kilometer (Van Sebille et al., 2015). As shown in Figure 1.4, this accumulation is the result of the convergence of the the large-scale Ekman transport in the mid-latitudes (Kubota, 1994; Maximenko et al., 2012; Van Sebille et al., 2015; Onink et al., 2019). However, microplastic concentrations show a high degree of spatial and temporal variability (van der Hal et al., 2017; Lebreton et al., 2018; Brach et al., 2018), and regular sampling is required to get a comprehensive understanding of plastic pollution within a given region.

To date, the majority of the surface microplastic samples have been collected in the North Atlantic and North Pacific (Van Sebille et al., 2015), although sampling in other basins has become more frequent in recent years (Li et al., 2020; Patti et al., 2020; da Rocha et al., 2021; Zhao et al., 2022). In addition, field campaigns are also placing more focus on sampling in near-shore regions, and show that microplastics concentrations increase with their proximity to shore (Ruiz-Orejón et al., 2016; Steer et al., 2017). The size of plastic debris also seems to play an important role in the near-shore distribution of plastic debris, as an global analysis of debris

types across aquatic environments suggests that plastic debris is less likely to be trapped in coastal areas as it gets smaller (Morales-Caselles et al., 2021). Coastal dynamics clearly have a strong influence on the transport and fate of marine plastic (Zhang, 2017), but the observational record in these regions remains limited.

While the observational record of plastic debris at the ocean surface is limited, it vastly

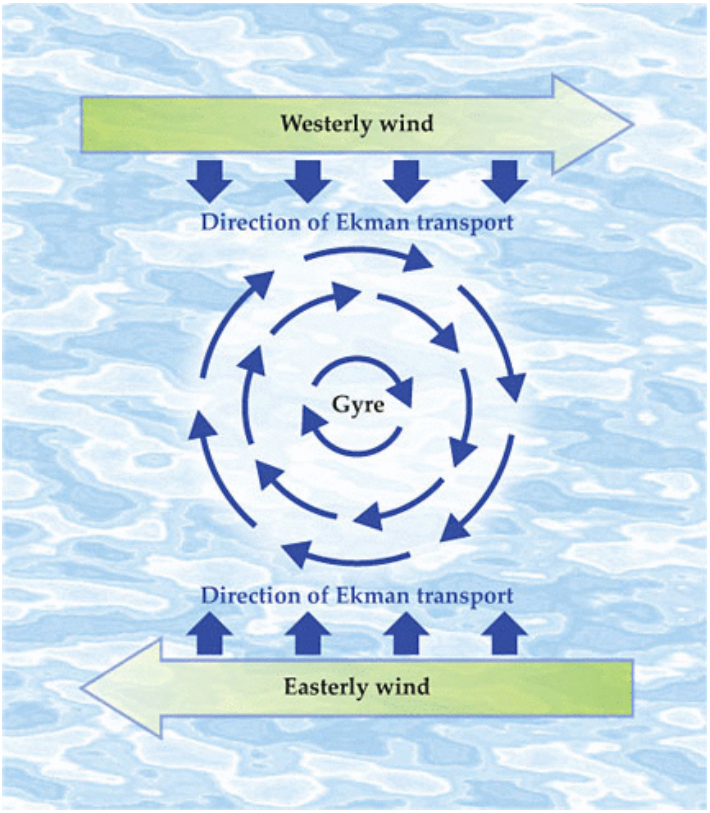

Figure 1.4: Schematic indicating the convergence of ocean currents in the subtropical ocean gyres. The high latitude westerlies and low latitude easterlies lead to Ekman transport in southwards and northwards directions, converging at the ocean gyres in the mid-latitudes. The schematic shows the large-scale from in the Nothern hemisphere, where the gyre flows clockwise, while in the Southern Hemisphere the flow is anticlockwise. Figure retrieved from Van Sebille (2015).

exceeds measurements of subsurface plastic concentrations. It has been theorized that the subsurface ocean could hold vast amounts of plastic debris (Woodall et al., 2014; Pabortsava & Lampitt, 2020), with Pabortsava & Lampitt (2020) proposing that the top 200 m of the Atlantic oceans alone could hold up to 21.1 million tons of microplastic debris. However, due to the difficulties and cost in collecting sufficient samples, the subsurface distribution and dynamics of marine plastic remain poorly understood. Vertical transport dynamics play an important role in the fate of marine plastics, as wind- and wave-driven turbulent mixing can result in the mixing of buoyant particles below the ocean surface (Kukulka et al., 2012; Kooi et al., 2016). Given that the ocean currents vary in depth (Webster, 1969), this can have consequences for the large-scale transport of plastic debris. Plastic has been found globally throughout the water column (Pieper et al., 2019b; Egger et al., 2020; Zhao et al., 2022) and down on the seafloor (Woodall et al., 2014; Brignac et al., 2019; Kane et al., 2020), with a conservative global estimate of 8.4 million tons of microplastic on the seabed (Barrett et al., 2020). However, until more measurements are available estimates of the subsurface plastic distribution and total amount of plastic debris remain uncertain.

Given the large number of studies reporting plastic concentrations on beaches worldwide

(Ribic et al., 2010, 2012; Browne et al., 2015; Monteiro et al., 2018), one might expect that the global distribution and amount of beached plastic is relatively well understood. However, due to a lack of methodological standardization it is difficult to compare concentrations reported by different studies, given the variability in sampling techniques, the size range of considered microplastics, and concentration units (Browne et al., 2015). For example, there is no standard for the minimum particle size considered within a beach study, but given that smaller particles are numerically more common, this can strongly influence reported debris counts per unit area or length (Smith & Turrell, 2021). Meanwhile, concentrations can be reported as both counts or mass per unit area (Taïbi et al., 2021) or unit length of coastline (Barnes & Milner, 2005), but it is not trivial to convert between these units and the total plastic load on a coastline when the total coastline or sampled surface area is unreported.

Despite these methodological challenges, some general trends are apparent for beached plastic. Beached plastic concentrations are generally highest near large population centers (Hardesty et al., 2017b; Ryan et al., 2018; Olivelli et al., 2020), with local concentrations reaching up to 647 kg km^{-1} on high-usage commercial beaches (Debrot et al., 2013). Beached plastic often originates from local land-based sources (Hardesty et al., 2017b; Ryan, 2020), although particularly islands often report high amounts of plastic debris originating from remote ocean-based sources (Lavers & Bond, 2017; Pieper et al., 2019a). In contrast, particularly isolated coastlines such as in Antarctica might be completely devoid of beached plastic (Convey et al., 2002). Beached plastic concentrations are dependent on factors such as local wind conditions and coastal geomorphology (Pieper et al., 2015; Hardesty et al., 2017b; Brignac et al., 2019), and it is difficult to establish clear statistical relations between these factors and observed plastic concentrations. As such, to date it has not been possible to establish a global, standardized beached plastic dataset such as was done for surface microplastic observations (Browne et al., 2015; Van Sebille et al., 2015), further underlining the urgent need for increased standardization of field measurement methodologies.

While field measurements have allowed insight into the general distribution of plastic de-

Figure 1.5: Biofouling of three plastic sheets immersed in the Bay of Bengal for 6 months, where the biofilm consists of macrofoulants such as barnacles. Figure adapted from Sudhakar et al. (2007).

bris in the global ocean, it is more difficult to draw conclusions on how processes such as fragmentation, biofouling and interactions with marine wildlife affect plastic debris. Over time, plastic debris changes physically and chemically as it remains in marine environments. Exposure to UV and physical abrasion can cause wear and tear on a plastic object (Barnes et al., 2009),

which can lead to oxidation and embrittlement of the object's surface (Corcoran et al., 2009). This can in turn result in the gradual production of small plastic fragments that break off of the original parent object (Andrady, 2011). Meanwhile the biofouling of a plastic object (Figure 1.5), which refers to the settling of fouling organisms on an object, can affect the overall density of an object, and result in an initially buoyant object gradually sinking over time (Fazey & Ryan, 2016).

There have been a number of experimental studies considering fragmentation and biofouling in laboratory and ocean settings (O'Brine & Thompson, 2010; Fazey & Ryan, 2016; Song et al., 2017; Gerritse et al., 2020; Xiong et al., 2022), but it is difficult to extrapolate these findings to other environmental conditions. For example, Fazey & Ryan (2016) demonstrated that biofouling can result in the sinking of initially buoyant plastic items after just 17 - 66 days, resulting in plastic debris being removed from the ocean surface over the course of weeks. However, the objects within the study were tethered to a pier in a South African harbor, and it is unclear whether biofouling would be equally fast for e.g. a freely drifting debris item in the open ocean or at different latitudes. Similarly, Song et al. (2017) and Gerritse et al. (2020) show that under laboratory conditions fragmentation is generally a relatively slow process over the course of decades to centuries, but it is challenging to generalize these findings to rates under variable environmental conditions in the physical world. Analysis of the relative size distribution of microplastic particles in the ocean can provide insight into the influence of variables such as the debris shape on plastic degradation (Ter Halle et al., 2016), but without a way to date microplastic fragments it is generally not possible to strongly constrain fragmentation rates in marine environments from observations alone. As such, processes such as biofouling and fragmentation under variable environmental conditions remain poorly understood.

Similar issues arise when considering interactions between plastic debris and marine wildlife. It has been established that marine wildlife and plastic debris interact in a variety of ways (Barnes et al., 2009), such as the afore-mentioned biofouling (Fazey & Ryan, 2016; Xiong et al., 2022), ingestion (Cole et al., 2013; Dawson et al., 2018; Zhu et al., 2019; Weitzel et al., 2021), and entanglement (Good et al., 2010; Gunn et al., 2010; Jepsen & de Bruyn, 2019; Dabrowska et al., 2021). Ingestion and entanglement can cause direct harm to marine wildlife, while wildlife rafting on plastic debris can have consequences for transporting alien species to new marine habitats (Barnes & Milner, 2005; Goldstein et al., 2014; Therriault et al., 2018). However, while a number of studies have examined the exposure of marine species to plastic pollution (Schuyler et al., 2016; Compa et al., 2019; Good et al., 2020), this isn't equivalent to quantifying the harm plastic pollution causes, as finding plastic within a creature's stomach is not an immediate indication that it caused harm to the creature (Rummel et al., 2016). Laboratory experiments have shown that microplastic ingestion cause harm to marine wildlife, with environmentally - relevant concentrations resulting in a long-term impact on zebrafish such as skin/gill inflamation and decreased repoductive capabilities (Boyle et al., 2020; Guimarães et al., 2021; Marana et al., 2022). However, most marine species can not be similarly studied within laboratory settings, and it is unclear to what extent (if at all) these findings with zebrafish can be applied to other species.

Finally, the observational record has indicated multiple marine debris sinks. What defines a sink is dependent on what timescale is being considered. For example, sea ice and beaches could be considered as plastic sinks, as they stop plastic particles from moving freely throughout the ocean (Obbard et al., 2014; Pham et al., 2020). However, over time this trapped debris can be released again, which makes it difficult to make a clear distinction between permanent and transitory sinks. One example of a permanent sink would be the removal of beached plastic from beaches through beach cleanups, but although numerous studies report this occurring (Pieper et al.,

2015; Debrot et al., 2013; Pervez et al., 2020), few make concrete estimates how much plastic is actually being removed. Other examples of permanent removals are catching fish with ingested plastics (Rochman et al., 2015), the cleanup of drifting ghost nets (Spirkovski et al., 2019) and even table salt production from sea water (Yang et al., 2015). However, given that a large amount of plastic removal goes unreported or has not been studied beyond anecdotal reporting, it is currently not possible to draw firm conclusions regarding the size of marine plastic sinks.

In conclusion, field measurements have shown that plastic debris, particularly microplastic, is ubiquitous in the ocean, with reports from all over the world and for all types of marine habitats. Despite this, sampling has generally been too sparse to set up a global marine plastic mass budget from field observations alone, and particularly the spatial and temporal variability in plastic concentrations is poorly understood. While more frequent and widespread sampling could at least partially address these issues, the difficulty and cost in collecting field measurements and the lack of methodological standardization means that this is unlikely to occur in the near future.

1.2 Modeling marine microplastics

Numerical modeling has been widely used within the plastic research community to gain insight into the fate of plastic debris once it enters the ocean (Van Sebille et al., 2015; Hardesty et al., 2017a; Onink et al., 2019; Mountford & Morales Maqueda, 2021; van Duinen et al., 2022). Compared to solely using field observations, numerical modeling provides a number of distinct advantages: it makes it possible to test various scenarios to isolate the influence of various physical processes on plastic transport (Onink et al., 2019; Wichmann et al., 2019; Lobelle et al., 2021), as well as to extrapolate from the available field measurements to larger scales (Eriksen et al., 2014; Van Sebille et al., 2015), and long-term scenarios can investigate possible impacts of plastic pollution over the decades to come (Koelmans et al., 2017; Lebreton et al., 2019). Numerical models come in a variety of different forms, with Eulerian (Mountford & Morales Maqueda, 2019, 2021), Lagrangian (Lebreton et al., 2012; Onink et al., 2019), box model (Koelmans et al., 2017; Kaandorp et al., 2021) and transition matrix (Van Sebille et al., 2012; Maximenko et al., 2012) models being a subset of the different types of models employed within the plastic modeling field. Given these advantages, models play an important role in furthering the understanding of the fate of plastic debris in the ocean (Hardesty et al., 2017a).

However, numerical models come with their own set of challenges. First, models are by definition simplifications of reality, with the model designer making assumptions about what processes and timescales are important to include. As such, ideally there should always be verification of model predictions based on available field measurements, which in the case of plastic research can be challenging. As described in section 1.1, measurements of plastic concentrations are sparse and it is not always possible to directly validate model predictions. For example, while in certain circumstances it is possible to identify a likely origin of a plastic object (Ryan, 2020; Ryan et al., 2021), this is generally not the case for most plastic debris. As such, while e.g. bayesian inference analysis can make very precise predictions regarding the origin of plastic debris at a given time and location (van Duinen et al., 2022), field observations are not always able to validate these predictions.

In addition, the majority of numerical models in the microplastic field are process-based, which requires a good understanding of the significant underlying physical processes. For example, the large-scale transport of plastic debris in the open ocean is relatively well understood, with the Ekman currents known to drive the accumulation of plastic in the subtropical gyres while Stokes drift contributes to the landward transport of debris (Kubota, 1994; Martinez et al., 2009; Onink et al., 2019). However, a process like biofouling is likely strongly dependent on

environmental conditions and the type of plastic debris, whereas an experimental study like Fazey & Ryan (2016) only considered biofouling rates within one particular environmental setting and with a limited range of debris items. Models can still investigate the influence biofouling could have on particle dynamics. For example, Kooi et al. (2017) demonstrated biofouling could result in particles vertically oscillating throughout the water column, while Lobelle et al. (2021) demonstrated sinking rates of microplastic particles can vary significantly depending on the particle sizes and algal concentrations. However, given the limited experimental basis these are generally exploratory studies that don't seek to provide exact predictions of plastic concentrations.

Finally, models often run scaling issues. Plastic transport in the ocean is governed by processes that operate on a variety of spatial and temporal scales, ranging from meters to thousands of kilometers and from seconds to decadal timescales (Van Sebille et al., 2020). Due to computational constraints it is not possible to consider all scales within a model. For example, a oceanic general ciculation model (OGCM) such as HYCOM or NEMO will typically have a spatial resolution on the order of kilometers, and a temporal resolution on the order of hours to days (Seo et al., 2013; Madec et al., 2017). This implies that any variability in e.g. the ocean currents on smaller and shorter timescales is not captured within a model, which can influence the overall transport of particles (Nooteboom et al., 2020). While parametrizations are developed that approximate the influence of these unresolved process in less computationally-expensive ways (e.g. Kukulka et al., 2012; Reijnders et al., 2022), the full dynamics are still not being considered. One approach is to use regional studies that can look at plastic dynamics on smaller scales (e.g. Kukulka et al., 2016; Critchell & Lambrechts, 2016; Alsina et al., 2020), but this then raises the challenge of how to generalize local results to larger scales. Finally, the ocean is a highly chaotic system (Tziperman et al., 1994; Prants, 2014; Cravatte et al., 2021), so even if all physical, chemical and geological processes were completely resolved, small changes in the initial model conditions can propagate throughout the entire ocean system (Vialard et al., 2003; Peng & Xie, 2006; Wakelin et al., 2009). Any ocean model is therefore at best an approximation of the true physical ocean state. In conclusion, while modeling studies can be used to investigate plastic debris scenarios that could not be studied with field observations alone, it is important to keep in mind the limitations when considering the results from numerical models.

One of the most common applications of numerical models has been to simulate the transport of plastic debris. Microplastic field measurements show elevated concentrations in the subtropical ocean gyres (Van Sebille, 2015), which is a pattern reproduced by large-scale transport models (Van Sebille et al., 2012; Maximenko et al., 2012; Lebreton et al., 2012). By individually considering the Ekman, geostrophic and Stokes drift current components, Lagrangian models have shown that this convergence is largely due to the Ekman currents (Kubota et al., 2005; Martinez et al., 2009; Onink et al., 2019). Geostrophic currents can play an important role in circulation patterns, such as driving eastward advection in the South Atlantic subtropics (Kubota et al., 2005; Martinez et al., 2009), but generally don't result in large-scale debris accumulation (Kubota et al., 2005; Martinez et al., 2009; Onink et al., 2019). Meanwhile, the wave-driven Stokes drift is found to oppose debris convergence in the subtropical gyres, instead contributing to the landward transport of floating debris (Onink et al., 2019). On a global scale, Stokes drift can therefore contribute to trapping debris near coastlines.

Near-shore transport and beaching of plastic debris has proven challenging to study with large-scale models, as it is affected by processes such as waves-breaking and coastal geomorphology that are typically not resolved in OGCMs (Van Sebille et al., 2020). Stokes drift likely plays an important role in near-shore transport (Alsina et al., 2020), but plastic transport dynamics in the surf zone prior to beaching are strongly dependent on local geomorphological conditions such as the bed profile and wave conditions (Kerpen et al., 2020). As such, there are no clear relations

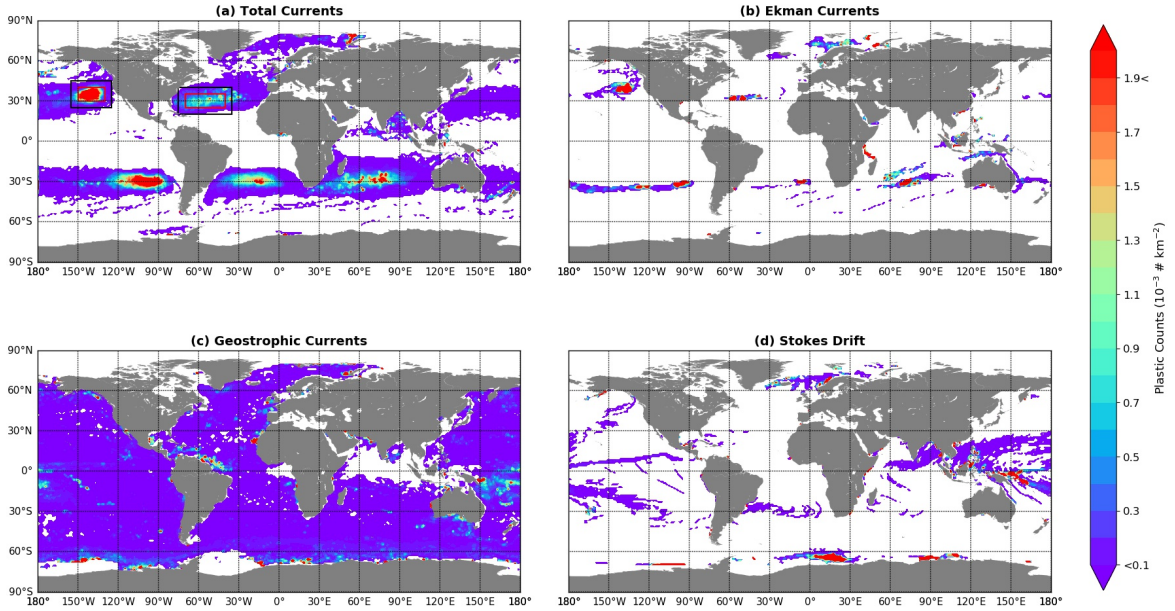

Figure 1.6: Average particle densities for global Lagrangian simulations with transport by (a) Ekman and geostrophic currents, (b) Ekman currents, (c) geostrophic currents and (d) Stokes drift. All simulations start from a spatially uniform distribution of particles with particles spaced at 1° intervals over all ocean cells. Figure retrieved from Onink et al. (2019).

between large-scale oceanographic variables (which could be calculated using an OGCM) and debris beaching probabilities, and plastic debris has been represented with a variety of approaches in modeling studies. This includes completely neglecting beaching altogether (Van Sebille et al., 2012; Onink et al., 2019; Miladinova et al., 2020), but more commonly beaching is represented either based on a coastal proximity condition (Lebreton et al., 2019; Guerrini et al., 2021) or by considering any particle advected onto a land cell to be beached (Lebreton et al., 2012; Critchell & Lambrechts, 2016). The resuspension of beached particles is also often not considered as a separate physical process, even as field studies such as Hinata et al. (2017) demonstrate that beached debris can be resuspended on timescales of days to weeks by processes such as wind, waves and storms (Pieper et al., 2015; Critchell & Lambrechts, 2016). Overall, numerical models have provided limited insight into the distribution of beached plastic debris on global scales, and improved parametrizations are required to represent beaching and resuspension processes within OGCM-based numerical simulations.

Large-scale modeling has largely focused on the horizontal transport of floating plastic debris, where this debris remains at the ocean surface over the entire simulation period (Onink et al., 2019; Van Sebille, 2015; Liubartseva et al., 2018; Kaandorp et al., 2020). Given that debris can persist at the ocean surface for decades (Lebreton et al., 2018), assuming that plastic particles remain at the ocean surface can generally be valid for highly buoyant debris and solely considering surface processes simplifies the model dynamics. In addition, there are more field measurements available at the ocean surface which can be used to validate model results. However, by not considering the full three-dimensional transport of plastic debris these models provide an incomplete picture of the fate of plastic in the ocean, and more attention ought to be given to understanding vertical transport processes. Mountford & Morales Maqueda (2019) considered the three-dimensional transport of particles with various buoyancies, and showed that the subsurface ocean can hold substantial amounts of neutrally and negatively buoyant plastic debris. The Eulerian model also showed that even positively buoyant plastic debris was mixed down to 300m below the ocean surface, emphasizing that it is crucial to also consider vertical transport processes for all particle types. Meanwhile, Kooi et al. (2017) showed that biofouling

can remove initially buoyant plastic debris from the ocean surface, as the formation of a biofilm can increase the overall particle density and eventually lead to sinking. However, the model also predicted that below the euphotic zone the microbes making up the biofilm would die and fall off of the particle, decreasing the particle density again and over time leading to the particles oscillating vertically. Building on the Kooi et al. (2017) biofouling model, Fischer et al. (2022) also showed similar oscillatory behavior under more realistic environmental conditions. These models have thus provided a new insight into a possible plastic debris transport mechanism that might not have been readily apparent from the observational record alone.

There have been various approaches to model plastic debris fragmentation, but in general the lack of sufficient observational data to evaluate model performance remains an issue. Eriksen et al. (2014) estimated the total number of plastic debris items in the global ocean, and assumed that the system was close to equilibrium with regards to fragmentation. As such, it was assumed there was a fixed 1:16 ratio in the number of macroplastic (200 mm) to mesoplastic (50 mm) particles, and similarly a fixed 1:625 ratio in the number of mesoplastic to large microplastic particles (2 mm). While this allowed very basic estimates of the number of plastic particles in the ocean, it does not provide much insight into the physical process of fragmentation. Based on the statistical analysis of microplastic fragments collected in the North Atlantic, Ter Halle et al. (2016) concluded that for particles with a mass greater than 1 mg the fragmentation rate appears constant. However, the lack of lighter particles could either indicates faster fragmentation processes for small particles, or be the result of other removal processes from the ocean surface such as vertical turbulent mixing. Inspection of the individual microplastics also suggested that the particle shape likely affected the fragmentation rate, as cubic-like fragments showed more even surface degradation than flat fragments. This is likely because cubic-like fragments more easily roll and change orientation, whereas flatter fragments typically have a more photodegraded face, which suggests they float with a preferred orientation. However, without a technique to date the fragments, it was not possible to estimate fragmentation rates. Kaandorp et al. (2021) developed a statistical fragmentation model where fragmentation leads to the generation of a cascade of smaller particles within a simple box model. When this model was tuned with field measurements from the Mediterranean Sea, beach-based fragmentation was shown to likely be a very slow process with timescales of years to decades (Kaandorp et al., 2021). While the box model was a simplification of the actual ocean circulation, the fragmentation model itself is a framework that could be applied in a different model setup to further investigate the role plastic transport, beaching and resuspension play in plastic fragmentation.

Numerical models have been essential in trying to establish a global marine plastic budget, although to date a closed budget has not yet been determined. By interpolating between the measurements available at the ocean surface, an estimated 93 - 236 000 tons of plastic debris floats at the ocean surface (Van Sebille, 2015), which is significantly less than estimated plastic inputs. However, this estimate was based on measurements of microplastics, and as larger items likely contain most of the total plastic mass in the ocean, including these items within estimates could lead to a higher overall estimate (Lebreton et al., 2018). For example, by including larger debris items Lebreton et al. (2018) estimated 79 000 tons of plastic debris at the surface of the North Pacific subtropical gyre, compared with just 4 800 - 21 000 tons when only considering microplastics (Cózar et al., 2014; Eriksen et al., 2014). In addition, the Van Sebille et al. (2015) estimate did not include many near-shore microplastic concentrations, and given that concentrations tend to be higher close to land (Ruiz-Orejón et al., 2016), the Van Sebille (2015) estimate might again be too low.

Overall though, the general conclusion is that a large amount of plastic debris appears to be 'missing' and many suggestions have been made where this plastic might be. Multiple studies have

suggested that subsurface ocean could be a significant reservoir (Egger et al., 2020; Pabortsava & Lampitt, 2020; Woodall et al., 2014), but due to the lack of sufficient field measurements for model calibration and validation estimates remain uncertain. As such, to date models have not been used to extrapolate field measurements collected by e.g. Egger et al. (2020) and Pabortsava & Lampitt (2020) to estimate the total amount of subsurface plastic mass. Due to the lack of standardized sampling methodologies (Browne et al., 2015) and the general inability of large-scale models to resolve plastic beaching, the amount of beached plastic is highly uncertain. Lebreton et al. (2019) estimates that in 2015 coastlines held 46.7 - 126.4 million tons of macroplastic and 22.3 - 60.4 millions tons of microplastic debris assuming increasing plastic inputs between 1950 - 2015. However, the model tuning was based on matching the mass of floating plastic debris at the ocean surface estimated by Van Sebille et al. (2015) and not on any direct measurements of beached plastic concentrations. In addition, Lebreton et al. (2019) does not consider the deep sea as a plastic debris sink, and as such it is unclear how much of the plastic mass allocated to coastlines might be in the deep sea. Finally, it has been proposed that sea ice might hold at least trillions of microplastic particles (Obbard et al., 2014; Peeken et al., 2018), but there has only been limited modeling work on the interaction between sea ice and plastic debris (Mountford & Morales Maqueda, 2021). As such, it is currently not possible to estimate the total plastic mass trapped in sea ice.

In conclusion, while the ocean surface might only hold around 1% of the $4.8 - 12.7$ millions tons of plastic that entered the ocean in 2010 alone (Van Sebille et al., 2015; Jambeck et al., 2015), observations and models have identified many possible reservoirs that might hold this missing plastic mass. Conservatively the seabed might hold over 8 millions tons of plastic mass (Barrett et al., 2020), while the top 5 - 200m of the Atlantic ocean might also hold up 21.1 million tons of microplastic alone. However, all these estimates of inputs and reservoirs are highly uncertain, and both models and additional field measurements are required to constrain the global plastic mass budget.

1.3 Thesis scope

To summarise sections 1.1 and 1.2, the large-scale distribution of plastic debris at the surface in the open ocean are relatively well understood. This is due to a combination of relatively extensive field sampling and a large number of modeling studies that have studied ocean surface plastic transport. However, it is less clear how plastic debris is distributed on coastlines and in coastal waters, nor how plastic is transported below the ocean surface. Given the difficulty in obtaining sufficient standardized field measurements in these domains, numerical models could provide useful insights. However, coastal and vertical plastic transport dynamics are currently not fully understood, which complicates the development of physically complete modeling frameworks.

The goal of this thesis is to better understand the transport of plastic debris in all regions of the global ocean, including coastal regions and vertical transport dynamics. In addition, this thesis investigates the physical transformation of plastic debris in the form of fragmentation. These processes are investigated using Lagrangian models based on the Parcels (Probably A Really Computationally Efficient Lagrangian Simulator) (Lange & van Sebille, 2017; Delandmeter & Van Sebille, 2019) framework using ocean circulation data from reanalysis products. The thesis consists of the following chapters:

- Chapter 2 provides a general overview of Lagrangian particle modeling, and covers the Parcels framework. In addition, a brief overview is given of the reanalysis data used to run the Lagrangian simulations.

- Chapter 3 investigates beaching and resuspension of plastic debris on a global scale. A novel parametrization of plastic beaching and resuspension within a large-scale ocean model is presented, followed by an extensive sensitivity analysis of how the distribution of beached marine plastic is influenced by the beaching and resuspension timescales.
- Chapter 4 presents parametrizations of wind-driven vertical turbulent mixing within the surface ocean mixed layer. Ocean reanalysis datasets generally do not provide turbulence data fields, and these parametrizations allow for the calculation of near-surface vertical turbulent mixing from wind and mixed layer depth data alone.
- Chapter 5 expands upon the beaching/resuspension parametrization from chapter 3 and a wind mixing parametrization from chapter 4 to investigate the influence particle size has on the three-dimensional transport of microplastic in the Mediterranean Sea. It also considers the influence of microplastic fragmentation, by applying the Kaandorp et al. (2021) fragmentation model within the size-dependent Lagrangian transport framework.
- Finally, chapter 6 is a general discussion of all the presented results, and provides an outlook for potential future research areas.

Bibliography

Alsina, J. M., Jongedijk, C. E., & van Sebille, E., 2020. Laboratory measurements of the wave-induced motion of plastic particles: Influence of wave period, plastic size and plastic density, *Journal of Geophysical Research: Oceans*, 125(12), e2020JC016294.

Andrady, A. L., 2011. Microplastics in the marine environment, *Marine pollution bulletin*, 62(8), 1596–1605.

Attademo, F. L. N., Balensiefer, D. C., da Bôaviagem Freire, A. C., de Sousa, G. P., da Cunha, F. A. G. C., & de Oliveira Luna, F., 2015. Debris ingestion by the antillean manatee (trichechus manatus manatus), *Marine pollution bulletin*, 101(1), 284–287.

Audrézet, F., Zaiko, A., Lear, G., Wood, S. A., Tremblay, L. A., & Pochon, X., 2021. Biosecurity implications of drifting marine plastic debris: current knowledge and future research, *Marine Pollution Bulletin*, 162, 111835.

Ballance, A., Ryan, P., Turpie, J., et al., 2000. How much is a clean beach worth? the impact of litter on beach users in the cape peninsula, south africa, *South African Journal of Science*, 96(5), 210–230.

Barnes, D. K., 2002. Invasions by marine life on plastic debris, *Nature*, 416(6883), 808–809.

Barnes, D. K. & Milner, P., 2005. Drifting plastic and its consequences for sessile organism dispersal in the atlantic ocean, *Marine Biology*, 146(4), 815–825.

Barnes, D. K., Galgani, F., Thompson, R. C., & Barlaz, M., 2009. Accumulation and fragmentation of plastic debris in global environments, *Philosophical transactions of the royal society B: biological sciences*, 364(1526), 1985–1998.

Barrett, J., Chase, Z., Zhang, J., Holl, M. M. B., Willis, K., Williams, A., Hardesty, B. D., & Wilcox, C., 2020. Microplastic pollution in deep-sea sediments from the great australian bight, *Frontiers in Marine Science*, p. 808.

Bessa, F., Barría, P., Neto, J. M., Frias, J. P., Otero, V., Sobral, P., & Marques, J., 2018. Occurrence of microplastics in commercial fish from a natural estuarine environment, *Marine pollution bulletin*, 128, 575–584.

Bond, A. L., Provencher, J. F., Elliot, R. D., Ryan, P. C., Rowe, S., Jones, I. L., Robertson, G. J., & Wilhelm, S. I., 2013. Ingestion of plastic marine debris by common and thick-billed murres in the northwestern atlantic from 1985 to 2012, *Marine Pollution Bulletin*, 77(1-2), 192–195.

Boyle, D., Catarino, A. I., Clark, N. J., & Henry, T. B., 2020. Polyvinyl chloride (pvc) plastic fragments release pb additives that are bioavailable in zebrafish, *Environmental Pollution*, 263, 114422.

Brach, L., Deixonne, P., Bernard, M.-F., Durand, E., Desjean, M.-C., Perez, E., van Sebille, E., & Ter Halle, A., 2018. Anticyclonic eddies increase accumulation of microplastic in the north atlantic subtropical gyre, *Marine pollution bulletin*, 126, 191–196.

Brandão, M. L., Braga, K. M., & Luque, J. L., 2011. Marine debris ingestion by magellanic penguins, spheniscus magellanicus (aves: Sphenisciformes), from the brazilian coastal zone, *Marine pollution bulletin*, 62(10), 2246–2249.

Brignac, K. C., Jung, M. R., King, C., Royer, S.-J., Blickley, L., Lamson, M. R., Potemra, J. T., & Lynch, J. M., 2019. Marine debris polymers on main hawaiian island beaches, sea surface, and seafloor, *Environmental science & technology*, 53(21), 12218–12226.

Browne, M. A., Chapman, M. G., Thompson, R. C., Amaral Zettler, L. A., Jambeck, J., & Mallos, N. J., 2015. Spatial and temporal patterns of stranded intertidal marine debris: is there a picture of global change?, *Environmental Science & Technology*, 49(12), 7082–7094.

Cole, M., Lindeque, P., Fileman, E., Halsband, C., Goodhead, R., Moger, J., & Galloway, T. S., 2013. Microplastic ingestion by zooplankton, *Environmental science & technology*, 47(12), 6646–6655.

Compa, M., Alomar, C., Wilcox, C., van Sebille, E., Lebreton, L., Hardesty, B. D., & Deudero, S., 2019. Risk assessment of plastic pollution on marine diversity in the mediterranean sea, *Science of The Total Environment*, 678, 188–196.

Convey, P., Barnes, D., & Morton, A., 2002. Debris accumulation on oceanic island shores of the scotia arc, antarctica, *Polar Biology*, 25(8), 612–617.

Corcoran, P. L., Biesinger, M. C., & Grifi, M., 2009. Plastics and beaches: a degrading relationship, *Marine pollution bulletin*, 58(1), 80–84.

Cózar, A., Echevarría, F., González-Gordillo, J. I., Irigoien, X., Úbeda, B., Hernández-León, S., Palma, Á. T., Navarro, S., García-de Lomas, J., Ruiz, A., et al., 2014. Plastic debris in the open ocean, *Proceedings of the National Academy of Sciences*, 111(28), 10239–10244.

Cózar, A., Sanz-Martín, M., Martí, E., González-Gordillo, J. I., Ubeda, B., Gálvez, J. Á., Irigoien, X., & Duarte, C. M., 2015. Plastic accumulation in the mediterranean sea, *PloS one*, 10(4), e0121762.

Cravatte, S., Serazin, G., Penduff, T., & Menkes, C., 2021. Imprint of chaotic ocean variability on transports in the southwestern pacific at interannual timescales, *Ocean Science*, 17(2), 487–507.

Critchell, K. & Lambrechts, J., 2016. Modelling accumulation of marine plastics in the coastal zone; what are the dominant physical processes?, *Estuarine, Coastal and Shelf Science*, 171, 111–122.

da Rocha, F. O. C., Martinez, S. T., Campos, V. P., da Rocha, G. O., & de Andrade, J. B., 2021. Microplastic pollution in southern atlantic marine waters: Review of current trends, sources, and perspectives, *Science of The Total Environment*, 782, 146541.

Dabrowska, A., Lopata, I., & Osial, M., 2021. The ghost nets phenomena from the chemical perspective, *Pure and Applied Chemistry*, 93(4), 479–496.

Dawson, A. L., Kawaguchi, S., King, C. K., Townsend, K. A., King, R., Huston, W. M., & Bengtson Nash, S. M., 2018. Turning microplastics into nanoplastics through digestive fragmentation by antarctic krill, *Nature communications*, 9(1), 1–8.

Debrot, A. O., van Rijn, J., Bron, P. S., & de León, R., 2013. A baseline assessment of beach debris and tar contamination in bonaire, southeastern caribbean, *Marine Pollution Bulletin*, 71(1-2), 325–329.

Delandmeter, P. & Van Sebille, E., 2019. The parcels v2. 0 lagrangian framework: new field interpolation schemes, *Geoscientific Model Development*, 12(8), 3571–3584.

Derraik, J. G., 2002. The pollution of the marine environment by plastic debris: a review, *Marine pollution bulletin*, 44(9), 842–852.

Egger, M., Sulu-Gambari, F., & Lebreton, L., 2020. First evidence of plastic fallout from the north pacific garbage patch, *Scientific reports*, 10(1), 1–10.

Enders, K., Lenz, R., Stedmon, C. A., & Nielsen, T. G., 2015. Abundance, size and polymer composition of marine microplastics ≤ 10 μm in the atlantic ocean and their modelled vertical distribution, *Marine pollution bulletin*, 100(1), 70–81.

Eo, S., Hong, S. H., Song, Y. K., Han, G. M., Seo, S., Park, Y.-G., & Shim, W. J., 2022. Underwater hidden microplastic hotspots: Historical ocean dumping sites, *Water Research*, p. 118254.

Eriksen, M., Lebreton, L. C., Carson, H. S., Thiel, M., Moore, C. J., Borerro, J. C., Galgani, F., Ryan, P. G., & Reisser, J., 2014. Plastic pollution in the world's oceans: more than 5 trillion plastic pieces weighing over 250,000 tons afloat at sea, *PloS one*, 9(12), e111913.

Faris, J. & Hart, K., 1994. Seas of debris: a summary of the third international conference on marine debris.

Fazey, F. M. & Ryan, P. G., 2016. Biofouling on buoyant marine plastics: An experimental study into the effect of size on surface longevity, *Environmental pollution*, 210, 354–360.

Fischer, R., Lobelle, D., Kooi, M., Koelmans, A., Onink, V., Laufkötter, C., Amaral-Zettler, L., Yool, A., & van Sebille, E., 2022. Modeling submerged biofouled microplastics and their vertical trajectories, *Biogeosciences*, pp. 1–29.

Gerritse, J., Leslie, H. A., de Tender, C. A., Devriese, L. I., & Vethaak, A. D., 2020. Fragmentation of plastic objects in a laboratory seawater microcosm, *Scientific reports*, 10(1), 1–16.

Goldstein, M. C., Carson, H. S., & Eriksen, M., 2014. Relationship of diversity and habitat area in north pacific plastic-associated rafting communities, *Marine Biology*, 161(6), 1441–1453.

Good, T. P., June, J. A., Etnier, M. A., & Broadhurst, G., 2010. Derelict fishing nets in puget sound and the northwest straits: Patterns and threats to marine fauna, *Marine Pollution Bulletin*, 60(1), 39–50.

Good, T. P., Samhouri, J. F., Feist, B. E., Wilcox, C., & Jahncke, J., 2020. Plastics in the pacific: Assessing risk from ocean debris for marine birds in the california current large marine ecosystem, *Biological Conservation*, 250, 108743.

Gregory, M. R., 2009. Environmental implications of plastic debris in marine settings - entanglement, ingestion, smothering, hangers-on, hitch-hiking and alien invasions, *Philosophical Transactions of the Royal Society B: Biological Sciences*, 364(1526), 2013–2025.

Guerrini, F., Mari, L., & Casagrandi, R., 2021. The dynamics of microplastics and associated contaminants: Data-driven lagrangian and eulerian modelling approaches in the mediterranean sea, *Science of the Total Environment*, 777, 145944.

Guimarães, A. T. B., Charlie-Silva, I., & Malafaia, G., 2021. Toxic effects of naturally-aged microplastics on zebrafish juveniles: a more realistic approach to plastic pollution in freshwater ecosystems, *Journal of Hazardous Materials*, 407, 124833.

Gunn, R., Hardesty, B. D., & Butler, J., 2010. Tackling 'ghost nets': local solutions to a global issue in northern australia, *Ecological Management & Restoration*, 11(2), 88–98.

Hardesty, B. D., Harari, J., Isobe, A., Lebreton, L., Maximenko, N., Potemra, J., Van Sebille, E., Vethaak, A. D., & Wilcox, C., 2017a. Using numerical model simulations to improve the understanding of micro-plastic distribution and pathways in the marine environment, *Frontiers in marine science*, 4, 30.

Hardesty, B. D., Lawson, T., van der Velde, T., Lansdell, M., & Wilcox, C., 2017b. Estimating quantities and sources of marine debris at a continental scale, *Frontiers in Ecology and the Environment*, 15(1), 18–25.

Henderson, J. R., 2001. A pre-and post-marpol annex v summary of hawaiian monk seal entanglements and marine debris accumulation in the northwestern hawaiian islands, 1982–1998, *Marine Pollution Bulletin*, 42(7), 584–589.

Hinata, H., Mori, K., Ohno, K., Miyao, Y., & Kataoka, T., 2017. An estimation of the average residence times and onshore-offshore diffusivities of beached microplastics based on the population decay of tagged meso-and macrolitter, *Marine pollution bulletin*, 122(1-2), 17–26.

Jambeck, J. R., Geyer, R., Wilcox, C., Siegler, T. R., Perryman, M., Andrady, A., Narayan, R., & Law, K. L., 2015. Plastic waste inputs from land into the ocean, *Science*, 347(6223), 768–771.

Jepsen, E. M. & de Bruyn, P. N., 2019. Pinniped entanglement in oceanic plastic pollution: A global review, *Marine pollution bulletin*, 145, 295–305.

Kaandorp, M. L., Dijkstra, H. A., & van Sebille, E., 2020. Closing the mediterranean marine floating plastic mass budget: inverse modeling of sources and sinks, *Environmental science & technology*, 54(19), 11980–11989.

Kaandorp, M. L., Dijkstra, H. A., & van Sebille, E., 2021. Modelling size distributions of marine plastics under the influence of continuous cascading fragmentation, *Environmental Research Letters*, 16(5), 054075.

Kane, I. A., Clare, M. A., Miramontes, E., Wogelius, R., Rothwell, J. J., Garreau, P., & Pohl, F., 2020. Seafloor microplastic hotspots controlled by deep-sea circulation, *Science*, 368(6495), 1140–1145.

Karlsson, T. M., Arneborg, L., Broström, G., Almroth, B. C., Gipperth, L., & Hassellöv, M., 2018. The unaccountability case of plastic pellet pollution, *Marine pollution bulletin*, 129(1), 52–60.

Kerpen, N. B., Schlurmann, T., Schendel, A., Gundlach, J., Marquard, D., & Hüpgen, M., 2020. Wave-induced distribution of microplastic in the surf zone, *Frontiers in Marine Science*, p. 979.

Koelmans, A. A., Kooi, M., Law, K. L., & Van Sebille, E., 2017. All is not lost: deriving a top-down mass budget of plastic at sea, *Environmental Research Letters*, 12(11), 114028.

Kooi, M., Reisser, J., Slat, B., Ferrari, F. F., Schmid, M. S., Cunsolo, S., Brambini, R., Noble, K., Sirks, L.-A., Linders, T. E., et al., 2016. The effect of particle properties on the depth profile of buoyant plastics in the ocean, *Scientific reports*, 6(1), 1–10.

Kooi, M., Nes, E. H. v., Scheffer, M., & Koelmans, A. A., 2017. Ups and downs in the ocean: effects of biofouling on vertical transport of microplastics, *Environmental science & technology*, 51(14), 7963–7971.

Kubota, M., 1994. A mechanism for the accumulation of floating marine debris north of hawaii, *Journal of Physical Oceanography*, 24(5), 1059–1064.

Kubota, M., Takayama, K., & Namimoto, D., 2005. Pleading for the use of biodegradable polymers in favor of marine environments and to avoid an asbestos-like problem for the future, *Applied Microbiology and Biotechnology*, 67(4), 469–476.

Kukulka, T., Proskurowski, G., Morét-Ferguson, S., Meyer, D. W., & Law, K. L., 2012. The effect of wind mixing on the vertical distribution of buoyant plastic debris, *Geophysical Research Letters*, 39(7).

Kukulka, T., Law, K. L., & Proskurowski, G., 2016. Evidence for the influence of surface heat fluxes on turbulent mixing of microplastic marine debris, *Journal of Physical Oceanography*, 46(3), 809–815.

Lange, M. & van Sebille, E., 2017. Parcels v0. 9: prototyping a lagrangian ocean analysis framework for the petascale age, *Geoscientific Model Development*, 10(11), 4175–4186.

Lavers, J. L. & Bond, A. L., 2017. Exceptional and rapid accumulation of anthropogenic debris on one of the world's most remote and pristine islands, *Proceedings of the National Academy of Sciences*, 114(23), 6052–6055.

Lavers, J. L., Bond, A. L., & Hutton, I., 2014. Plastic ingestion by flesh-footed shearwaters (puffinus carneipes): Implications for fledgling body condition and the accumulation of plastic-derived chemicals, *Environmental Pollution*, 187, 124–129.

Law, K. L., 2017. Plastics in the marine environment, *Annual review of marine science*, 9, 205–229.

Law, K. L., Morét-Ferguson, S., Maximenko, N. A., Proskurowski, G., Peacock, E. E., Hafner, J., & Reddy, C. M., 2010. Plastic accumulation in the north atlantic subtropical gyre, *Science*, 329(5996), 1185–1188.

Lebreton, L., Van Der Zwet, J., Damsteeg, J.-W., Slat, B., Andrady, A., & Reisser, J., 2017. River plastic emissions to the world's oceans, *Nature communications*, 8(1), 1–10.

Lebreton, L., Slat, B., Ferrari, F., Sainte-Rose, B., Aitken, J., Marthouse, R., Hajbane, S., Cunsolo, S., Schwarz, A., Levivier, A., et al., 2018. Evidence that the great pacific garbage patch is rapidly accumulating plastic, *Scientific reports*, 8(1), 1–15.

Lebreton, L., Egger, M., & Slat, B., 2019. A global mass budget for positively buoyant macroplastic debris in the ocean, *Scientific reports*, 9(1), 1–10.

Lebreton, L.-M., Greer, S., & Borrero, J. C., 2012. Numerical modelling of floating debris in the world's oceans, *Marine pollution bulletin*, 64(3), 653–661.

Lee, J., Hong, S., Song, Y. K., Hong, S. H., Jang, Y. C., Jang, M., Heo, N. W., Han, G. M., Lee, M. J., Kang, D., et al., 2013. Relationships among the abundances of plastic debris in different size classes on beaches in south korea, *Marine pollution bulletin*, 77(1-2), 349–354.

Li, D., Liu, K., Li, C., Peng, G., Andrady, A. L., Wu, T., Zhang, Z., Wang, X., Song, Z., Zong, C., et al., 2020. Profiling the vertical transport of microplastics in the west pacific ocean and the east indian ocean with a novel in situ filtration technique, *Environmental Science & Technology*, 54(20), 12979–12988.

Li, W. C., Tse, H., & Fok, L., 2016. Plastic waste in the marine environment: A review of sources, occurrence and effects, *Science of the total environment*, 566, 333–349.

Liubartseva, S., Coppini, G., Lecci, R., & Clementi, E., 2018. Tracking plastics in the mediterranean: 2d lagrangian model, *Marine pollution bulletin*, 129(1), 151–162.

Lobelle, D., Kooi, M., Koelmans, A. A., Laufkötter, C., Jongedijk, C. E., Kehl, C., & van Sebille, E., 2021. Global modeled sinking characteristics of biofouled microplastic, *Journal of Geophysical Research: Oceans*, 126(4), e2020JC017098.

Madec, G., Bourdallé-Badie, R., Bouttier, P.-A., Bricaud, C., Bruciaferri, D., Calvert, D., Chanut, J., Clementi, E., Coward, A., Delrosso, D., et al., 2017. Nemo ocean engine.

Marana, M. H., Poulsen, R., Thormar, E. A., Clausen, C. G., Thit, A., Mathiessen, H., Jaafar, R., Korbut, R., Hansen, A. M. B., Hansen, M., et al., 2022. Plastic nanoparticles cause mild inflammation, disrupt metabolic pathways, change the gut microbiota and affect reproduction in zebrafish: A full generation multi-omics study, *Journal of Hazardous Materials*, 424, 127705.

Martinez, E., Maamaatuaiahutapu, K., & Taillandier, V., 2009. Floating marine debris surface drift: convergence and accumulation toward the south pacific subtropical gyre, *Marine Pollution Bulletin*, 58(9), 1347–1355.

Mascarenhas, R., Santos, R., & Zeppelini, D., 2004. Plastic debris ingestion by sea turtles in paraíba, brazil, *Marine pollution bulletin*, 49(4), 354–355.

Maximenko, N., Hafner, J., & Niiler, P., 2012. Pathways of marine debris derived from trajectories of lagrangian drifters, *Marine pollution bulletin*, 65(1-3), 51–62.

Meijer, L. J., van Emmerik, T., van der Ent, R., Schmidt, C., & Lebreton, L., 2021. More than 1000 rivers account for 80% of global riverine plastic emissions into the ocean, *Science Advances*, 7(18), eaaz5803.

Mercogliano, R., Avio, C. G., Regoli, F., Anastasio, A., Colavita, G., & Santonicola, S., 2020. Occurrence of microplastics in commercial seafood under the perspective of the human food chain. a review, *Journal of agricultural and food chemistry*, 68(19), 5296–5301.

Miladinova, S., Macias, D., Stips, A., & Garcia-Gorriz, E., 2020. Identifying distribution and accumulation patterns of floating marine debris in the black sea, *Marine Pollution Bulletin*, 153, 110964.

Monteiro, R. C., do Sul, J. A. I., & Costa, M. F., 2018. Plastic pollution in islands of the atlantic ocean, *Environmental Pollution*, 238, 103–110.

Morales-Caselles, C., Viejo, J., Martí, E., González-Fernández, D., Pragnell-Raasch, H., González-Gordillo, J. I., Montero, E., Arroyo, G. M., Hanke, G., Salvo, V. S., et al., 2021. An inshore–offshore sorting system revealed from global classification of ocean litter, *Nature Sustainability*, 4(6), 484–493.

Morét-Ferguson, S., Law, K. L., Proskurowski, G., Murphy, E. K., Peacock, E. E., & Reddy, C. M., 2010. The size, mass, and composition of plastic debris in the western north atlantic ocean, *Marine Pollution Bulletin*, 60(10), 1873–1878.

Mountford, A. & Morales Maqueda, M., 2019. Eulerian modeling of the three-dimensional distribution of seven popular microplastic types in the global ocean, *Journal of Geophysical Research: Oceans*, 124(12), 8558–8573.

Mountford, A. S. & Morales Maqueda, M. A., 2021. Modeling the accumulation and transport of microplastics by sea ice, *Journal of Geophysical Research: Oceans*, 126(2), e2020JC016826.

Nooteboom, P. D., Delandmeter, P., van Sebille, E., Bijl, P. K., Dijkstra, H. A., & von der Heydt, A. S., 2020. Resolution dependency of sinking lagrangian particles in ocean general circulation models, *PloS one*, 15(9), e0238650.

Obbard, R. W., Sadri, S., Wong, Y. Q., Khitun, A. A., Baker, I., & Thompson, R. C., 2014. Global warming releases microplastic legacy frozen in arctic sea ice, *Earth's Future*, 2(6), 315–320.

O'Brine, T. & Thompson, R. C., 2010. Degradation of plastic carrier bags in the marine environment, *Marine pollution bulletin*, 60(12), 2279–2283.

Olivelli, A., Hardesty, B. D., & Wilcox, C., 2020. Coastal margins and backshores represent a major sink for marine debris: insights from a continental-scale analysis, *Environmental Research Letters*, 15(7), 074037.

Onink, V., Wichmann, D., Delandmeter, P., & van Sebille, E., 2019. The role of ekman currents, geostrophy, and stokes drift in the accumulation of floating microplastic, *Journal of Geophysical Research: Oceans*, 124(3), 1474–1490.

Pabortsava, K. & Lampitt, R. S., 2020. High concentrations of plastic hidden beneath the surface of the atlantic ocean, *Nature communications*, 11(1), 1–11.

Patti, T. B., Fobert, E. K., Reeves, S. E., & da Silva, K. B., 2020. Spatial distribution of microplastics around an inhabited coral island in the maldives, indian ocean, *Science of The Total Environment*, 748, 141263.

Peeken, I., Primpke, S., Beyer, B., Gütermann, J., Katlein, C., Krumpen, T., Bergmann, M., Hehemann, L., & Gerdts, G., 2018. Arctic sea ice is an important temporal sink and means of transport for microplastic, *Nature communications*, 9(1), 1–12.

Peng, S.-Q. & Xie, L., 2006. Effect of determining initial conditions by four-dimensional variational data assimilation on storm surge forecasting, *Ocean Modelling*, 14(1-2), 1–18.

Pervez, R., Wang, Y., Mahmood, Q., Zahir, M., & Jattak, Z., 2020. Abundance, type, and origin of litter on no. 1 bathing beach of qingdao, china, *Journal of Coastal Conservation*, 24(3), 1–10.

Pham, C. K., Pereira, J. M., Frias, J. P., Ríos, N., Carriço, R., Juliano, M., & Rodríguez, Y., 2020. Beaches of the azores archipelago as transitory repositories for small plastic fragments floating in the north-east atlantic, *Environmental Pollution*, 263, 114494.

Piccardo, M., Renzi, M., & Terlizzi, A., 2020. Nanoplastics in the oceans: Theory, experimental evidence and real world, *Marine Pollution Bulletin*, 157, 111317.

Pieper, C., Ventura, M. A., Martins, A., & Cunha, R. T., 2015. Beach debris in the azores (ne atlantic): Faial island as a first case study, *Marine pollution bulletin*, 101(2), 575–582.

Pieper, C., Amaral-Zettler, L., Law, K. L., Loureiro, C. M., & Martins, A., 2019a. Application of matrix scoring techniques to evaluate marine debris sources in the remote islands of the azores archipelago, *Environmental Pollution*, 249, 666–675.

Pieper, C., Martins, A., Zettler, E., Loureiro, C. M., Onink, V., Heikkilä, A., Epinoux, A., Edson, E., Donnarumma, V., Vogel, F. d., et al., 2019b. Into the med: Searching for microplastics from space to deep-sea, in *International Conference on Microplastic Pollution in the Mediterranean Sea*, pp. 129–138, Springer.

Prants, S., 2014. Chaotic lagrangian transport and mixing in the ocean, *The European Physical Journal Special Topics*, 223(13), 2723–2743.

Puskic, P. S., Lavers, J. L., & Bond, A. L., 2020. A critical review of harm associated with plastic ingestion on vertebrates, *Science of The Total Environment*, 743, 140666.

Redford, D. P., Trulli, H. K., & Trulli, W. R., 1997. Sources of plastic pellets in the aquatic environment, in *Marine Debris*, pp. 335–343, Springer.

Reijnders, D., Deleersnijder, E., & van Sebille, E., 2022. Simulating lagrangian subgrid-scale dispersion on neutral surfaces in the ocean, *Journal of Advances in Modeling Earth Systems*, 14(2), e2021MS002850.

Ribic, C. A., Sheavly, S. B., Rugg, D. J., & Erdmann, E. S., 2010. Trends and drivers of marine debris on the atlantic coast of the united states 1997–2007, *Marine pollution bulletin*, 60(8), 1231–1242.

Ribic, C. A., Sheavly, S. B., Rugg, D. J., & Erdmann, E. S., 2012. Trends in marine debris along the us pacific coast and hawai'i 1998–2007, *Marine Pollution Bulletin*, 64(5), 994–1004.

Richardson, K., Hardesty, B. D., & Wilcox, C., 2019. Estimates of fishing gear loss rates at a global scale: A literature review and meta-analysis, *Fish and Fisheries*, 20(6), 1218–1231.

Rochman, C. M., Tahir, A., Williams, S. L., Baxa, D. V., Lam, R., Miller, J. T., Teh, F.-C., Werorilangi, S., & Teh, S. J., 2015. Anthropogenic debris in seafood: Plastic debris and fibers from textiles in fish and bivalves sold for human consumption, *Scientific reports*, 5(1), 1–10.

Ruiz-Orejón, L. F., Sardá, R., & Ramis-Pujol, J., 2016. Floating plastic debris in the central and western mediterranean sea, *Marine Environmental Research*, 120, 136–144.

Rummel, C. D., Löder, M. G., Fricke, N. F., Lang, T., Griebeler, E.-M., Janke, M., & Gerdts, G., 2016. Plastic ingestion by pelagic and demersal fish from the north sea and baltic sea, *Marine pollution bulletin*, 102(1), 134–141.

Ryan, P. G., 2018. Entanglement of birds in plastics and other synthetic materials, *Marine Pollution Bulletin*, 135, 159–164.

Ryan, P. G., 2020. Land or sea? what bottles tell us about the origins of beach litter in kenya, *Waste Management*, 116, 49–57.

Ryan, P. G., Perold, V., Osborne, A., & Moloney, C. L., 2018. Consistent patterns of debris on south african beaches indicate that industrial pellets and other mesoplastic items mostly derive from local sources, *Environmental Pollution*, 238, 1008–1016.

Ryan, P. G., Dilley, B. J., Ronconi, R. A., & Connan, M., 2019. Rapid increase in asian bottles in the south atlantic ocean indicates major debris inputs from ships, *Proceedings of the National Academy of Sciences*, 116(42), 20892–20897.

Ryan, P. G., Weideman, E. A., Perold, V., Hofmeyr, G., & Connan, M., 2021. Message in a bottle: Assessing the sources and origins of beach litter to tackle marine pollution, *Environmental Pollution*, 288, 117729.

Schmidt, C., Krauth, T., & Wagner, S., 2017. Export of plastic debris by rivers into the sea, *Environmental science & technology*, 51(21), 12246–12253.

Schuyler, Q. A., Wilcox, C., Townsend, K. A., Wedemeyer-Strombel, K. R., Balazs, G., van Sebille, E., & Hardesty, B. D., 2016. Risk analysis reveals global hotspots for marine debris ingestion by sea turtles, *Global Change Biology*, 22(2), 567–576.

Seo, S., Park, Y.-G., Park, J.-H., Lee, H. J., & Hirose, N., 2013. The tsushima warm current from a high resolution ocean prediction model, hycom, *Ocean and Polar Research*, 35(2), 135–146.

Smith, L. & Turrell, W. R., 2021. Monitoring plastic beach litter by number or by weight: The implications of fragmentation, *Frontiers in Marine Science*, p. 1359.

Song, Y. K., Hong, S. H., Jang, M., Han, G. M., Jung, S. W., & Shim, W. J., 2017. Combined effects of uv exposure duration and mechanical abrasion on microplastic fragmentation by polymer type, *Environmental science & technology*, 51(8), 4368–4376.

Spirkovski, Z., Ilik-Boeva, D., Ritterbusch, D., Peveling, R., & Pietrock, M., 2019. Ghost net removal in ancient lake ohrid: A pilot study, *Fisheries Research*, 211, 46–50.

Steer, M., Cole, M., Thompson, R. C., & Lindeque, P. K., 2017. Microplastic ingestion in fish larvae in the western english channel, *Environmental Pollution*, 226, 250–259.

Sudhakar, M., Trishul, A., Doble, M., Kumar, K. S., Jahan, S. S., Inbakandan, D., Viduthalai, R., Umadevi, V., Murthy, P. S., & Venkatesan, R., 2007. Biofouling and biodegradation of polyolefins in ocean waters, *Polymer Degradation and Stability*, 92(9), 1743–1752.

Taïbi, N.-E., Bentaallah, M. E. A., Alomar, C., Compa, M., & Deudero, S., 2021. Micro-and macro-plastics in beach sediment of the algerian western coast: First data on distribution, characterization, and source, *Marine Pollution Bulletin*, 165, 112168.

Ter Halle, A., Ladirat, L., Gendre, X., Goudouneche, D., Pusineri, C., Routaboul, C., Tenailleau, C., Duployer, B., & Perez, E., 2016. Understanding the fragmentation pattern of marine plastic debris, *Environmental science & technology*, 50(11), 5668–5675.

Therriault, T. W., Nelson, J. C., Carlton, J. T., Liggan, L., Otani, M., Kawai, H., Scriven, D., Ruiz, G. M., & Clarke Murray, C., 2018. The invasion risk of species associated with japanese tsunami marine debris in pacific north america and hawaii, *Marine Pollution Bulletin*, 132, 82–89.

Tramoy, R., Gasperi, J., Dris, R., Colasse, L., Fisson, C., Sananes, S., Rocher, V., & Tassin, B., 2019. Assessment of the plastic inputs from the seine basin to the sea using statistical and field approaches, *Frontiers in Marine Science*, 6, 151.

Tziperman, E., Stone, L., Cane, M. A., & Jarosh, H., 1994. El niño chaos: Overlapping of resonances between the seasonal cycle and the pacific ocean-atmosphere oscillator, *Science*, 264(5155), 72–74.

Van Cauwenberghe, L., Vanreusel, A., Mees, J., & Janssen, C. R., 2013. Microplastic pollution in deep-sea sediments, *Environmental pollution*, 182, 495–499.

van der Hal, N., Ariel, A., & Angel, D. L., 2017. Exceptionally high abundances of microplastics in the oligotrophic israeli mediterranean coastal waters, *Marine pollution bulletin*, 116(1-2), 151–155.

van Duinen, B., Kaandorp, M. L., & van Sebille, E., 2022. Identifying marine sources of beached plastics through a bayesian framework: Application to southwest netherlands, *Geophysical Research Letters*, p. e2021GL097214.

Van Emmerik, T., Loozen, M., Van Oeveren, K., Buschman, F., & Prinsen, G., 2019. Riverine plastic emission from jakarta into the ocean, *Environmental Research Letters*, 14(8), 084033.

Van Sebille, E., 2015. The oceans' accumulating plastic garbage, *Physics Today*, 68, 60–61.

Van Sebille, E., England, M. H., & Froyland, G., 2012. Origin, dynamics and evolution of ocean garbage patches from observed surface drifters, *Environmental Research Letters*, 7(4), 044040.

Van Sebille, E., Wilcox, C., Lebreton, L., Maximenko, N., Hardesty, B. D., Van Franeker, J. A., Eriksen, M., Siegel, D., Galgani, F., & Law, K. L., 2015. A global inventory of small floating plastic debris, *Environmental Research Letters*, 10(12), 124006.

Van Sebille, E., Aliani, S., Law, K. L., Maximenko, N., Alsina, J. M., Bagaev, A., Bergmann, M., Chapron, B., Chubarenko, I., Cózar, A., et al., 2020. The physical oceanography of the transport of floating marine debris, *Environmental Research Letters*, 15(2), 023003.

Vialard, J., Menkes, C., Anderson, D. L., & Balmaseda, M. A., 2003. Sensitivity of pacific ocean tropical instability waves to initial conditions, *Journal of physical oceanography*, 33(1), 105–121.

Votier, S. C., Archibald, K., Morgan, G., & Morgan, L., 2011. The use of plastic debris as nesting material by a colonial seabird and associated entanglement mortality, *Marine Pollution Bulletin*, 62(1), 168–172.

Wakelin, S. L., Holt, J. T., & Proctor, R., 2009. The influence of initial conditions and open boundary conditions on shelf circulation in a 3d ocean-shelf model of the north east atlantic, *Ocean Dynamics*, 59(1), 67–81.

Webster, F., 1969. Vertical profiles of horizontal ocean currents, in *Deep Sea Research and Oceanographic Abstracts*, vol. 16, pp. 85–98, Elsevier.

Weitzel, S. L., Feura, J. M., Rush, S. A., Iglay, R. B., & Woodrey, M. S., 2021. Availability and assessment of microplastic ingestion by marsh birds in mississippi gulf coast tidal marshes, *Marine Pollution Bulletin*, 166, 112187.

Wichmann, D., Delandmeter, P., Dijkstra, H. A., & van Sebille, E., 2019. Mixing of passive tracers at the ocean surface and its implications for plastic transport modelling, *Environmental Research Communications*, 1(11), 115001.

Woodall, L. C., Sanchez-Vidal, A., Canals, M., Paterson, G. L., Coppock, R., Sleight, V., Calafat, A., Rogers, A. D., Narayanaswamy, B. E., & Thompson, R. C., 2014. The deep sea is a major sink for microplastic debris, *Royal Society open science*, 1(4), 140317.

Xiong, X., Siddique, M. S., Graham, N. J., & Yu, W., 2022. Towards microplastics contribution for membrane biofouling and disinfection by-products precursors: The effect on microbes, *Journal of Hazardous Materials*, 426, 127797.

Yang, D., Shi, H., Li, L., Li, J., Jabeen, K., & Kolandhasamy, P., 2015. Microplastic pollution in table salts from china, *Environmental science & technology*, 49(22), 13622–13627.

Zhang, H., 2017. Transport of microplastics in coastal seas, *Estuarine, Coastal and Shelf Science*, 199, 74–86.

Zhao, S., Zettler, E. R., Bos, R. P., Lin, P., Amaral-Zettler, L. A., Mincer, T. J., et al., 2022. Large quantities of small microplastics permeate the surface ocean to abyssal depths in the south atlantic gyre, *Global Change Biology*.

Zhu, L., Wang, H., Chen, B., Sun, X., Qu, K., & Xia, B., 2019. Microplastic ingestion in deep-sea fish from the south china sea, *Science of the Total Environment*, 677, 493–501.

Chapter 2

Methods

2.1 Lagrangian modeling framework

All the work within this thesis utilizes a Lagrangian modeling framework, where plastic particles are represented by virtual particles. Using reanalysis or other ocean circulation data, the trajectory of a virtual particle can be calculated with the following equation of motion:

$$\vec{x}(t+dt) = \vec{x}(t) + \int_t^{t+\Delta t} \vec{v}\big(\vec{x},\tau\big)d\tau \tag{2.1}$$

where $\vec{x} = (\lambda, \phi, z)$ is the particle position with longitude λ, latitude ϕ and depth z and $\vec{v}(\vec{x}, t)$ is the ocean currents at the particle position (Van Sebille et al., 2018). Assuming that the particle is passive, in that it only follows the general ocean flow and does not exhibit any other transport behavior, the full transport of a particle can be calculated from the ocean currents $\vec{u}$. However, depending on the type of particle other processes might be relevant to model the full particle transport. For example, depending on the particle size, shape, density and orientation (Enders et al., 2015; DiBenedetto et al., 2018; Clark et al., 2020), a particle can be either positively or negatively buoyant and exhibit a rise velocity w_r. Meanwhile, the ocean current velocity fields $\vec{u}$ typically originate from the output from oceanic general circulation models (OGCM), which don't resolve physical processes on all spatial and temporal scales (Van Sebille et al., 2018). As such, equation (2.1) often includes a diffusion term to at least partially account for unresolved sub-grid processes:

$$\vec{x}(t+\Delta t) = \vec{x}(t) + \int_t^{t+\Delta t} \vec{v}\big(\vec{x},\tau\big)d\tau + \vec{K}(\vec{x},t)d\vec{W}(t) \tag{2.2}$$

where $\vec{K}$ is a diffusion tensor and $d\vec{W}(t)$ is a Wiener increment with zero mean and variance dt. Since the relevant physical processes for calculating the transport of virtual particles are highly dependent on the particle type, it is vital to have a flexible model framework that easily adapts to various transport scenarios.

All the Lagrangian model scenarios described in chapters 3, 4 and 5 utilize Parcels (**P**robably **A** **R**eally **C**omputationally **E**fficient **L**agrangian **S**imulator), which is a set of Python classes and methods (Lange & van Sebille, 2017; Delandmeter & Van Sebille, 2019) that has been used to model the Lagrangian transport of a wide array of passive and active particles such as ice masses (Sutter et al., 2021), sea turtles (Le Gouvello et al., 2020), plastic (Onink et al., 2019) and fish (Phillips et al., 2018). Parcels is developed to easily allow for the use of customized Kernels that represent particle transport or transformation processes, and as such Parcels is highly suited for running the wide range of simulation scenarios described in subsequent

chapters. While the specific physical processes included in specific scenarios are covered in-depth in each chapter, this section will provide a general overview of the Parcels model framework.

The basic structure of Parcels is shown in Figure 2.1. All hydrodynamic data fields are

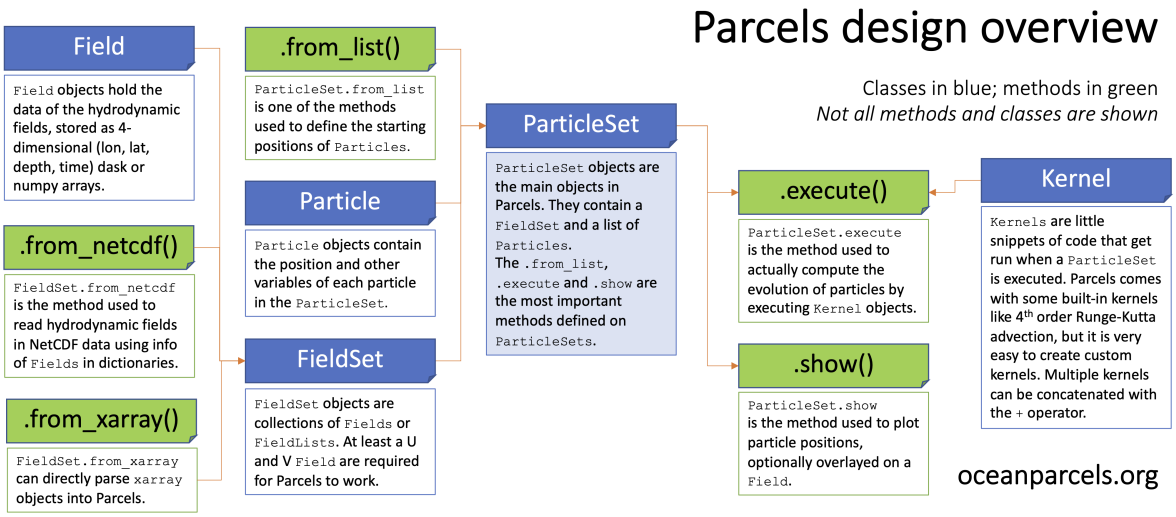

Figure 2.1: Diagram showing the basic structure of Parcels. Figure retrieved from Lange & van Sebille (2017).

contained within Field objects, where the FieldSet object is a collection of all the fields. For example, the FieldSet could contain Field objects for meridional and zonal ocean currents, the mixed layer depth, ocean salinity, etc., where this data can originate from OGCM output products such as HYCOM (Bleck, 2002). The ParticleSet object is the main component of any Parcels simulation, containing both the FieldSet and the Particle objects that contain all the particle positions. Depending on the particular scenario, a Particle object can be modified to store other variables, such as the particle's age or the sea surface temperature at the particle's location.

The final components of a Parcels simulation are the Kernels, which are code snippets that when executed define the behavior of the particles within the ParticleSet. A number of standard Kernels are provided as part of Parcels, such as Kernels for 4th order Runge-Kutta particle advection and various schemes for zonal and meridional diffusion. Parcels also allows the use of customized Kernels, such as for particle beaching (Chapter 3) or fragmentation (Chapter 5). Multiple Kernels can be chained together to define the full particle behavior, and these Kernels are executed every timestep to calculate the full particle transport.

Once all model components have been defined, the method ParticleSet.execute() runs the simulation, with the full procedure shown in Figure 2.2. For each time interval, the Kernel is executed for each particle within the ParticleSet. For example, if the Kernel includes particle advection, the Kernel will calculate the new particle positions for each time interval. The value of the time interval, generally referred to as the integration timestep Δt, is dependent on the specific model setup, as the physical processes included within a simulation impose constraints on Δt. For example, for global-scale simulations with solely horizontal transport processes, $\Delta t = 10$ minutes can be appropriate (Chapter 3), as shorter timesteps do not significantly affect the model performance and would increase the computational costs. However, for simulations involving vertical particle transport such long timesteps would not be numerically stable, as vertical transport processes generally act on much smaller spatial and temporal scales compared to horizontal transport (Chapter 4). As such, shorter timesteps on the order of $\Delta t = 30$ seconds are necessary for large-scale simulations involving vertical transport (Chapter 5). While it is

possible to save the particle positions and other variables for each integration timestep into the ParticleFile output file, this increases the storage requirements for all the output data. Given that the particle position data at this high temporal resolution does not necessarily provide much additional physical insight, it is generally acceptable to store particle variable data for every 12 - 24 hours depending on the model study (Chapters 3 and 5).

The field data, the number of particles and the Kernels are specific to each model scenario

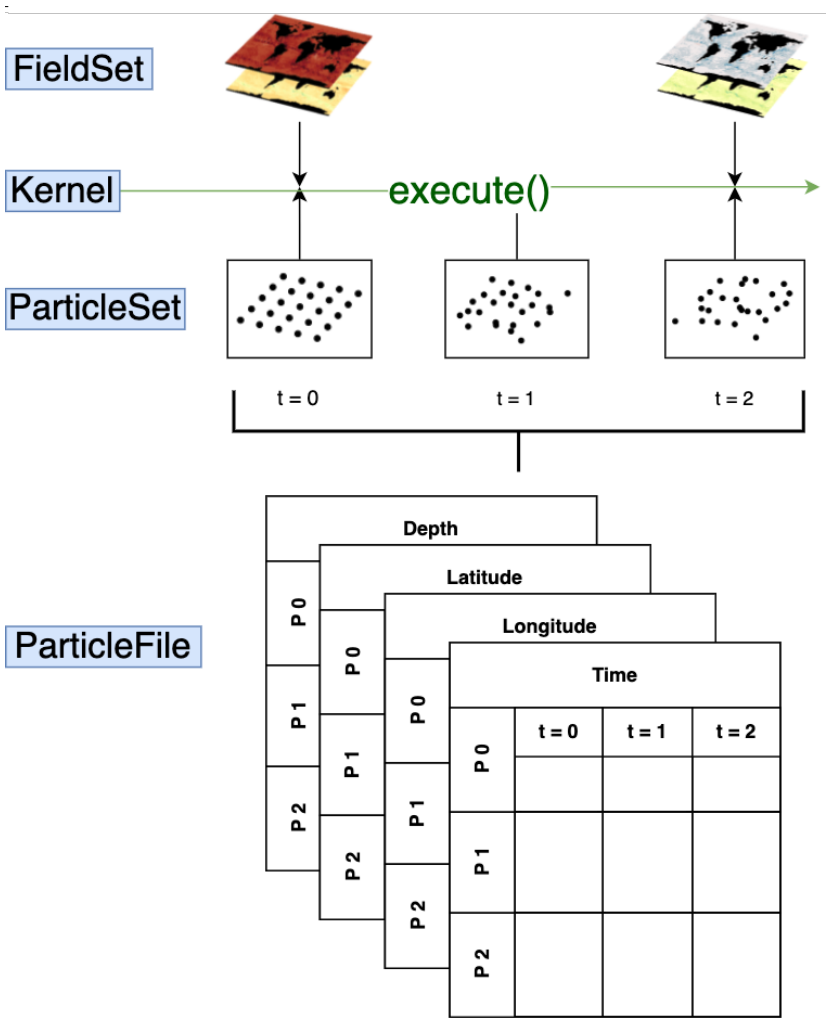

Figure 2.2: Diagram showing the execution of the ParticleSet.execute() method for time intervals $t = 0, 1, 2$. Using data loaded from the FieldSet, the Kernel is executed for each particle, resulting in changes in the particle positions. Variables such as the particle longitude, latitude and depth are saved within the ParticleFile. Figure created by Reint Fischer.

and are described in the subsequent chapters. However, a common feature with large-scale Lagrangian simulations is that ocean currents can advect a particle onto a land cell where it can get stuck. While this is sometimes employed as a parametrization of plastic beaching (Lebreton et al., 2012; Liubartseva et al., 2018), it is a numerical issue related to the improper resolution of boundary currents (Lynch et al., 2014) and not a representation of physical beaching processes. Given that over 40% of the particles within a simulation can get stuck if this numerical issue is not accounted for (Sterl et al., 2020), the model scenarios in chapters 3 and 5 include artificial anti-beaching currents (Onink et al., 2019). When a particle is within 500 m of the nearest model land cell, a current with a magnitude of 1 m s^{-1} pushes the particle away from land. While this does not significantly influence the large-scale distribution of plastic particles (Onink

et al., 2019; Sterl et al., 2020), it prevents particles from getting stuck due to numerical errors and as such, particles within the model scenarios described in chapters 3 and 5 only beach according to the specified beaching parametrizations.

2.2 Ocean reanalysis datasets

All Lagrangian model scenarios included within this thesis utilize offline data, in that the ocean current data has been computed prior to running the Lagrangian simulation. Given the high computational cost in running a large-scale high resolution OGCM, this saves computational resources for running the Lagrangian component of the model. This does assume that the plastic debris represented by the virtual Lagrangian particle does not influence the modeled ocean flow, but even the largest debris items such as fishing nets, that can be over a 100 m in length, are significantly smaller than the spatial scales resolved within OGCMs (Napper & Thompson, 2020; Bleck, 2002).

The model scenarios within this thesis use reanalysis data to run the Lagrangian simulations, where an ocean reanalysis is "a physically consistent set of optimally merged simulation model states and historical observational data, using data assimilation" (Baatz et al., 2021). In other words, an ocean reanalysis product uses a numerical model such as an OGCM to compute variables such as meridional/zonal currents, temperature and salinity, where observational records are continuously integrated into the model via data assimilation so that the reanalysis matches observational records as closely as possible. A reanalysis can thus provide crucial insight into the past states of the global climate, and be used as input for other models (e.g. an atmospheric reanalysis such as the ERA5 reanalysis (Hersbach et al., 2020) can be used as forcing of an ocean reanalysis). Ocean reanalyses have generally focused on the retrospective analysis of physical properties such as current velocities, but state-of-the-art reanalyses can also include processes such as sea ice dynamics and biogeochemistry (Baatz et al., 2021).

The work in this thesis utilizes two ocean reanalysis datasets. The global-scale beaching scenarios described in chapter 3 use the GOFS 3.1 HYCOM + NCODA Global 1/12° reanalysis, which is based on the HYCOM modeling framework (Bleck, 2002) and the NCODA data assimilation system (Cummings, 2005; Cummings & Smedstad, 2013). The size-dependent transport and fragmentation scenarios described in chapter 5 use the CMEMS Mediterranean Sea Physics Reanalysis (CMSPR) (Escudier et al., 2020), which is based on the NEMO version 3.6 (Madec et al., 2017) OGCM. While the details of the underlying model structures and algorithms for the reanalysis products are beyond the scope of this thesis, there are a number of common features that are relevant for the work contained within this thesis.

The underlying model grid of HYCOM is a bipolar rectilinear/curvilinear grid, but in both the HYCOM and CMSPR reanalysis products the data variables are regridded onto Arakawa A-grids (Arakawa & Lamb, 1977). While Parcels supports Fields with data on any curvilinear grid (Delandmeter & Van Sebille, 2019), having all data variables on the same numerical grid simplifies the implementation of various model components. For example, all the Lagrangian model scenarios described in chapters 3 and 5 require calculating the distance of the virtual particle to the nearest model land cell. Given that all tracers are on the same model grid, this is relatively easy to define and compute on an A-grid, but with e.g. staggered Arakawa C-grids there are multiple approaches that could be taken to define the particle distance to the nearest model land cell. While the beaching parametrization introduced in chapter 3 can be adapted for scenarios using C-grid flow field data, exact definitions such as the distance to shore might need to be adapted.

The HYCOM and CMSPR products have comparable spatial and temporal resolutions, where the HYCOM reanalysis has a temporal resolution of 3 hours and a spatial resolution of 1/12° (≈ 10 km at the equator) while the CMSPR data has a temporal resolution of 1 hour and a spatial resolution of 1/24°. The implementation of ocean physics varies between the two models, but both reanalysis products produce good reproductions of large-scale circulation patterns (Chi et al., 2018; Escudier et al., 2021). However, the models are unable to resolve sub-mesoscale horizontal circulation features. Within a Lagrangian model framework sub-grid processes are often parametrized by a diffusion term (Van Sebille et al., 2018), where the choices in horizontal and vertical diffusion coefficients depend on the particular model scenario (Lacerda et al., 2019; Reijnders et al., 2022; Kukulka et al., 2016). However, this doesn't correct for the fact that OGCMs are unable to adequately model coastal dynamics (Liu & Weisberg, 2011; de Souza et al., 2021), as these can demonstrate variability on a spatial scale of meters (Van Sebille et al., 2020) while the spatial resolution of an OGCM is on the order of tens of kilometers. As such, nearshore processes such as particle beaching and resuspension can not be represented with OGCM data alone. Given that OGCM are a vital component of most global-scale plastic transport modeling studies, this has resulted in a limited understanding of the role of plastic debris beaching and resuspension on a global scale.

As demonstrated by Onink et al. (2019), surface wave dynamics play an important role in the large-scale transport of floating plastic debris. However, both HYCOM and CMSPR do not resolve wave dynamics, and surface wave reanalysis products are used to model the large-scale Stokes drift. In the chapter 3 beaching scenarios, Stokes drift data is used from the WaveWatch III (WW3) hindcast product (Tolman, 1997, 2009), which is a global hindcast with a 1/2° spatial and 3 hour temporal resolution. For the size-dependent transport and fragmentation scenarios described in chapter 5, the Mediterranean Sea Waves Reanalysis (MSWR) (Korres et al., 2019) is used, which has a 1/24° spatial and 1 hour temporal resolution. Both the WW3 and MSWR products have been validated relative to field measurements, and show high correlations in the direction and magnitude of surface Stokes drift compared with *in situ* drifter measurements (Tamura et al., 2012; Rascle & Ardhuin, 2013; Zacharioudaki et al., 2020). However, the relative coarse resolutions with the WW3 and MSWR datasets implies that nearshore wave processes such as wave breaking, shoaling and refraction are not resolved. As with earlier modeling studies like (Onink et al., 2019) and (Lebreton et al., 2018), the wave-driven transport in the various model scenarios is added to the advection by the large-scale currents. While the interactions between Stokes drift and the Eulerian mean flow can affect particle transport (Higgins et al., 2020), it is uncertain how this affects large-scale particle transport.

Bibliography

Arakawa, A. & Lamb, V. R., 1977. Computational design of the basic dynamical processes of the ucla general circulation model, *General circulation models of the atmosphere*, 17(Supplement C), 173–265.

Baatz, R., Hendricks Franssen, H., Euskirchen, E., Sihi, D., Dietze, M., Ciavatta, S., Fennel, K., Beck, H., De Lannoy, G., Pauwels, V., et al., 2021. Reanalysis in earth system science: Toward terrestrial ecosystem reanalysis, *Reviews of Geophysics*, 59(3), e2020RG000715.

Bleck, R., 2002. An oceanic general circulation model framed in hybrid isopycnic-cartesian coordinates, *Ocean modelling*, 4(1), 55–88.

Chi, L., Wolfe, C. L., & Hameed, S., 2018. Intercomparison of the gulf stream in ocean reanalyses: 1993- 2010, *Ocean Modelling*, 125, 1–21.

Clark, L. K., DiBenedetto, M. H., Ouellette, N. T., & Koseff, J. R., 2020. Settling of inertial nonspherical particles in wavy flow, *Physical Review Fluids*, 5(12), 124301.

Cummings, J. A., 2005. Operational multivariate ocean data assimilation, *Quarterly Journal of the Royal Meteorological Society: A journal of the atmospheric sciences, applied meteorology and physical oceanography*, 131(613), 3583–3604.

Cummings, J. A. & Smedstad, O. M., 2013. Variational data assimilation for the global ocean, in *Data Assimilation for Atmospheric, Oceanic and Hydrologic Applications (Vol. II)*, pp. 303–343, Springer.

de Souza, J. M. A. C., Couto, P., Soutelino, R., & Roughan, M., 2021. Evaluation of four global ocean reanalysis products for new zealand waters–a guide for regional ocean modelling, *New Zealand Journal of Marine and Freshwater Research*, 55(1), 132–155.

Delandmeter, P. & Van Sebille, E., 2019. The parcels v2. 0 lagrangian framework: new field interpolation schemes, *Geoscientific Model Development*, 12(8), 3571–3584.

DiBenedetto, M. H., Ouellette, N. T., & Koseff, J. R., 2018. Transport of anisotropic particles under waves, *Journal of Fluid Mechanics*, 837, 320–340.

Enders, K., Lenz, R., Stedmon, C. A., & Nielsen, T. G., 2015. Abundance, size and polymer composition of marine microplastics ≤ 10 μm in the atlantic ocean and their modelled vertical distribution, *Marine pollution bulletin*, 100(1), 70–81.

Escudier, R., Clementi, E., Omar, M., Cipollone, A., Pistoia, J., Aydogdu, A., Drudi, M., Grandi, A., Lyubartsev, V., Lecci, R., CretÃ, S., Masina, S., Coppini, G., & Pinardi, N., 2020. Mediterranean sea physical reanalysis (cmems med-currents, e3r1 system).

Escudier, R., Clementi, E., Nigam, T., Pistoia, J., Grandi, A., & Aydogdu, A., 2021. Quality information document (cmems-med-quid-006-004).

Hersbach, H., Bell, B., Berrisford, P., Hirahara, S., Horányi, A., Muñoz-Sabater, J., Nicolas, J., Peubey, C., Radu, R., Schepers, D., et al., 2020. The era5 global reanalysis, *Quarterly Journal of the Royal Meteorological Society*, 146(730), 1999–2049.

Higgins, C., Vanneste, J., & van den Bremer, T., 2020. Unsteady ekman-stokes dynamics: Implications for surface wave-induced drift of floating marine litter, *Geophysical Research Letters*, 47(18), e2020GL089189.

Korres, G., Ravdas, M., & Zacharioudaki, A., 2019. Mediterranean sea waves hindcast (cmems med-waves).

Kukulka, T., Law, K. L., & Proskurowski, G., 2016. Evidence for the influence of surface heat fluxes on turbulent mixing of microplastic marine debris, *Journal of Physical Oceanography*, 46(3), 809–815.

Lacerda, A. L. d. F., Rodrigues, L. d. S., van Sebille, E., Rodrigues, F. L., Ribeiro, L., Secchi, E. R., Kessler, F., & Proietti, M. C., 2019. Plastics in sea surface waters around the antarctic peninsula, *Scientific reports*, 9(1), 3977.

Lange, M. & van Sebille, E., 2017. Parcels v0. 9: prototyping a lagrangian ocean analysis framework for the petascale age, *Geoscientific Model Development*, 10(11), 4175–4186.

Le Gouvello, D. Z., Hart-Davis, M. G., Backeberg, B. C., & Nel, R., 2020. Effects of swimming behaviour and oceanography on sea turtle hatchling dispersal at the intersection of two ocean current systems, *Ecological Modelling*, 431, 109130.

Lebreton, L., Slat, B., Ferrari, F., Sainte-Rose, B., Aitken, J., Marthouse, R., Hajbane, S., Cunsolo, S., Schwarz, A., Levivier, A., et al., 2018. Evidence that the great pacific garbage patch is rapidly accumulating plastic, *Scientific reports*, 8(1), 1–15.

Lebreton, L.-M., Greer, S., & Borrero, J. C., 2012. Numerical modelling of floating debris in the world's oceans, *Marine pollution bulletin*, 64(3), 653–661.

Liu, Y. & Weisberg, R. H., 2011. Evaluation of trajectory modeling in different dynamic regions using normalized cumulative lagrangian separation, *Journal of Geophysical Research: Oceans*, 116(C9).

Liubartseva, S., Coppini, G., Lecci, R., & Clementi, E., 2018. Tracking plastics in the mediterranean: 2d lagrangian model, *Marine pollution bulletin*, 129(1), 151–162.

Lynch, D. R., Greenberg, D. A., Bilgili, A., McGillicuddy Jr, D. J., Manning, J. P., & Aretxabaleta, A. L., 2014. *Particles in the coastal ocean: Theory and applications*, Cambridge University Press.

Madec, G., Bourdallé-Badie, R., Bouttier, P.-A., Bricaud, C., Bruciaferri, D., Calvert, D., Chanut, J., Clementi, E., Coward, A., Delrosso, D., et al., 2017. Nemo ocean engine.

Napper, I. E. & Thompson, R. C., 2020. Plastic debris in the marine environment: history and future challenges, *Global Challenges*, 4(6), 1900081.

Onink, V., Wichmann, D., Delandmeter, P., & van Sebille, E., 2019. The role of ekman currents, geostrophy, and stokes drift in the accumulation of floating microplastic, *Journal of Geophysical Research: Oceans*, 124(3), 1474–1490.

Phillips, J. S., Gupta, A. S., Senina, I., van Sebille, E., Lange, M., Lehodey, P., Hampton, J., & Nicol, S., 2018. An individual-based model of skipjack tuna (katsuwonus pelamis) movement in the tropical pacific ocean, *Progress in Oceanography*, 164, 63–74.

Rascle, N. & Ardhuin, F., 2013. A global wave parameter database for geophysical applications. part 2: Model validation with improved source term parameterization, *Ocean Modelling*, 70, 174–188.

Reijnders, D., Deleersnijder, E., & van Sebille, E., 2022. Simulating lagrangian subgrid-scale dispersion on neutral surfaces in the ocean, *Journal of Advances in Modeling Earth Systems*, 14(2), e2021MS002850.

Sterl, M. F., Delandmeter, P., & van Sebille, E., 2020. Influence of barotropic tidal currents on transport and accumulation of floating microplastics in the global open ocean, *Journal of Geophysical Research: Oceans*, 125(2), e2019JC015583.

Sutter, J., Fischer, H., & Eisen, O., 2021. Investigating the internal structure of the antarctic ice sheet: the utility of isochrones for spatiotemporal ice-sheet model calibration, *The Cryosphere*, 15(8), 3839–3860.

Tamura, H., Miyazawa, Y., & Oey, L.-Y., 2012. The stokes drift and wave induced-mass flux in the north pacific, *Journal of Geophysical Research: Oceans*, 117(C8).

Tolman, H. L., 1997. *User manual and system documentation of WAVEWATCH-III version 1.15*, US Department of Commerce, National Oceanic and Atmospheric Administration, National Weather Service, National Centers for Environmental Prediction.

Tolman, H. L., 2009. User manual and system documentation of wavewatch iii tm version 3.14, *Technical note, MMAB Contribution*, 276, 220.

Van Sebille, E., Griffies, S. M., Abernathey, R., Adams, T. P., Berloff, P., Biastoch, A., Blanke, B., Chassignet, E. P., Cheng, Y., Cotter, C. J., et al., 2018. Lagrangian ocean analysis: Fundamentals and practices, *Ocean Modelling*, 121, 49–75.

Van Sebille, E., Aliani, S., Law, K. L., Maximenko, N., Alsina, J. M., Bagaev, A., Bergmann, M., Chapron, B., Chubarenko, I., Cózar, A., et al., 2020. The physical oceanography of the transport of floating marine debris, *Environmental Research Letters*, 15(2), 023003.

Zacharioudaki, A., Ravdas, M., Korres, G., & Lyubartsev, V., 2020. Quality information document (cmems-med-quid-006-012).

Chapter 3

Global simulations of marine plastic transport show plastic trapping in coastal zones

Victor Onink, Cleo E. Jongedijk, Matthew J. Hoffman, Erik van Sebille and Charlotte Laufkötter

Published in *Environmental Research Letters*, Volume 16, 064053, 2021.

Abstract

Global coastlines potentially contain significant amounts of plastic debris, with harmful implications for marine and coastal ecosystems, fisheries and tourism. However, the global amount, distribution and origin of plastic debris on beaches and in coastal waters is currently unknown. Here we analyse beaching and resuspension scenarios using a Lagrangian particle transport model. Throughout the first 5 years after entering the ocean, the model indicates that at least 77% of positively buoyant marine plastic debris (PBMPD) released from land-based sources is either beached or floating in coastal waters, assuming no further plastic removal from beaches or the ocean surface. The highest concentrations of beached PBMPD are found in Southeast Asia, caused by high plastic inputs from land and limited offshore transport, although the absolute concentrations are generally overestimates compared to field measurements. The modelled distribution on a global scale is only weakly influenced by local variations in resuspension rates due to coastal geomorphology. Furthermore, there are striking differences regarding the origin of the beached plastic debris. In some Exclusive Economic Zones (EEZ), such as the Indonesian Archipelago, plastic originates almost entirely from within the EEZ while in other EEZs, particularly remote islands, almost all beached plastic debris arrives from remote sources. Our results highlight coastlines and coastal waters as important reservoirs of marine plastic debris and limited transport of PBMPD between the coastal zone and the open ocean.

3.1 Introduction

Marine plastic debris is found in almost all marine habitats, specifically on coastlines worldwide (Browne et al., 2015). Coastal ecosystems can be particularly sensitive to plastic pollution (Li et al., 2020), and plastic debris on beaches can reduce the economic value of a beach by up to 97% (Ballance et al., 2000). Furthermore, while an estimated 1.15-12.7 million tons of plastic enter the ocean per year (Jambeck et al., 2015; Lebreton et al., 2017; Schmidt et al., 2017), the amount of positively buoyant marine plastic debris (PBMPD) found floating at the ocean surface is estimated to be significantly lower (Cózar et al., 2014; Eriksen et al., 2014; van Sebille et al., 2015; Lebreton et al., 2018). Some of the plastic entering the ocean likely immediately sinks, as 34.5% of all plastics produced between 1950-2015 were made of neutrally or negatively buoyant polymers (Geyer et al., 2017; Lebreton et al., 2019), yet a significant amount of PBMPD is still unaccounted for. A large fraction of this missing PBMPD is potentially distributed on coastlines (Hardesty et al., 2017a; Schwarz et al., 2019; Lebreton et al., 2019), with local concentrations varying between 0 - 647 kg km^{-1} (Convey et al., 2002; Debrot et al., 2013). However, given the scarcity of measurements relative to the length of coastlines, limited insight into local temporal and spatial fluctuations in beached PBMPD concentrations and the lack of a standardized sampling methodology, it is currently not possible to estimate the total amount of beached plastic debris from field measurements alone, or to describe the global pattern of beached plastic (Browne et al., 2015).

Using a simple box model, Lebreton et al. (2019) suggest that 66.8% of PBMPD released into the ocean since 1950 is stored on coastlines, however assuming a very high beaching probability and a resuspension probability below the observed range (Hinata et al., 2017). More complex global Lagrangian simulations of PBMPD have either not included beaching at all (Onink et al., 2019; Miladinova et al., 2020) or use simple best guess implementations without considering resuspension (Lebreton et al., 2012; Critchell et al., 2015; Carlson et al., 2017). Most of these studies have focused on plastic debris in the open ocean (van Sebille et al., 2015; Onink et al., 2019), and do not report how global estimates of the amount and distribution of beached plastic vary with different beaching and resuspension parametrizations.

Here we present a series of idealised beaching experiments, using a Lagrangian particle tracking model with beaching and resuspension parameterizations. We estimate upper and lower bounds for the fraction of positively buoyant terrestrial plastic debris in coastal waters, on beaches and in the open ocean within the first years of release into the marine environment. Additionally, we describe the global relative distribution of beached plastic debris, and we analyse the relative amount of plastic with local versus remote origin.

3.2 Methods

3.2.1 Ocean Surface Current Data

For the 2005-2015 global surface currents, we use the HYCOM + NCODA Global 1/12° surface current reanalysis (Bleck, 2002) and the surface Stokes drift estimates from the WaveWatch III hindcast dataset (Tolman, 1997, 2009). The HYCOM + NCODA Global 1/12° reanalysis (Bleck, 2002) has a temporal resolution of 3 hours and a equatorial spatial resolution of 1/12° (≈9.3 km). The HYCOM + NCODA Global 1/12° reanalysis does not incorporate Stokes drift, which has been shown to play an important role in shoreward surface transport (Onink et al., 2019). Therefore, we add surface Stokes drift estimates from the WaveWatch III hindcast dataset (Tolman, 1997, 2009), which has a temporal resolution of 3 hours and a spatial resolution of 1/2°. Comparison of Stokes drift estimates from the WaveWatch III dataset with *in situ* measurements

from drifters have shown high correlations (Tamura et al., 2012; Rascle & Ardhuin, 2013), where root mean square errors have been on orders of centimeters per second (Tamura et al., 2012). Unless otherwise mentioned, simulations discussed in this paper have been done with surface currents obtained by the sum of the HYCOM currents and Stokes drift, as has been done in earlier modeling studies (Fraser et al., 2018; Lebreton et al., 2018; Lacerda et al., 2019). Not including Stokes drift reduces the amount of PBMPD that beaches by 6-7% (Supplementary Figure 3.A.7) and reduces the trapping of PBMPD near the coast (Supplementary Figure 3.A.8). Stokes drift is thus an important component of the ocean circulation to consider in global PBMPD transport and beaching modeling.

PBMPD floating at the surface can be exposed to winds, with the strength of this effect depending on the size of the object that is exposed to winds above the ocean surface (Van Den Bremer & Breivik, 2018). However, for the open ocean, the best model performance for modeling PBMPD is without including a separate windage term (Lebreton et al., 2018). Furthermore, windage and Stokes drift are shown to be similar on a global scale (Onink et al., 2019). Given that we include Stokes drift, we therefore do not consider an additional term for windage.

3.2.2 Lagrangian Transport

We use Parcels (Lange & van Sebille, 2017; Delandmeter & Van Sebille, 2019) to model plastic as virtual particles which are advected using surface ocean flow field data. A change in the position $\vec{x}$ of a particle is calculated according to

$$\vec{x}(t+\Delta t) = \vec{x}(t) + \int_{t}^{t+\Delta t} \vec{v}(\vec{x}(\tau),\tau)d\tau + R\sqrt{\frac{2\,dt\,K_h}{r}} \tag{3.1}$$

where $\vec{v}(\vec{x}(t),t)$ is the surface flow velocity at the particle location $\vec{x}(t)$ at time t, $R \in [-1,1]$ is a random process representing subgrid motion with a mean of zero and variance $r = 1/3$, dt is the integration timestep, and K_h is the horizontal diffusion coefficient. The seed value of the random number generator does not influence the amount of beached plastic (Supplementary Figure 3.A.7). Equation (3.1) is integrated with a 4th order Runge-Kutta scheme with an integration timestep of $dt = 10$ minutes, and particle positions are saved every 24 hours. We take $K_h = 10$ $\mathrm{m^2\ s^{-1}}$ (Lacerda et al., 2019; Liubartseva et al., 2018) to parameterize sub-grid processes.

3.2.3 Plastic emissions into the ocean

We use a terrestrial plastic input estimate based on the low end estimates of Jambeck et al. (2015), where 15% of mismanaged plastic from the population living within 50km of the coast enters the ocean. To obtain high-resolution estimates we multiply the country-specific mismanaged waste estimates with population densities (Center for International Earth Science Information Network–CIESIN–Columbia University, 2016) for 2010. This results in estimates of total mismanaged plastic for all cells on the HYCOM grid. Polypropylene, polyethylene and polystyrene constitute 54% of primary plastic production in 2010 (Geyer et al., 2017), and we assume that this fraction is indicative of how much mismanaged plastic is initially buoyant. We acknowledge that this 54% is a rough estimate, as it assumes that mismanaged plastic inputs have the same composition as global plastic production, whereas it has also been reported that heavier polymers can float with sufficient trapped air bubbles (Ryan, 2015) and light polymers have been found submerged (Brignac et al., 2019). This leads to a total buoyant plastic input of 2.16×10^6 tons in 2010 (71.70% Asia, 4.39% North America, 3.94% South America, 2.16% Europe, 17.36% Africa and 0.45% Oceania). The release of the virtual particles is scaled

according to the estimate of buoyant plastic entering the ocean, where each particle represents up to 5.4 tons of buoyant plastic. To save computational resources we neglect sources smaller than 0.06 tons per year per grid cell, which represent 0.007% of the total input. In each run particles are released every 31 days during the first year of the simulation starting in 2010 (628,236 particles in total) and advected for 5 years (Supplementary Figure 3.A.6). Starting the simulation in 2005 barely affects the amount of beached plastic (Supplementary Figure 3.A.7). We refer to this input scenario as the Jambeck input.

To test the model sensitivity to the plastic input, we calculate one simulation using a low end estimate of plastic waste entering the ocean from rivers (Lebreton et al., 2017). Again assuming 54% of plastic entering the ocean is initially buoyant, we have an input of 6.21×10^5 tons for 2010 (87.04% Asia, 0.78% North America, 4.58% South America, 0.13% Europe, 7.45% Africa, 0.02% Oceania). Due to the smaller total input, no sources were neglected. We refer to this input scenario as the Lebreton input.

Particles are released in the shore-adjacent ocean cell nearest to the total mismanaged plastic cell in question. Since it is unlikely that real plastic always enters the ocean at exactly the same location, at the first timestep particles are distributed randomly throughout the shore-adjacent ocean cell prior to the start of advection by the ocean currents.

3.2.4 Beaching Parametrizations

3.2.4.1 Stochastic Beaching & Resuspension

Many processes are hypothesized to influence the amount of beached plastic on coastlines, such wind direction and speed, coast angle, aspect and morphology, local runoff, the proximity to urban centers and the degree of human usage of the beach (Debrot et al., 1999; Smith, 2012; Thiel et al., 2013; Browne et al., 2015; Pieper et al., 2015; Hardesty et al., 2017b; Ryan et al., 2018; Brignac et al., 2019). Many of these factors have some limited predictive power in statistical models that attempt to explain patterns of beached plastic (Hardesty et al., 2017b; Ryan et al., 2018). However, it is unclear from these studies whether these factors influence beaching, resuspension or both. They can also partially cancel each other out as they might work in opposite directions and in general it is unclear how these factors should be parameterized. We therefore decided to implement the simplest model possible, where we assume that on a global average, the main drivers of plastic beaching are the surface currents and the location of plastic input.

To account for the uncertainty of the ocean current data in land-adjacent ocean cells, we parametrize beaching as a stochastic process in the coastal zone, within which we consider the currents unreliable. For any given timestep, we calculate the beaching probability p_B as:

$$p_b = \begin{cases} \text{if } d \leq D,\ p_B = 1 - \exp(-dt/\lambda_B) \\ \text{if } d > D,\ p_B = 0 \end{cases} \tag{3.2}$$

where d is the distance of particle to the nearest coastal cell, D is a predefined distance to the shore within which beaching can occur, dt is the integration timestep and λ_B is the characteristic timescale of plastic beaching. Beaching is therefore only possible within a beaching zone set by D. To account for the fact that global-scale ocean current datasets are inaccurate in ocean cells adjacent to land (referred to henceforth as coastal cells), we set D such that all coastal cells are fully contained within the beaching zone, resulting in a beaching zone of 10km.

The probability of beaching is set by the beaching timescale λ_B, where λ_B is the number of

days that a particle must spend within the beaching zone such that there is a 63.2% chance that the particle has beached. There is no experimental study to base the value of λ_B on, nor how it might vary for different types of plastic debris, so we selected a range of possibilities to investigate the sensitivity. For the sensitivity analysis we take $\lambda_B \in [1, 2, 5, 10, 26, 35, 100]$ days. Given the mean current speed in the coastal cells in the HYCOM dataset, $\lambda_B = 1$ day is the time a particle would require to travel 10km in a straight line, representing a lower bound for the beaching probability. In the Mediterranean, analysis of GPS trajectories of drifter buoys suggests $\lambda_B = 76$ days (Kaandorp et al., 2020), and an inverse modeling study suggests $\lambda_B = 26$ days for plastic debris (Kaandorp et al., 2020). We consider $\lambda_B = 100$ days to represent scenarios in which particles have very low beaching probabilities. A wooden drifter experiment in the North Sea found 46.88% of drifters beached within 91 days, traveling geodesic distances between 452-559 km (Stanev et al., 2019). Given that the drifters crossed the North Sea in this time and therefore spent time outside of the coastal zone, this suggests that λ_B is less than 100 days. However, we acknowledge that the values for λ_B remain a major source of uncertainty. Furthermore, unless specifically mentioned we parameterize beaching (and also resuspension) rates as global constants.

Particle resuspension is also implemented stochastically, where the resuspension probability p_R of a beached particle is defined as:

$$p_R = 1 - \exp(-dt/\lambda_R) \tag{3.3}$$

where dt is the timestep and λ_R is the characteristic timescale of plastic resuspension. Hinata et al. (2017) has experimentally studied the resuspension timescale of plastic objects with different sizes and found $\lambda_R = 69 - 273$ days. For our sensitivity analysis we take $\lambda_R \in [69, 171, 273]$ days. When a particle beaches, we save its last floating position, and when a particle resuspends it continues its trajectory from this position.

3.2.4.2 Coast-dependent resuspension

There have been a number of studies that have tried to explain the pattern of beached plastic using statistical models that among others factors take geomorphology into account (Hardesty et al., 2017b; Ryan et al., 2018). However, it is unclear whether plastic beaching, resuspension or both are affected by geomorphology, and the influence of geomorphology likely differs for different types of plastic debris (Weideman et al., 2020). We are not aware of any studies investigating how geomorphology affects beaching probabilities. However, the dependence of resuspension probabilities on beach types have been studied with regard to the resuspension of oil (Samaras et al., 2014). Oil resuspension rates for sandy and rocky shores were found to be 24 and 18 hours, respectively, and while these timescales are much shorter than the resuspension timescales for plastic (Hinata et al., 2017), we use the ratio of the timescales of different coast types as a starting point for a sensitivity analysis.

For coastal geomorphology, we use data from Luijendijk et al. (2018) to determine the relative amount of sandy coastline s of each model cell of the HYCOM grid, where $s = 0$ indicates a completely not-sandy coastline while $s = 1$ indicates a completely sandy coastline (Supplementary Figure 3.A.5). Note that "not sandy" covers multiple shore geomorphologies, such as rocky shores, cliffs and shorelines covered by vegetation such as mangrove forests. The resuspension timescale is determined by:

$$\lambda_R = \begin{cases} \text{3:4 Dependence} \ \rightarrow \lambda_R = 69 \times (0.75 + 0.25 \times s) \\ \text{1:4 Dependence} \rightarrow \lambda_R = 69 \times (0.25 + 0.75 \times s) \end{cases} \tag{3.4}$$

where with 3:4 Dependence we use the resuspension timescale coastline dependence for oil (Samaras et al., 2014), whereas with 1:4 Dependence there a stronger dependence on the coastline type to check the sensitivity. In both cases we use $\lambda_{RT,s=1} = 69$ days.

There is currently little knowledge about how resuspension timescales vary with the coastline type and the classification of coastlines as sandy and not-sandy is overly simplistic, as coastlines such as rocky beaches, cliffs and mangroves are now considered equivalent. However, to our knowledge there have not been any studies that consider how plastic resuspension might depend on coastal geomorphology, and therefore we consider these runs as a first exploration of the potential role of coastal geomorphology on the global beached plastic budget and distribution.

3.2.5 Model concentration units

Model concentrations are computed by binning beached particle masses onto the same grid as the HYCOM reanalysis data, and then dividing the total beached mass in each cell by the length of model coastline (sum of cell edges shared with land cells) for that cell. This is because the beached plastic is not distributed homogeneously over the entire cell, but is instead concentrated on the shoreline interface between land and water, such as beaches. Since there is no global dataset of beach area, concentrations are instead reported as the amount of plastic per length of model coastline (kg km^{-1}), which is commonly used for reporting field measurements (see Table 3.1). However, due to the coarse resolution of the HYCOM grid, the length of the model coastline is an approximation of the true coastline length for a given cell.

3.3 Results

3.3.1 Global beached plastic budget

A systematic test of the effect of different beaching and resuspension probabilities on the global plastic budget is shown in Figure 3.1. In all scenarios, the model reaches an equilibrium between the beaching and resuspension fluxes after the initial release within less than two years. At the end of our five years of simulations, between 31-95% of PBMPD is beached depending on parameter values. High beaching probabilities combined with small resuspension probabilities lead to a large amount of plastic stored on beaches and vice versa. With the Jambeck input, and assuming 54% of the input is buoyant, this corresponds to $0.72 - 2.06 \times 10^6$ tons of beached PBMPD originating from plastic debris released in 2010 alone.

Rather than being a function of the absolute values of λ_B and λ_R, our model shows that the average beached fraction is dependent on the ratio λ_B/λ_R (Figure 3.2a). At very low ratios, i.e. high beaching but low resuspension probabilities, up to 99% of PBMPD is beached in the 5th year of the simulations. As the ratio increases, the beached fraction decreases to 31%. However, at least 77% of the PBMPD remains within 10 km of the model coastline in all scenarios(Figure 3.2a) and only a small fraction escapes to the open ocean. Multiple studies report decreasing concentrations of floating PBMPD with increasing distance from shore, which is commonly attributed to PBMPD being removed from the ocean surface over time (Ryan, 2013, 2015; Pedrotti et al., 2016; Ruiz-Orejón et al., 2018). However, such trends could also be partially due to PBMPD remaining trapped nearshore by the surface ocean currents.

While PBMPD can leave and return to the coastal zone, a large portion of PBMPD never travels far from the coastline (Figure 3.2b). Over 25% of PBMPD mass never travels beyond 50 km from the nearest coastline even with the lowest beaching probability (Supplementary Table

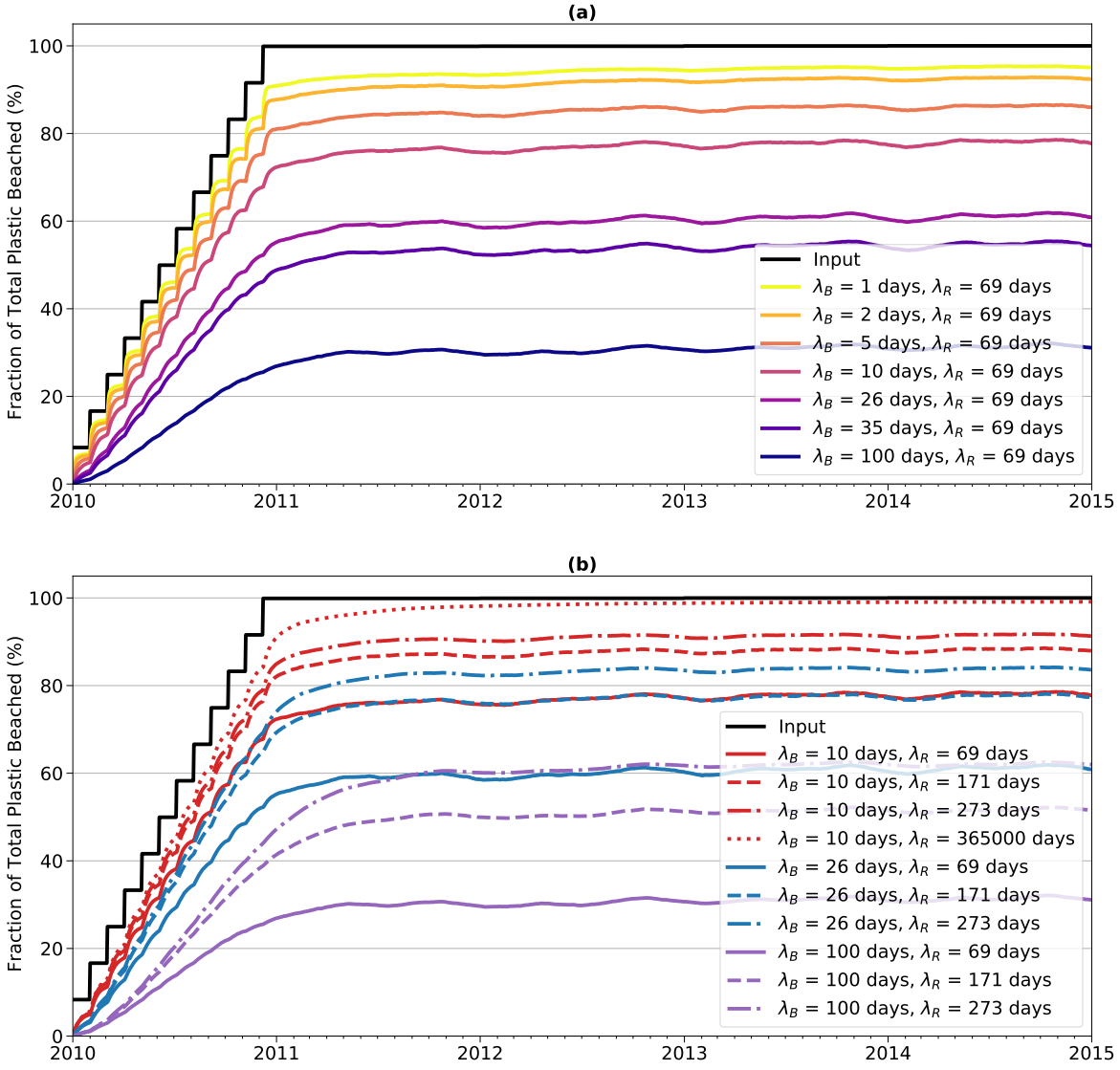

Figure 3.1: The global percentage of beached PBMPD, using the Jambeck input. (a) The beached fractions as a function of the beaching timescale λ_B in days. (b) The beached fractions as a function of the resuspension timescale λ_R in days.

3.A.2). The likelihood for plastic to leave the coastal zone is not uniform worldwide, as PBMPD that enters the ocean from island sources or from sources close to energetic boundary currents is more likely to travel further from shore (Figure 3.2c). However, there are long stretches of coastline where most plastic remains near shore, as the median of the maximum distances from shore reached by particles released from those coastlines is less than 20km offshore.

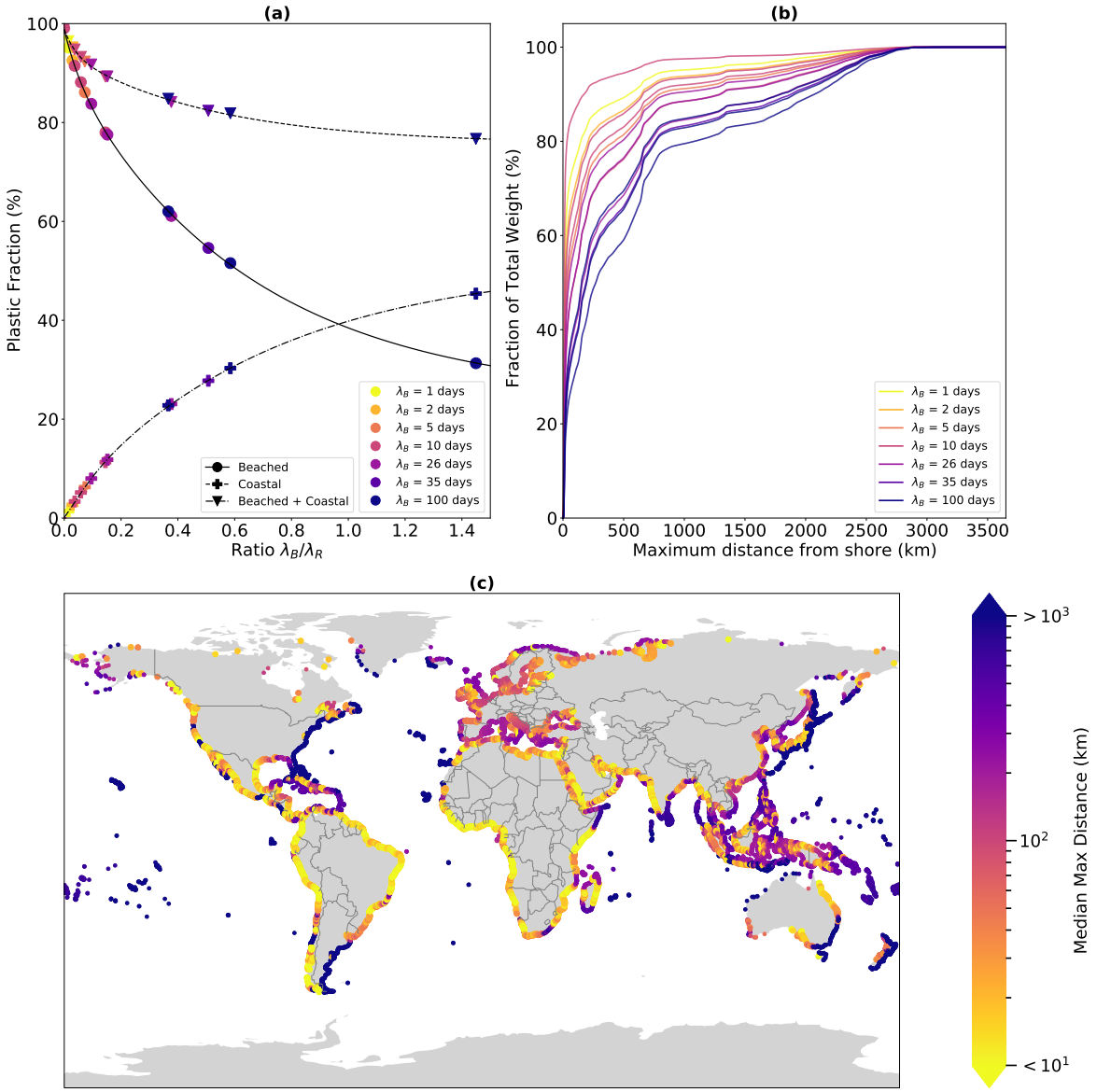

Figure 3.2: (a) The global PBMPD budget of beached, coastal and coastal + beached PBMPD as a percentage of the total of amount of PBMPD that enters the ocean. The fractions are averages over the fifth year of the simulation. Coastal PBMPD is defined as non-beached PBMPD floating within 10km from shore. The lines indicate fits ($a \times \exp(x * k1) + b \times \exp(x * k2) + c$) for the beached, coastal and coastal + beached fractions. (b) The cumulative fraction of PBMPD as a function of the maximum distance from land that particles reach during their entire trajectory. (c) The median maximum distance from shore reached by particles over the course of their entire trajectories, with each point indicating an input location. The median is calculated over all simulations shown in 2a.

3.3.2 Global beached plastic distribution

Across all simulations, the highest beached PBMPD concentrations are found near regions with the largest PBMPD sources. These include areas such as Southeast Asia and the Mediterranean

Sea (Figure 3.3a), and have concentrations up to 10^6 kg km^{-1}. The lowest concentrations are in areas with low population densities, such as polar regions, the Chilean coastline and parts of the Australian coast. No PBMPD reaches the Antarctic mainland in any of our simulations. This is largely in line with measurements of plastic in Antarctica, which have been very low both on beaches (Convey et al., 2002) and afloat (Suaria et al., 2020). The lack of PBMPD in Antarctica is due to a lack of terrestrial input sources and the Antarctic Circumpolar Current blocking transport of PBMPD to Antarctic coastlines.

The global pattern of beached plastic is fairly robust towards the choice of beaching and resuspension probabilities (Supplementary Figure 3.A.9) but strongly depends on the plastic input distribution. With the Lebreton input, the relative global fraction of PBMPD that is beached over the last year of simulation is 3% higher in comparison to using the Jambeck input (Supplementary Figure 3.A.7). However, absolute beached PBMPD concentrations are significantly lower, and a larger fraction of beached PBMPD is concentrated in Southeast Asia (Figure 3.3b), reflecting higher inputs in this region. Therefore, detailed knowledge of the distribution and size of marine plastic debris sources are essential for understanding the global distribution of beached PBMPD.

While the overall distribution of beached plastic is largely shaped by the plastic input scenario, the ocean currents can play an important local role for beached PBMPD concentrations. For example, while higher beaching probabilities lead to higher global beached fractions, certain coastlines exhibit lower beached concentrations, such as Kenya, the Indian west coast and Libya (Supplementary Figure 3.A.9). More beached PBMPD globally results in less PBMPD afloat, and therefore reduced transport of PBMPD by the ocean currents to these areas.

3.3.3 Local versus remote origin of beached plastic debris

On a global average, 48.5% of beached PBMPD within all Exclusive Economic Zones (EEZ) (Institute, 2019) is local, in that it originates from a source within the EEZ. However, the local fraction of beached PBMPD is highly variable (Figure 3.4). Generally, the local fraction for island EEZs is relatively low, matching recent reports for individual islands in various oceans (Lavers & Bond, 2017; Brignac et al., 2019; Pieper et al., 2019; Ryan et al., 2019). This is likely since their location in the open ocean exposes them to floating PBMPD originating from a wide range of EEZ's, while at the same time, PBMPD originating from an island EEZ itself is less likely to beach locally than on a mainland shore due to the comparatively small coastline of islands on which beaching can occur. In the field the fraction from local sources is further reduced due to the contribution of maritime sources (Lavers & Bond, 2017; Ryan et al., 2019; Brignac et al., 2019), which are not included in this model.

Higher local fractions of beached PBMPD are due to a combination of factors. Large local inputs generally lead to a higher local fractions, as a large fraction of PBMPD beaches close to its initial input. Examples of such EEZ's include China, Indonesia and Brazil. In addition, the ocean currents can play a critical role (see also Figure 3.2c). Eastern Africa has relatively low local beached fractions, partly due to receiving high amounts of PBMPD from Indonesia transported by the Indian Ocean South Equatorial Current (matching observations by Ryan (2020)). Meanwhile, coastlines such as the Russian Arctic and Chilean mainland have high local fractions despite low local inputs, since the prevailing local currents do not carry much PBMPD from other regions.

However, our local beached fraction estimates are only based on PBMPD that enters the ocean

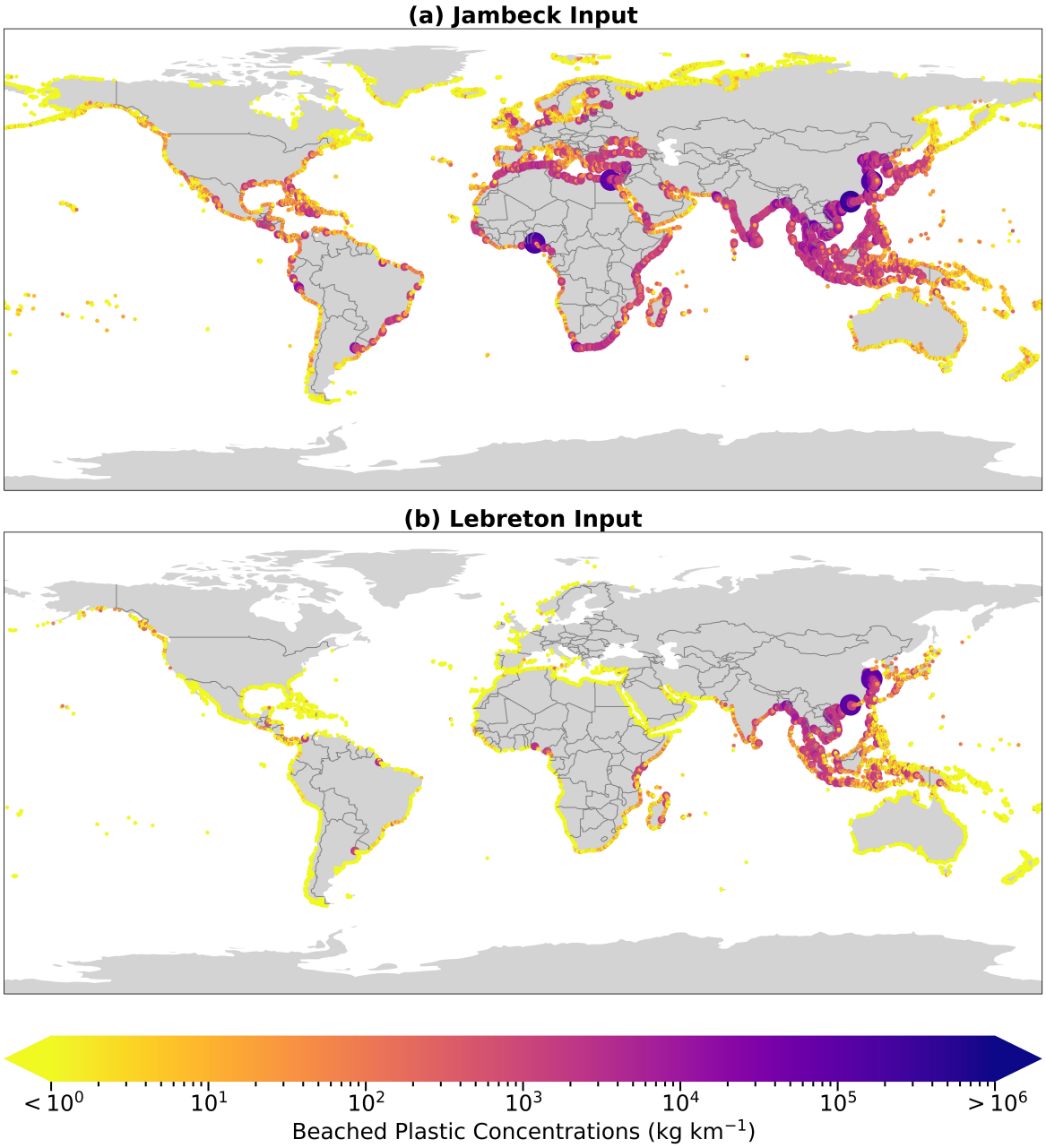

Figure 3.3: Average beached PBMPD concentrations over the final year of the simulation. (a) The beached PBMPD concentrations with the Jambeck input. (b) The beached PBMPD concentrations with the Lebreton input. Both simulations use $\lambda_B = 10$ days and $\lambda_R = 69$ days.

and subsequently beaches. Coastlines can also contain debris that is littered onto the coastline directly and never enters the ocean, and plastic debris that originates from maritime sources. Furthermore, ocean surface plastic removal processes such as sinking can further reduce the non-local fraction, but it is uncertain how large an effect this would have. As such, our estimates are only approximations of the actual local fraction of beached PBMPD.

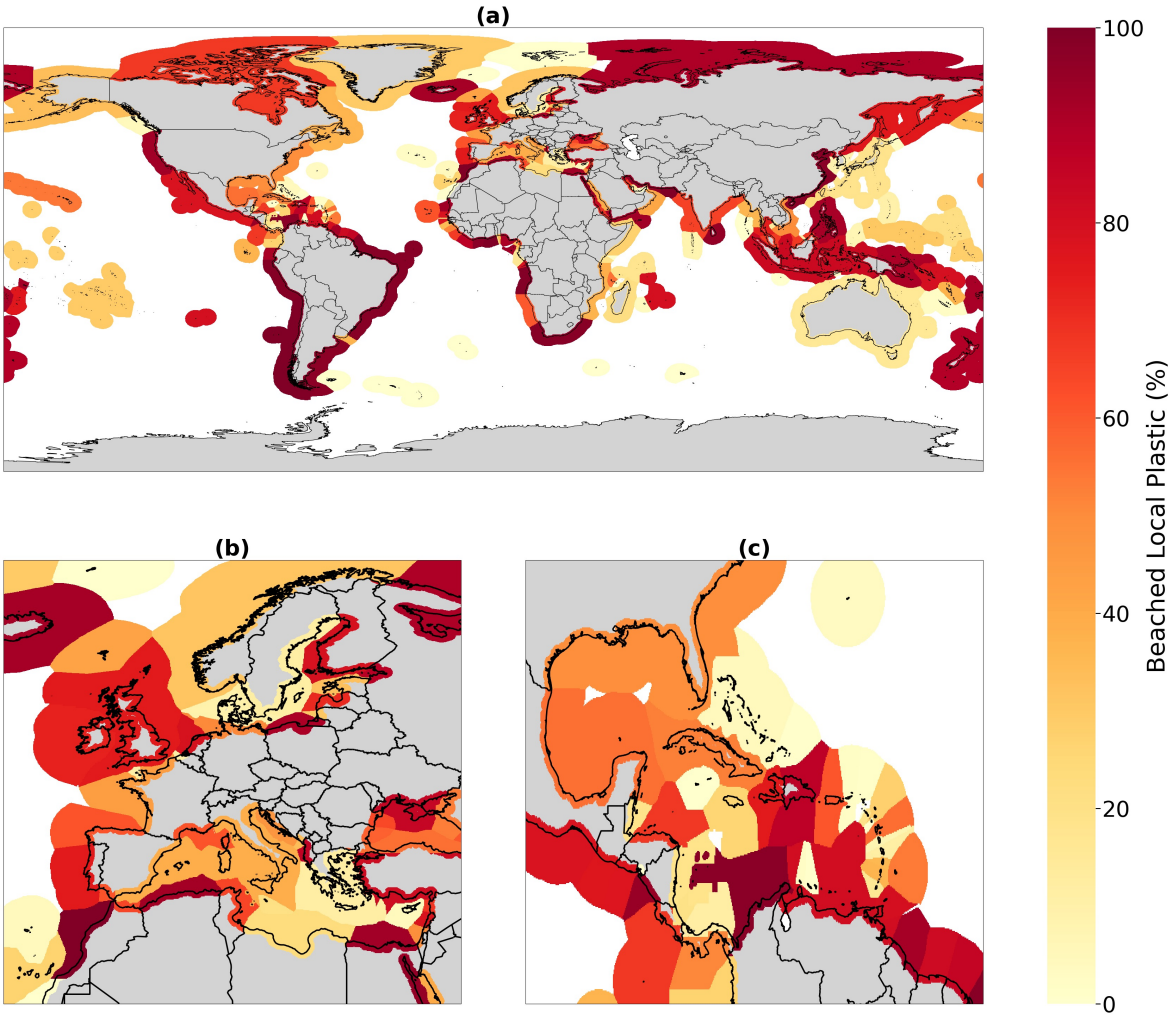

Figure 3.4: The percentage of beached PBMPD that originates from within the EEZ for each EEZ. (a) Global (b) Europe (c) Central America & the Caribbean. The shown values are averages over all stochastic simulations, and over all beached plastic over the course of each simulation. Data for EEZs are not shown if beaching didn't occur in this EEZ in each considered stochastic simulation. Some EEZs are split where one EEZ consisted of multiple distinct regions (e.g. the United States EEZ has been split into the US East coast, West coast, Alaska and Hawaii).

3.4 Discussion

A systematic evaluation of our model based on a large number of field observations is currently impossible due to the lack of a standardized measurement methodology of beached plasti (Browne et al., 2015), which prevents comparisons of plastic debris concentrations reported by different studies. Beached plastic concentrations are reported either as counts or masses, per unit area or unit length of coastline, and considering different debris sizes. Furthermore, our parameterizations do not account for beach cleanups, which are known to occur at many study sites (Table 3.1). Additionally our simulations represent idealized scenarios: there is only

Table 3.1: A comparison of measurements of plastic debris with model simulations. The average, minimum and maximum model outputs are calculated over all stochastic simulations with the Jambeck input. Studies that don't report the occurrence of beach cleanups are indicated by a hyphen. [a]concentrations as reported in Monteiro et al. (2018), [b]total of marine debris, not solely plastic.

Study	**Location**	**Concentration (items km^{-1})**	**Cleanup**	**Model mean [min max] (kg km^{-1})**
Barnes & Milner (2005)[a,b]	Iceland	40	-	3.28 [0.72 8.98]
	Faeroe Islands	210	-	6.41 [0.04 30.58]
	La Gomera, Canary Islands	1910	-	69.58 [0.55 178.99]
	Ascension	3400	-	0.45 [0.00 6.14]
	Falkland Islands	430	-	2.49 [0.68 7.68]
	Dominica	1500	-	124.54 [0.00 918.14]
Pieper et al. (2015)[a]	Faial, Azores	4610	Regular during summer, none during the study period	93.59 [0.00 285.74]
Ryan (1987)[a]	Tristan da Cunha	240	-	16.31 [0.00 100.53]
	Gough Island	100	-	9.12 [0.00 96.57]
Otley & Ingham (2003)[a]	Falkland Islands	370	-	2.49 [0.68 7.68]
Convey et al. (2002)	Candlemas Island	31	None	0.00 [0.00 0.00]
	Saunders Island	50	None	0.00 [0.00 0.00]
	Adelaide Island	0	None	0.00 [0.00 0.00]
Ribic et al. (2010)[b]	Northeast US Atlantic Coast	102	-	12.46 [1.96 43.55]
	Middle US Atlantic Coast	429	-	106.09 [5.86 397.56]
	Southeast US Atlantic Coast	83	-	220.50 [64.85 683.85]
Ribic et al. (2012)[b]	Northern US Pacific Coast	56	Not regularly	56.65 [35.00 116.03]
	Southern California Bight	139	Not regularly	160.80 [43.92 623.58]
	Hawaii	134	Not regularly	33.24 [4.90 120.65]
Study	**Location**	**Concentration (kg km^{-1})**	**Cleanup**	**Model mean [min max] (kg km^{-1})**
Corbin & Singh (1993)	Dominica	8	-	124.54 [0.00 918.14]
	St. Lucia	3	-	110.18 [0.00 550.12]
Debrot et al. (2013)	Bonaire	647	-	53.26 [0.00 285.57]
Debrot et al. (1999)	CuraÃ§ao	506	Occasionally	43.12 [0.00 362.68]
Claereboudt (2004)	Northern Oman	15	Occur, but frequency not specified	86.43 [10.08 449.02]
Ali & Shams (2015)	Clifton Beach, Karachi, Pakistan	11	Periodically, but frequency not specified	4718.88 [167.62 55688.46]
Hong et al. (2014)	South Korea	262	Not regularly	970.65 [263.95 1611.52]
Pervez et al. (2020a)	Shilaoren Beach, Qingdao, China	5	Daily	2721.28 [327.44 13124.59]
Pervez et al. (2020b)	No. 1 Bathing Beach, Qingdao, China	73	Daily	2721.28 [327.44 13124.59]
Madzena & Lasiak (1997)	Transkei Coast, South Africa	47	Not regularly	1383.42 [111.45 5084.47]
Study	**Location**	**Total Plastic (metric tons)**	**Cleanup**	**Model mean [min max] (metric tons)**
Lavers & Bond (2017)	Henderson Island	17.6	Never	0.08 [0.00 0.49]

one year of input; we don't consider loss processes such as sinking, ingestion, or burial in sediment (Van Sebille et al., 2020); maritime sources of PBMPD and beach littering are not considered.

Nevertheless, we compare the modeled relative distribution of beached plastic with studies that measured beached plastic concentrations with a standardized method over multiple study sites. The modeled beached PBMPD distribution for South Africa closely resembles the distribution from field measurements (Ryan et al., 2018), likewise our model captures the very low concentrations found on the Australian Northwestern coast (Hardesty et al., 2017b). However, the model appears to over-predict the amount of beached plastic on the Northeastern Australian coastline, potentially due an overestimated input of plastic from Polynesian islands. In the United States, the concentration ratio between the Northern Pacific coast and the Southern California Bight is approximately equal to the ratio reported in Ribic et al. (2012), but the relative amount of beached plastic in Hawaii is underestimated (Table 3.1). PBMPD from maritime sources is often an important contributor of beached plastic on remote shores and islands (Browne et al., 2015; Lavers & Bond, 2017), and the lack of maritime sources in the input scenarios might partially account for this discrepancy. The overall relative similarity of the measured and modeled distribution is encouraging and indicates that we may have captured the dominant drivers of beaching on a continental scale. However, these studies only allow comparisons of the relative patterns, as the model units (kg km^{-1}) do not match the field measurement concentrations. Compared to studies that do report concentrations in terms of mass, the model generally overestimates field concentrations by a factor of 5 - 560 (Table 3.1). This either indicates that substantial losses of beached and floating plastic occur on short timescales that our model does not account for (such as burial within sediments (Lavers & Bond, 2017; Martin et al., 2020), sinking (Ryan, 2015; Choy et al., 2019; Egger et al., 2020) and beach cleanups (Uneputty et al., 1998; Willis et al., 2018)), and/or that the input estimates are too high. The sites where beached concentrations are underestimated (both in absolute and relative terms) are all islands, which could be due to neglecting maritime sources in the model.

Our results depend strongly on the representation of the ocean currents, the accuracy of the plastic input estimate, the beaching/resuspension parameterizations and the relative importance of processes that are not included. HYCOM has been shown to represent circulation patterns well in various parts of the world (Metzger et al., 2010; Savage et al., 2015; Wang et al., 2019). However, HYCOM does not account for Stokes drift, which plays an important role in shoreward surface transport (Onink et al., 2019). In line with earlier modeling studies (Fraser et al., 2018; Lebreton et al., 2018; Lacerda et al., 2019), we take the sum of the HYCOM currents and Stokes drift from the WaveWatch III reanalysis (Tolman, 1997, 2009), and we consider this the best available representation of global scale circulation. Nevertheless, we acknowledge that trajectory modeling is more accurate in the open ocean than on the coastal shelf, where we also miss the effects of tidal currents (Liu & Weisberg, 2011; Liu et al., 2014; Sterl et al., 2020).

With an estimated global beached fraction of 31-95%, we show that the beached amount of plastic is a lot less constrained than suggested in Lebreton et al. (2019), whose simple 6-box model predicted that 69% of plastic that has entered the ocean since 1950 is found beached. In this box model, the authors assumed a 97% annual beaching rate of coastal PBMPD (equivalent to $\lambda_B = 104$ days), which is at the upper end of our tested range of plausible λ_B values ($1 - 100$ days), and they tuned their resuspension rate to match the global amount of floating PBMPD, resulting in a 1% annual resuspension rate of beached plastic (equivalent to $\lambda_R = 36,317$ days) that is much slower than what is indicated by field experiments (69-273 days, Hinata et al. (2017)). In addition, the box model of Lebreton et al. (2019) assumes uniform offshore transport, while we show that transport varies strongly in different regions (Figure 3.2c).

We mostly use the Jambeck input scenario for our model Jambeck et al. (2015). There have been a number of estimates for plastic inputs into the ocean (Jambeck et al., 2015; Lebreton et al., 2017; Schmidt et al., 2017; Lebreton & Andrady, 2019), but it is unclear which are most accurate. Furthermore, all alternative estimates also neglect contributions from maritime sources and primary microplastics. There are indications that the amount of plastic entering the ocean is lower than estimated in the Jambeck input (Tramoy et al., 2019; Van Emmerik et al., 2019) and given how strongly the modeled global distribution of PBMPD is influenced by the input scenario, it is crucial to get better estimates of plastic debris input sources, both terrestrial and maritime.

The model assumes that there are no PBMPD loss processes, or at least that they don't play a significant role during the first 5 years. For example, we assume PBMPD remains at the ocean surface, but processes such as biofouling can cause the density of PBMPD to increase until it starts to sink (Fazey & Ryan, 2016). PBMPD can also be removed through ingestion by wildlife (Van Franeker & Law, 2015). Experiments with tethered PBMPD biofouling show sinking of cm-sized plastic sheets after 17-66 days underneath a floating dock (Fazey & Ryan, 2016), but it is unclear how this translates to sinking rates for free floating PBMPD for different sizes, shape and regions. PBMPD has been found at the surface up to 50 years after its estimated production date (Lebreton et al., 2018), and while this PBMPD might not have floated at the ocean surface over this entire time period, it does suggest biofouling requires more than 66 days to sink PBMPD in the open ocean. Given these uncertainties, sinking was not included as PBMPD removal process in this study. Plastic ingestion has been found to occur with a wide range of species (Derraik, 2002), but it is unclear how much total plastic has been ingested and at what rate this occurs. We also assume beached PBMPD remains available for resuspension indefinitely, but PBMPD can be transported towards the backshore (Pham et al., 2020) or be buried (Browne et al., 2015). As a consequence, the beached PBMPD budgets are upper estimates given that PBMPD is unable to exit the cycle of beaching and resuspension in our model.

Finally, we assume globally uniform beaching and resuspension probabilities. Exploratory tests with shore type dependent resuspension affects the global budget and distribution of beached plastic only minimally (Supplementary Figures 3.A.10 and 3.A.11), even when applying substantial differences in resuspension probability. These results indicate that on a global scale, local variations in resuspension probability driven by factors such as wind direction or coastal geomorphology play only a minor role. Nevertheless, more research is needed to understand how both beaching and resuspension are influenced by geomorphology and climatological factors, particularly on local to regional scales.

3.5 Conclusion

Our results indicate that part of the discrepancy between current plastic input estimates and estimates of floating plastic debris in the open ocean is due to high amounts of beached and coastal PBMPD. We have also identified coastlines where PBMPD is much more likely to reach the open ocean, such as the Eastern United States, Eastern Japan and Indonesia. Here, cleanups would be particularly effective in intercepting PBMPD before it escapes to the open ocean. However, more work needs to be done investigating the behavior of PBMPD in coastal waters, specifically the role of wind, waves, tides, and coastal morphology in PBMPD transport, beaching and resuspension. This would be strongly aided by standardized beached PBMPD field measurements, allowing comparisons of PBMPD concentrations at different measurement sites. Furthermore, future studies ought to consider the influence of maritime sources on beached PBMPD, as this study only considers terrestrial inputs.

Acknowledgements

Calculations were performed on UBELIX (http://www.id.unibe.ch/hpc), the HPC cluster at the University of Bern. VO and CL acknowledge support from the Swiss National Science Foundation (project PZ00P2_174124 Global interactions between microplastics and marine ecosystems). EvS was supported by the European Research Council (ERC) under the European Unions Horizon 2020 research and innovation programme (grant agreement No 715386). CEJ is supported by a Skempton Scholarship.

Author Information

Development of the beaching and resuspension parametrizations was done by VO, CEJ, and CL, with input from MJH. The manuscript was written by VO and CL, with extensive input from CEJ, MJH and EvS. Everyone contributed to the study design and discussion of the analysis, with VO carrying out the analysis.

Competing Interests

The authors declare no competing interests.

Code Availability

The code for the Lagrangian simulations is available at:
https://github.com/VictorOnink/Modeling-Global-Plastic-Beaching.

3.A Supplementary material

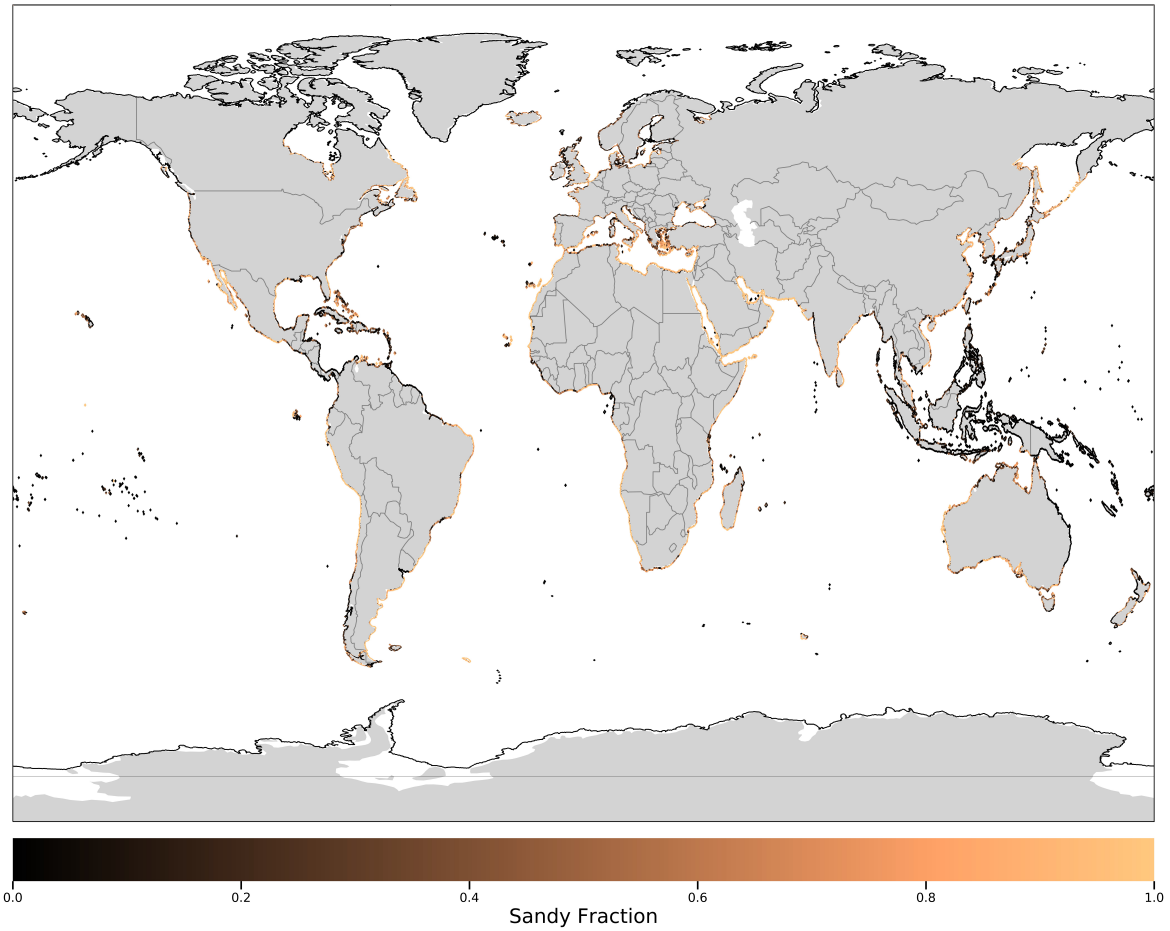

Figure 3.A.5: The sandy fraction of coastlines used for the coast dependent resuspension. The data is adapted from Luijendijk et al. (2018).

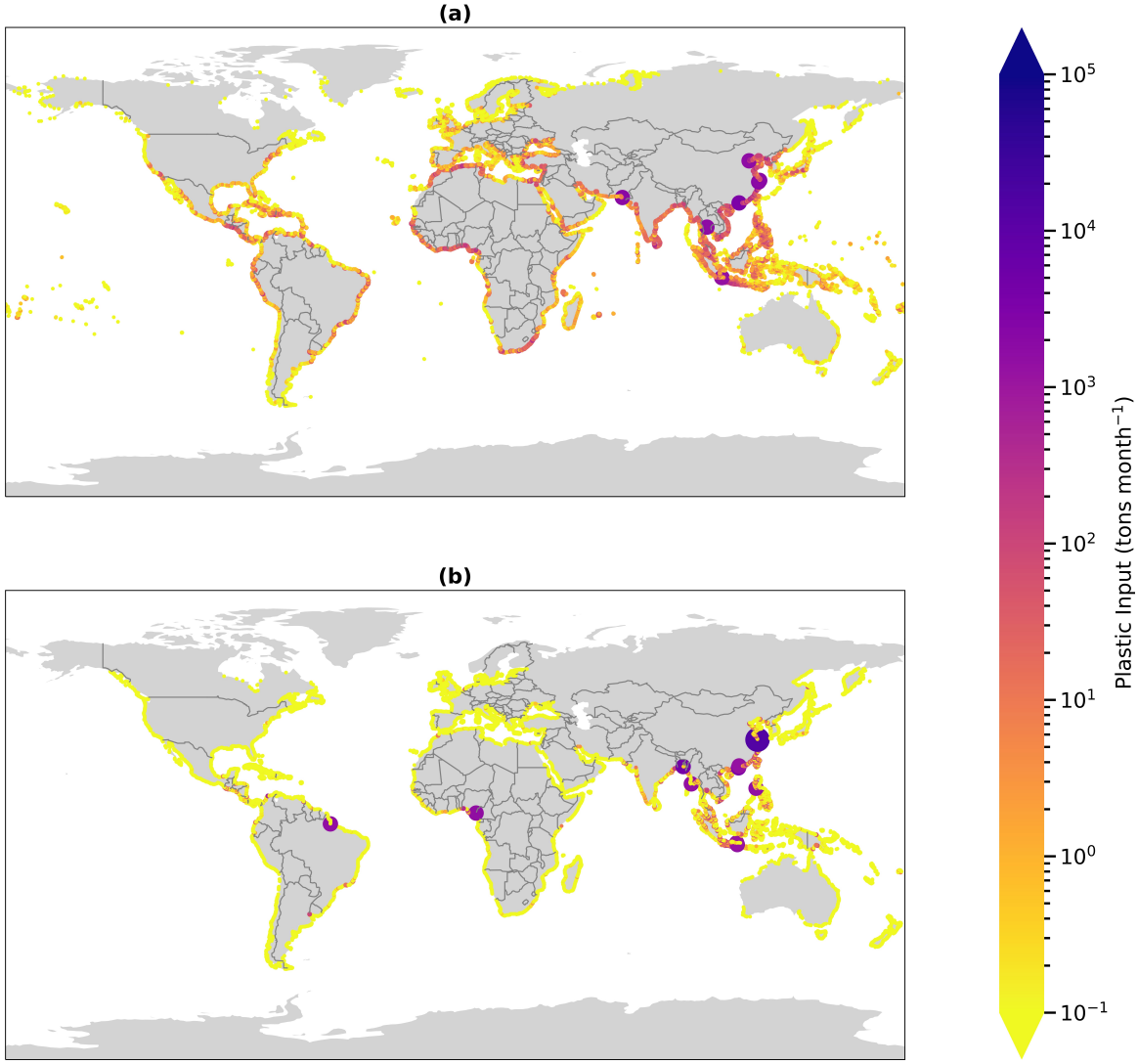

Figure 3.A.6: The monthly PBMPD inputs in the first year of the simulations. (a) Jambeck input. (b) Lebreton input.

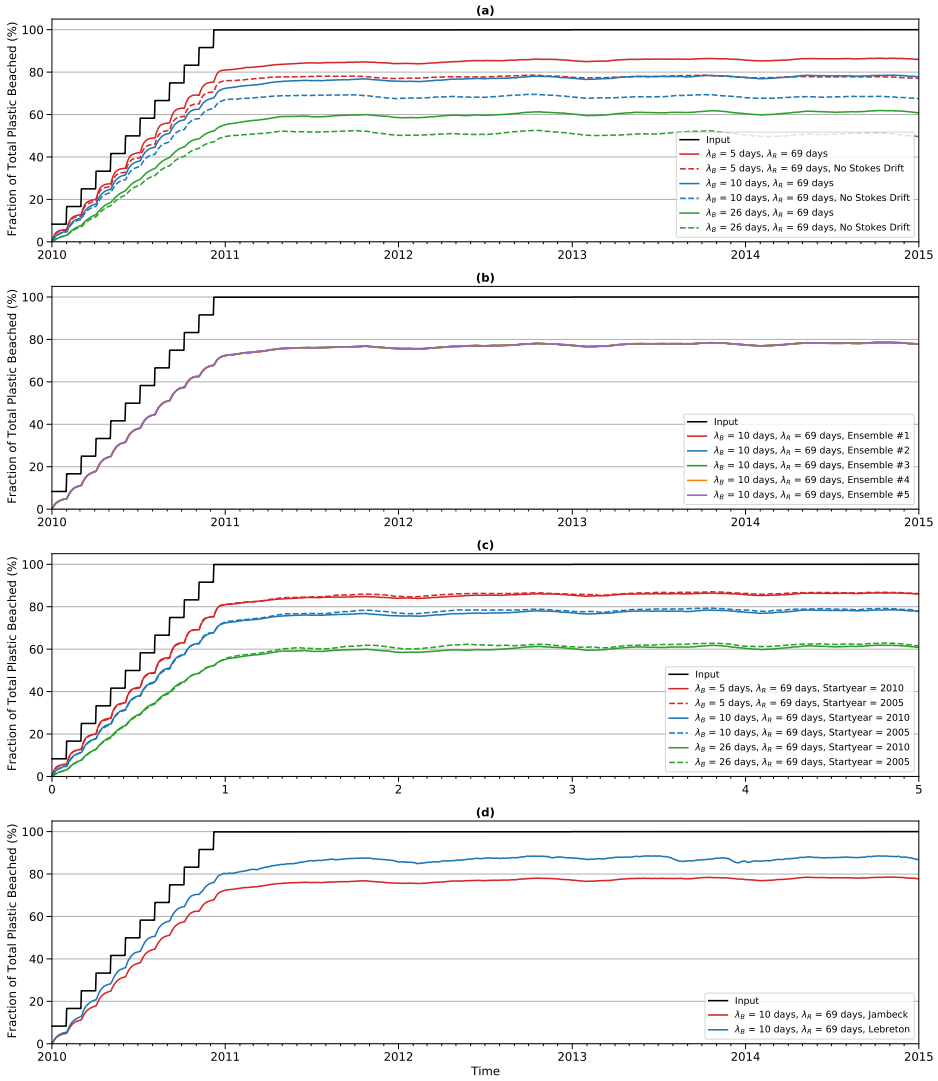

Figure 3.A.7: Sensitivity tests of how the global beached PBMPD fractions vary under various model parameters. (a) The inclusion of Stokes drift. (b) Different seedings of the random number generator. (c) Using the same input, but running the simulation for 2005-2010 and 2010-2015. (d) Using the Jambeck and Lebreton input scenarios. The solid black line indicates the total amount of plastic in the simulation. All simulations except those shown in (c) start in 2010 and all simulations except those shown in (a) include Stokes drift. All simulations use the Jambeck input except where specified otherwise.

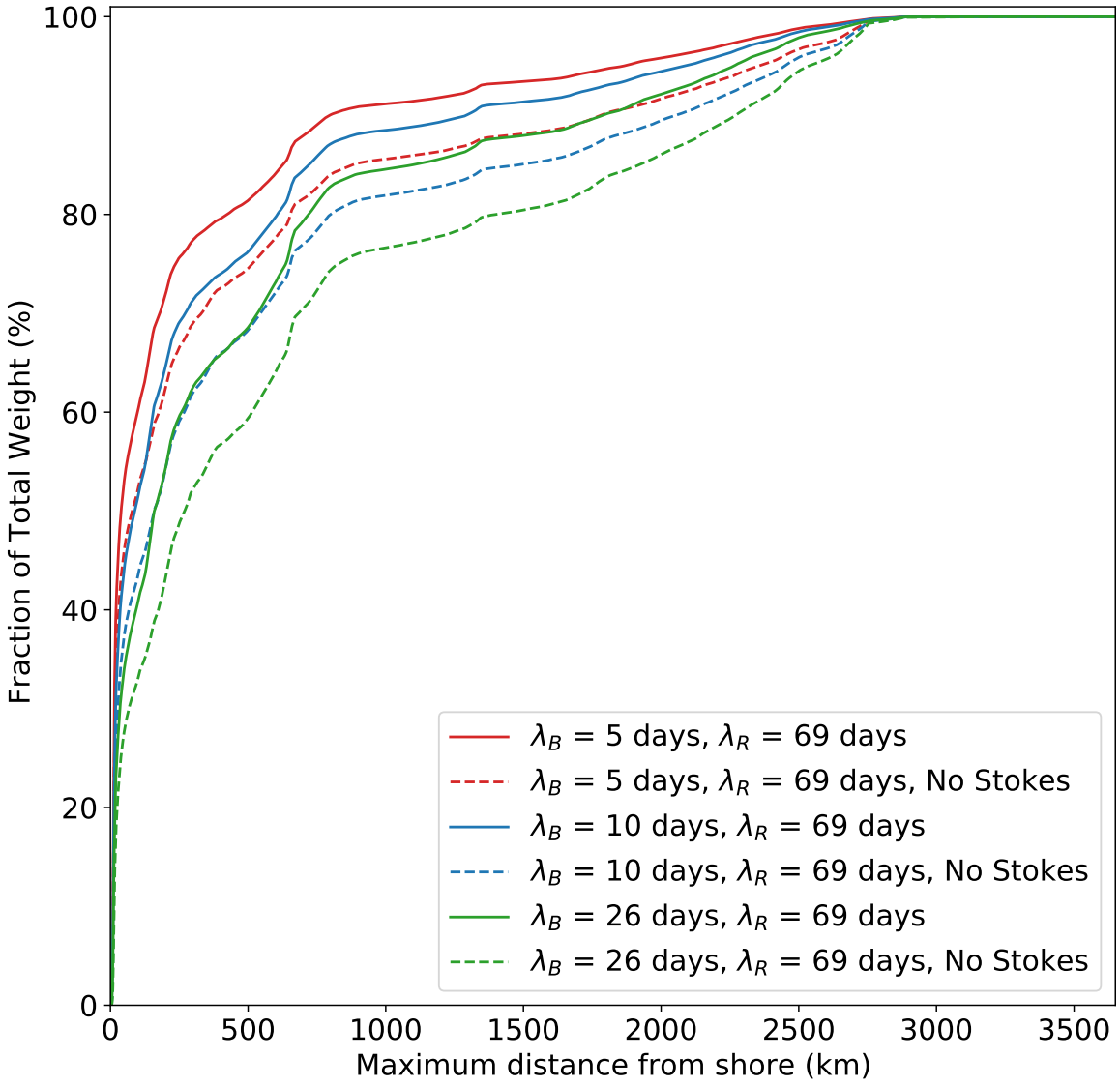

Figure 3.A.8: The cumulative fraction of PBMPD as a function of the maximum distance that a particle is removed from the nearest land cell over the course of its entire trajectory. All simulations start in 2010 using the Jambeck input, where the solid lines indicate simulations that included Stokes drift while the dashed lines exclude Stokes drift.

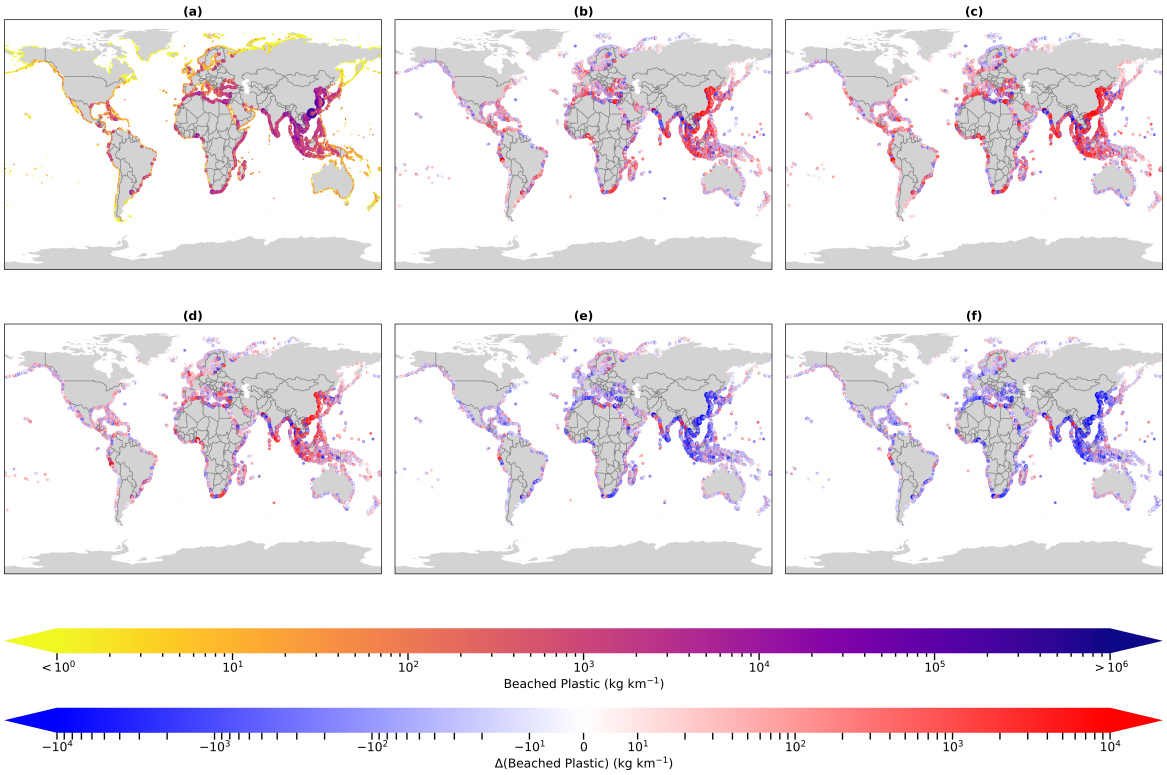

Figure 3.A.9: Differences in average beached PBMPD concentrations over the final year of the simulation with varying beaching and resuspension timescales. (a) $\lambda_B = 10$ days, $\lambda_R = 69$ days. (b) difference relative to (a) for $\lambda_B = 10$ days, $\lambda_R = 171$ days. (c) difference relative to (a) for $\lambda_B = 10$ days, $\lambda_R = 273$ days. (d) difference relative to (a) for $\lambda_B = 5$ days, $\lambda_R = 69$ days. (e) difference relative to (a) for $\lambda_B = 26$ days, $\lambda_R = 69$ days. (f) difference relative to (a) for $\lambda_B = 35$ days, $\lambda_R = 69$ days.

Table 3.A.2: The cumulative fractions of the maximum distance from land that PBMPD mass reaches over each particle trajectory for all stochastic model runs starting in 2010 with the Jambeck input and including Stokes drift. The columns 50% and 70% show the maximum distances from nearest land for each model past which 50% and 70% of the total PBMPD mass were never further from land. The columns <50 km and <150 km indicate the fraction of total PBMPD mass that remain these distances from the nearest land throughout the entire simulation.

Model	**50% (km)**	**70% (km)**	**<50 km (%)**	**<150 km (%)**
$\lambda_B = 1$, $\lambda_R = 69$	15	47	70.55	80.31
$\lambda_B = 2$, $\lambda_R = 69$	19	97	64.23	75.85
$\lambda_B = 5$, $\lambda_R = 69$	39	180	53.05	67.32
$\lambda_B = 10$, $\lambda_R = 69$	89	273	44.16	59.16
$\lambda_B = 10$, $\lambda_R = 171$	32	152	56.04	69.85
$\lambda_B = 10$, $\lambda_R = 273$	22	117	61.78	74.33
$\lambda_B = 10$, $\lambda_R = 365000$	11	18	83.07	89.23
$\lambda_B = 26$, $\lambda_R = 69$	160	535	34.03	48.26
$\lambda_B = 26$, $\lambda_R = 171$	88	269	44.14	59.36
$\lambda_B = 26$, $\lambda_R = 273$	48	199	50.50	65.21
$\lambda_B = 35$, $\lambda_R = 69$	190	579	31.50	45.11
$\lambda_B = 100$, $\lambda_R = 69$	273	657	25.33	37.12
$\lambda_B = 100$, $\lambda_R = 171$	153	512	30.68	44.52
$\lambda_B = 100$, $\lambda_R = 273$	195	587	34.85	49.42

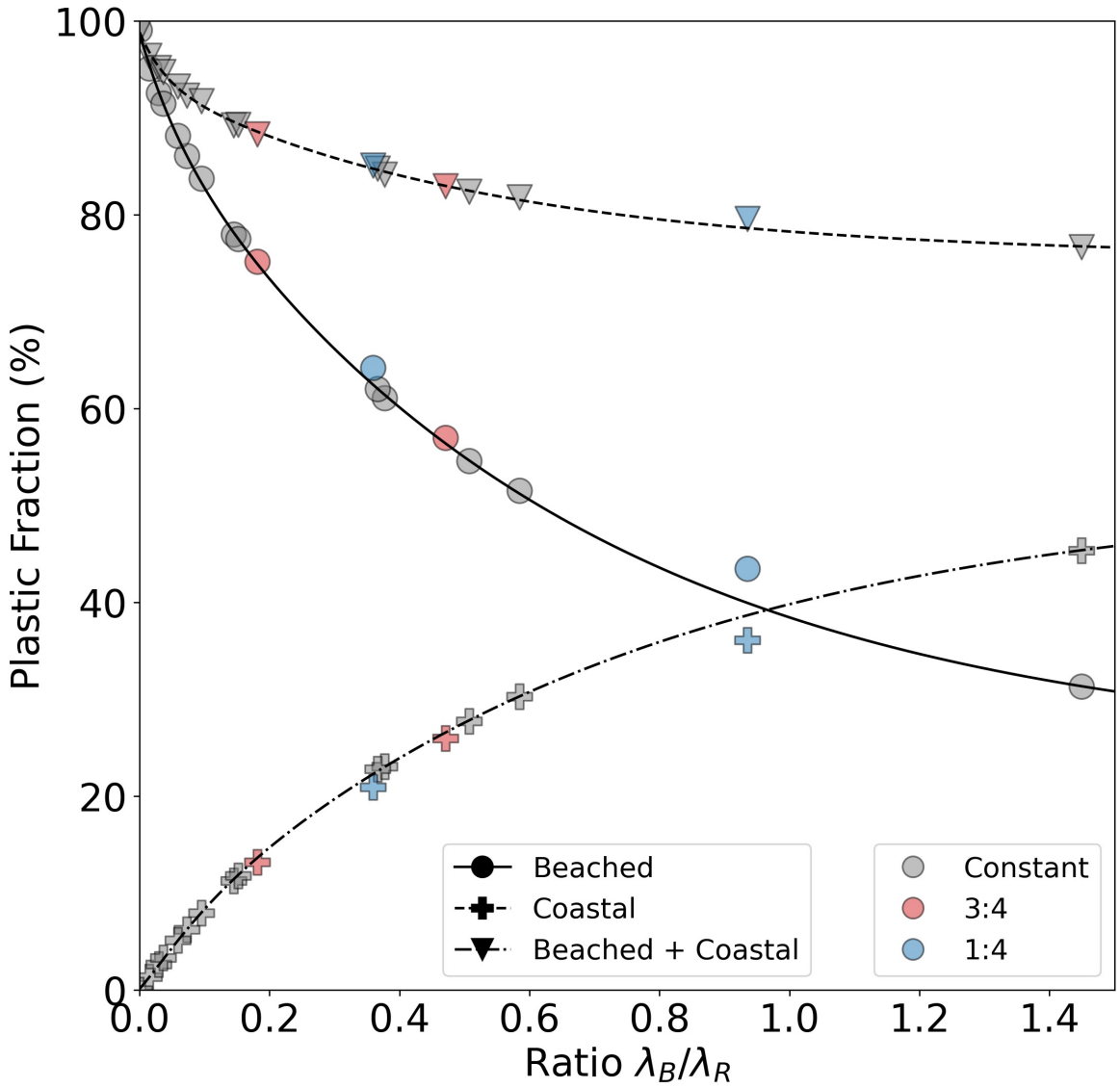

Figure 3.A.10: The global PBMPD budget of beached, coastal and coastal + beached PBMPD as a percentage of the total of amount of PBMPD that enters the ocean, for global constant resuspension (grey markers) and shore dependent resuspension (red and blue markers). Ratios λ_B/λ_R for shore dependent resuspension simulations are calculated using the global average sandy fraction of coastlines. The lines indicate fits for the beached, coastal and coastal + beached fractions for constant resuspension alone. Since the beached fractions with shore dependent resuspension are close to these fit lines, spatially varying resuspension does not seem to have a strong influence globally on the amount of beached plastic. The fractions are averages over the fifth year of the simulation. Coastal PBMPD is defined as non-beached PBMPD within 10 km of the nearest land cell.

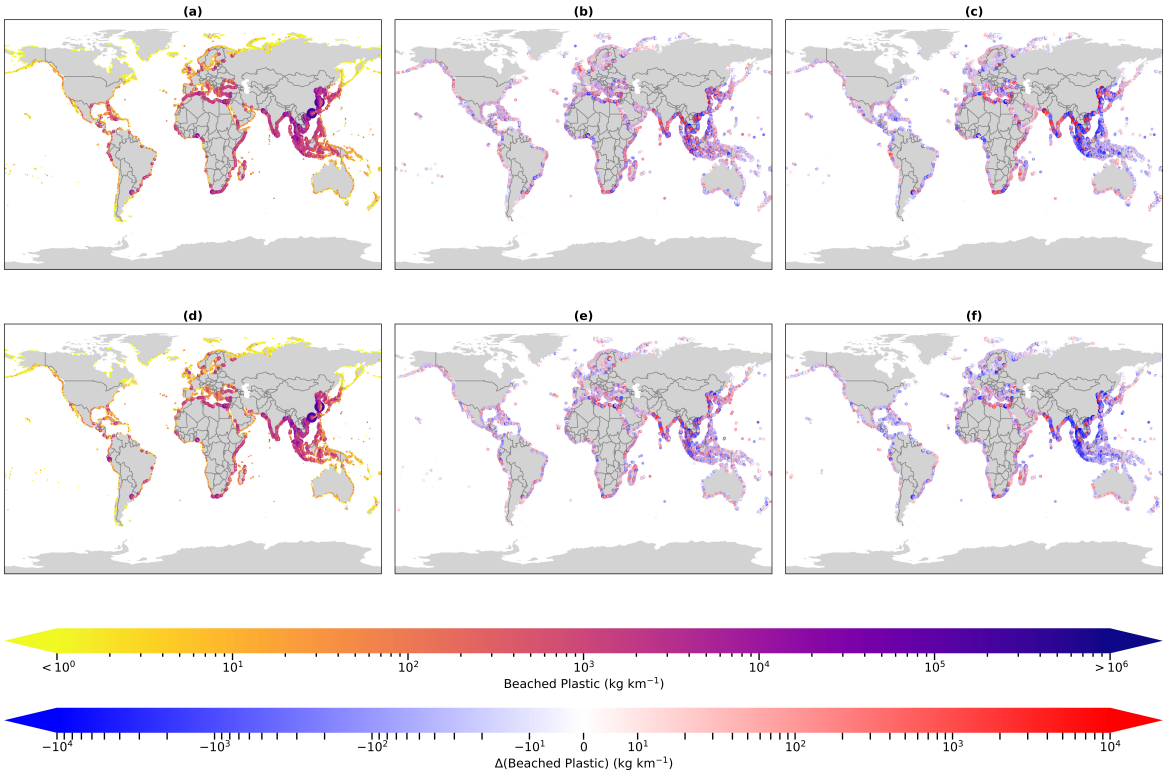

Figure 3.A.11: Differences in average beached PBMPD concentrations over the final year of the simulation of shore dependent resuspension timescales relative to global constant resuspension. (a) Stochastic $\lambda_B = 10$ days, $\lambda_R = 69$ days. (b) Difference relative to (a) for shore dependent resuspension $\lambda_B = 10$ days, $\lambda_R = 69$ days, Ratio = 3:4. (c) Difference relative to (a) for shore dependent resuspension $\lambda_B = 10$ days, $\lambda_R = 69$ days, Ratio = 1:4. (d) Stochastic $\lambda_B = 26$ days, $\lambda_R = 69$ days. (e) Difference relative to (d) for shore dependent resuspension $\lambda_B = 26$ days, $\lambda_R = 69$ days, Ratio = 3:4. (f) Difference relative to (d) for shore dependent resuspension $\lambda_B = 26$ days, $\lambda_R = 69$ days, Ratio = 1:4. All simulations start in 2010, use the Jambeck input and include Stokes drift.

Bibliography

Ali, R. & Shams, Z. I., 2015. Quantities and composition of shore debris along clifton beach, karachi, pakistan, *Journal of coastal conservation*, 19(4), 527–535.

Ballance, A., Ryan, P., Turpie, J., et al., 2000. How much is a clean beach worth? the impact of litter on beach users in the cape peninsula, south africa, *South African Journal of Science*, 96(5), 210–230.

Barnes, D. K. & Milner, P., 2005. Drifting plastic and its consequences for sessile organism dispersal in the atlantic ocean, *Marine Biology*, 146(4), 815–825.

Bleck, R., 2002. An oceanic general circulation model framed in hybrid isopycnic-cartesian coordinates, *Ocean modelling*, 4(1), 55–88.

Brignac, K. C., Jung, M. R., King, C., Royer, S.-J., Blickley, L., Lamson, M. R., Potemra, J. T., & Lynch, J. M., 2019. Marine debris polymers on main hawaiian island beaches, sea surface, and seafloor, *Environmental science & technology*, 53(21), 12218–12226.

Browne, M. A., Chapman, M. G., Thompson, R. C., Amaral Zettler, L. A., Jambeck, J., & Mallos, N. J., 2015. Spatial and temporal patterns of stranded intertidal marine debris: is there a picture of global change?, *Environmental Science & Technology*, 49(12), 7082–7094.

Carlson, D. F., Suaria, G., Aliani, S., Fredj, E., Fortibuoni, T., Griffa, A., Russo, A., & Melli, V., 2017. Combining litter observations with a regional ocean model to identify sources and sinks of floating debris in a semi-enclosed basin: the adriatic sea, *Frontiers in Marine Science*, 4, 78.

Center for International Earth Science Information Network–CIESIN–Columbia University, 2016. Gridded population of the world, version 4 (gpwv4): population density.

Choy, C. A., Robison, B. H., Gagne, T. O., Erwin, B., Firl, E., Halden, R. U., Hamilton, J. A., Katija, K., Lisin, S. E., Rolsky, C., et al., 2019. The vertical distribution and biological transport of marine microplastics across the epipelagic and mesopelagic water column, *Scientific reports*, 9(1), 1–9.

Claereboudt, M. R., 2004. Shore litter along sandy beaches of the gulf of oman, *Marine pollution bulletin*, 49(9-10), 770–777.

Convey, P., Barnes, D., & Morton, A., 2002. Debris accumulation on oceanic island shores of the scotia arc, antarctica, *Polar Biology*, 25(8), 612–617.

Corbin, C. & Singh, J., 1993. Marine debris contamination of beaches in st. lucia and dominica, *Marine Pollution Bulletin*, 26(6), 325–328.

Cózar, A., Echevarría, F., González-Gordillo, J. I., Irigoien, X., Úbeda, B., Hernández-León, S., Palma, Á. T., Navarro, S., García-de Lomas, J., Ruiz, A., et al., 2014. Plastic debris in the open ocean, *Proceedings of the National Academy of Sciences*, 111(28), 10239–10244.

Critchell, K., Grech, A., Schlaefer, J., Andutta, F., Lambrechts, J., Wolanski, E., & Hamann, M., 2015. Modelling the fate of marine debris along a complex shoreline: Lessons from the great barrier reef, *Estuarine, Coastal and Shelf Science*, 167, 414–426.

Debrot, A. O., Tiel, A. B., & Bradshaw, J. E., 1999. Beach debris in curacao, *Marine Pollution Bulletin*, 38(9), 795–801.

Debrot, A. O., van Rijn, J., Bron, P. S., & de León, R., 2013. A baseline assessment of beach debris and tar contamination in bonaire, southeastern caribbean, *Marine pollution bulletin*, 71(1-2), 325–329.

Delandmeter, P. & Van Sebille, E., 2019. The parcels v2. 0 lagrangian framework: new field interpolation schemes, *Geoscientific Model Development*, 12(8), 3571–3584.

Derraik, J. G., 2002. The pollution of the marine environment by plastic debris: a review, *Marine pollution bulletin*, 44(9), 842–852.

Egger, M., Sulu-Gambari, F., & Lebreton, L., 2020. First evidence of plastic fallout from the north pacific garbage patch, *Scientific reports*, 10(1), 1–10.

Eriksen, M., Lebreton, L. C., Carson, H. S., Thiel, M., Moore, C. J., Borerro, J. C., Galgani, F., Ryan, P. G., & Reisser, J., 2014. Plastic pollution in the world's oceans: more than 5 trillion plastic pieces weighing over 250,000 tons afloat at sea, *PloS one*, 9(12), e111913.

Fazey, F. M. & Ryan, P. G., 2016. Biofouling on buoyant marine plastics: An experimental study into the effect of size on surface longevity, *Environmental Pollution*, 210, 354–360.

Fraser, C. I., Morrison, A. K., Hogg, A. M., Macaya, E. C., van Sebille, E., Ryan, P. G., Padovan, A., Jack, C., Valdivia, N., & Waters, J. M., 2018. Antarctica's ecological isolation will be broken by storm-driven dispersal and warming, *Nature climate change*, 8(8), 704–708.

Geyer, R., Jambeck, J. R., & Law, K. L., 2017. Production, use, and fate of all plastics ever made, *Science advances*, 3(7), e1700782.

Hardesty, B. D., Harari, J., Isobe, A., Lebreton, L., Maximenko, N., Potemra, J., van Sebille, E., Vethaak, A. D., & Wilcox, C., 2017a. Using numerical model simulations to improve the understanding of micro-plastic distribution and pathways in the marine environment, *Frontiers in Marine Science*, 4, 30.

Hardesty, B. D., Lawson, T., van der Velde, T., Lansdell, M., & Wilcox, C., 2017b. Estimating quantities and sources of marine debris at a continental scale, *Frontiers in Ecology and the Environment*, 15(1), 18–25.

Hinata, H., Mori, K., Ohno, K., Miyao, Y., & Kataoka, T., 2017. An estimation of the average residence times and onshore-offshore diffusivities of beached microplastics based on the population decay of tagged meso-and macrolitter, *Marine pollution bulletin*, 122(1-2), 17–26.

Hong, S., Lee, J., Kang, D., Choi, H.-W., & Ko, S.-H., 2014. Quantities, composition, and sources of beach debris in korea from the results of nationwide monitoring, *Marine pollution bulletin*, 84(1-2), 27–34.

Institute, F. M., 2019. Union of the esri country shapefile and the exclusive economic zones (version 3).

Jambeck, J. R., Geyer, R., Wilcox, C., Siegler, T. R., Perryman, M., Andrady, A., Narayan, R., & Law, K. L., 2015. Plastic waste inputs from land into the ocean, *Science*, 347(6223), 768–771.

Kaandorp, M. L. A., Dijkstra, H. A., & van Sebille, E., 2020. Closing the mediterranean marine floating plastic mass budget: Inverse modeling of sources and sinks, *Environmental Science & Technology*, 54(19), 11980–11989.

Lacerda, A. L. d. F., Rodrigues, L. d. S., van Sebille, E., Rodrigues, F. L., Ribeiro, L., Secchi, E. R., Kessler, F., & Proietti, M. C., 2019. Plastics in sea surface waters around the antarctic peninsula, *Scientific reports*, 9(1), 3977.

Lange, M. & van Sebille, E., 2017. Parcels v0.9: Prototyping a lagrangian ocean analysis frameworkfor the petascale age, *Geoscientific Model Development Discussions*, 10, 4175–4186.

Lavers, J. L. & Bond, A. L., 2017. Exceptional and rapid accumulation of anthropogenic debris on one of the world's most remote and pristine islands, *Proceedings of the National Academy of Sciences*, 114(23), 6052–6055.

Lebreton, L. & Andrady, A., 2019. Future scenarios of global plastic waste generation and disposal, *Palgrave Communications*, 5(1), 1–11.

Lebreton, L., Slat, B., Ferrari, F., Sainte-Rose, B., Aitken, J., Marthouse, R., Hajbane, S., Cunsolo, S., Schwarz, A., Levivier, A., et al., 2018. Evidence that the great pacific garbage patch is rapidly accumulating plastic, *Scientific reports*, 8(1), 1–15.

Lebreton, L., Egger, M., & Slat, B., 2019. A global mass budget for positively buoyant macroplastic debris in the ocean, *Scientific reports*, 9(1), 1–10.

Lebreton, L. C., Van Der Zwet, J., Damsteeg, J.-W., Slat, B., Andrady, A., & Reisser, J., 2017. River plastic emissions to the world's oceans, *Nature communications*, 8, 15611.

Lebreton, L.-M., Greer, S., & Borrero, J. C., 2012. Numerical modelling of floating debris in the world's oceans, *Marine pollution bulletin*, 64(3), 653–661.

Li, R., Yu, L., Chai, M., Wu, H., & Zhu, X., 2020. The distribution, characteristics and ecological risks of microplastics in the mangroves of southern china, *Science of The Total Environment*, 708, 135025.

Liu, Y. & Weisberg, R. H., 2011. Evaluation of trajectory modeling in different dynamic regions using normalized cumulative lagrangian separation, *Journal of Geophysical Research: Oceans*, 116(C9).

Liu, Y., Weisberg, R. H., Vignudelli, S., & Mitchum, G. T., 2014. Evaluation of altimetry-derived surface current products using lagrangian drifter trajectories in the eastern gulf of mexico, *Journal of Geophysical Research: Oceans*, 119(5), 2827–2842.

Liubartseva, S., Coppini, G., Lecci, R., & Clementi, E., 2018. Tracking plastics in the mediterranean: 2d lagrangian model, *Marine pollution bulletin*, 129(1), 151–162.

Luijendijk, A., Hagenaars, G., Ranasinghe, R., Baart, F., Donchyts, G., & Aarninkhof, S., 2018. The state of the world's beaches, *Scientific reports*, 8(1), 1–11.

Madzena, A. & Lasiak, T., 1997. Spatial and temporal variations in beach litter on the transkei coast of south africa, *Marine Pollution Bulletin*, 34(11), 900–907.

Martin, C., Baalkhuyur, F., Valluzzi, L., Saderne, V., Cusack, M., Almahasheer, H., Krishnakumar, P., Rabaoui, L., Qurban, M., Arias-Ortiz, A., et al., 2020. Exponential increase of plastic burial in mangrove sediments as a major plastic sink, *Science advances*, 6(44), eaaz5593.

Metzger, E. J., Hurlburt, H., Xu, X., Shriver, J. F., Gordon, A. L., Sprintall, J., Susanto, R. D., & Van Aken, H., 2010. Simulated and observed circulation in the indonesian seas: 1/12 global hycom and the instant observations, *Dynamics of Atmospheres and Oceans*, 50(2), 275–300.

Miladinova, S., Macias, D., Stips, A., & Garcia-Gorriz, E., 2020. Identifying distribution and accumulation patterns of floating marine debris in the black sea, *Marine Pollution Bulletin*, 153, 110964.

Monteiro, R. C., do Sul, J. A. I., & Costa, M. F., 2018. Plastic pollution in islands of the atlantic ocean, *Environmental Pollution*, 238, 103–110.

Onink, V., Wichmann, D., Delandmeter, P., & van Sebille, E., 2019. The role of ekman currents, geostrophy, and stokes drift in the accumulation of floating microplastic, *Journal of Geophysical Research: Oceans*, 124(3), 1474–1490.

Otley, H. & Ingham, R., 2003. Marine debris surveys at volunteer beach, falkland islands, during the summer of 2001/02, *Marine Pollution Bulletin*, 46(12), 1534–1539.

Pedrotti, M. L., Petit, S., Elineau, A., Bruzaud, S., Crebassa, J.-C., Dumontet, B., Martí, E., Gorsky, G., & Cózar, A., 2016. Changes in the floating plastic pollution of the mediterranean sea in relation to the distance to land, *PloS one*, 11(8), e0161581.

Pervez, R., Wang, Y., Ali, I., Ali, J., & Ahmed, S., 2020a. The analysis of the accumulation of solid waste debris in the summer season along the shilaoren beach qingdao, china, *Regional Studies in Marine Science*, 34, 101041.

Pervez, R., Wang, Y., Mahmood, Q., Zahir, M., & Jattak, Z., 2020b. Abundance, type, and origin of litter on no. 1 bathing beach of qingdao, china, *Journal of Coastal Conservation*, 24, 34.

Pham, C. K., Pereira, J. M., Frias, J. P., Ríos, N., Carriço, R., Juliano, M., & Rodríguez, Y., 2020. The azores archipelago as a transitory repository for small plastic fragments floating in the north-east atlantic, *Environmental Pollution*, 263, 114494.

Pieper, C., Ventura, M. A., Martins, A., & Cunha, R. T., 2015. Beach debris in the azores (ne atlantic): Faial island as a first case study, *Marine pollution bulletin*, 101(2), 575–582.

Pieper, C., Amaral-Zettler, L., Law, K. L., Loureiro, C. M., & Martins, A., 2019. Application of matrix scoring techniques to evaluate marine debris sources in the remote islands of the azores archipelago, *Environmental Pollution*, 249, 666–675.

Rascle, N. & Ardhuin, F., 2013. A global wave parameter database for geophysical applications. part 2: Model validation with improved source term parameterization, *Ocean Modelling*, 70, 174–188.

Ribic, C. A., Sheavly, S. B., Rugg, D. J., & Erdmann, E. S., 2010. Trends and drivers of marine debris on the atlantic coast of the united states 1997–2007, *Marine Pollution Bulletin*, 60(8), 1231–1242.

Ribic, C. A., Sheavly, S. B., Rugg, D. J., & Erdmann, E. S., 2012. Trends in marine debris along the us pacific coast and hawai'i 1998–2007, *Marine Pollution Bulletin*, 64(5), 994–1004.

Ruiz-Orejón, L. F., Sardá, R., & Ramis-Pujol, J., 2018. Now, you see me: High concentrations of floating plastic debris in the coastal waters of the balearic islands (spain), *Marine pollution bulletin*, 133, 636–646.

Ryan, P. G., 1987. The origin and fate of artefacts stranded on islands in the african sector of the southern ocean, *Environmental Conservation*, 14(4), 341–346.

Ryan, P. G., 2013. A simple technique for counting marine debris at sea reveals steep litter gradients between the straits of malacca and the bay of bengal, *Marine pollution bulletin*, 69(1-2), 128–136.

Ryan, P. G., 2015. Does size and buoyancy affect the long-distance transport of floating debris?, *Environmental Research Letters*, 10(8), 084019.

Ryan, P. G., 2020. Land or sea? what bottles tell us about the origins of beach litter in kenya, *Waste Management*, 116, 49–57.

Ryan, P. G., Perold, V., Osborne, A., & Moloney, C. L., 2018. Consistent patterns of debris on south african beaches indicate that industrial pellets and other mesoplastic items mostly derive from local sources, *Environmental Pollution*, 238, 1008–1016.

Ryan, P. G., Dilley, B. J., Ronconi, R. A., & Connan, M., 2019. Rapid increase in asian bottles in the south atlantic ocean indicates major debris inputs from ships, *Proceedings of the National Academy of Sciences*, 116(42), 20892–20897.

Samaras, A. G., De Dominicis, M., Archetti, R., Lamberti, A., & Pinardi, N., 2014. Towards improving the representation of beaching in oil spill models: A case study, *Marine pollution bulletin*, 88(1-2), 91–101.

Savage, J. A., Tokmakian, R. T., & Batteen, M. L., 2015. Assessment of the hycom velocity fields during agulhas return current cruise 2012, *Journal of Operational Oceanography*, 8(1), 11–24.

Schmidt, C., Krauth, T., & Wagner, S., 2017. Export of plastic debris by rivers into the sea, *Environmental science & technology*, 51(21), 12246–12253.

Schwarz, A., Ligthart, T., Boukris, E., & Van Harmelen, T., 2019. Sources, transport, and accumulation of different types of plastic litter in aquatic environments: a review study, *Marine pollution bulletin*, 143, 92–100.

Smith, S. D., 2012. Marine debris: A proximate threat to marine sustainability in bootless bay, papua new guinea, *Marine Pollution Bulletin*, 64(9), 1880–1883.

Stanev, E., Badewien, T., Freund, H., Grayek, S., Hahner, F., Meyerjürgens, J., Ricker, M., Schöneich-Argent, R., Wolff, J.-O., & Zielinski, O., 2019. Extreme westward surface drift in the north sea: public reports of stranded drifters and lagrangian tracking, *Continental Shelf Research*, 177, 24–32.

Sterl, M. F., Delandmeter, P., & van Sebille, E., 2020. Influence of barotropic tidal currents on transport and accumulation of floating microplastics in the global open ocean, *Journal of Geophysical Research: Oceans*, 125(2), e2019JC015583.

Suaria, G., Perold, V., Lee, J. R., Lebouard, F., Aliani, S., & Ryan, P. G., 2020. Floating macro-and microplastics around the southern ocean: Results from the antarctic circumnavigation expedition, *Environment International*, 136, 105494.

Tamura, H., Miyazawa, Y., & Oey, L.-Y., 2012. The stokes drift and wave induced-mass flux in the north pacific, *Journal of Geophysical Research: Oceans*, 117(C8).

Thiel, M., Hinojosa, I., Miranda, L., Pantoja, J., Rivadeneira, M., & Vásquez, N., 2013. Anthropogenic marine debris in the coastal environment: a multi-year comparison between coastal waters and local shores, *Marine pollution bulletin*, 71(1-2), 307–316.

Tolman, H. L., 1997. *User manual and system documentation of WAVEWATCH-III version 1.15*, US Department of Commerce, National Oceanic and Atmospheric Administration, National Weather Service, National Centers for Environmental Prediction.

Tolman, H. L., 2009. User manual and system documentation of wavewatch iii tm version 3.14, *Technical note, MMAB Contribution*, 276, 220.

Tramoy, R., Gasperi, J., Dris, R., Colasse, L., Fisson, C., Sananes, S., Rocher, V., & Tassin, B., 2019. Assessment of the plastic inputs from the seine basin to the sea using statistical and field approaches, *Frontiers in Marine Science*, 6, 151.

Uneputty, P., Evans, S., & Suyoso, E., 1998. The effectiveness of a community education programme in reducing litter pollution on shores of ambon bay (eastern indonesia), *Journal of Biological Education*, 32(2), 143–147.

Van Den Bremer, T. & Breivik, Ø., 2018. Stokes drift, *Philosophical Transactions of the Royal Society A: Mathematical, Physical and Engineering Sciences*, 376(2111), 20170104.

Van Emmerik, T., Loozen, M., Van Oeveren, K., Buschman, F., & Prinsen, G., 2019. Riverine plastic emission from jakarta into the ocean, *Environmental Research Letters*, 14(8), 084033.

Van Franeker, J. A. & Law, K. L., 2015. Seabirds, gyres and global trends in plastic pollution, *Environmental Pollution*, 203, 89–96.

van Sebille, E., Wilcox, C., Lebreton, L., Maximenko, N., Hardesty, B. D., Van Franeker, J. A., Eriksen, M., Siegel, D., Galgani, F., & Law, K. L., 2015. A global inventory of small floating plastic debris, *Environmental Research Letters*, 10(12), 1–11.

Van Sebille, E., Aliani, S., Law, K. L., Maximenko, N., Alsina, J. M., Bagaev, A., Bergmann, M., Chapron, B., Chubarenko, I., Cózar, A., et al., 2020. The physical oceanography of the transport of floating marine debris, *Environmental Research Letters*, 15(2), 023003.

Wang, M., Liu, Z., Zhu, X., Yan, X., Zhang, Z., & Zhao, R., 2019. Origin and formation of the ryukyu current revealed by hycom reanalysis, *Acta Oceanologica Sinica*, 38(11), 1–10.

Weideman, E. A., Perold, V., Omardien, A., Smyth, L. K., & Ryan, P. G., 2020. Quantifying temporal trends in anthropogenic litter in a rocky intertidal habitat, *Marine pollution bulletin*, 160, 111543.

Willis, K., Maureaud, C., Wilcox, C., & Hardesty, B. D., 2018. How successful are waste abatement campaigns and government policies at reducing plastic waste into the marine environment?, *Marine Policy*, 96, 243–249.

Chapter 4

Empirical Lagrangian parametrization for wind-driven mixing of buoyant particles at the ocean surface

Victor Onink, Erik van Sebille and Charlotte Laufkötter

Published in *Geoscientific Model Development*, Volume 15, issue 5, 1995-2012, 2022.

Abstract

Turbulent mixing is a vital component of vertical particulate transport, but ocean global circulation models (OGCMs) generally have low resolution representations of near-surface mixing. Furthermore, turbulence data is often not provided in OGCM model output. We present 1D parametrizations of wind-driven turbulent mixing in the ocean surface mixed layer, which are designed to be easily included in 3D Lagrangian model experiments. Stochastic transport is computed by Markov-0 or Markov-1 models, and we discuss the advantages/disadvantages of two vertical profiles for the vertical diffusion coefficient K_z. All vertical diffusion profiles and stochastic transport models lead to stable concentration profiles for buoyant particles, which for particles with rise velocities of 0.03 and 0.003 m s^{-1} agree relatively well with concentration profiles from field measurements of microplastics when Langmuir-circulation-driven turbulence is accounted for. Markov-0 models provide good model performance for integration timesteps of $\Delta t \approx 30$ seconds, and can be readily applied in studying the behaviour of buoyant particulates in the ocean. Markov-1 models do not consistently improve model performance relative to Markov-0 models, and require an additional parameter that is poorly constrained.

4.1 Introduction

Lagrangian models are essential tools to examine the transport of particulates in the ocean on a variety of spatial and temporal scales (Van Sebille et al., 2018), and have been used to study

the movement of plastic particulates (Onink et al., 2019), oil (Samaras et al., 2014) and fish larvae (Paris et al., 2013). However, especially in the field of marine plastic modeling, most large scale modeling studies consider only virtual particles (henceforth referred to as particles) that float and remain at the ocean surface (Lebreton et al., 2018; Liubartseva et al., 2018; Onink et al., 2019, 2021), essentially simplifying the three dimensional ocean into a 2D system. While this does reduce the complexity of models, ultimately vertical transport processes need to be considered in order to have a complete understanding of oceanic particulate transport (Wichmann et al., 2019; Van Sebille et al., 2020).

In the case of buoyant particulates (particulates with a density lower than seawater), buoyancy is expected to return any particulates to the ocean surface. However, instead of all buoyant particulates accumulating at the ocean surface, both field measurements (Kukulka et al., 2012; Kooi et al., 2016b) and regional large-eddy simulations (LES) model studies (e.g. Liang et al., 2012; Yang et al., 2014; Brunner et al., 2015; Taylor, 2018) indicate vertical concentration profiles throughout the mixed layer (ML). These profiles arise due to the balance between the particulate buoyancy and turbulent mixing flows, which are largely driven by wind and wave breaking at the ocean surface (Chamecki et al., 2019). While such profiles are commonly used to correct surface measurements of particulates such as microplastics (e.g. Law et al., 2014; Egger et al., 2020), it is difficult to recreate such vertical mixing profiles in the ML outside of LES models, as vertical turbulent processes generally act on much smaller scales than is explicitly resolved in ocean global circulation models (OGCMs) (Taylor, 2018). In addition, while it is possible to represent mixing using the parametrization from Kukulka et al. (2012), this approach is only valid for depths up to several meters, while the mixed layer depth (MLD) can be hundreds of meters deep (Chamecki et al., 2019).

In this study we present numerical simulations of buoyant virtual particles in the ML with four 1D wind-driven mixing parametrizations. These mixing parametrizations have been specifically designed such that the code can be easily adapted to function within large-scale 3D Lagrangian models running with OGCM data, for cases where the vertical spatial scales might be too coarse to explicitly represent turbulent processes or where turbulence data might not be provided as model output. Using these parametrizations we calculate the vertical equilibrium profiles of buoyant particles within the ML as a function of the particle rise velocities, the 10m wind speed and the MLD. Buoyant particles are found below the ML (Pieper et al., 2019; Choy et al., 2019; Egger et al., 2020), but diffusive mixing at such depths is likely not due to wind-driven turbulent mixing and therefore goes beyond the scope of this study. We test two methods for solving stochastic differential equations, and consider vertical diffusion coefficient profiles based on the KPP model (Large et al., 1994) and on Kukulka et al. (2012) extended by Poulain (2020). The modelled concentration profiles are then compared with measurements of vertical concentration profiles of microplastics.

4.2 Methods

Turbulence in the ocean occurs over a wide range of spatial and temporal scales, with Kolmogorov length and timescales of $\eta = (\nu^3/\epsilon)^{1/4} = 3 \times 10^{-4}$ m and $\tau_n = (\nu/\epsilon)^{1/2} = 0.1$ s (Landahl & Christensen, 1998) for turbulent kinetic energy $\epsilon = 10^{-4}$ m^2 s^{-2} (Gaspar et al., 1990) and kinematic viscosity of seawater $\nu = 10^{-6}$ m^2 s^{-1} (Riisgård & Larsen, 2007). The vertical resolution of OGCMs is typically on the order of meters and is therefore not capable of explicitly resolving all turbulent processes. Instead, turbulence due to sub-grid scale processes is generally represented stochastically. In our 1D vertical model, we simulate positively buoyant particles that are vertically transported due to stochastic turbulence and the particle rise velocity w_{rise}.

For such particles, the particle trajectory $Z(t)$ can be computed with a stochastic differential equation (SDE) (Gräwe et al., 2012) as:

$$Z(t+dt) = Z(t) + (w_{rise} + \partial_z K_z)dt + \sqrt{2K_z}dW \tag{4.1}$$

$$Z(0) = 0 \tag{4.2}$$

where $K_z = K_z\big(Z(t)\big)$ is the vertical diffusion coefficient, $\partial_z K_z = \partial K_z/\partial z$, dW is a Wiener increment with zero mean and variance dt and we define the vertical axis z as positive upward with $z = 0$ at the air-sea interface. The Euler-Maruyama (EM) scheme (Maruyama, 1955) is the simplest numerical approximation of equation 4.1, where infinitesimal terms dt and dW are replaced with the finite Δt and ΔW. Equation 4.1 can then be rewritten as (Gräwe et al., 2012):

$$w'(t) = \partial_z K_z + \frac{1}{\Delta t}\sqrt{2K_z}\Delta W \tag{4.3}$$

$$Z(t+\Delta t) = Z(t) + \big(w_{rise} + w'(t)\big)\Delta t \tag{4.4}$$

where w' is the stochastic velocity perturbation due to turbulence. The turbulent transport has both a deterministic drift term and a stochastic term. This is the most basic form of representing turbulent particle transport, as turbulent perturbations on the particle position are assumed to be uncorrelated (Berloff & McWilliams, 2003). The drift term assures that the well-mixed condition is met, which states that an initially uniform particle distribution must remain uniform even with inhomogeneous turbulence (Brickman & Smith, 2002; Ross & Sharples, 2004). This approach, termed a Markov-0 (M-0) or random walk model, assumes that turbulent fluctuations exhibit no autocorrelation on timescales Δt, which for global-scale Lagrangian simulations can range from 30 seconds (Lobelle et al., 2021) to 30 minutes (Onink et al., 2019). However, measurements from Lagrangian ocean floats show this is an oversimplification, as coherent oceanic flow structures can induce velocity autocorrelations that can persist for significantly longer timescales (Denman & Gargett, 1983; Brickman & Smith, 2002).

A higher order approach is the Markov-1 (M-1) model, which assumes a degree of auto-correlation of particle velocities set by the Lagrangian integral timescale T_L. The turbulent velocity perturbation is now expressed as a Langevin equation, and with an EM numerical scheme the particle trajectory $Z(t)$ is computed as (Mofakham & Ahmadi, 2020):

$$Z(t+\Delta t) = Z(t) + \big(w_{rise} + w'(t)\big)\Delta t \tag{4.5}$$

$$w'(t+\Delta t) = \alpha w'(t) + \partial_z \sigma_w^2 \Delta t + \sqrt{\frac{2(1-\alpha)\sigma_w^2}{\Delta t}}\Delta W \tag{4.6}$$

where $\alpha = 1 - \Delta t/T_L$ and $\sigma_w^2 = \sigma_w^2(z,t)$ is the variance of w', and we assume $\Delta t \leq T_L$. The influence of the initial turbulent fluctuations on subsequent fluctuations is set by α, which in turn depends on the ratio between the integration timestep Δt and T_L. However, empirical and theoretical estimates for T_L range from 6-7 seconds (Kukulka & Veron, 2019) to 15-30 minutes (Denman & Gargett, 1983), and T_L can also be depth dependent (Brickman & Smith, 2002). In large-eddy simulation (LES) models, $T_L = 4e/3C_0\epsilon$ where e is the sub-grid scale turbulent kinetic energy, C_0 is a model constant determining diffusion in the velocity space and ϵ is the turbulent kinetic energy dissipation rate (Kukulka & Veron, 2019), but e and ϵ are not commonly available variables in the output of OGCMs. However, it does indicate why model T_L estimates vary widely, as T_L describes the autocorrelation of the particle velocity from its initial velocity due to unresolved sub-grid processes, which depends on the model resolution and setup in a given study. Since there is not a clear indication of the true value of T_L, we consider a range of values $\alpha \in [0, 0.1, 0.3, 0.5, 0.7, 0.95]$, corresponding to $T_L \in [1, 1.1, 1.4, 2, 3.3, 20] \times \Delta t$. As the depth dependence of T_L is uncertain, we make the simplification that $\partial_z T_L = \partial_z \alpha = 0$. Since $\Delta t \leq T_L$,

we use $K_z = \sigma_w^2 \Delta t$ (Brickman & Smith, 2002), which means that equation 4.6 becomes:

$$w'(t) = \alpha w'(t) + \partial_z K_z + \frac{1}{dt}\sqrt{2(1-\alpha)K_z}\Delta W \tag{4.7}$$

In this form, it is clear that equation 4.7 is equivalent to equation 4.4 when $\alpha = 0$. This is because when $\alpha = 0$, velocity perturbations w' are assumed to be uncorrelated over timescales $\geq \Delta t$, which is equivalent to the M-0 formulation. M-1 stochastic models generally should lead to improved representation of diffusion in Lagrangian models (Berloff & McWilliams, 2003; Van Sebille et al., 2018), but it does require insight into turbulence statistics that have not yet been extensively studied in Lagrangian settings. For that reason, while even higher order Markov models are theoretically possible (Berloff & McWilliams, 2003), we limit this study to just the M-0 and M-1 approaches.

All Lagrangian simulations are run using Parcels v2.2.1 (Delandmeter & Sebille, 2019), which has been used for 1D, 2D and 3D particle oceanographic simulations (Fischer et al., 2021; Onink et al., 2021; Lobelle et al., 2021). The simulations start with 100,000 particles released at $Z(0) = 0$ and run for 12 hours. The model is one dimensional with horizontal velocities set to zero. The time-invariant vertical diffusion profiles are calculated with a 0.1 m vertical resolution, where the K_z value at the exact particle location is linearly interpolated from these profiles. The vertical transport is calculated according to Equations 4.3 and 4.4 for M-0 simulations, and Equations 4.5 and 4.7 for M-1 simulations. We take $\Delta t = 30$ seconds, where the integration timestep is a compromise between accounting for turbulent transport on short timescales and computational cost for when the 1D model is integrated into a larger 3D Lagrangian model. We consider high, medium and low buoyancy particles with rise velocities of $w_{rise} \in [0.03, 0.003, 0.0003]$ m s^{-1}, which for plastic polyethylene ($\rho = 980$ kg m^{-3}) particles corresponds to spherical particles with diameters of 2.2, 0.4 and 0.1 mm (Enders et al., 2015). However, these particle sizes are rough indications of approximate particle sizes, as the buoyancy of particle depends on a combination of the particle size, shape, polymer density and degree of biofouling (Kooi et al., 2016b; Kaiser et al., 2017; Brignac et al., 2019). Relative to peak stochastic velocity perturbations w' calculated from the vertical diffusion coefficients described in Section 4.2.1, the rise velocity of the high buoyancy particles dominate w' except for the highest wind speeds, while turbulence dominates buoyancy for the medium and low buoyancy particles for almost all wind conditions (Table 4.A.2). The surface wind stress is computed from $u_{10} \in [0.85, 2.4, 4.35, 6.65, 9.3]$ m s^{-1}. The model domain is $z \in [-100, 0]$m, where we apply a ceiling boundary condition (BC) in which particles that cross the surface boundary are placed at $z = 0$. This BC assures that neither buoyancy or turbulence can transport particles out of the water column. Vertical concentration profiles are computed by binning the final particle locations into 0.5 m bins, and the concentrations are then normalized by the total number of particles in the simulation. The variability of the profiles at each depth level is calculated as the standard deviation over the final hour of each simulation.

4.2.1 Vertical diffusion profiles

Two vertical diffusion coefficient profiles are used, with the first based on Kukulka et al. (2012) and Poulain (2020). Kukulka et al. (2012) parametrized the near-surface vertical diffusion coefficient K_z^S due to breaking waves as:

$$K_z^S = 1.5 u_{*w} \kappa H_s \tag{4.8}$$

for $z > -1.5H_s$, where $\kappa = 0.4$ is the von Karman constant, H_s is the significant wave height and u_{*w} is the friction velocity of water. The significant wave height H_s is parametrized as $H_s = 0.96 g^{-1} \beta_*^{3/2} u_{*a}^2$, where $g = 9.81$ m s^{-2} is the accelation of gravity, $\beta_* = c_p/u_{*a}$ is the

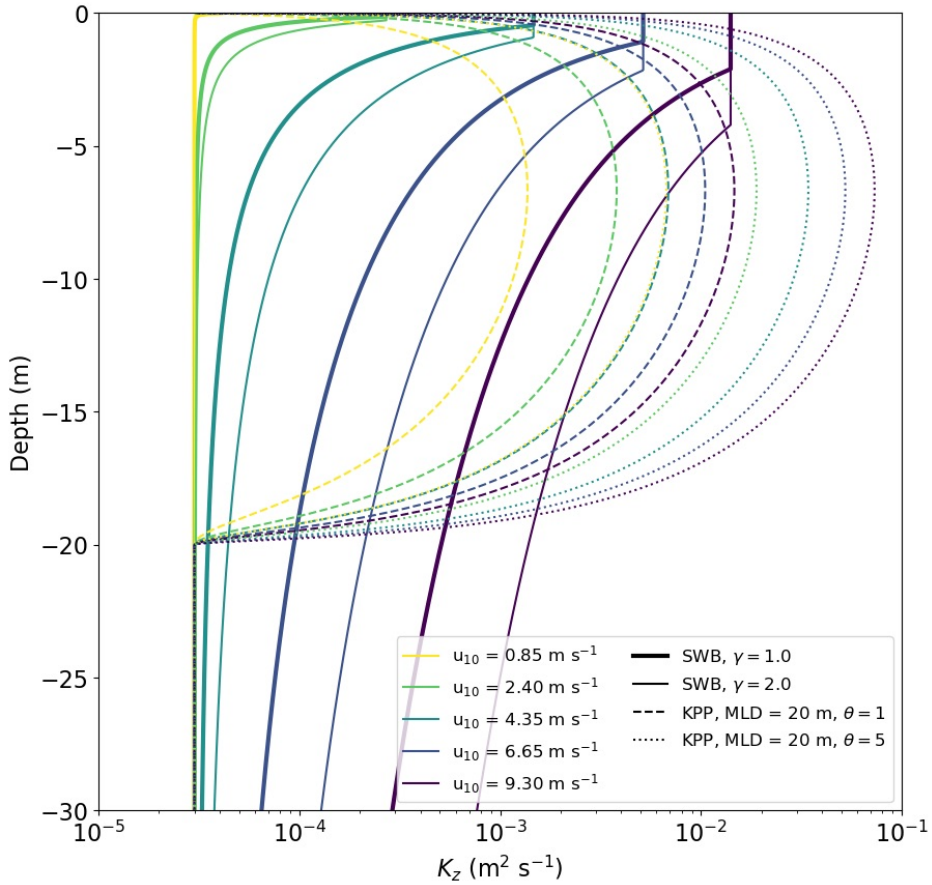

Figure 4.1: Vertical diffusion coefficient profiles for SWB and KPP diffusion under varying wind conditions. The KPP diffusion profile is calculated with z_0 according to Equation 4.12.

wave age, c_p being the characteristic phase speed of the surface waves and $u_{*a} = \tau/\rho_a$ is the friction velocity of water. The friction velocity of air is based on the air density $\rho_a = 1.22$ kg m^{-3} and the surface wind stress $\tau = C_D \rho_a u_{10}^2$, where u_{10} is the 10m wind speed and C_D is the drag coefficient (Large & Pond, 1981). Similarly, $u_{*w} = \tau/\rho_w$ with the seawater density $\rho_w = 1027$ kg m^{-3}. Following Kukulka et al. (2012), we assume a fully developed sea-state with $\beta_* = 35$. The Kukulka et al. (2012) parametrization is valid only for $z \approx -1.5 H_s$, and we extend the parametrization for greater depths using the eddy viscosity profile ν_z as found for oscillating grid turbulence by Poulain (2020):

$$\nu_z = \begin{cases} \nu^S \text{ if } z > -\gamma H_s \\ \nu^S (\gamma H_s)^{3/2} |z|^{-3/2} \text{ if } z < -\gamma H_s \end{cases} \tag{4.9}$$

where ν^S is the near surface eddy viscosity and $\gamma = 1.0$ is a multiple of H_s that sets the depth to which ν^S is constant. This approach agrees with Kukulka et al. (2012) in predicting constant mixing for $z > -H_s$, where the eddy viscosity then drops proportional to $z^{-3/2}$ for greater depths. Oscillating grid turbulence (OGT) experiments are commonly used to study wave and wind induced turbulence (Fernando, 1991). As OGT experiments have been shown to reproduce turbulence decay laws of velocities and dissipation rates observed in the ocean ML (Thompson & Turner, 1975; Hopfinger & Toly, 1976; Craig & Banner, 1994), this provides some confidence in the modeling of the decay of near-surface eddy viscosity, although direct validation with field measurements of eddy viscosity have yet to occur. The diffusion coefficient K_z depends on ν_z as $K_z = \nu_z / Sc_t$, where Sc_t is the turbulent Schmidt number, and assuming $\partial_z Sc_t = 0$, combining

equations 4.8 and 4.9 results in:

$$K_z = \begin{cases} K_z^S + K_B = 1.5 u_{*w} \kappa H_s + K_B \text{ if } z > -\gamma H_s \\ K_z^S (\gamma H_s)^{3/2} |z|^{-3/2} + K_B = 1.5 u_{*w} \kappa \gamma^{3/2} H_s^{5/2} |z|^{-3/2} + K_B \text{ if } z < -\gamma H_s \end{cases} \tag{4.10}$$

where $K_B = 3 \times 10^{-5}$ m^2 s^{-1} is the dianeutral diffusion below the MLD (Waterhouse et al., 2014). The diffusion is thus constant for $z > -\gamma H_s$, below which $K_z \propto |z|^{-3/2}$, while the magnitude of K_z increases for higher wind speeds (Fig. 4.1). Poulain (2020) implies $\gamma = 1.0$ while Kukulka et al. (2012) estimates $\gamma \approx 1.5$, so to test the model sensitivity we consider $\gamma \in [0.5, 1.0, 1.5, 2.0]$ (Figure 4.1). As $z \to -\infty$, $|z|^{-3/2} \to 0$, and therefore we include the bulk dianeutral diffusion K_B to account for vertical mixing at depths below the influence of surface wave-driven turbulence. As both Kukulka et al. (2012) and Poulain et al. (2019) considered turbulence generated by breaking surface waves, we refer to this diffusion approach as Surface Wave Breaking (SWB) diffusion.

The second vertical diffusion coefficient profile is a local form of the K-profile parameterization (KPP) (Large et al., 1994; Boufadel et al., 2020), where K_z is given by:

$$K_z = \left(\frac{\kappa u_{*w}}{\phi} \theta \right) (|z| + z_0) \left(1 - \frac{|z|}{MLD} \right) + K_B \tag{4.11}$$

where $\phi = 0.9$ is the "stability function" of the Monin-Obukov boundary layer theory, θ is a Langmuir circulation (LC) enhancement factor, and z_0 is the roughness scale of turbulence. As such, K_Z rises from a small non-zero value at $z = 0$ to a maxima at $z = 1/3MLD$, before dropping to $K_z = K_B$ for $z \leq MLD$ (Fig. 4.1). In the original KPP formulation $K_z(z \leq MLD) = 0$ since the theory only applies to the surface mixed layer, so we add the same bulk dianeutral diffusion term K_B as with the SWB profile (equation 4.10). Boufadel et al. (2020) examined a case where LC-driven turbulence was considered negligible and so $\theta = 1.0$. However, the presence of LC can increase turbulent mixing by a factor $\theta = 3 - 4$ (McWilliams & Sullivan, 2000) and has been shown to strongly affect the vertical concentration profiles of buoyant microplastic particles in LES experiments (Brunner et al., 2015; Kukulka & Brunner, 2015). Therefore, we examine $\theta \in [1.0, 2.0, 3.0, 4.0, 5.0]$. The roughness scale z_0, which can represent the surface roughness due to surface waves, depends on the wind speed and the wave age (Zhao & Li, 2019), and following Kukulka et al. (2012) we consider a wave age $\beta_* = c_p/u_{*a} = 35$ that is equivalent to $\beta = c_p/u_{10} = 1.21$. According to Zhao & Li (2019), the roughness scale is given by:

$$z_0 = 3.5153 \times 10^{-5} \beta^{-0.42} u_{10}^2 / g \tag{4.12}$$

For $w_{10} = 0.85 - 9.30$ m s^{-1}, this means $z_0 = 2.38 \times 10^{-6} - 2.86 \times 10^{-4}$ m. To test the model sensitivity to z_0, we also consider an alternative scenario where $z_0 = 0.1 \times H_s = 1.76 \times 10^{-3} - 2.10 \times 10^{-1}$ m, following the same formulation $H_s = 0.96 g^{-1} \beta_*^{3/2} u_{*a}^2$ as in Kukulka et al. (2012). This increases K_z for $z \approx 0$, but does not significantly affect the magnitude K_z at greater depths (Figure 4.A.8). The original KPP theory does not explicitly account for surface wave breaking, which would lead to larger non-zero K_z at $z = 0$. While we do not claim that setting $z_0 = 0.1 \times H_s$ means that our KPP profile accounts for surface wave breaking turbulent mixing, it allows us to investigate the influence higher near-surface mixing would have on the modelled vertical concentration profiles. The MLD is the maximum depth of the surface ocean boundary layer formed due to interaction with the atmosphere, and in KPP theory the MLD is defined as the depth where the bulk Richardson number Ri_B is first equal to a critical value Ri_{crit}. In the original formulation $Ri_{crit} = 0.3$ (Large et al., 1994), but Ri_B can be difficult to compute in the field as this requires data for both vertical density and velocity shear profiles. In this study we prescribe MLD= 20 m, as this falls within the range of the MLD for field data

used to evaluate the model (see Section 4.2.2).

4.2.2 Field data

We compiled a dataset of vertical plastic concentration profiles collected within the surface mixing layer to validate the modelled concentration profiles (Table 4.1), with a total of 90 profiles with 741 data points. Only Kooi et al. (2016b) directly measured the rise velocity of a subsample of the collected microplastic particulates, and showed that these particles were positively buoyant. However, the presence of all the other sampled particulates near the open ocean surface indicates they are unlikely to be negatively buoyant. For all stations the wind speed was recorded and the MLD was determined from CTD data based on a temperature threshold (de Boyer Montégut et al., 2004). The majority of samples were collected in the North Atlantic (Kukulka et al., 2012; Kooi et al., 2016b; Pieper et al., 2019), and in regions with a relatively shallow MLD. Since wind-driven turbulent mixing isn't expected to influence the concentration depth profile below the MLD, we don't consider any measurements collected below 73 m. Measurements were collected with surface wind speeds up to 10.7 m s^{-1}, with the majority of sampled concentrations being collected for $u_{10} = 3.4-7.9$ m s^{-1} (535/741 data points).

Almost all measurements were collected with neuston nets, either multi-level nets simultaneously sampling fixed depth intervals (Kooi et al., 2016b) or using multi-stage nets that consecutively sample fixed depths or depth ranges (Kukulka et al. (2012); Egger et al. (2020); Amaral-Zettler (unpublished data)). These nets have mesh-sizes of 0.33 mm, and will generally sample high and medium ($w_{rise} = 0.03 - 0.003$ m s^{-1}) buoyancy particulates, which for non-biofouled polyethylene would have a diameter greater than the mesh size (2.2 and 0.4 mm). In contrast, low buoyancy particulates ($w_{rise} = 0.0003$ m s^{-1}) are typically not sampled in neuston nets (Kooi et al., 2016b), likely in part due to smaller particulate sizes. Pieper et al. (2019) filtered samples collected via Niskin bottles with a 0.8μm filter and thus was able to filter out smaller particulates with lower rise velocities.

All measured microplastic concentrations are normalized by total amount of plastic measured within a vertical profile. In order to compare the average normalized field concentration with the modelled profiles, we bin the normalized field concentrations into 0.5 m depth bins and calculate the standard deviation for each depth bin. Comparison of the modelled concentration profiles with the binned normalized field measurements is done via the root mean square error (RMSE):

$$RMSE = \sqrt{\frac{1}{n}\sum_{i=0}^{n}(C_{f,i} - C_{m,i})} \tag{4.13}$$

where $C_{f,i}$ and $C_{m,i}$ are the binned normalized field measurement and modelled concentration within depth bin i. Model evaluation for the low buoyancy particles is not possible with the available field measurements as low buoyancy particles are typically too small to be sampled with neuston nets, and the Pieper et al. (2019) dataset alone is too small.

4.3 Results

Starting with all particles at $z = 0$ for $t = 0$, M-0 models with both KPP and SWB diffusion lead to stable vertical concentration profiles (Fig. 4.2), where the equilibrium concentration profile is already established within 1 - 2 hours (Fig. 4.A.9). For both diffusion profiles, there is progressively deeper mixing of particles with increasing wind speeds and decreasing buoyancy.

Table 4.1: Overview of the sources of field measurements of microplastic concentration profiles. The uncertainty in the mean MLD is the standard deviation.

Source	Measurement Approach	Number of concentration profiles	Number of data points	Mean MLD [min max] (z)
Kooi et al. (2016b)	Neuston net	46	506	15.4±3.6 [10.0, 26.2]
Pieper et al. (2019)	Niskin bottles	12	152	17.1±5.5 [11.0, 28.0]
Kukulka et al. (2012)	Neuston net	13	47	24.3±8.9 [11.0, 45.1]
Egger et al. (2020)	Neuston net	16	20	55.8±19.2 [12.3, 72.8]
Amaral-Zettler (unpublished data)	Neuston net	3	16	17.8±4.8 [14.0, 26.0]
Total		90	741	17.5±8.8 [10.0, 72.8]

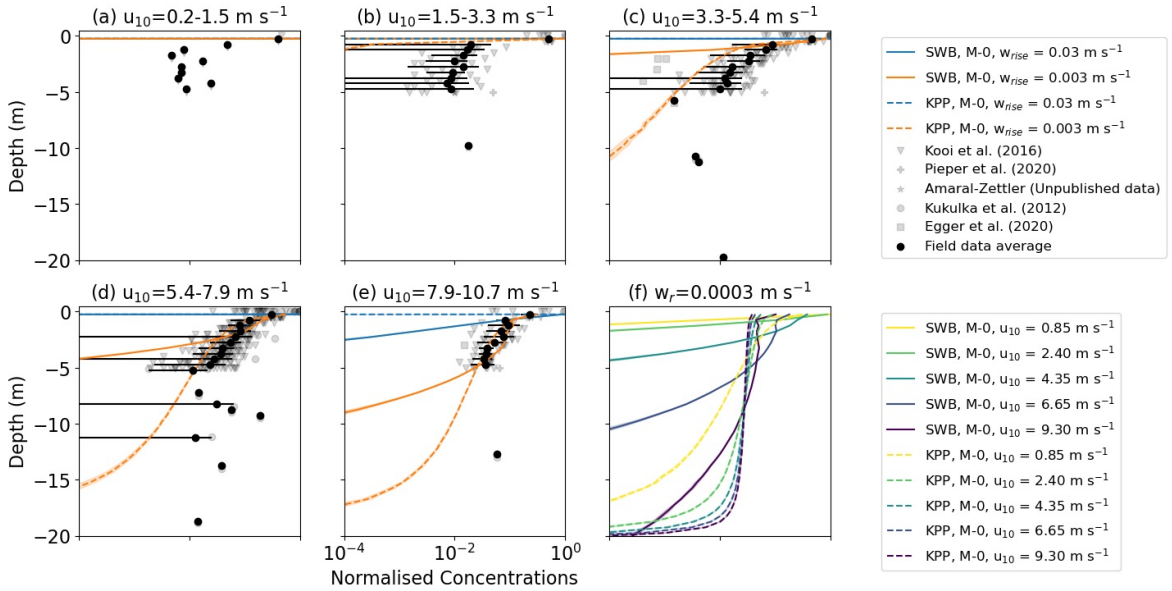

Figure 4.2: Vertical concentrations of buoyant particles for KPP and SWB diffusion using M-0 models. Subfigures (a) - (e) show the vertical concentration profiles for high and medium buoyancy particles with increasing wind speeds. The KPP profiles are calculated for $\theta = 1.0$ and z_0 according to Equation 4.12. The grey markers indicate field measurements, with darker shades indicating more measurements, while the binned field measurement average and standard deviation are shown by the black markers. Subfigure (f) shows the vertical concentration profiles for low buoyancy particles under increasing wind conditions. Shading around the profiles indicates the profile's standard deviation at each depth level.

While with both SWB and KPP diffusion low buoyancy particles always get mixed below the surface, for medium and high buoyancy particles there exist minimum wind speeds below which all particles remain at the surface. These limits are similar for both diffusion types for medium buoyancy particles ($u_{10} \geq 2.40$ m s^{-1}), but high buoyancy particles only mix below the surface with SWB diffusion if $u_{10} \geq 9.30$ m s^{-1}. However, once mixing below the ocean surface occurs, KPP diffusion always leads to deeper mixing of particles than SWB diffusion due to higher subsurface K_z values.

The concentration profiles for medium and low buoyancy particles are largely unaffected by reducing Δt below 30 seconds (Fig. 4.A.14). However, for high buoyancy particles with SWB diffusion the concentration profile more strongly depends on Δt due to the applied boundary condition. For $\Delta t = 30$ s, the M-0 model shows all particles remain near the ocean surface, but shorter Δt values indicate that deeper mixing of particles already occurs for $u_{10} = 6.65$ m s^{-1}. With KPP diffusion, all high buoyancy particles remain at the surface even with $\Delta t = 1$ second, as K_z at $z = 0$ remains too low to overcome the high rise velocity.

Even though KPP diffusion with $\theta = 1.0$ and z_0 following (Zhao & Li, 2019) predicts deeper

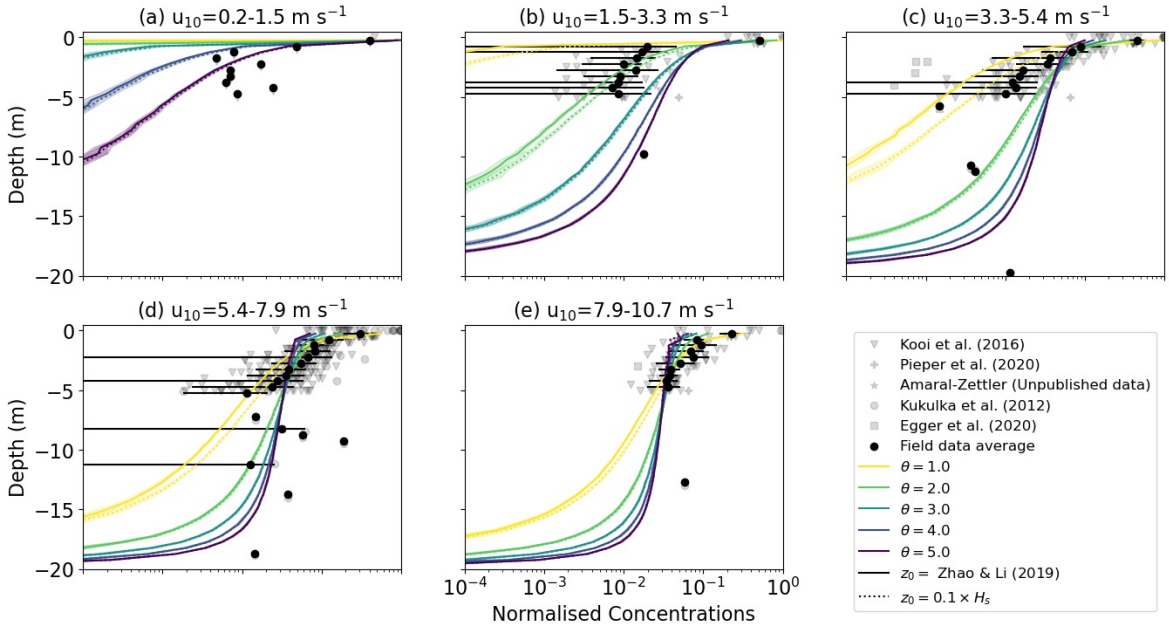

Figure 4.3: Vertical concentrations of buoyant particles for KPP diffusion using M-0 models for $w_r = 0.003$ m s^{-1}. The KPP profiles are calculated for $\theta = [1.0, 2.0, 3.0, 4.0, 5.0]$ and with either $z_0 = 0.1 \times H_s$ or according to Equation 4.12. The grey markers indicate field measurements, with darker shades indicating more measurements, while the binned field measurement average and standard deviation are shown by the black markers. Shading around the profiles indicates the profile's standard deviation at each depth level.

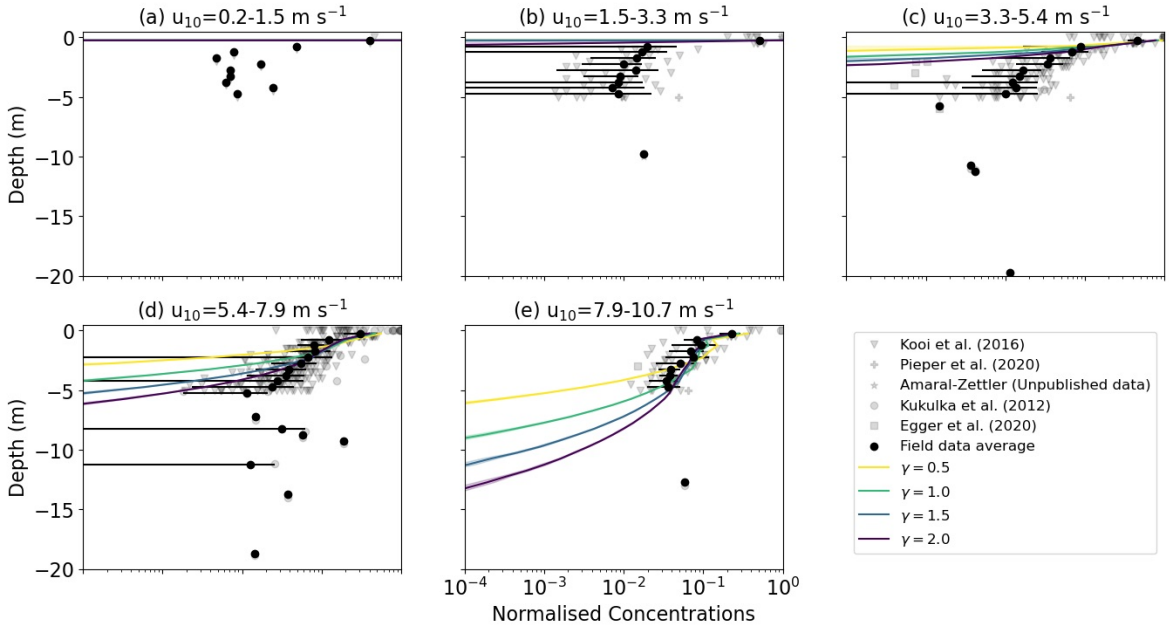

Figure 4.4: Vertical concentrations of buoyant particles for SWB diffusion under varying wind conditions with $w_r = 0.003$ m s^{-1}. The SWB diffusion profile is calculated with $\gamma \in [0.5, 1.0, 1.5, 2.0]$. The grey markers indicate field measurements, with darker shades indicating more measurements, while the binned field measurement average and standard deviation are shown by the black markers. Shading around the profiles indicates the profile's standard deviation at each depth level.

mixing of particles than with SWB diffusion ($\gamma = 1.0$), both approaches underpredict the mixing of particles relative to field observations. For KPP diffusion, this can be corrected by accounting for LC-driven mixing, which leads to deeper mixing of particles for both medium and low buoyancy particles (Figures 4.3 & 4.A.10). For medium buoyancy particles this generally leads to better model agreement with lower RMSE values between the modelled and averaged field data concentration profiles (Figure 4.5). However, for high buoyancy particles LC-driven circulation is not enough as particles remain at the ocean surface for all wind conditions even for $\theta = 5.0$ (Figure 4.A.11), as K_z for $z \approx 0$ is too low to overcome the inherent particle buoyancy. Only when LC-driven is combined with higher near-surface K_z values by setting $z_0 = 0.1 \times H_s$ do we see any below-surface mixing of high buoyancy particles when $\theta > 3.0$ and $u_{10} \geq 9.30$ m s^{-1}. Increased near-surface K_z values have a lesser influence on the concentration profiles of medium and low density particles, as these particles were already being mixed below the surface even without larger z_0 values. For SWB diffusion we obtain deeper mixing of all particles by increasing $\gamma > 1.0$ (Figures 4.4, 4.A.12 & 4.A.13), which improves model performance relative to observations (Figure 4.5). While increasing γ does not affect the peak magnitude of the near-surface K_z values, it increases the depth until which K_z is constant. This therefore results in stronger overall mixing (Figure 4.1), which in turn leads to the deeper mixing of the particles.

With both KPP and SWB diffusion, M-1 models show deeper mixing of particles as $\alpha \to 1$ (Fig. 4.6). Relative to the field measurements, M-1 models can at best slightly improve model performance over M-0 models (Fig. 4.7). However, improved model performance is not shown across all particle sizes and wind conditions, and there is not a consistent α value leading to the smallest RMSE values.

4.4 Discussion

The parametrizations presented in this study are intended for use in 3D Lagrangian experiments using OGCM data, and therefore should yield numerically stable results for the relatively large integration timesteps used in large-scale Lagrangian vertical transport modeling (Lobelle et al., 2021). While there are more stable schemes available than the EM scheme used in this study (Gräwe et al., 2012), the EM scheme is computationally the cheapest and yields concentration profiles that match reasonably well with observations. Both M-0 and M-1 models show largely convergent concentration profiles for $\Delta t = 30$ seconds, which would make both approaches feasible with regards to computational cost. However, we would currently recommend using a M-0 model. M-1 models have the additional tuning parameter α representing the autocorrelation of turbulent velocity fluctuations, which is poorly constrained in the literature. Using spatially invariant α values at best slightly improved model performance in comparison with M-0 models, and constraining α is not possible from these results. M-1 models may improve modeling of vertical diffusive transport, but more work is required to further constrain the value and vertical profile of α. Finally, numerous formulations of the M-1 drift term have been proposed (Brickman & Smith, 2002; Mofakham & Ahmadi, 2020, e.g.) which can lead to large differences in the modelled profiles. In this study we used the non-normalized Langevin equation from Mofakham & Ahmadi (2020), but other formulations could be explored in future work.

While the concentration profiles of medium and low buoyancy particles are unaffected by decreasing the integration timestep $\Delta t < 30$ seconds, using higher Δt values underestimates the depth to which high buoyancy particles are mixed when using SWB diffusion. This is because for high Δt values, the upward non-stochastic component of equation 4.6, which scales with Δt, dominates the stochastic component, which scales with $\sqrt{\Delta t}$. With KPP diffusion the vertical profile for high buoyancy particles appears unaffected by Δt, but this is because the near-surface K_z values are significantly lower than with SWB diffusion. One

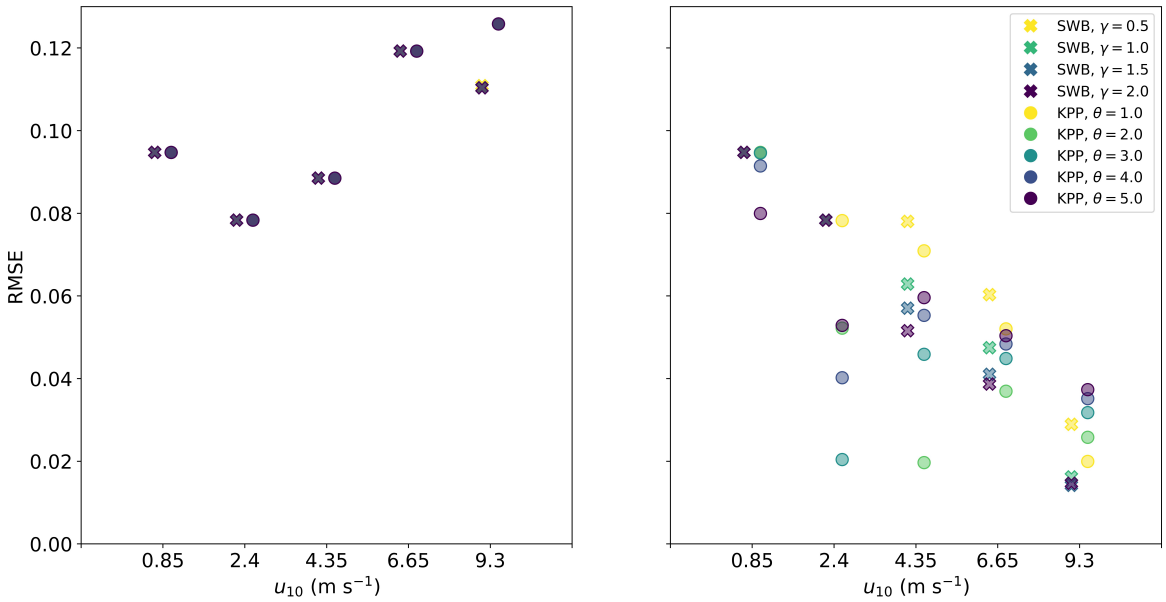

Figure 4.5: RMSE between field measurements and modelled concentration profiles for M-0 models with KPP and SWB diffusion under different wind conditions. All KPP diffusion simulations were with z_0 according to Equation 4.12.

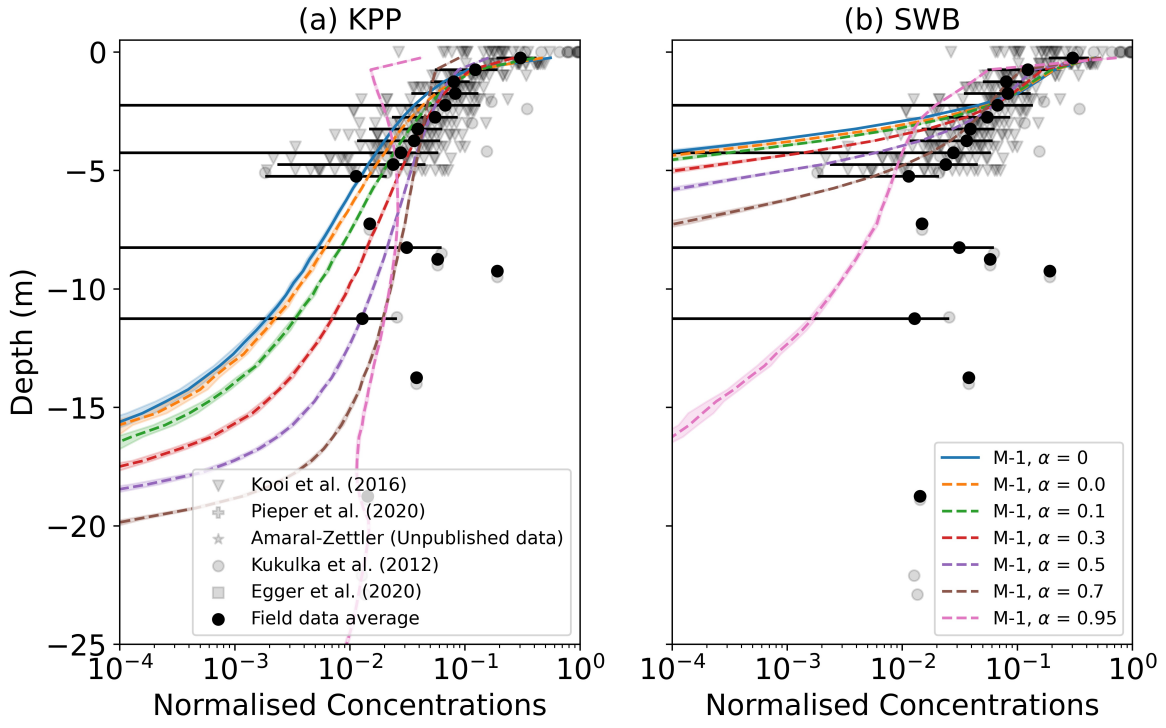

Figure 4.6: Vertical concentrations of buoyant particles for (a) KPP and (b) SWB diffusion using M-0 and M-1 models with varying values for α. The grey markers indicate field measurements, with darker shades indicating more measurements, while the binned field measurement average and standard deviation are shown by the black markers. Shading around the profiles indicates the profile's standard deviation at each depth level. The KPP profiles are for $\theta = 1.0$ and z_0 according to 4.12. All profiles are for $u_{10} = 6.65$ m s^{-1} and medium buoyancy particles ($w_{rise} = 0.003$ m s^{-1}).

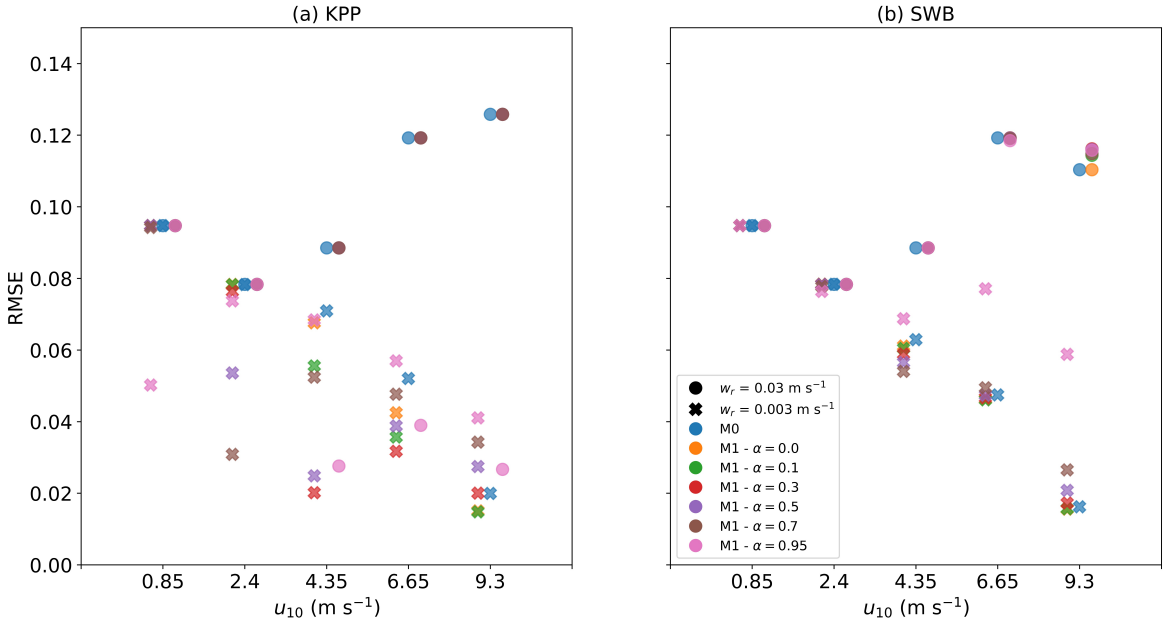

Figure 4.7: RMSE between field measurements and modelled concentration profiles for M-0 and M-1 models with (a) KPP and (b) SWB diffusion under different wind conditions and with varying values of α. All KPP diffusion simulations were with $\theta = 1.0$ and z_0 according to 4.12.

possibility to correct for this is to apply a different BC, such as a reflective BC. While the concentration profiles for medium and low buoyancy particles are not strongly affected by such a reflective BC (Fig. 4.A.15), the reflective BC does show deeper particle mixing with SWB diffusion. However, for $\Delta t = 30$ seconds the depth of mixing is now overestimated compared to smaller Δt values (Fig. 4.A.16), as with $\Delta t = 30$ seconds and $w_r = 0.03$ m s^{-1} the particle would be reflected up to 0.9 m below the ocean surface solely due to the model numerics. In addition, earlier studies have shown that reflecting BC can cause spurious increases in particle concentration near the boundary (Ross & Sharples, 2004; Nordam et al., 2019). Therefore, changing the BC to a reflective BC would not improve the concentration profiles of high buoyancy particles. Depending on the model application and setup, the error in the concentration profile depth ($\mathcal{O}(1)$ m for high buoyancy particles) might be acceptable. Otherwise, the error can be reduced by using a smaller integration timestep where that is computationally feasible.

Considering the KPP and SWB diffusion profiles, the results in this study are inconclusive with regards to which approach performs better relative to field observations. For high buoyancy particles, SWB diffusion leads to slightly deeper particle mixing, while only if the KPP diffusion profile accounts for LC-driven turbulence and has higher near-surface K_z values can it similarly show below-surface mixing of high buoyancy particles for $u_{10} \geq 9.30$ m s^{-1}. With medium and low buoyancy particles the KPP profile leads to much deeper mixing compared with SWB diffusion where $\gamma = 1.0$ (Poulain, 2020), especially when accounting for LC-driven turbulence, and this appears to agree better with field observations. However, for SWB diffusion the value of γ is uncertain, as Poulain (2020) and Kukulka et al. (2012) respectively define $\gamma = 1.0$ and $\gamma \approx 1.5$. Higher γ values leads to approximately equal model performance relative to field observations as with KPP diffusion. However, the model evaluation is largely based on field measurements collected in the top 5 m of the water column, and it is below this depth that we see greater differences in the KPP and SWB vertical concentration profiles. In addition, the currently available data collected with Neuston nets does not allow for model evaluation for the low-buoyancy particles in either scenario. As such, more field measurements (including smaller-sized particles) would be necessary to fully evaluate model performance for all particles

sizes with the two diffusion profiles.

With regards to necessary data to calculate the diffusion profiles, the SWB approach has the benefit that it only requires surface wind stress data, while KPP diffusion additionally requires MLD data. In addition, while our results indicate that accounting for LC-driven turbulent mixing improves KPP diffusion model performance, determining which θ value to use is not trivial. McWilliams & Sullivan (2000) demonstrated that θ is inversely proportional to the Langmuir number La, which is defined as $La = \sqrt{u_{*w}/U_S}$ with U_S as the surface Stokes drift. The Langmuir number can conceivably be calculated using OGCM data, but the details of such an implementation will be left for future work with 3D Lagrangian models. However, KPP diffusion does have the advantage that it has been widely used and validated in various model setups (Large et al., 1994; McWilliams & Sullivan, 2000; Boufadel et al., 2020), while such extensive validation has not yet occured for SWB diffusion. Finally, the influence of wind forcing on turbulence is generally assumed to be limited to the surface mixed layer (Chamecki et al., 2019), while with the SWB profile wind-generated turbulence can extend far below the MLD (Figures 4.1 & 4.4), possibly overestimating turbulent mixing at such depths. KPP theory does limit wind-driven turbulent mixing to the surface mixed layer, while either a constant K_z value or other K_z profiles could be used for sub-MLD mixing, such as the K_z estimates for internal tide mixing as proposed by de Lavergne et al. (2020).

Ideally, KPP theory would be expanded to account for surface wave breaking, which could lead to higher near-surface K_z values as seen with MLD diffusion. While such a theoretical approach is beyond the scope of this paper, we show that artificially elevating near-surface K_z values by increasing the surface roughness z_0 has a smaller influence on the overall concentration profile than LC-driven mixing, as similarly shown by Brunner et al. (2015). Therefore, although we recommend future work incorporating surface wave breaking into KPP theory, our current KPP diffusion approach representing LC-driving mixing through θ does already seem to capture the majority of turbulent mixing dynamics.

In all cases, the vertical concentration profiles stabilized to vertical equilibrium profiles, similar to what has been shown for buoyant particles in LES model studies (Liang et al., 2012; Yang et al., 2014; Brunner et al., 2015; Taylor, 2018). The modelled concentration profiles generally resembled the profiles from field measurements of microplastic concentrations under different wind conditions (Kukulka et al., 2012; Kooi et al., 2016b), but the averaged concentration profiles of the field measurements are quite noisy. Partly, this could be due to inhomogeneity in the particle buoyancy, as the collected microplastic particulates have varying sizes and rise velocities (Kooi et al., 2016b; Egger et al., 2020). Additionally, we sorted the field measurements based on wind conditions, but other underlying oceanographic conditions such as the MLD can still vary significantly even with similar wind speeds. Unfortunately, we lack additional data of the oceanographic conditions at the of sampling, which currently prohibits more high-level comparisons of the field and model concentration profiles. Compared with the field data, the variance in the modelled concentration profiles is significantly smaller. This is in part also due to assuming constant environmental conditions over 12 hours for the model simulations, while wind and other oceanographic conditions can change on much shorter timescales over the ocean surface. To further improve vertical transport model verification, more measurements would be required, covering a wider range of oceanographic conditions (such as for wind conditions higher than $u_{10} = 10.7$ m s^{-1}) and with a high spatial sampling resolution also for depths $z < -5$m. Ideally these measurements would also sample small, neutrally buoyant particulates, but we acknowledge this is difficult with the sampling techniques commonly used today. At the same time, we would encourage conducting more ocean field measurements of near-surface vertical eddy diffusion coefficient and/or eddy viscosity profiles, as this will allow further validation of the K_z profiles predicted by the KPP and SWB theory with actual ocean near-surface mixing measurements.

The parameterizations have been validated for high/medium rise velocities, and at least for KPP diffusion with $\theta > 1.0$ the concentration profiles resemble those calculated from field observations. This provides confidence in the turbulence estimates from the KPP approach, and as these are independent of the type of particle that might be present, this would suggest the KPP approach can also be applied to to neutral or negatively buoyant particles. However, as model verification was only possible for microplastic particulates with rise velocities approximately between 0.03 - 0.003 m s^{-1}, we would advise additional model verification for other particle types where the necessary field data is available. In the case of SWB diffusion, turbulent mixing seems underestimated when further from the ocean surface when $\gamma = 1.0$, but increasing to $\gamma = 1.5 - 2.0$ does correct for this. However, as SWB diffusion has not yet been as extensively tested and verified as KPP diffusion, we advice more caution and additional validation with field observations before applying this diffusion approach to other particle types.

4.5 Conclusion

We have developed a number of 1D surface-mixing parametrizations designed to be readily applied in large-scale oceanic Lagrangian model experiments using OGCM data. Where possible, we would recommend using the turbulence fields from the OGCM to assure turbulent transport of the particles is consistent with that of other model tracers. However, if the turbulence fields are unavailable then particularly parametrizations with KPP diffusion with LC-driven mixing are shown to produce modelled vertical concentration profiles that match relatively well with field observations of microplastics. The parametrizations generally perform well for timesteps of $\Delta t = 30$ seconds, but for high buoyancy particles users need to take care to use sufficiently short timesteps, especially with SWB diffusion. Verification was only possible for positively buoyant particles larger than 0.33 mm (which generally have rise velocities ≤ 0.003 m s^{-1}), but the parametrizations should also be applicable to other particle types. The parametrizations can therefore be applied to investigate the influence of turbulent mixing on the vertical transport of (microplastic) particles within a 3D model setup, and ultimately gain a more complete understanding of the fate of such particles in the ocean.

Acknowledgements

VO and CL acknowledge support from the Swiss National Science Foundation (project PZ00P2_174124 Global interactions between microplastics and marine ecosystems). EvS was supported by the European Research Council (ERC) under the European Unions Horizon 2020 research and innovation programme (grant agreement No 715386). Calculations were performed on UBELIX (http://www.id.unibe.ch/hpc), the HPC cluster at the University of Bern. We would like to thank Dr. Tobias Kukulka, Dr. Catharina Pieper, Dr. Matthias Egger, Dr. Linda Amaral-Zettler and Dr. Erik Zettler for providing field measurements, Dr. Marie Poulain-Zarcos for providing data on vertical mixing, and Dr. Thomas Stocker and Daan Reijnders for fruitful discussions regarding the Markov-1 numerical schemes.

Author contributions

Development of the parametrizations and the analysis was done by VO, with CL helping with improving the code performance. The manuscript was written by VO, with extensive input from CL and EvS. Everyone contributed to the study design and discussion of the analysis.

Code availability

The code for the 1D model, the subsequent analysis and all figures is available at zenodo (Onink, 2021). The field data for Kooi et al. (2016b) is available at figshare (Kooi et al., 2016a). For the field data from Kukulka et al. (2012), Pieper et al. (2019), Egger et al. (2020) and Amaral-Zettler (unpublished data), please contact the corresponding authors of the respective studies.

4.A Supplementary material

4.A.1 w_r/w' ratios for various turbulence scenarios

Table 4.A.2: Ratios w_r/w' between the rise velocity w_r and the peak stochastic velocity perturbation w' for KPP and SWB diffusion. The peak w' is the maximum value of Equation 4.3. The peak w' values for KPP diffusion are calculated for $\theta \in [1.0, 3.0, 5.0]$ and for z_0 following Equation 4.12. The peak w' values for SWB diffusion are independent of γ.

Wind Speed (m s^{-1})	Diffusion Type	$w_r = 0.03$ m s^{-1}	$w_r = 0.003$ m s^{-1}	$w_r = 0.0003$ m s^{-1}
0.85	KPP, $\theta = 1.0$	1.818	0.182	0.018
	KPP, $\theta = 3.0$	1.055	0.106	0.011
	KPP, $\theta = 5.0$	0.818	0.082	0.008
	SWB	10.512	1.051	0.105
2.40	KPP, $\theta = 1.0$	1.087	0.109	0.011
	KPP, $\theta = 3.0$	0.628	0.063	0.006
	KPP, $\theta = 5.0$	0.486	0.049	0.005
	SWB	4.077	0.408	0.041
4.35	KPP, $\theta = 1.0$	0.808	0.081	0.008
	KPP, $\theta = 3.0$	0.465	0.047	0.005
	KPP, $\theta = 5.0$	0.359	0.036	0.004
	SWB	1.753	0.175	0.018
6.65	KPP, $\theta = 1.0$	0.654	0.065	0.007
	KPP, $\theta = 3.0$	0.373	0.037	0.004
	KPP, $\theta = 5.0$	0.288	0.029	0.003
	SWB	0.935	0.094	0.009
9.30	KPP, $\theta = 1.0$	0.553	0.055	0.006
	KPP, $\theta = 3.0$	0.313	0.031	0.003
	KPP, $\theta = 5.0$	0.241	0.024	0.002
	SWB	0.566	0.057	0.006

4.A.2 Influence of z_0 on diffusion profiles

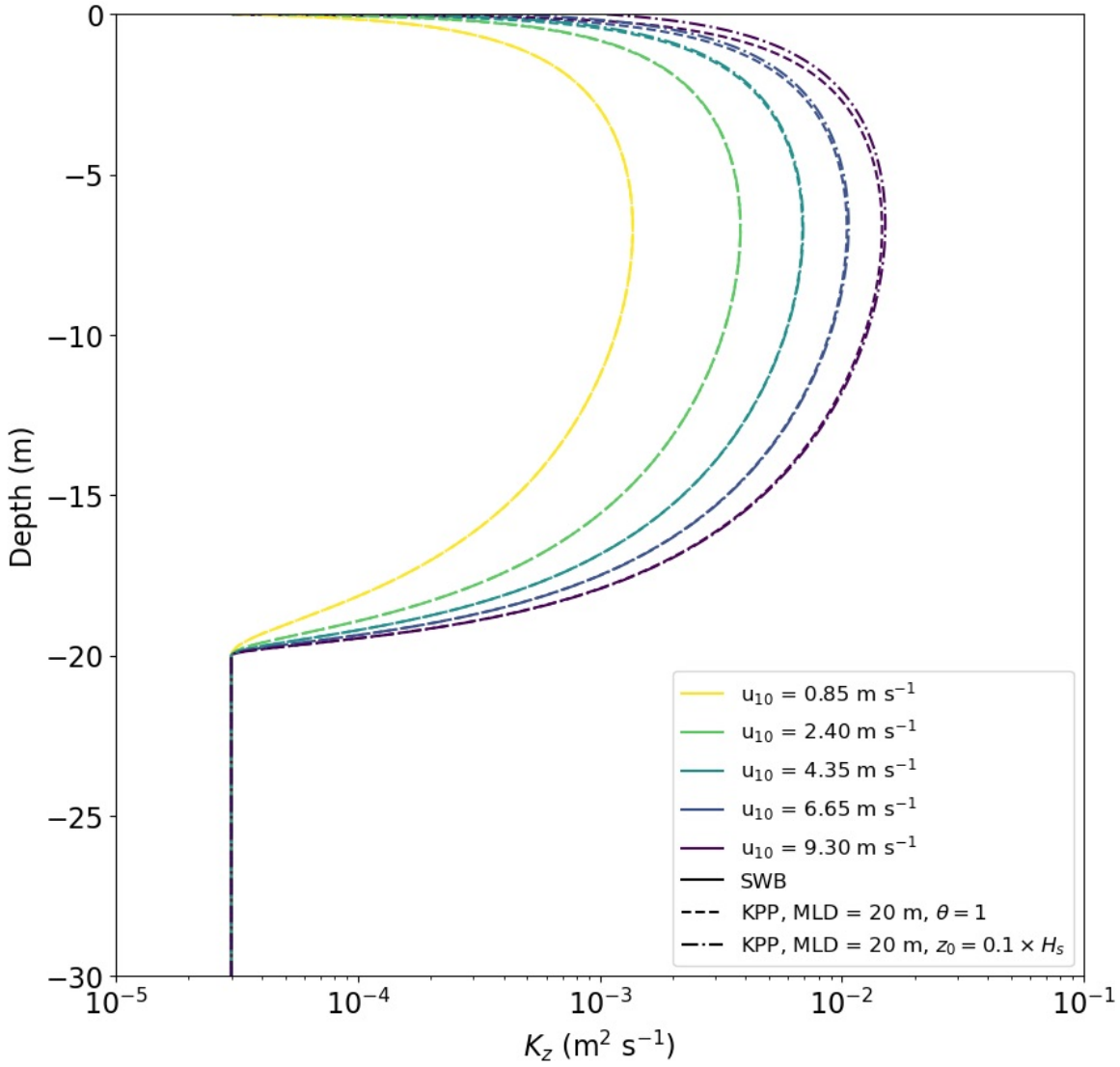

Figure 4.A.8: Vertical diffusion coefficient profiles for KPP diffusion under varying wind conditions with $\theta = 1.0$. The KPP diffusion profile is calculated either with z_0 according to Equation 4.12 or $z_0 = 0.1 \times H_s$.

4.A.3 Time evolution of concentration profiles

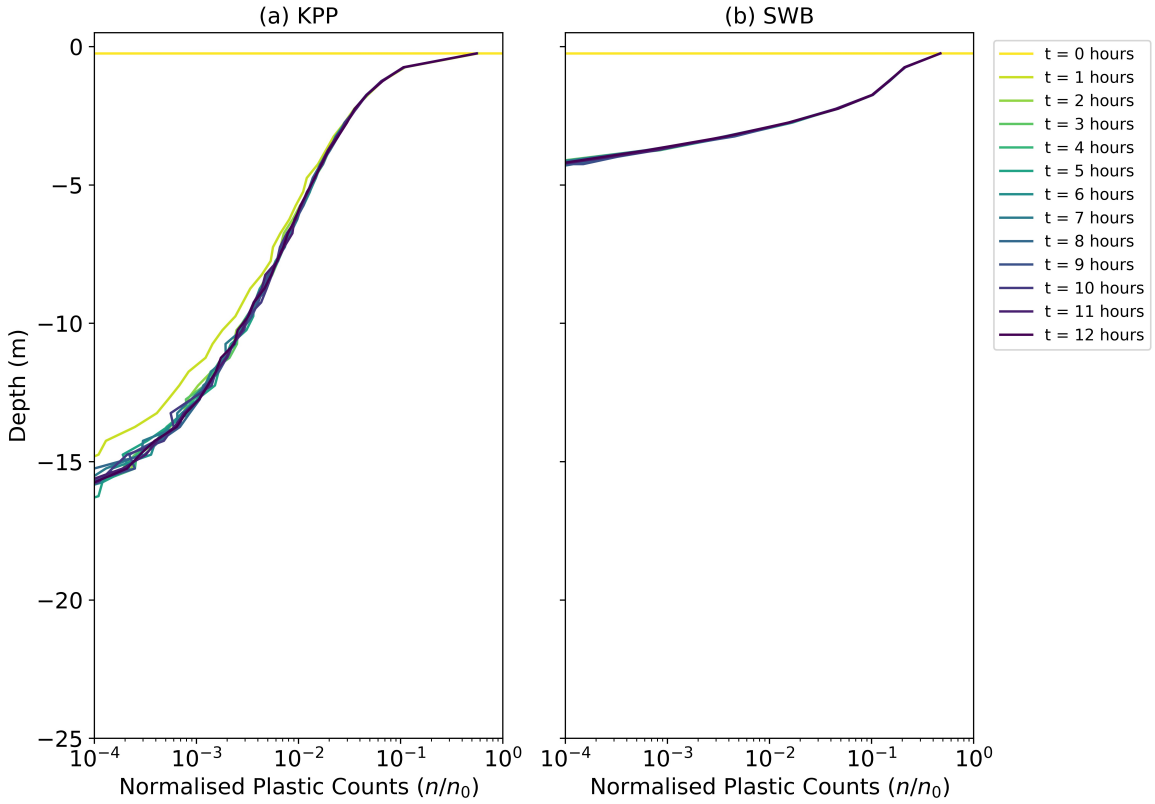

Figure 4.A.9: Vertical concentrations of buoyant particles for KPP diffusion at times $t = 0 - 12$ hours. The KPP diffusion profile is calculated with $\theta = 1.0$, $u_{10} = 6.65$ m s^{-1}, and z_0 according to Equation 4.12.

4.A.4 Influence of θ for KPP diffusion

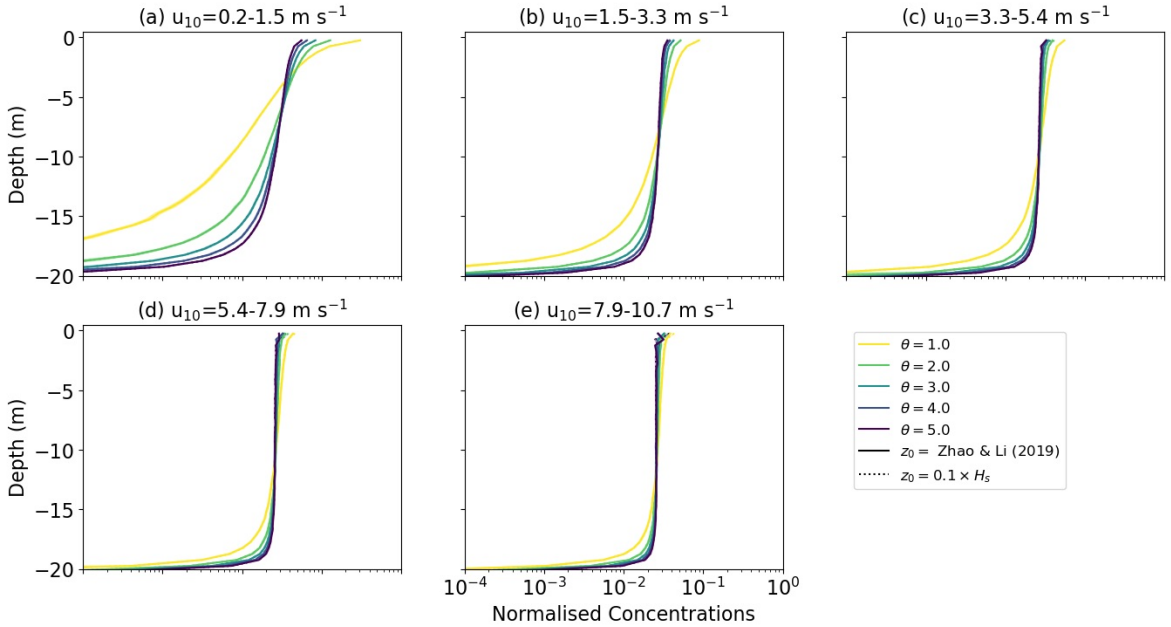

Figure 4.A.10: Vertical concentrations of buoyant particles for KPP diffusion under varying wind conditions with $w_r = 0.0003$ m s^{-1}. The KPP diffusion profile is calculated either with z_0 according to Equation 4.12 or $z_0 = 0.1 \times H_s$, and for $\theta \in [1.0, 2.0, 3.0, 4.0, 5.0]$. The grey markers indicate field measurements, with darker shades indicating more measurements, while the binned field measurement average and standard deviation are shown by the black markers. Shading around the profiles indicates the profile's standard deviation at each depth level.

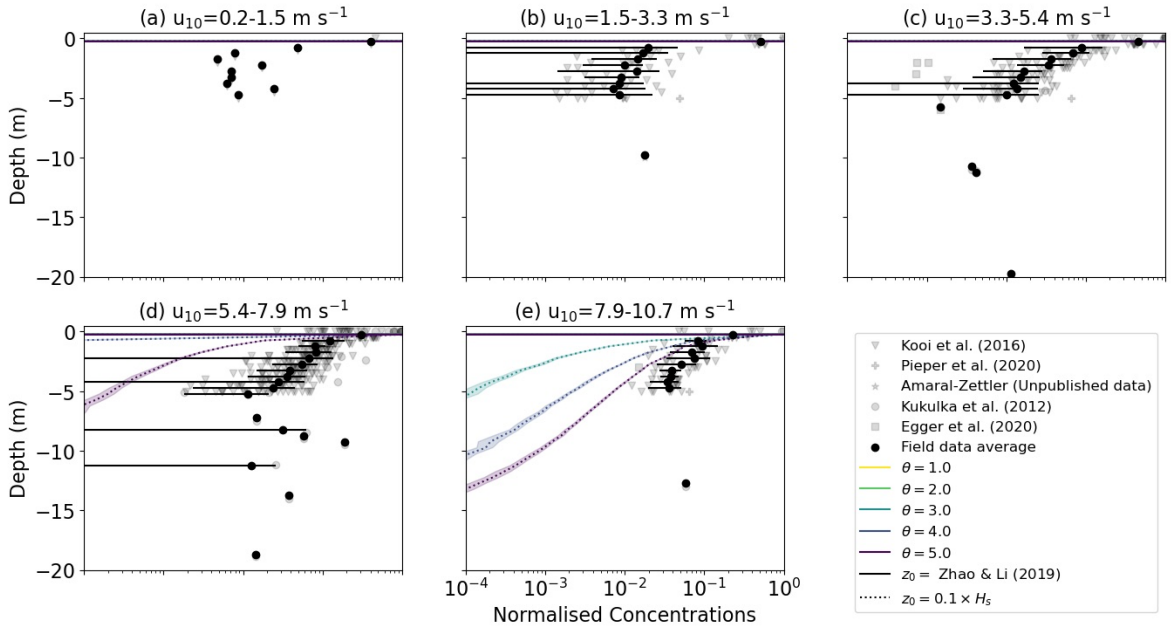

Figure 4.A.11: Vertical concentrations of buoyant particles for KPP diffusion under varying wind conditions with $w_r = 0.03$ m s^{-1}. The KPP diffusion profile is calculated either with z_0 according to Equation 4.12 or $z_0 = 0.1 \times H_s$, and for $\theta \in [1.0, 2.0, 3.0, 4.0, 5.0]$. The grey markers indicate field measurements, with darker shades indicating more measurements, while the binned field measurement average and standard deviation are shown by the black markers. Shading around the profiles indicates the profile's standard deviation at each depth level.

4.A.5 Influence of γ for SWB diffusion

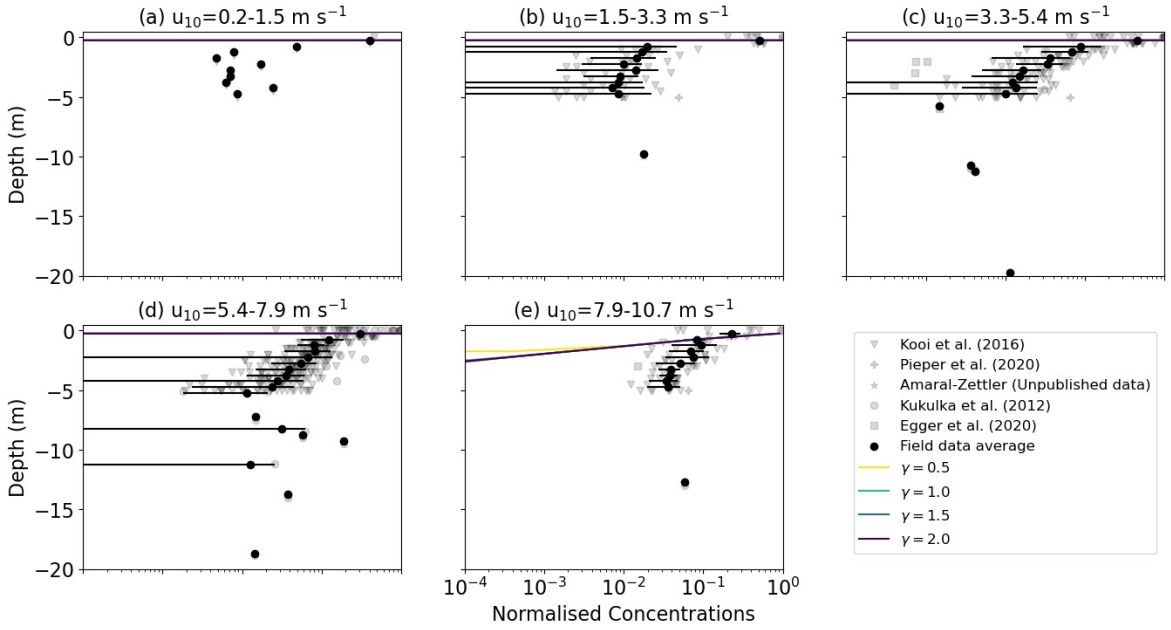

Figure 4.A.12: Vertical concentrations of buoyant particles for SWB diffusion under varying wind conditions with $w_r = 0.0003$ m s^{-1}. The SWB diffusion profile is calculated with $\gamma \in [0.5, 1.0, 1.5, 2.0]$. The grey markers indicate field measurements, with darker shades indicating more measurements, while the binned field measurement average and standard deviation are shown by the black markers. Shading around the profiles indicates the profile's standard deviation at each depth level.

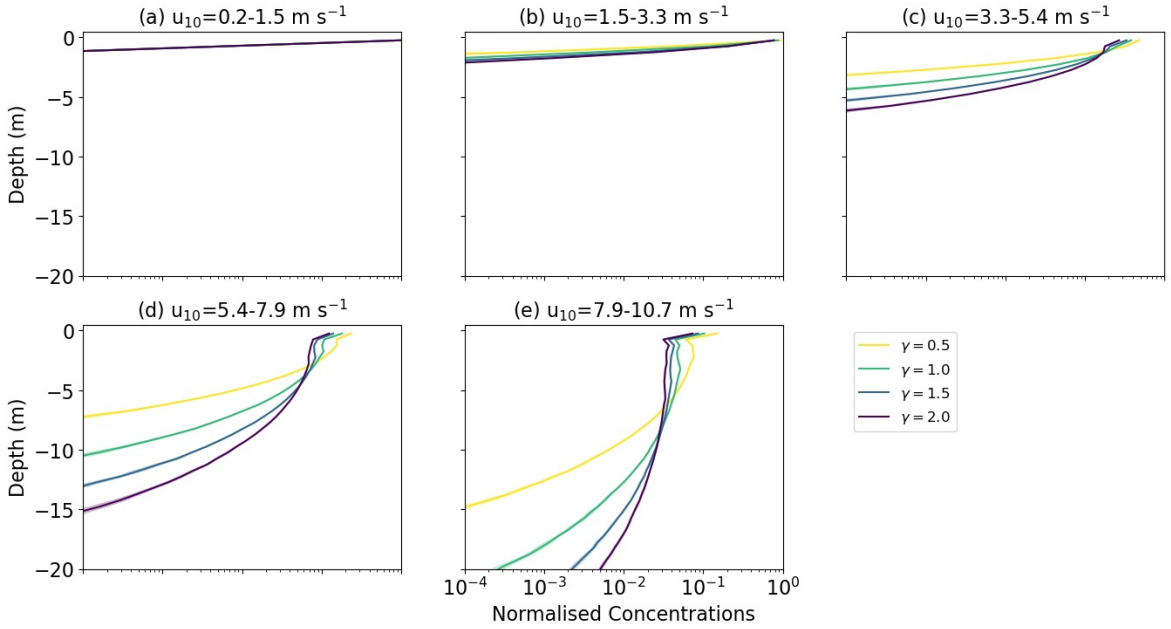

Figure 4.A.13: Vertical concentrations of buoyant particles for KPP diffusion under varying wind conditions with $w_r = 0.03$ m s^{-1}. The SWB diffusion profile is calculated with $\gamma \in [0.5, 1.0, 1.5, 2.0]$. The grey markers indicate field measurements, with darker shades indicating more measurements, while the binned field measurement average and standard deviation are shown by the black markers. Shading around the profiles indicates the profile's standard deviation at each depth level.

4.A.6 Influence of Δt

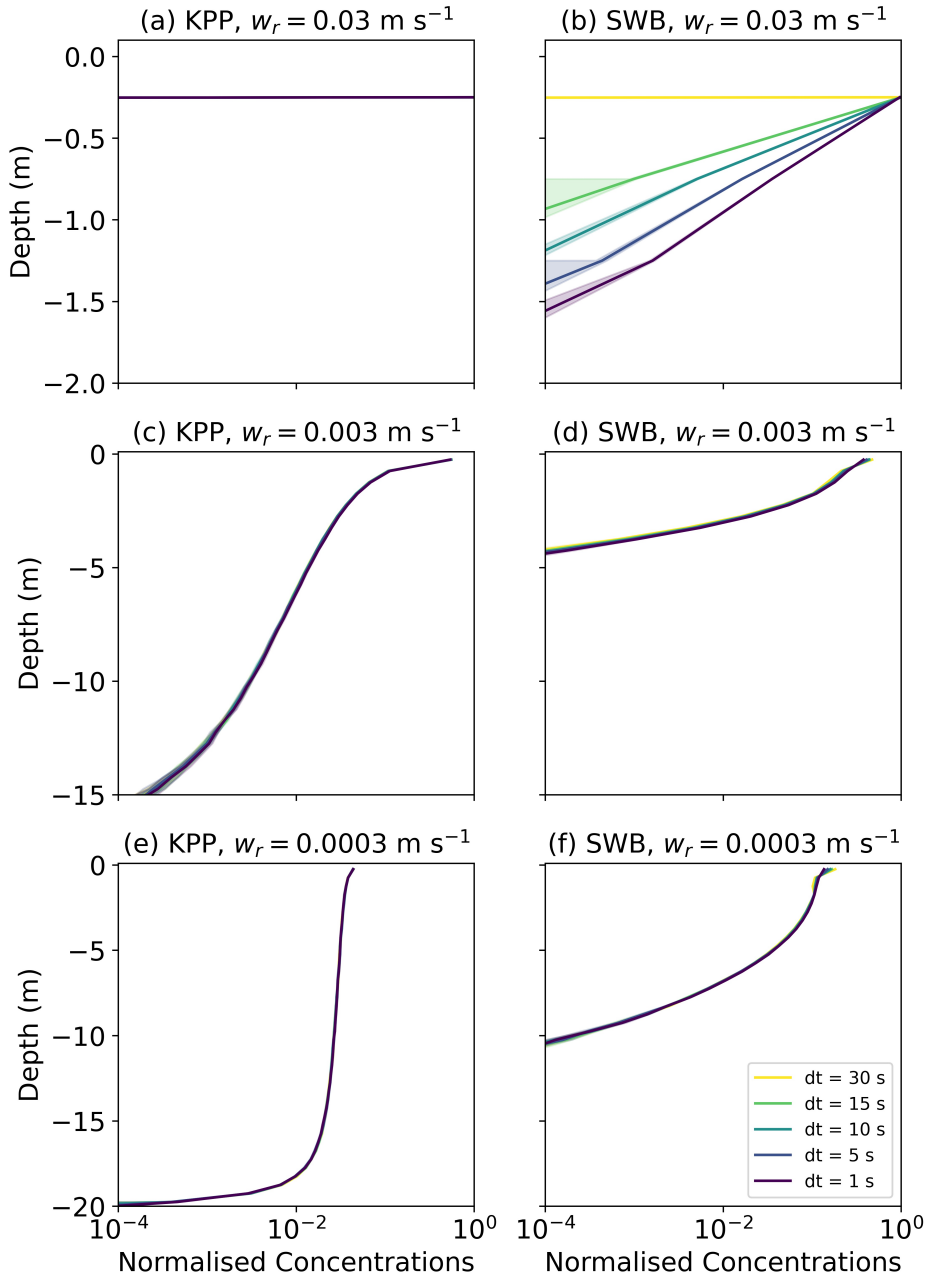

Figure 4.A.14: Vertical concentrations of buoyant particles for (a, c, e) KPP and (b, d, f) SWB diffusion using M-0 models with varying values for w_{rise} and $\Delta t \in [30, 15, 10, 5, 1]$ second(s). All profiles are for $u_{10} = 6.65$ m s^{-1}. Shading around the profiles indicates the profile's standard deviation at each depth level. The KPP profiles are computed with $\theta = 1.0$ and z_0 according to Equation 4.12, while the SWB profile is computed with $\gamma = 1.0$.

4.A.7 Influence of boundary conditions

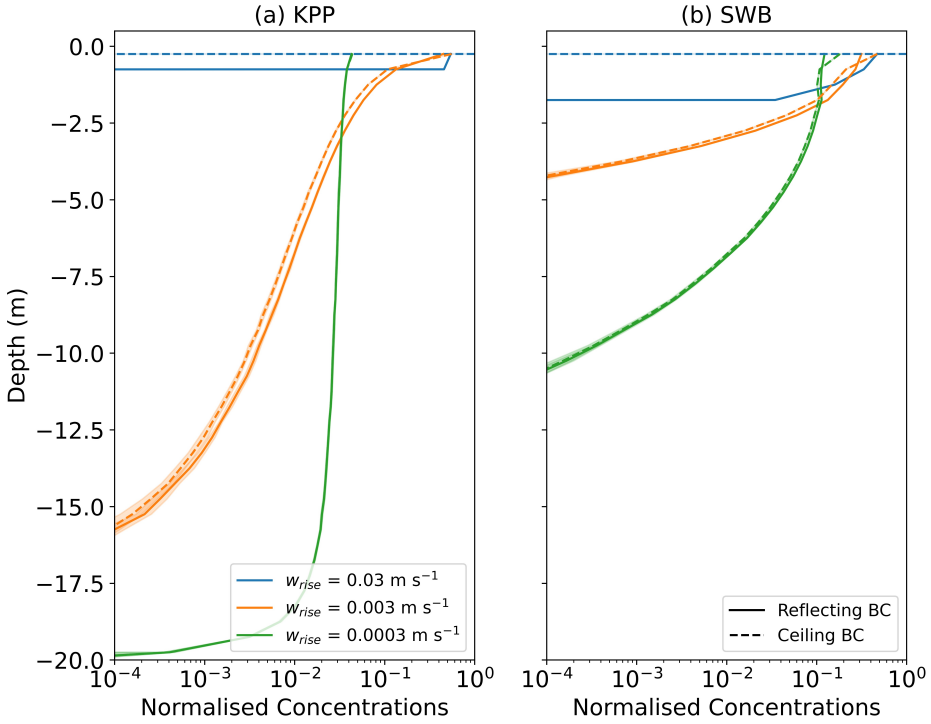

Figure 4.A.15: Vertical concentrations of buoyant particles for (a) KPP and (b) SWB diffusion using M-0 models for reflective and ceiling BC's. Shading around the profiles indicates the profile's standard deviation at each depth level. All profiles are for $u_{10} = 6.65$ m s^{-1}. The KPP profiles are computed with $\theta = 1.0$ and z_0 according to Equation 4.12, while the SWB profile is computed with $\gamma = 1.0$.

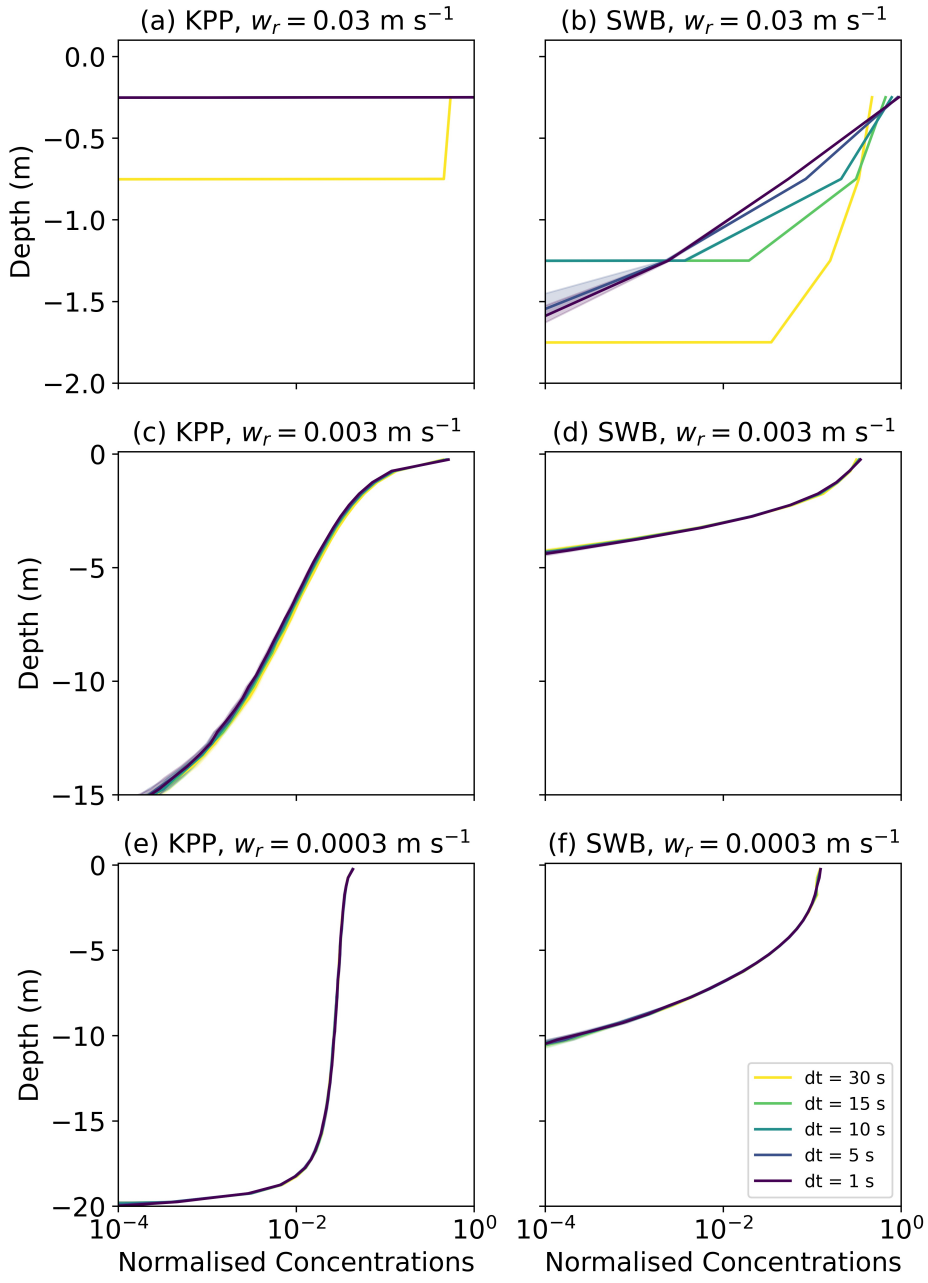

Figure 4.A.16: Vertical concentrations of buoyant particles for (a, c, e) KPP and (b, d, f) SWB diffusion using M-0 models with varying values for w_{rise} and $\Delta t \in [30, 15, 10, 5, 1]$ second(s) with a reflective BC. All profiles are for $u_{10} = 6.65$ m s^{-1}. Shading around the profiles indicates the profile's standard deviation at each depth level. The KPP profiles are computed with $\theta = 1.0$ and z_0 according to Equation 4.12, while the SWB profile is computed with $\gamma = 1.0$.

Bibliography

Berloff, P. S. & McWilliams, J. C., 2003. Material transport in oceanic gyres. part iii: Randomized stochastic models, *Journal of physical oceanography*, 33(7), 1416–1445.

Boufadel, M., Liu, R., Zhao, L., Lu, Y., Özgökmen, T., Nedwed, T., & Lee, K., 2020. Transport of oil droplets in the upper ocean: impact of the eddy diffusivity, *Journal of Geophysical Research: Oceans*, 125(2), e2019JC015727.

Brickman, D. & Smith, P., 2002. Lagrangian stochastic modeling in coastal oceanography, *Journal of atmospheric and oceanic technology*, 19(1), 83–99.

Brignac, K. C., Jung, M. R., King, C., Royer, S.-J., Blickley, L., Lamson, M. R., Potemra, J. T., & Lynch, J. M., 2019. Marine debris polymers on main hawaiian island beaches, sea surface, and seafloor, *Environmental science & technology*, 53(21), 12218–12226.

Brunner, K., Kukulka, T., Proskurowski, G., & Law, K. L., 2015. Passive buoyant tracers in the ocean surface boundary layer: 2. observations and simulations of microplastic marine debris, *Journal of Geophysical Research: Oceans*, 120(11), 7559–7573.

Chamecki, M., Chor, T., Yang, D., & Meneveau, C., 2019. Material transport in the ocean mixed layer: recent developments enabled by large eddy simulations, *Reviews of Geophysics*, 57(4), 1338–1371.

Choy, C. A., Robison, B. H., Gagne, T. O., Erwin, B., Firl, E., Halden, R. U., Hamilton, J. A., Katija, K., Lisin, S. E., Rolsky, C., et al., 2019. The vertical distribution and biological transport of marine microplastics across the epipelagic and mesopelagic water column, *Scientific reports*, 9(1), 1–9.

Craig, P. D. & Banner, M. L., 1994. Modeling wave-enhanced turbulence in the ocean surface layer, *Journal of Physical Oceanography*, 24(12), 2546–2559.

de Boyer Montégut, C., Madec, G., Fischer, A. S., Lazar, A., & Iudicone, D., 2004. Mixed layer depth over the global ocean: An examination of profile data and a profile-based climatology, *Journal of Geophysical Research: Oceans*, 109(C12).

de Lavergne, C., Vic, C., Madec, G., Roquet, F., Waterhouse, A. F., Whalen, C., Cuypers, Y., Bouruet-Aubertot, P., Ferron, B., & Hibiya, T., 2020. A parameterization of local and remote tidal mixing, *Journal of Advances in Modeling Earth Systems*, 12(5), e2020MS002065.

Delandmeter, P. & Sebille, E. v., 2019. The parcels v2. 0 lagrangian framework: new field interpolation schemes, *Geoscientific Model Development*, 12(8), 3571–3584.

Denman, K. & Gargett, A., 1983. Time and space scales of vertical mixing and advection of phytoplankton in the upper ocean, *Limnology and oceanography*, 28(5), 801–815.

Egger, M., Sulu-Gambari, F., & Lebreton, L., 2020. First evidence of plastic fallout from the north pacific garbage patch, *Scientific reports*, 10(1), 1–10.

Enders, K., Lenz, R., Stedmon, C. A., & Nielsen, T. G., 2015. Abundance, size and polymer composition of marine microplastics ≤ 10 μm in the atlantic ocean and their modelled vertical distribution, *Marine pollution bulletin*, 100(1), 70–81.

Fernando, H. J., 1991. Turbulent mixing in stratified fluids, *Annual review of fluid mechanics*, 23(1), 455–493.

Fischer, R., Lobelle, D., Kooi, M., Koelmans, A., Onink, V., Laufkötter, C., Amaral-Zettler, L., Yool, A., & van Sebille, E., 2021. Modeling submerged biofouled microplastics and their vertical trajectories, *Biogeosciences Discussions*, pp. 1–29.

Gaspar, P., Grégoris, Y., & Lefevre, J.-M., 1990. A simple eddy kinetic energy model for simulations of the oceanic vertical mixing: Tests at station papa and long-term upper ocean study site, *Journal of Geophysical Research: Oceans*, 95(C9), 16179–16193.

Gräwe, U., Deleersnijder, E., Shah, S. H. A. M., & Heemink, A. W., 2012. Why the euler scheme in particle tracking is not enough: the shallow-sea pycnocline test case, *Ocean Dynamics*, 62(4), 501–514.

Hopfinger, E. & Toly, J.-A., 1976. Spatially decaying turbulence and its relation to mixing across density interfaces, *Journal of fluid mechanics*, 78(1), 155–175.

Kaiser, D., Kowalski, N., & Waniek, J. J., 2017. Effects of biofouling on the sinking behavior of microplastics, *Environmental Research Letters*, 12(12), 124003.

Kooi, M., Reisser, J., Slat, B., Ferrari, F., Schmid, M., Cunsolo, S., Brambini, R., Noble, K., Sirks, L.-A., Linders, T. E., Schoeneich-Argent, R. I., & Koelmans, A. A., 2016a. Data from 'the effect of particle properties on the depth profile of buoyant plastics in the ocean'.

Kooi, M., Reisser, J., Slat, B., Ferrari, F. F., Schmid, M. S., Cunsolo, S., Brambini, R., Noble, K., Sirks, L.-A., Linders, T. E., et al., 2016b. The effect of particle properties on the depth profile of buoyant plastics in the ocean, *Scientific reports*, 6(1), 1–10.

Kukulka, T. & Brunner, K., 2015. Passive buoyant tracers in the ocean surface boundary layer: 1. influence of equilibrium wind-waves on vertical distributions, *Journal of Geophysical Research: Oceans*, 120(5), 3837–3858.

Kukulka, T. & Veron, F., 2019. Lagrangian investigation of wave-driven turbulence in the ocean surface boundary layer, *Journal of Physical Oceanography*, 49(2), 409–429.

Kukulka, T., Proskurowski, G., Morét-Ferguson, S., Meyer, D., & Law, K., 2012. The effect of wind mixing on the vertical distribution of buoyant plastic debris, *Geophysical Research Letters*, 39(7).

Landahl, M. T. & Christensen, E. M., 1998. *Turbulence and random processes in fluid mechanics*, Cambridge University Press.

Large, W. & Pond, S., 1981. Open ocean momentum flux measurements in moderate to strong winds, *Journal of physical oceanography*, 11(3), 324–336.

Large, W. G., McWilliams, J. C., & Doney, S. C., 1994. Oceanic vertical mixing: A review and a model with a nonlocal boundary layer parameterization, *Reviews of geophysics*, 32(4), 363–403.

Law, K. L., Morét-Ferguson, S. E., Goodwin, D. S., Zettler, E. R., DeForce, E., Kukulka, T., & Proskurowski, G., 2014. Distribution of surface plastic debris in the eastern pacific ocean from an 11-year data set, *Environmental science & technology*, 48(9), 4732–4738.

Lebreton, L., Slat, B., Ferrari, F., Sainte-Rose, B., Aitken, J., Marthouse, R., Hajbane, S., Cunsolo, S., Schwarz, A., Levivier, A., et al., 2018. Evidence that the great pacific garbage patch is rapidly accumulating plastic, *Scientific reports*, 8(1), 1–15.

Liang, J.-H., McWilliams, J. C., Sullivan, P. P., & Baschek, B., 2012. Large eddy simulation of the bubbly ocean: New insights on subsurface bubble distribution and bubble-mediated gas transfer, *Journal of Geophysical Research: Oceans*, 117(C4).

Liubartseva, S., Coppini, G., Lecci, R., & Clementi, E., 2018. Tracking plastics in the mediterranean: 2d lagrangian model, *Marine pollution bulletin*, 129(1), 151–162.

Lobelle, D., Kooi, M., Koelmans, A. A., Laufkötter, C., Jongedijk, C. E., Kehl, C., & van Sebille, E., 2021. Global modeled sinking characteristics of biofouled microplastic, *Journal of Geophysical Research: Oceans*, 126(4), e2020JC017098.

Maruyama, G., 1955. Continuous markov processes and stochastic equations, *Rendiconti del Circolo Matematico di Palermo*, 4(1), 48.

McWilliams, J. C. & Sullivan, P. P., 2000. Vertical mixing by langmuir circulations, *Spill Science & Technology Bulletin*, 6(3-4), 225–237.

Mofakham, A. A. & Ahmadi, G., 2020. On random walk models for simulation of particle-laden turbulent flows, *International Journal of Multiphase Flow*, 122, 103157.

Nordam, T., Kristiansen, R., Nepstad, R., & Röhrs, J., 2019. Numerical analysis of boundary conditions in a lagrangian particle model for vertical mixing, transport and surfacing of buoyant particles in the water column, *Ocean Modelling*, 136, 107–119.

Onink, V., 2021. Model and analysis code for: "empirical lagrangian parametrization for wind-driven mixing of buoyant particulates at the ocean surface".

Onink, V., Wichmann, D., Delandmeter, P., & van Sebille, E., 2019. The role of ekman currents, geostrophy, and stokes drift in the accumulation of floating microplastic, *Journal of Geophysical Research: Oceans*, 124(3), 1474–1490.

Onink, V., Jongedijk, C. E., Hoffman, M. J., van Sebille, E., & LaufkÃ¶tter, C., 2021. Global simulations of marine plastic transport show plastic trapping in coastal zones, *Environmental Research Letters*, 16(6), 064053.

Paris, C. B., Atema, J., Irisson, J.-O., Kingsford, M., Gerlach, G., & Guigand, C. M., 2013. Reef odor: a wake up call for navigation in reef fish larvae, *PloS one*, 8(8), e72808.

Pieper, C., Martins, A., Zettler, E., Loureiro, C. M., Onink, V., Heikkilä, A., Epinoux, A., Edson, E., Donnarumma, V., de Vogel, F., et al., 2019. Into the med: Searching for microplastics from space to deep-sea, in *International Conference on Microplastic Pollution in the Mediterranean Sea*, pp. 129–138, Springer.

Poulain, M., 2020. *Etude de la distribution verticale de particules plastiques dans l'océan : caractérisation, modélisation et comparaison avec des observations*, Ph.D. thesis, Institut National Polytechnique de Toulouse, 6 allée Emile Monso - BP 34038 31029 Toulouse.

Poulain, M., Mercier, M. J., Brach, L., Martignac, M., Routaboul, C., Perez, E., Desjean, M. C., & Ter Halle, A., 2019. Small microplastics as a main contributor to plastic mass balance in the north atlantic subtropical gyre, *Environmental science & technology*, 53(3), 1157–1164.

Riisgård, H. U. & Larsen, P. S., 2007. Viscosity of seawater controls beat frequency of water-pumping cilia and filtration rate of mussels mytilus edulis, *Marine Ecology Progress Series*, 343, 141–150.

Ross, O. N. & Sharples, J., 2004. Recipe for 1-d lagrangian particle tracking models in space-varying diffusivity, *Limnology and Oceanography: Methods*, 2(9), 289–302.

Samaras, A. G., De Dominicis, M., Archetti, R., Lamberti, A., & Pinardi, N., 2014. Towards improving the representation of beaching in oil spill models: A case study, *Marine pollution bulletin*, 88(1-2), 91–101.

Taylor, J. R., 2018. Accumulation and subduction of buoyant material at submesoscale fronts, *Journal of Physical Oceanography*, 48(6), 1233–1241.

Thompson, S. & Turner, J., 1975. Mixing across an interface due to turbulence generated by an oscillating grid, *Journal of Fluid Mechanics*, 67(2), 349–368.

Van Sebille, E., Griffies, S. M., Abernathey, R., Adams, T. P., Berloff, P., Biastoch, A., Blanke, B., Chassignet, E. P., Cheng, Y., Cotter, C. J., et al., 2018. Lagrangian ocean analysis: Fundamentals and practices, *Ocean Modelling*, 121, 49–75.

Van Sebille, E., Aliani, S., Law, K. L., Maximenko, N., Alsina, J. M., Bagaev, A., Bergmann, M., Chapron, B., Chubarenko, I., Cózar, A., et al., 2020. The physical oceanography of the transport of floating marine debris, *Environmental Research Letters*, 15(2), 023003.

Waterhouse, A. F., MacKinnon, J. A., Nash, J. D., Alford, M. H., Kunze, E., Simmons, H. L., Polzin, K. L., St. Laurent, L. C., Sun, O. M., Pinkel, R., et al., 2014. Global patterns of diapycnal mixing from measurements of the turbulent dissipation rate, *Journal of Physical Oceanography*, 44(7), 1854–1872.

Wichmann, D., Delandmeter, P., & van Sebille, E., 2019. Influence of near-surface currents on the global dispersal of marine microplastic, *Journal of Geophysical Research: Oceans*, 124(8), 6086–6096.

Yang, D., Chamecki, M., & Meneveau, C., 2014. Inhibition of oil plume dilution in langmuir ocean circulation, *Geophysical Research Letters*, 41(5), 1632–1638.

Zhao, D. & Li, M., 2019. Dependence of wind stress across an air–sea interface on wave states, *Journal of Oceanography*, 75(3), 207–223.

Chapter 5

The influence of particle size and fragmentation on large-scale microplastic transport in the Mediterranean Sea

Victor Onink, Mikael Kaandorp, Erik van Sebille and Charlotte Laufkötter

Manuscript in preparation.

Abstract

Microplastic particles move three-dimensionally through the ocean, but modeling studies often do not consider size-dependent vertical transport processes. In addition, microplastic fragmentation in ocean environments remains poorly understood, despite fragments making up the majority of microplastic pollution in terms of number of particles, and despite its potential role in mass removal. Here we first investigate the role of particle size and density on the large-scale transport of microplastic in the Mediterranean Sea, and next analyse how fragmentation may affect transport and mass loss of plastic. For progressively smaller particle sizes, microplastic is shown to be less likely to be beached and more likely to reach open water. Smaller particles also generally get mixed deeper, resulting in lower near-surface concentrations of small particles despite their higher total abundance. Microplastic fragmentation is shown to be dominated by beach-based fragmentation, with ocean-based fragmentation processes likely having negligible influence. However, fragmentation remains a slow process acting on decadal timescales and as such likely does not have a major influence in the large-scale distribution of microplastics and mass loss over periods of at least 3 years.

5.1 Introduction

Marine plastic pollution has negative ecological and economic impacts, including harming marine wildlife through ingestion and entanglement (Mascarenhas et al., 2004; Molnar et al., 2008; Van Franeker & Law, 2015), acting as a vector for harmful chemicals and bacterial pathogens (Gregory, 2009; Viršek et al., 2017) and reducing tourism at commercial beaches (Ballance et al., 2000; Beaumont et al., 2019). Plastic is already ubiquitous in marine habitats, with microplastic (< 5 mm) particles being found everywhere from coastlines to the deep sea (Browne et al., 2015; Brignac et al., 2019). Yet, the pathways and ultimate fate of plastic once it enters the ocean are

not fully understood, complicating a full assessment of the associated risk of marine plastic pollution. A complete understanding of the fate of plastic once it enters the ocean is therefore necessary and urgent.

Lagrangian models are commonly used to explore various (micro)plastic scenarios and interpolate between the available measurements (Lebreton et al., 2012; van Sebille et al., 2015; Liubartseva et al., 2018; Onink et al., 2019, 2021a), since there is an insufficient number of standardized field measurements to capture the full spatial and temporal variation of microplastic concentrations on a range of time- and spatial scales (Browne et al., 2015). However, many models assume that all plastic in the model is buoyant and remains at the ocean surface throughout the entire simulation. Furthermore, microplastic particles come in a wide array of sizes and densities but models often assume one generic particle (Lebreton et al., 2012; van Sebille et al., 2015; Critchell et al., 2015; Carlson et al., 2017; Liubartseva et al., 2018; Onink et al., 2019, 2021a). While these assumptions reduce model complexity, such models ignore all vertical transport processes and cannot be used to examine microplastic distributions below the surface. However, even positively buoyant microplastic particles can be mixed below the ocean surface due to wave-driven turbulence (Kukulka et al., 2012; Kooi et al., 2016; Onink et al., 2021b) and buoyant polymers have been found on the seabed up to thousands of meters below the ocean surface (Bergmann et al., 2017; Woodall et al., 2014; Brignac et al., 2019). Field measurements also indicate that the debris size affects the likelihood of the object reaching the open ocean, with smaller particles being more likely to escape coastal regions (Morales-Caselles et al., 2021). On a global scale, Mountford & Morales Maqueda (2019) showed that the particle buoyancy can influence the large-scale transport both horizontally and vertically, but did not explicitly relate these different buoyancies to particle sizes, while also using a relatively coarse spatial resolution for the flow fields. In addition, plastic transport is further complicated by the various transformations that microplastic particles undergo, such as changes in particle density due to biofouling (Fazey & Ryan, 2016; Fischer et al., 2021) and decreasing particle size due to fragmentation (Song et al., 2017; Gerritse et al., 2020), and the influence of particle shape anisotropy on flow behavior (DiBenedetto et al., 2018; Clark et al., 2020). The fragmentation of microplastics into gradually smaller particles has been suggested as a possible mass sink (Lebreton et al., 2019), and it is important to understand the rate at which this occurs in order to set up a global microplastic mass balance. Furthermore, while it is assumed that fragmentation generally occurs more quickly on beaches than in the open ocean due to higher UV exposure, higher oxygen levels and greater temperature fluctuations (Andrady, 2017), there is limited experimental work that validates this assumption.

Understanding the influence that particle size has on large-scale transport is crucial, as it can affect the particle buoyancy and therefore susceptibility to vertical mixing, as well as the bioavailability of the particles to marine organisms (Wright et al., 2013). Here, we first present a series of Lagrangian experiments to investigate the influence of microplastic particle size and density on the large-scale transport. We limit our scope to the Mediterranean Sea, due to the availability of both field measurements (Cózar et al., 2015; Ruiz-Orejón et al., 2018; Merlino et al., 2020; de Haan et al., 2022) and modeling studies (Kaandorp et al., 2020, 2021; Tsiaras et al., 2021) to compare our results with. We then include microplastic fragmentation into our size-dependent transport framework, building upon the work from Kaandorp et al. (2021), to investigate the relative influence of ocean-based fragmentation. We also estimate the rate of mass transfer to plastic particles smaller than 0.156 mm (below the commonly used mesh size in microplastic observations).

5.2 Methods

5.2.1 Ocean surface current data

For the 2010 - 2013 zonal and meridional currents, temperature, salinity and Mixed Layer Depth (MLD) data, we use the CMEMS Mediterranean Sea Physics Reanalysis (CMSPR) (Escudier et al., 2020). This reanalysis product has a temporal resolution of 3 hours, a horizontal spatial resolution of 1/24° and 141 vertical depth levels. The model code is based on the NEMO version 3.6 (Madec et al., 2017) oceanic general circulation model (OGCM), and the reanalysis is forced with hourly ECMWF ERA5 atmospheric forcing fields (Hersbach et al., 2020). Compared with observations, the main characteristics of the Mediterranean circulation is reproduced, while the errors in sea temperature and salinity relative to observations are small(Escudier et al., 2021). The CMSPR MLD correctly represents the climatological MLD (Houpert et al., 2015; Escudier et al., 2021).

Since the CMSPR does not account for wave forcing, we use the Mediterranean Sea Waves Reanalysis (MSWR) (Korres et al., 2019) for the meridional and zonal surface Stokes drift, and peak wave period. This reanalysis product has a temporal resolution of 1 hour and a horizontal spatial resolution of 1/24°. The model code is based on the ECMWF WAM 4.6.2 wave model (ECMWF, 2017) and is forced with with hourly 10m surface wind fields from the ECMWF ERA5 atmospheric reanalysis (Hersbach et al., 2020). Direct validation of the Stokes drift is difficult, but this is expected to be a function of both the spectral significant wave height and the spectral wave period (Breivik et al., 2016), which are both simulated reasonable well compared to observations (Zacharioudaki et al., 2020).

For calculating the wind-driven turbulent mixing within the surface mixed layer, we use hourly 10m surface wind fields from the ECMWF ERA5 atmospheric reanalysis (Hersbach et al., 2020). Using the ERA5 reanalysis provides consistency with the forcing used for the CMSPR and MSWR products, and the ERA5 product has been shown to have the closest match in near-surface winds with observations compared to other reanalysis products (Ramon et al., 2019).

5.2.2 Lagrangian transport

We use Parcels (Lange & van Sebille, 2017; Delandmeter & Van Sebille, 2019) to model plastic as virtual particles that are advected by the surface ocean currents. A change in the horizontal particle position $\vec{x}$ =(lon, lat) is calculated according to:

$$\vec{x}(t+\Delta t) = \vec{x}(t) + \int_t^{t+\Delta t} \left(\vec{v}\big(\vec{x},\tau\big) + \vec{v_S}\big(\vec{x},z,\tau\big) \right) d\tau + R\sqrt{\frac{2dtK_h}{r}} \tag{5.1}$$

where $\vec{v}(\vec{x},t)$ is the horizontal surface velocity at the particle location $\vec{x}(t)$ at time t, $\vec{v_S}\big(\vec{x},z,\tau\big)$ is the horizontal Stokes drift due to the surface wave field, $R \in [-1,1]$ is a random process representing subgrid motion with mean zero and variance $r = 1/3$, dt is the integration timestep and $K_h = 10$ m^2 s^{-1} is the horizontal diffusion coefficient (Lacerda et al., 2019; Onink et al., 2021a). To calculate the horizontal Stokes drift at depth z from the surface Stokes drift, we use the approximation based on the Phillips spectrum from Breivik et al. (2016). Equation 5.1 is integrated with a 4th order Runge-Kutta scheme with $dt = 30$ seconds, and particle position are saved every 12 hours.

The turbulent vertical particle transport is modelled as a Markov-0 process following Onink et al.

(2021b), where the vertical particle position $z(t)$ is calculated by:

$$z(t+\Delta t) = z(t) + \big(w_r + \partial_z K_z(\vec{x}, z, t)\big)dt + \sqrt{2K_z(\vec{x}, z, t)}dW \tag{5.2}$$

where w_r is the particle rise velocity, $K_z\big(\vec{x}, z, t\big)$ is the vertical diffusion coefficient, $\partial_z K_z = \partial K_z/\partial z$, dW is a Wiener increment with zero mean and variance dt, and the vertical axis z is defined positively upward with $z = 0$ at the air-sea interface. Since the vertical and horizontal diffusion fields are not provided within the CMSPR dataset, we use a local form of the K-profile parametrization (KPP) (Large et al., 1994; Boufadel et al., 2020) for the vertical K_z profile:

$$K_(\vec{x}, z, t) = \left(\frac{\kappa u_{*w}(\vec{x}, t)}{\phi}\theta\right)(|z| + z_0)\left(1 - \frac{|z|}{MLD(\vec{x}, t)}\right) \tag{5.3}$$

where $\kappa = 0.4$ is the von Karman constant, $u_{*w}(\vec{x}, t) = \tau(\vec{x}, t)/\rho_w(\vec{x}, t)$ is the frictional velocity of water for surface wind stress $\tau(\vec{x}, t)$ and surface sea water density $\rho_w(\vec{x}, 0, t)$, $\phi = 0.9$ is the stability function in Monin-Obuokov boundary layer theory, θ is the Langmuir circulation enhancement factor and z_0 is the roughness scale of turbulence following (Zhao & Li, 2019) for a wave age $\beta = 1.21$ (Kukulka et al., 2012; Onink et al., 2021b). Langmuir circulation (LC) turbulent mixing can increase turbulent mixing up to $\theta = 3 - 4$ (McWilliams & Sullivan, 2000), but as calculating θ is not trivial we assume conservative wind mixing with negligible LC-driven mixing where $\theta = 1.0$. Aside from wind-driven turbulent mixing within the mixed layer, we also account for tidal mixing throughout the water column based on time-invariant tidal mixing climatologies (de Lavergne et al., 2020) as in Fischer et al. (2021). The particle rise velocity w_r is dependent on the particle size, and for a spherical particle with diameter d is calculated as:

$$w_r = \sqrt{\frac{(1 - \frac{\rho_p}{\rho_w(\vec{x}, z, t)}) * 8/3 * d * g}{24/Re(\vec{x}, z, t) + 5/\sqrt{Re(\vec{x}, z, t)} + 2/5}} \tag{5.4}$$

for the particle density ρ_p, gravitational acceleration $g = 9.81$ m s^{-2} and Reynolds number $Re(\vec{x}, z, t) = p_D w_r/\nu(\vec{x}, z, t)$ with the kinematic viscosity of sea water ν (Enders et al., 2015). The kinematic viscosity $\nu(\vec{x}, z, t)$ at the particle position is calculated following the procedure from (Kooi et al., 2017).

Following (Onink et al., 2021b), the boundary condition at the ocean surface has the particle depth set at $z = 0$ if the particle crosses the air-surface interface. At the seabed, we apply a reflecting boundary condition. Microplastic particles have been found at seafloor worldwide (Woodall et al., 2014), and there have been a number of studies that have examined particle settling and entrainment (Carvajalino-Fernandez et al., 2020; Waldschläger & Schüttrumpf, 2019b; Ballent et al., 2013). However, overall microplastic entrainment remains a highly uncertain process and there is insufficient field and laboratory data to properly parametrize seabed settling and entrainment. Therefore, seabed processes were not included in the current model setup.

The beaching and resuspension of particles on coastlines is modelled following Onink et al. (2021a). Concentrations of beached microplastics are influenced by a wide range of processes, such as wind direction and speeds, coast angle, aspect and morphology, tides, local runoff and the degree of human usage of the beach (Debrot et al., 1999; Browne et al., 2015; Pieper et al., 2015; Hardesty et al., 2017; Ryan et al., 2018; Brignac et al., 2019; Kaandorp et al., 2022). However, such processes typically act on smaller spatial and temporal scales than those resolved in ocean reanalysis products. To at least partially account for unresolved nearshore processes, particle beaching is implemented as a stochastic process where the beaching probability p_B for a

particle for timestep dt is:

$$p_B = \begin{cases} \text{if } d \leq D,\ p_B = 1 - \exp(-dt/\lambda_B) \\ \text{if } d > D,\ p_B = 0 \end{cases} \tag{5.5}$$

where d is the distance from the particle to the nearest model land cell, D sets the outer limit of the beaching zone within which beaching is possible and λ_B is the beaching timescale in days. Following Onink et al. (2021a), we set the beaching zone $D = 6$ km such that all land-adjacent ocean cells are fully contained within the beaching zone. The probability p_R of beached particles being resuspended for for a time increment dt is:

$$p_R = 1 - \exp(-dt/\lambda_R(w_r)) \tag{5.6}$$

where the resuspension timescale $\lambda_R(w_r)$ is dependent on the particle size. Based on field experiments with drifters of various sizes, Hinata et al. (2017) found a linear relationship between the particle rise velocity and the resuspension timescale in days:

$$\lambda_R(w_r) = 260 * w_r + 7.1. \tag{5.7}$$

Following equation 5.4, smaller particles have smaller rise velocities and are therefore more likely to be resuspended. While Hinata et al. (2017) only considered a single beach in Japan, it is the only field study that has studied the relation between the particle size and the residence time on a beach and therefore we apply the relation to the Mediterranean. There is likely also a relation between the particle size and the beaching probability, but as this has not been sufficiently studied to date we set λ_B to be size-independent. The beaching timescale remains a highly uncertain parameter, and while the extensive sensitivity study by Onink et al. (2021a) showed that it is actually the ratio between the beaching resuspension timescale that sets the large-scale beaching behavior, there was insufficient field data to constrain this ratio to a specific value range. We set λ_B to a uniform value of 26 days, based on the model calibration study in Kaandorp et al. (2020).

Objects floating at the ocean surface can be exposed to surface winds, but we do not include a separate windage term in the current model setup. The strength of the effect depends on the size of the object that is exposed above the ocean surface (Van Den Bremer & Breivik, 2018), and for the particle sizes within this study that effect is likely negligible.

5.2.3 Fragmentation model

5.2.3.1 Kaandorp box model and ocean fragmentation

The fragmentation model is based on Kaandorp et al. (2021), where plastic particles split into smaller fragments based on fractal theory (Turcotte, 1986; Charalambous, 2014). For a spatial dimension $D_N = 3$, one starts from a cubic parent object with dimensions L in size class $k = 0$. Over time this parent object splits into smaller fragments, where fragments in size class $k = n$ have size $L/2^n$. The probability mass function (pmf) giving the mass m in size class k at fragmentation index f is:

$$m(k; f, p) = \frac{\Gamma(k+f)}{\Gamma(k+1)\Gamma(f)} p^k (1-p)^f \tag{5.8}$$

where p is the fraction of the original parent object that has been lost to smaller size classes at $f = 1$ and Γ is the gamma function. The number of fragments $n(k, f, p)$ in each size class is:

$$n(k, f, p) = 2^{D_N k} m(k; f, p) \tag{5.9}$$

While a spatial dimension of $D_N = 3$ indicates a cubic parent object, $D_N = 2$ corresponds to a sheet and a non-integer D_N would indicate a mixture of various particle types. A value of $p = 0.4$ was reported to be suitable for pellets made out of polymers such as polyethylene and polypropylene. The fragmentation rate is highly uncertain, ranging from $1.8 \times 10^{-2} f$ week^{-1} based on data from laboratory experiments (Song et al., 2017), to $2.0 \times 10^{-4} f$ week-1 based on fitting the fragmentation model to observational data of particle sizes (Kaandorp et al., 2021). Defining the fragmentation timescale λ_f as the time in days such that $f = 1$ (implying 40% mass loss of the parent object with $p = 0.4$), this implies $\lambda_f = 388 - 35000$ days (Song et al., 2017; Kaandorp et al., 2021).

To study the transport and fragmentation of microplastic in the Mediterranean, Kaandorp et al. (2021) developed a box model representing microplastic transport between beaches, coastal (¡15 km) waters, and open water for various particle size classes. The transition probabilities between the coastal and open waters are based on Lagrangian simulations using the same CMSPR and MSWR data products used in this study (Kaandorp et al., 2020), while the particle resuspension followed equation 5.7. Kaandorp et al. (2021) assumed that fragmentation only occurrs on beaches, as higher temperatures, UV radiation exposure and oxygen availability are assumed to lead to faster fragmentation compared to microplastics in (sea)water (Andrady, 2017). For the full details of the implementation of the box model we refer to Kaandorp et al. (2021). In order to test the sensitivity of the box model to ocean fragmentation we modify the box model to also allow for fragmentation in coastal and open waters. We therefore differentiate between the beach-based fragmentation timescale $\lambda_{f,B}$ and the coastal/open water fragmentation timescale $\lambda_{f,O}$.

Kaandorp et al. (2021) included a sink term P_S in the box model, such that the amount of plastics in the ocean system steady state matched observed plastic quantities. The steady state concentrations in the beach and coastal/open water reservoirs can then be solved by matrix inversion, where depending on the fragmentation rate a steady state is reached after approximately a decade of simulation time.

In our sensitivity analysis of ocean fragmentation, we consider a base scenario where we solely have beach-based fragmentation particles in 12 size classes ($d = 0.002 - 5.000$ mm) with $\lambda_{f,B} \in [388, 35000]$ days. We then add coastal/open water fragmentation, where we set $\lambda_{f,O} \in [1, 5, 10, 100, 1000, 10000] \times \lambda_{f,B}$. We assume a continuous weekly microplastic input of size class $k = 0$ for the purpose of the sensitivity analysis. We set $\lambda_B = 26$ days (Kaandorp et al., 2020) and λ_R according to equation 5.7.

5.2.3.2 Lagrangian model

Over time, the Kaandorp et al. (2021) fragmentation model predicts an exponential rise in the number of microplastic fragments in the system. While this does not pose numerical challenges within a box model, this does constrain the duration of any Lagrangian fragmentation simulation. Given that it is not computationally feasible to represent each microplastic fragment as an individual virtual particle, we instead have each virtual particle represent a certain microplastic number/mass within a given size class. Similarly, while fragmentation is continuous and gradual process, it is not computationally feasible to add new virtual particles after each integration

timestep. Instead, further discretization is required.

To illustrate our Lagrangian fragmentation implementation, consider a single virtual particle which represents microplastic particles in the $k = 0$ size class ($d = 5.000$ mm). Initially, this particle will have a number and mass weight of 1. When this particle is released, it will be transported horizontally and vertically following equations 5.1 and 5.2, and cycle through beaching and resuspension with probabilities corresponding to equations 5.5 and 5.6. Assuming that fragmentation only occurs when a particle is beached, we keep a timer that tracks the cumulative time that the particle has been beached (even if it is resuspended intermittently). Once this timer indicates that a particle has been beached for 90 days, it fragments and we add 5 new particles corresponding to size classes $k = 1 - 5$. Based on the fragmentation timescale λ_f, we can convert the beached time to the equivalent fragmentation index f, which in turns allows us to calculate the particle number and mass for each of the virtual particles using equations 5.8 and 5.9. For example, if $\lambda_f = 90$ days, this would imply $f = 1.0$, and in turn that we would have $n(0, f = 1, p = 0.4) = 0.6$. The beached timer then resets for the $k = 0$ particle, with all newly created particles starting as beached at the same location as the parent particle with beached timers initialized at zero.

The described procedure applies to all particles in our fragmentation scenario (e.g. fragmentation of a $k = 2$ particle can create $k = 3 - 5$ fragments), where we track these particles for up to 3 years with $\lambda_f \in [388, 1000, 10000, 35000, 50000]$ days. We only consider 6 size classes ($d = 0.156 - 5.000$ mm) with particle densities $\rho = 920$ kg m^{-3}, both due to computational constraints and since our fragmentation validation rests almost solely on manta trawl measurements, which generally have a mesh size of 0.33 mm. Any particle mass transfer to smaller size classes ($d < 0.156$ mm) is considered lost from the system.

5.2.4 Lagrangian model input

For both the size-dependent transport and fragmentation simulations, we scale the spatial distribution of microplastic input according to riverine plastic inputs (Lebreton et al., 2017), where we always release the particles in the shore-adjacent ocean cells. For each particle size in the size-dependent transport scenario, we release 85 196 particles at the beginning of the simulation. We consider 12 size classes ($d = 0.002 - 5.000$ mm) with particle densities $\rho \in [30, 920, 980, 1020]$ kg m^{-3}, which correspond to expanded polystyrene (PS), polypropylene (PP), polyethylene (PE) and approximately neutrally buoyant polymers (Brignac et al., 2019). With the fragmentation scenarios, we release 2 718 particles per month (97,848 in total), where these are evenly divided over the six size classes. We base the initial weighing of the particles in each size class on river microplastic size distributions (Zeri et al., 2021). While the size distribution of microplastic entering the ocean can vary in space and time (Lebreton et al., 2017; Simon-Sánchez et al., 2019; Zeri et al., 2021), we currently lack the necessary field data to represent such input variability, and therefore assume temporal and spatial invariance in the input size distribution.

All simulations in both the size-dependent transport and fragmentation scenarios run for three years (2010 - 2012). While this is insufficient time the system to reach any equilibrium in the fragmentation scenarios, the exponential increase in the number of virtual particles with each additional simulation year means that longer simulations become too computationally costly. However, three years is sufficient to study the horizontal and vertical spread of microplastics throughout the Mediterranean, and in the case of the fragmentation scenario to quantify the mass loss rate of microplastic to smaller, unresolved size classes ($d < 0.156$ mm).

5.3 Results

5.3.1 Size-dependent transport

Figure 5.1 shows the relative distribution of particles between beaches, coastal waters (< 10 km from the model coastline) and open water (> 10 km from the model coastline), averaged over 3 years of simulations, each simulation corresponding to a given particle size and density. Almost all the large ($d = 5$ mm) particles are near coastlines, either beached ($35.24 - 81.96\%$, depending on the density) or adrift in the coastal zone ($17.01 - 59.01\%$), with only a small fraction in open water ($1.04 - 5.74\%$). For the smallest particles ($d = 0.002$ mm) the open water fraction rises to $21.85 - 25.08\%$, with the coastal zone holding the majority of the particles ($59.37 - 61.84\%$). Microplastic particles are less likely to be beached as the particle size decreases, as smaller rise velocities result in shorter resuspension timescales. However, with the exception of the $\rho = 30$ kg m^{-3} particles, only around 1% of particles reach open water for sizes $d > 0.156$ mm, as even as the number of particles that are adrift rises, they remain close to land. While the exact distribution of particles over the beached, coastal and open water slightly varies with particle density, the general trends with decreasing size are the same across all considered microplastic densities. The nearshore trapping of almost all microplastic $d > 0.1$mm is also a feature we see under size-independent resuspension timescales (Figure 5.1b & 5.A.9b).

The nearshore trapping of microplastics is dependent on local circulation patterns, and we see

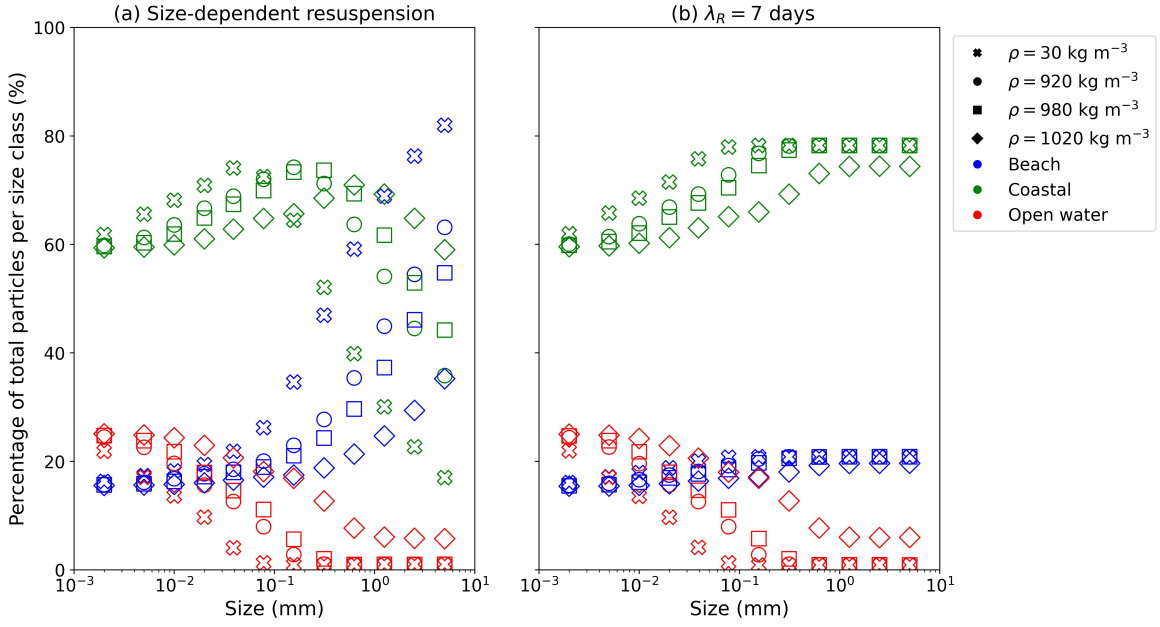

Figure 5.1: The Mediterranean beach (blue symbols), coastal (green) and open water reservoirs (red) as percentages of the total number of particles in each size class and in each microplastic density for (a) size dependent resuspension and (b) $\lambda_R = 7$ days. The fractions are averaged over the entire three year simulations. Each size class/particle density represent an individual model simulation.

spatial variability in the likelihood of microplastic to reach the open ocean (Figure 5.2). While certain areas, such as the Spanish and French coastlines, show relatively little nearshore trapping for any particle size (Figure 5.A.10), generally small microplastic particles are much more likely to reach the open ocean than large particles. However on local scales, such as the Adriatic Southern Italian coastline, opposite trends can occur.

We find strong differences in both the vertical and horizontal distribution of different sizes of

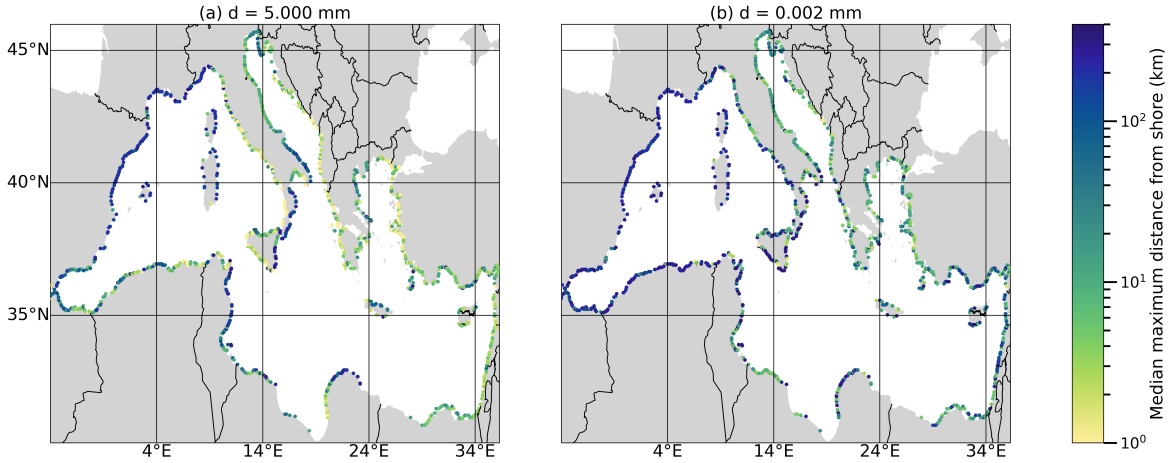

Figure 5.2: The median maximum distance from shore reached by particles (a) 5.000 mm and (b) 0.002 mm particles over the course of their entire trajectories, with each point indicating an input location. All simulations are for size-dependent resuspension with $\rho = 920$ kg m^{-3}.

microplastic. Smaller and denser microplastic particles are mixed deeper below the ocean surface (Figure 5.3 & 5.A.11), where for the smallest and heaviest microplastics up to 58.21% of all the particles are below 10 m from the ocean surface (Table 5.A.2). The vertical transport of particles also shows a strong seasonal influence, as stronger stratification during the spring and summer months generally leads to shallower mixing due to the lower MLD (Figure 5.3 & Table 5.A.2). However, vertical mixing from the internal tides can transport particles down far below the MLD, with a small number of particles of various sizes and densities being mixed over 2,000 m below the ocean surface.

In summary, large particles remain at the ocean surface whereas smaller particles can get mixed far below the ocean surface, and this is also reflected in the horizontal distribution. The open water column-integrated concentrations are orders of magnitude lower for large ($d = 5.000$ mm) particles (Figure 5.4a & 5.A.12) than for small ($d = 0.002$ mm) particles (Figure 5.4c & 5.A.12) in the first year of the simulation. This is in large part due to larger particles being more likely to be beached and less likely to be transported from coastal to open water. The horizontal distribution is strongly dependent on the input scenario, as we see the highest concentrations near the Algerian coast and in the Levantine Sea. However, by the third simulation year the smaller ($d < 0.078$ mm) particles are distributed more homogeneously throughout the entire Mediterranean basin, with slightly higher concentrations in the Eastern Mediterranean (Figure S5g-l). In contrast, almost all larger ($d > 0.078$ mm) particles are either beached or in coastal areas (Figure 5.A.14a-f). However, as smaller microplastic particles are more easily mixed below the surface, the near-surface microplastic concentrations are higher for large microplastics than small particles (Figure 5.4b, 5.4d & 5.A.13). As such, while smaller microplastic particles are more likely to reach open waters in the Mediterranean, solely considering surface field measurements would indicate an opposite trend.

5.3.2 Ocean fragmentation

We next examine the effect of fragmentation on the size distribution of microplastic particles, using the Kaandorp box model. Figure 5.5 shows the calculated steady-state size distributions assuming different ocean-based fragmentation timescales $\lambda_{f,O}$, separated into open water, coastal and beach reservoirs. The baseline steady state microplastic size distributions show an exponential increase in the number of particles for smaller size classes (note the logarithmic scale). The

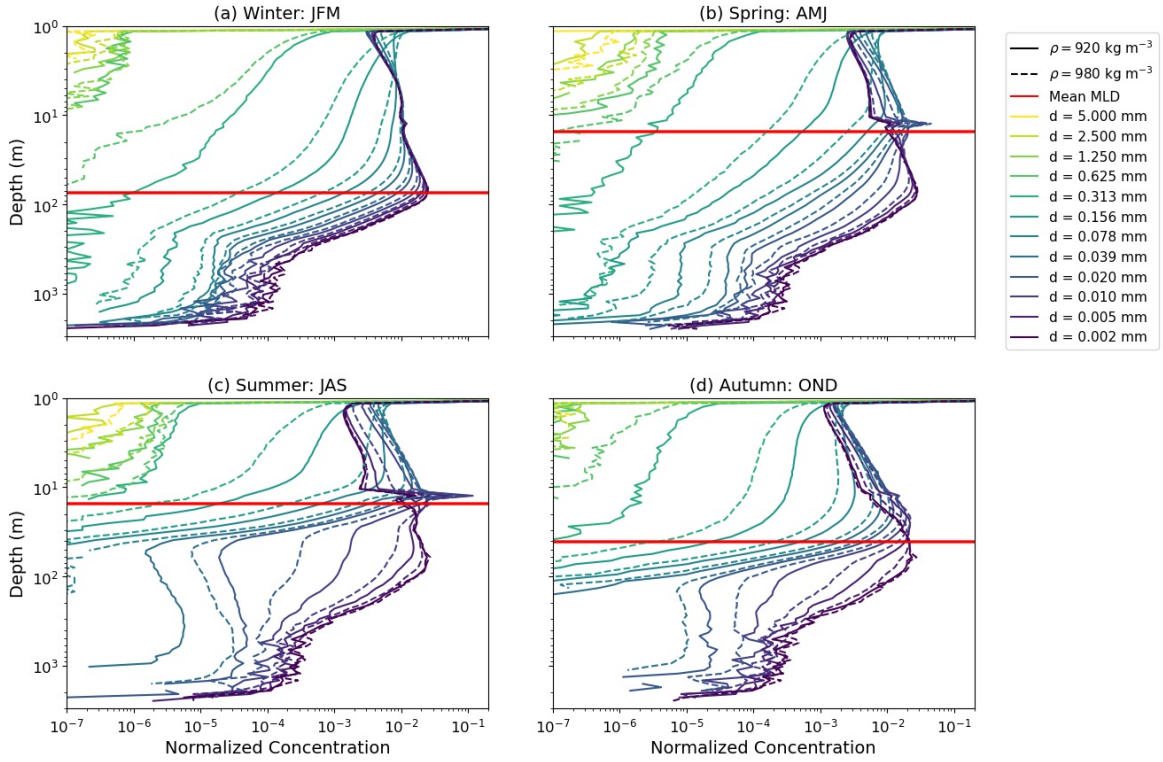

Figure 5.3: Normalized vertical microplastic concentrations during different seasons and for $5.000 - 0.002$ mm particles with $\rho \in [920, 980]$ kg m^{-3} with size-dependent resuspension. All profiles are averaged over the three year simulation period and are normalized by the total number of particles in each simulation ($n = 85,196$)

faster beach fragmentation timescale $\lambda_{f,B} = 388$ days results in 4 orders of magnitude more particles and mass in smaller size classes compared to $\lambda_{f,B} = 35,000$ days. The addition of ocean fragmentation has a minimal influence on the modelled size distribution unless $\lambda_{f,O} \approx \lambda_{f,B}$, i.e. ocean fragmentation is equally fast as fragmentation on beaches.

Based on laboratory experiments, the ocean fragmentation timescale $\lambda_{f,O}$ is highly variable and dependent on the object polymer, object type and experimental setup (Table 5.1). Assuming a fragmentation fraction $p = 0.4$, a parent object would lose 40% of its initial mass over a full fragmentation cycle ($f = 1$) and this is estimated to take anywhere from years to centuries in marine environments. However, for the type of PP and PE fragments considered in this study, $\lambda_{f,O}$ appears to be on the order of decades. Compared with the $\lambda_{f,B}$ estimates from (Song et al., 2017) of 0.3 - 1.1 years, this would suggest that to first order, ocean-based fragmentation is negligible relative to beach-based fragmentation, at least within the Mediterranean.

5.3.3 Lagrangian fragmentation

Based on the sensitivity study performed with the box model, we solely consider beach-based fragmentation in our Lagrangian fragmentation scenario and λ_f henceforth refers to the beach-based fragmentation timescale $\lambda_{f,B}$. A simulation time of three years is insufficient for any form of steady state to be established, and instead the size distributions are still heavily influenced by the initial input size distribution (Figure 5.6). It is only in the smallest size classes ($d = 0.156, 0.313$ mm) that clear differences arise between the various λ_f values. The fragmentation with $\lambda_f = 388$ days is over two orders of magnitude faster than with $\lambda_f = 50,000$ days, and in the coastal and beached reservoirs the $k = 5$ size class correspondingly has two orders of magnitude more particles and mass with $\lambda_f = 388$ days compared to $\lambda_f = 50,000$ days.

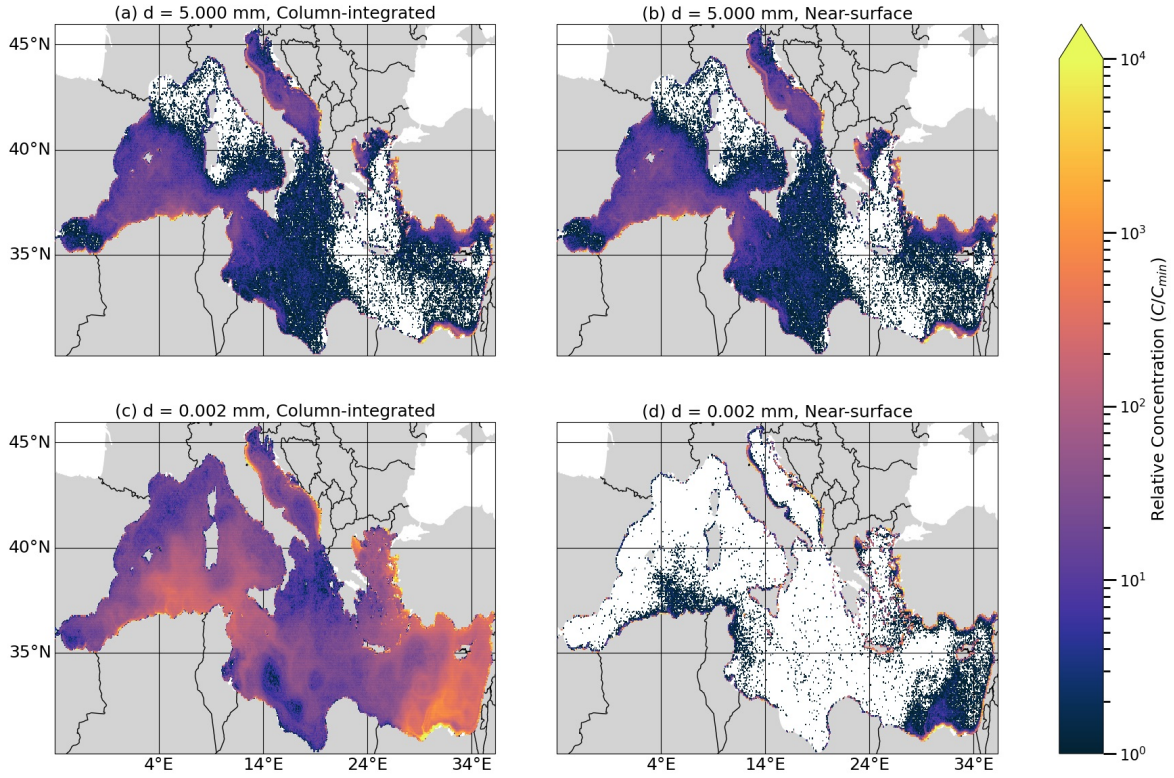

Figure 5.4: The column-integrated and near surface (particle depth $z < 1$ m) horizontal microplastic concentrations for (a - b) 5.0 mm and (c - d) 0.002 mm particles. All concentrations represent the first year of the simulation with size-dependent resuspension and $\rho = 920$ kg m^{-3}.

However, in the open water these differences are smaller due to the relatively small number of particles that reach the open water. A gradual mass transfer to smaller size classes is apparent, but the overall mass loss to size classes smaller than 0.156 mm (smaller than the regular Manta Trawl mesh size) is only $0.24 - 2.45\%$.

The horizontal spread of the various microplastic size classes closely resembles the distribution in the size-dependent transport scenarios (Figure 5.7), with the concentrations of microplastics near coastlines being orders of magnitude higher than in the open ocean. Smaller size classes generally show higher concentrations in open water due to the shorter resuspension timescales and decreased coastal trapping, but even as smaller particles are more numerous (Figure 5.7), the larger size classes still hold a large portion of the total microplastic mass (Figure 5.8). For example, with $\lambda_f = 388$ days by counts 53.25% of the particles have a size $d = 0.156$ mm (assuming spherical particles), but only 1.98% of the microplastic mass is in the size class. In contrast, the three largest size classes make up only 5.61% of the microplastic particles by count, but 76.04% of the microplastic mass. Given that all size classes in the Lagrangian fragmentation scenario are relatively large, the particles generally remain at the surface, with at most 0.07% of the total microplastic mass below 10 m.

5.4 Discussion

The distinct differences in the column-integrated and near-surface concentrations highlight the importance in considering the full 3D transport of microplastics. Particles with near-zero rise velocities, either due to their small size or being nearly neutrally buoyant relative to the sea water, are much more likely to be mixed below the ocean surface. As suggested by Cózar et al. (2014), this

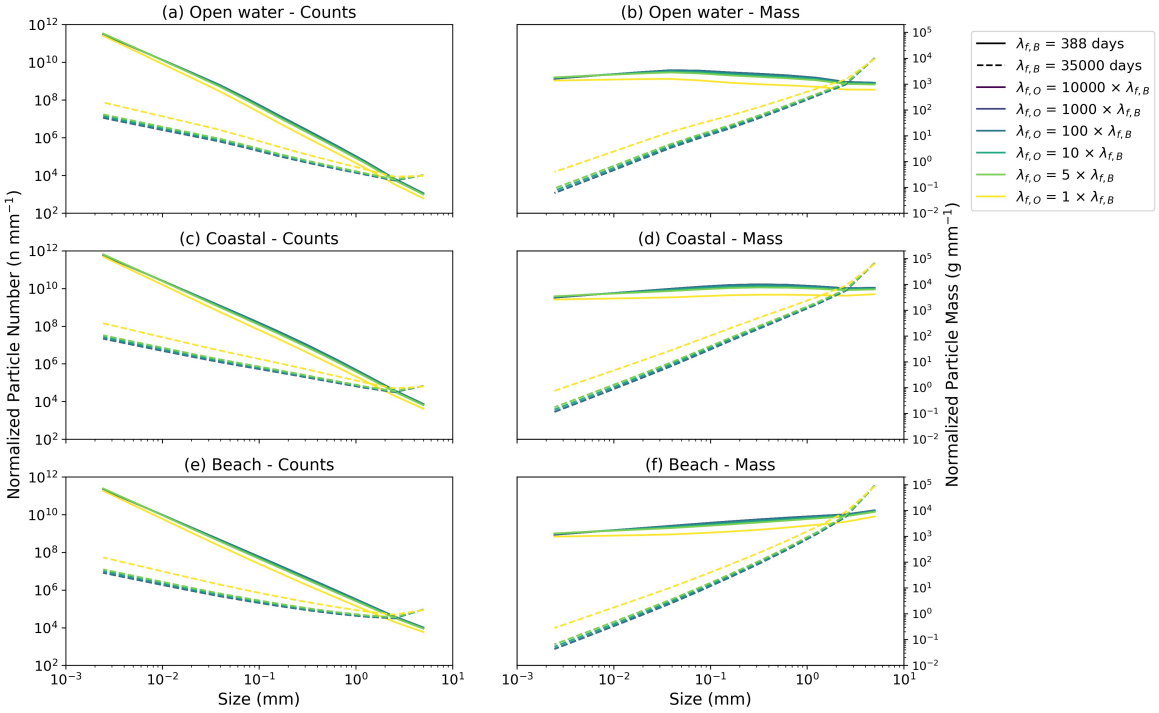

Figure 5.5: Steady-state normalized microplastic size distributions of microplastic particles with varying beach and ocean fragmentation timescales using the Kaandorp et al. (2021) box model.

can be a partial explanation of why size distributions of microplastic measurements collected with neuston nets show fewer small particles than expected. The near-surface concentration distribution in the first model year closely resembles that of Tsiaras et al. (2021), which despite using a different input scenario and model setup, similarly showed the highest concentrations in coastal areas of Egypt, Algeria and the Adriatic Sea. For the larger size classes ($d > 0.313$ mm), this also matches well with field measurements throughout the Mediterranean basin (Cózar et al., 2015; Pedrotti et al., 2018). However, validating the horizontal distribution of particles smaller than $\approx 0.1 - 0.33$ mm is currently not possible, as these particles are generally not captured within neuston nets and alternative sampling methodologies are either not available or not extensively used to study the distribution of the smallest microplastic particles in the ocean. Similarly, while the high subsurface concentrations predicted by the model are in line with observations (Egger et al., 2020; Poulain et al., 2018; Pieper et al., 2019; Pabortsava & Lampitt, 2020), these observational records do not have sufficiently high temporal and spatial resolutions to validate the modelled vertical concentration profiles, and its seasonal variability. This would also require sampling techniques other than neuston nets, such as niskin bottles (Pieper et al., 2019) or high-volume filtration systems (Zhao et al., 2022), to study the distribution of microplastic particles < 0.33 mm.

The transformation of microplastic particles due to fragmentation is critical for understanding the long-term fate of microplastics, as changes in the particle size can affect the large-scale transport and the bio-availability to various trophic levels in the marine ecosystems. While a host of different processes are known to affect the fragmentation rate, such as polymer type, UV exposure and oxidation (Song et al., 2017), isolating which is the dominant processes is vital for developing basic fragmentation models. One simplifying assumption made by Kaandorp et al. (2021) was that fragmentation predominantly occurred on beaches, where plastic is generally exposed to higher UV levels, higher oxygen levels, greater temperature fluctuations and more mechanical stresses. Based on the results in this current study, this assumption appears justified, given that ocean-based fragmentation only significantly affects the overall particle size distribution if $\lambda_{f,O} \approx \lambda_{f,B}$. While

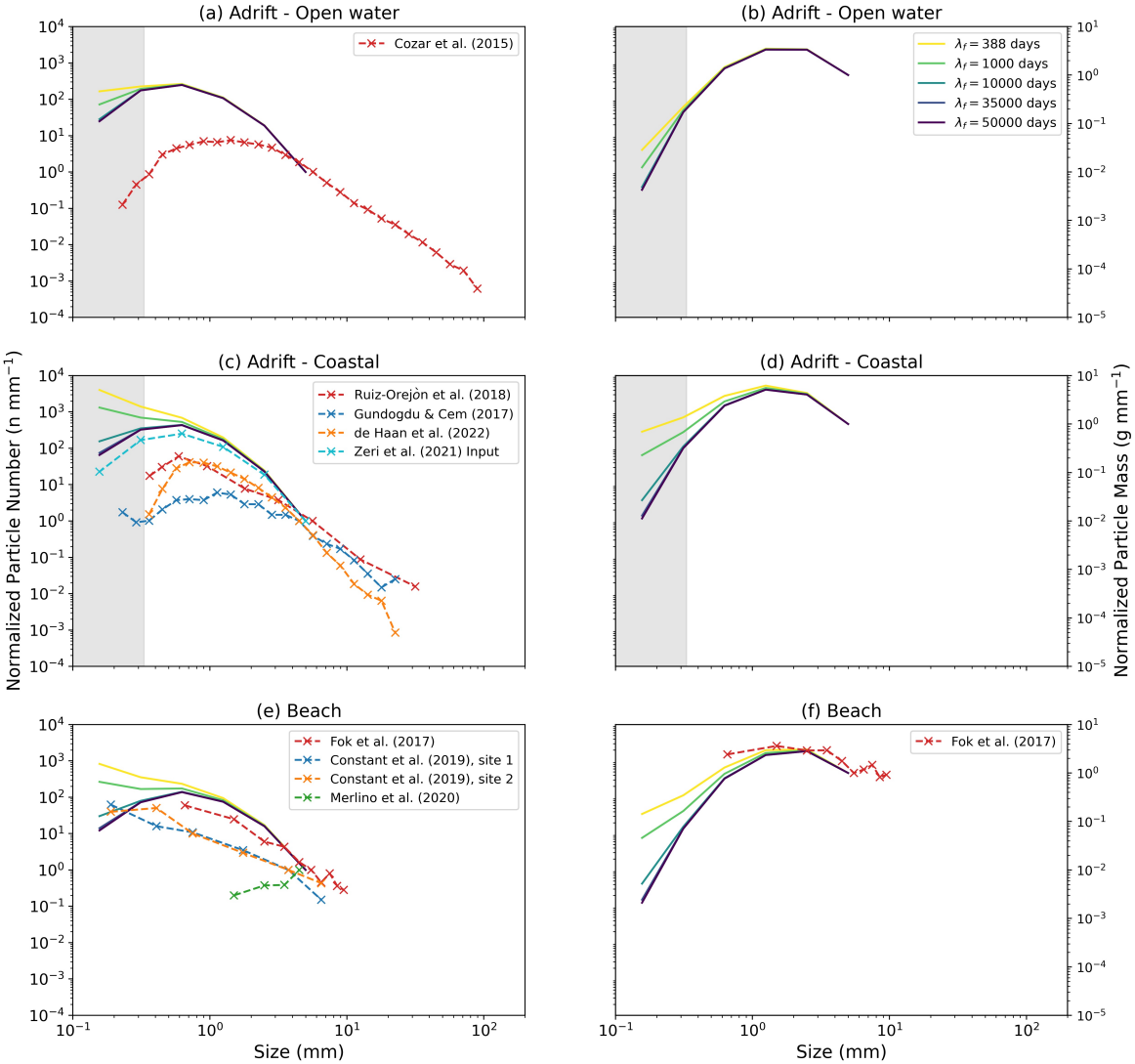

Figure 5.6: Comparisons of the surface (< 0.26 m) Lagrangian modelled and measured microplastic size distributions (MSDs). All modelled MSDs are normalized to the maximum size class, and all measured MSD are normalized by the relative to the measured size class closest to 5 mm. The Zeri et al. (2021) data in panel (c) indicates the size distribution of particles entering the simulation. In panels (a - d), they grey-shaded area indicates particle sizes < 0.33 mm, representing particle sizes below the detection limits of typical manta trawl nets used to collect surface microplastics.

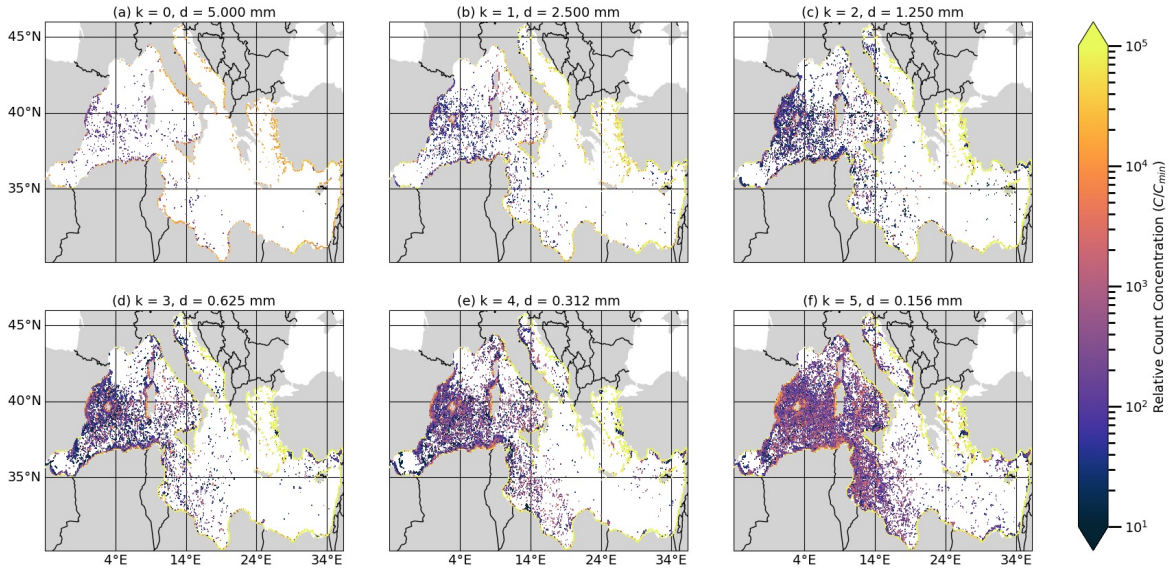

Figure 5.7: Columnn-integrated horizontal microplastic concentrations for size classes $k = 0 - 5$ in the third simulation year. The concentrations are weighed based on the particle counts.

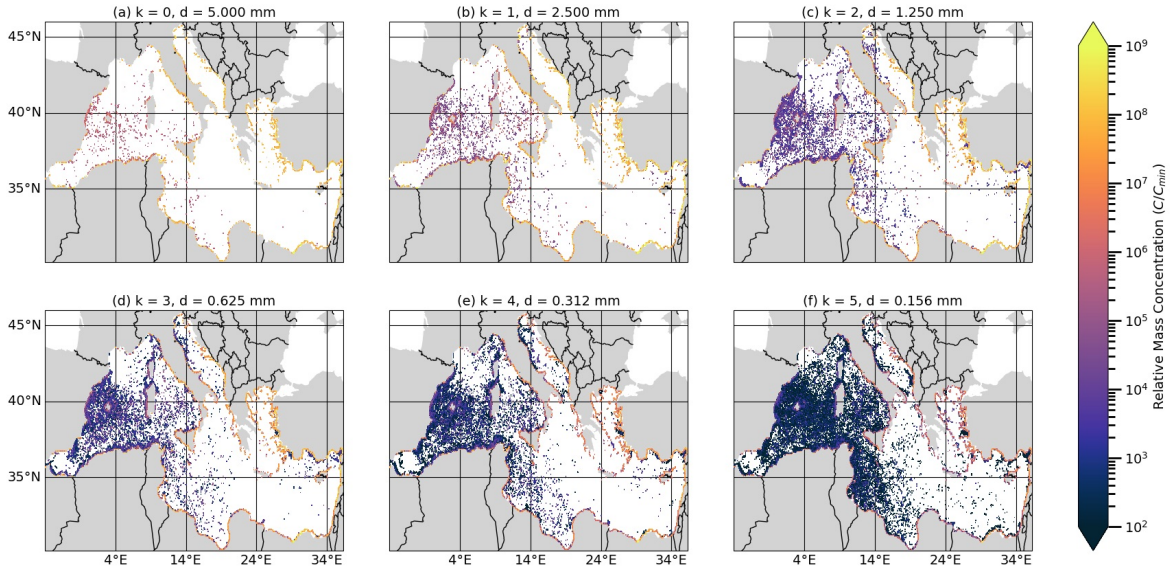

Figure 5.8: Columnn-integrated horizontal microplastic concentrations for size classes $k = 0 - 5$ in the third simulation year. The concentrations are weighed based on the particle mass.

Table 5.1: Estimates of the ocean-based fragmentation timescale $\lambda_{f,O}$ from literature sources. Unless otherwise noted, the lower and upper bounds are estimates of the time for the parent object to lose 40% of its original mass assuming linear and exponential mass loss rates. [1]Assumes the loss of strip surface area is equivalent to the loss of mass. [2]Estimate of the timescale for the parent object to lose all mass provided directly by the literature source.

Study	Plastic object	$\lambda_{f,O}$
O'Brine & Thompson (2010)	PE strip	15.3 - 19.2 years[1,2]
	Compostable polyester strip	<0.5 years [1,2]
Resmerită et al. (2018)	PP strip	20.2 - 25.8 years
Zhu et al. (2020)	Postconsumer expanded PS fragment	0.3 - 2.7 years [2]
	Postconsumer PP fragment	0.3 - 4.3 years [2]
	Postconsumer PE fragment	33 years [2]
	PE pellet	0.5 - 49 years [2]
	North Pacific Gyre (NPG) fragments	2.8 years [2]
	NPG fragments (no UV)	58 years [2]
Gerritse et al. (2020)	Low-density PE air pouch	50 - 63.6 years
	High-density PE air pouch	66.6 - 84.9 years
	PS packaging foam	33.3 - 42.3 years
	PS beaker	400.0 - 510.6 years
	Latex balloon	8.7 - 10.8 years
	Sillicon tube	40.0 - 50.8 years
	PET bottle	8.2 -14.3 years
	PET fleece	13.8 - 17.4 years
	PU foam	13.3 - 16.8 years
	Cellulose beaker	5.1 - 6.2 years
	CA cigarette filter	2.7 - 3.2 years
	Compostable postal bag	2.6 - 3.1 years
	Compostable trash bag	1.5 - 1.6 years
	PLA food bag	5.6 - 6.9 years

comparing fragmentation rates determined with different experimental setups is challenging, the fragmentation timescale for polyethylene and polypropylene polymers is generally on the order of decades in water, compared to years in a beach-like environment (Song et al., 2017). As such, neglecting ocean-based fragmentation likely will have a negligible impact on the results on this study. However, for other plastic polymers outside of the immediate scope on this study, such as cellulose, PLA and compostable polymers, $\lambda_{f,O}$ appears to be on the order of years, and neglecting ocean-based fragmentation may result in underestimating the fragmentation of such plastic objects.

Over a three year period, fragmentation is not shown to lead to significant amounts of 'lost' microplastic mass, as the mass transfer to size classes smaller than $d < 0.156$ mm is at most shown to be 2.45%. In reality, this mass fraction loss is likely to be even smaller, as the majority of plastic mass would be contained in objects larger than the 5 mm particles considered in this modeling study. Given the slow rate at which microplastic fragmentation occurs, after three years the modelled size distributions still closely resemble the input size distribution (Zeri et al., 2021). As such, greater understanding of the size distribution of microplastic inputs would already provide great insight to the size distribution of microplastics in the Mediterranean as a whole. Compared to size distributions from field measurements, the model predicts relatively higher amounts of microplastic in size classes $k = 0 - 5$ than in field measurements. In part this could be due to the lack of microplastic particles larger than $d = 5.000$ mm in the model, which could affect the overall relative number of particles in each size class. However, it is also possible that three years is simply not long enough for the model to

stabilize to a long-term size distribution. Due to exponential growth in the number of virtual particles in the simulation, three years is at or near the limit of what is currently computationally feasible, and for long-term fragmentation modeling e.g. the box model approach such as in Kaandorp et al. (2021) would be more fit for purpose. However, the current Lagrangian model setup provides insight into the distribution of the microplastic fragments in the Mediterranean. While observational studies often report microplastic concentrations as particle counts (e.g. Figure 5.6), it is shown in Figures 5.7 & 5.8 that microplastic mass and counts show different relative distributions. While the number concentration of microplastics is dominated by smaller particles, the distribution of microplastic mass is more strongly influenced by the distribution of larger particles. Dependent on the research question at hand, this difference could have important consequences when for example quantifying risks associated with microplastic pollution.

Considering the results of both the size-dependent transport and Lagrangian fragmentation scenario, the fate of microplastic when it enters the Mediterranean is strongly size-dependent. Large microplastic particles tend to remain close to shore, where they are more likely to beach and gradually fragment into smaller and smaller particles. Gradually, as the particles get smaller and especially for particles $d \approx 0.156$ mm or smaller, particles are more likely to escape from coastal areas and reach open water. At this point the particles are also sufficiently small that vertical transport processes start to play a more important role, leading to greater mixing of the particles throughout the water column. Overall, the work in this study reiterates the importance of coastal regions in the overall fate of microplastics suggested by Onink et al. (2021a). Given that many coastal processes occur on spatial and temporal timescales that are unresolved by large-scale circulation models such as CMSPR and MSWR (Van Sebille et al., 2020), it is possible that such coastal trapping is weaker when all nearshore processes are represented. This still highlights an urgent need for greater understanding of the nearshore microplastic transport (Kerpen et al., 2020; Alsina et al., 2020). However, it is promising that the model shows the same size-dependent trapping pattern as Morales-Caselles et al. (2021), who found that larger debris appears more likely to remain trapped close to shore than smaller debris.

We consider a range of size-dependent processes, which have various degrees of uncertainty. There are numerous studies that calculate the rise velocity of a particle based on its density and size under a range of conditions (Kooi et al., 2017; Waldschläger & Schüttrumpf, 2019a; Semcesen & Wells, 2021), but we decided to base our parameterization on Enders et al. (2015) due to relative ease of calculation within our model setup. However, depending on a particle's particular shape or spatial orientation we acknowledge the rise velocity could vary (DiBenedetto et al., 2018; Clark et al., 2020). There is higher uncertainty in the size-dependent resuspension timescale, and similarly in assuming size-independent beaching timescales. The resuspension timescale is based on empirical experiments by Hinata et al. (2017), but the relation is an extrapolation for microplastic particles as Hinata et al. (2017) used drifters at least 1.3 cm in size. However, considering size-independent resuspension timescale $\lambda_R \in [7, 50]$ days only affected the relative distribution of particles over the beached and coastal reservoirs, with the percentage of particles that reached open water remaining unaffected. Similarly, while we assumed a single beaching timescale $\lambda_B = 26$ days for the entire Mediterranean, this likely will vary depending on the particle characteristics and local geomorphology. Given that the beaching timescale remains uncertain for any type of particle and that there are no field experiments which can be used to estimate it (Onink et al., 2021a), we used $\lambda_B = 26$ days based on an inverse modeling study that best fit with field measurements in the Mediterranean (Kaandorp et al., 2020). Furthermore, given that spatially varying beaching and resuspension timescales do not seem to affect the large-scale distribution of microplastic particles (Daily et al., 2021), assuming spatial invariance in these timescales is the best available option until additional field experiments have been conducted.

Another assumption in the current model setup is that the particle density remains unchanged over the three year simulation period. Biofouling was not included in this study in order to focus solely on the influence of particle size. However, even without biofouling microplastic particles are shown to be mixed throughout the entire water column, including down the seabed up to 3000 m deep. This is even the case for particles up to 5 mm in size if the particle is nearly neutrally buoyant (up to 10% of all particles). Yet, by excluding biofouling the current study could be underestimating the amount of subsurface microplastic. The amount of vertical mixing might also be underestimated by assuming negligible LC-driving mixing. The KPP wind mixing parametrization can account for LC-driven turbulence through the LC enhancement factor θ, but computing θ from relatively spatially and temporally coarse reanalysis data is not trivial and beyond the scope of this study. Ideally the CMSPR dataset would include vertical turbulent mixing data, as the Onink et al. (2021b) parametrization now had to use the MLD data from the CMSPR dataset. Since the MLD in the CMSPR dataset is defined by a density criteria relative to the sea water density at 10 m, during the spring and summer months this results in almost the entire Mediterranean basin having a MLD= 10 m, which resulted in the artificial spike at $z = 10$ m in the vertical microplastic concentration profiles (Figure 5.3). However, with no readily available alternative parametrization for wind mixing that doesn't have its own set of limitations, this is the best possible approach.

5.5 Conclusion

Our results show that the size of microplastic particles significantly influences the large-scale transport of microplastic particles in the Mediterranean Sea, with smaller particles being more likely to escape coastal waters into open water and get mixed below the ocean surface up to depths of 3000 m. As a consequence, the near-surface microplastic concentrations are more likely to contain large ($d > 1.0$ mm) particles, even though throughout the entire Mediterranean Sea smaller particles ($d < 1.0$ mm) are more numerous. To first order, the fragmentation of microplastic particles is dominated by beach-based fragmentation, with ocean-based fragmentation having a non-negligible effect only if the ocean-based fragmentation rate occurs approximately at the same rate as beach-based fragmentation. However, more experimental work is required to investigate the fragmentation rate of various polymers in both beach-like and aqueous environments. With just beach-based fragmentation, the mass transfer of microplastic to fragments $d < 0.156$ mm is at most 2.45% over a three year period. Future work would require a lot more field measurements of small microplastic fragments, as neuston nets alone are unable to sample particles smaller than $d < 0.20 - 0.33$ mm. In addition, the modeling framework would need to be applied on a global scale to investigate whether the observed trends are Mediterranean-specific or hold more generally.

Acknowledgements

Calculations were performed on UBELIX (www.id.unibe.ch/hpc), the HPC cluster at the University of Bern. VO and CL acknowledge support from the Swiss National Science Foundation (Project PZ00P2_174124 Global interactions between microplastics and marine ecosystems). EvS and MLAK was supported by the European Research Council (ERC) under the European Unions Horizon 2020 research and innovation programme (Grant Agreement No. 715386). We would like to thank William de Haan, Anna Sànchez Vidal, Christina Zeri, Sedat Gündoğdu and Silvia Merlino for providing field measurements.

Author contributions

Development of the size-dependent transport scenario was done by VO, with input from MLAK, EvS and CL. Adapting the Kaandorp et al. (2021) box model to the Lagrangian fragmentation scenario was done by VO and MLAK, with input from CL. The manuscript was written by VO and CL, with extensive input from EvS and MLAK. Everyone contributed to the overall study design and discussion of the analysis, with VO carrying out the analysis.

Competing interests

The authors declare no competing interests.

Code availability

The model code is available at https://github.com/VictorOnink/Lagrangian-Transport-Scenarios

5.A Supplementary material

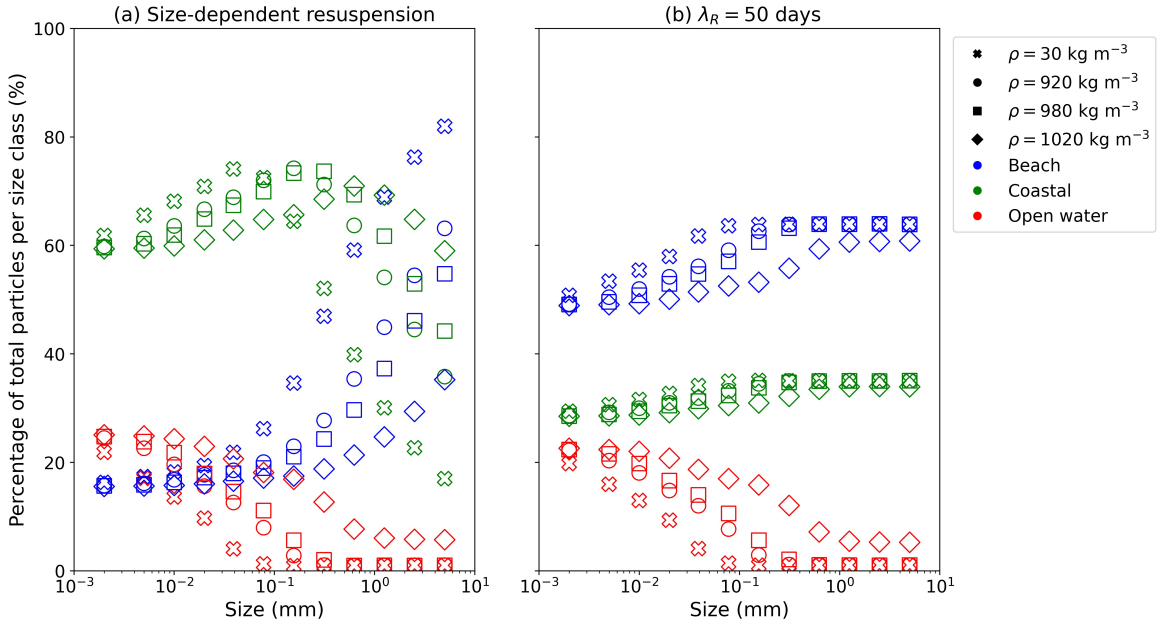

Figure 5.A.9: The Mediterranean beach, coastal and open water reservoirs as percentages of the total number of particles in each size class for (a) size dependent resuspension and (b) $\lambda_R = 7$ days. The fractions are averaged over the entire three year simulations.

Table 5.A.2: Seasonal and overall average fraction of particles at $z < 10$ m from the ocean surface. All percentages are relative to total number of particles in each simulation ($n = 85196$), and all averages are calculated over all three simulation years. JFM = January, February, March; AMJ = April, May, June; JAS = July, August, September; OND = October, November, December.

Size (mm)	Density (kg m^3)	JFM (%)	AMJ (%)	JAS (%)	OND (%)	Average (%)	Size (mm)	Density (kg m^3)	JFM (%)	AMJ (%)	JAS (%)	OND (%)	Average (%)
5.000	30	0.00	0.00	0.00	0.00	0.00	0.078	30	0.02	0.10	0.00	0.00	0.00
	920	0.00	0.00	0.00	0.00	0.00		920	4.91	11.31	1.20	3.07	5.12
	980	0.00	0.00	0.00	0.00	0.00		980	8.96	18.29	3.78	7.06	9.52
	1020	1.03	9.59	9.20	8.13	6.99		1020	21.30	36.29	20.77	23.24	25.40
2.500	30	0.00	0.00	0.00	0.00	0.00	0.039	30	1.52	3.24	0.16	0.60	1.38
	920	0.00	0.00	0.00	0.00	0.00		920	11.42	21.95	5.98	9.75	12.28
	980	0.00	0.00	0.00	0.00	0.00		980	15.09	27.69	10.39	14.14	16.83
	1020	1.02	9.98	9.28	8.00	7.07		1020	25.74	48.00	34.95	30.56	34.81
1.250	30	0.00	0.00	0.00	0.00	0.00	0.020	30	7.05	15.35	2.41	5.09	7.48
	920	0.00	0.00	0.00	0.00	0.00		920	16.93	31.77	13.82	16.66	19.80
	980	0.00	0.00	0.00	0.00	0.00		980	21.01	40.27	22.66	22.56	26.62
	1020	1.07	10.16	9.32	8.02	7.14		1020	29.28	54.31	49.50	39.72	43.20
0.625	30	0.00	0.00	0.00	0.00	0.00	0.010	30	13.29	25.01	8.22	11.93	14.62
	920	0.00	0.00	0.00	0.00	0.00		920	23.71	45.94	30.74	27.15	31.89
	980	0.00	0.00	0.00	0.00	0.00		980	27.27	51.57	43.84	34.22	39.22
	1020	2.94	10.52	8.15	7.60	7.30		1020	31.53	57.01	53.72	46.19	47.11
0.313	30	0.00	0.00	0.00	0.00	0.00	0.005	30	19.46	37.17	18.96	20.22	23.95
	920	0.00	0.00	0.00	0.00	0.00		920	28.66	53.38	48.35	38.78	42.29
	980	0.11	0.47	1.00	0.02	0.15		980	30.63	55.98	52.24	44.01	45.71
	1020	10.36	19.27	9.05	11.46	12.54		1020	32.36	57.88	54.79	48.02	48.26
0.156	30	0.00	0.00	0.00	0.00	0.00	0.002	30	27.39	51.82	45.09	35.21	39.88
	920	0.52	1.45	0.04	0.14	0.54		920	31.80	57.21	53.94	46.73	47.42
	980	2.70	5.98	0.39	1.36	2.61		980	32.17	57.62	54.51	47.81	48.03
	1020	18.14	28.98	14.06	18.90	20.02		1020	32.77	58.21	55.23	48.73	48.74

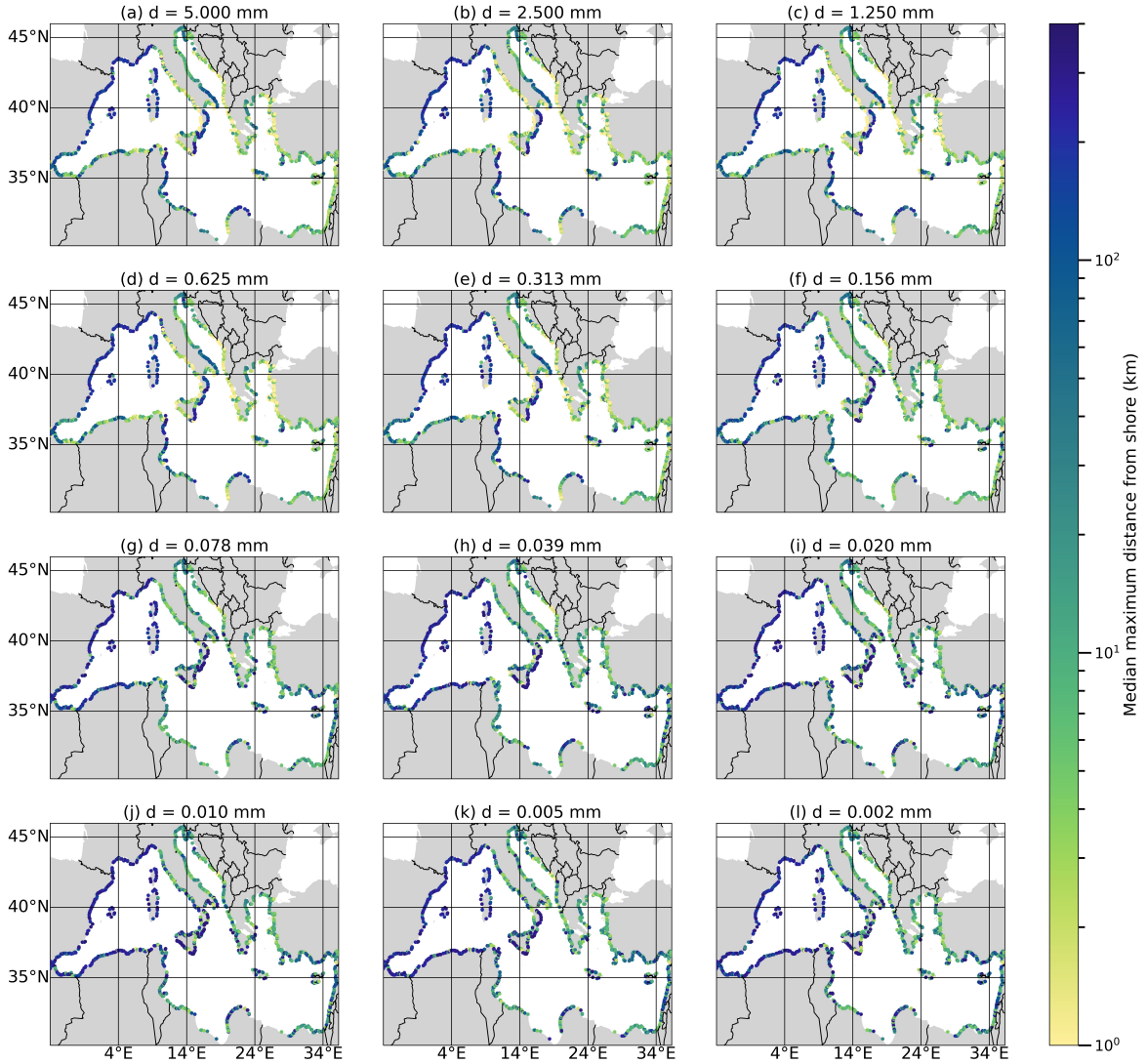

Figure 5.A.10: The median maximum distance from shore reached by particles $5.000 - 0.002$ mm particles over the course of their entire trajectories, with each point indicating an input location. All simulations are for size-dependent resuspension with $\rho = 920$ kg m^{-3}.

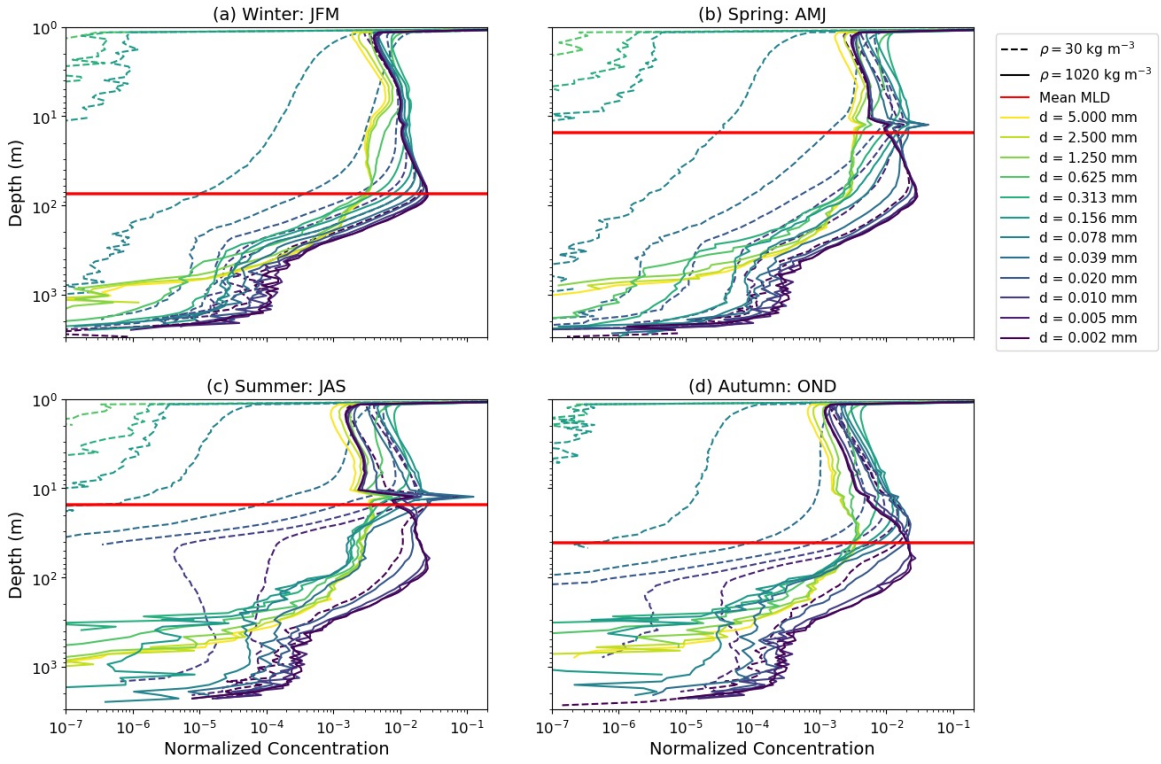

Figure 5.A.11: The seasonal normalized vertical microplastic concentrations for $5.000 - 0.002$ mm particles with $\rho \in [30, 1020]$ kg m^{-3} with size-dependent resuspension. All seasonal concentrations profiles are averaged over the three year simulation period. All profiles are normalized by the total number of particles in each simulation ($n = 85,196$).

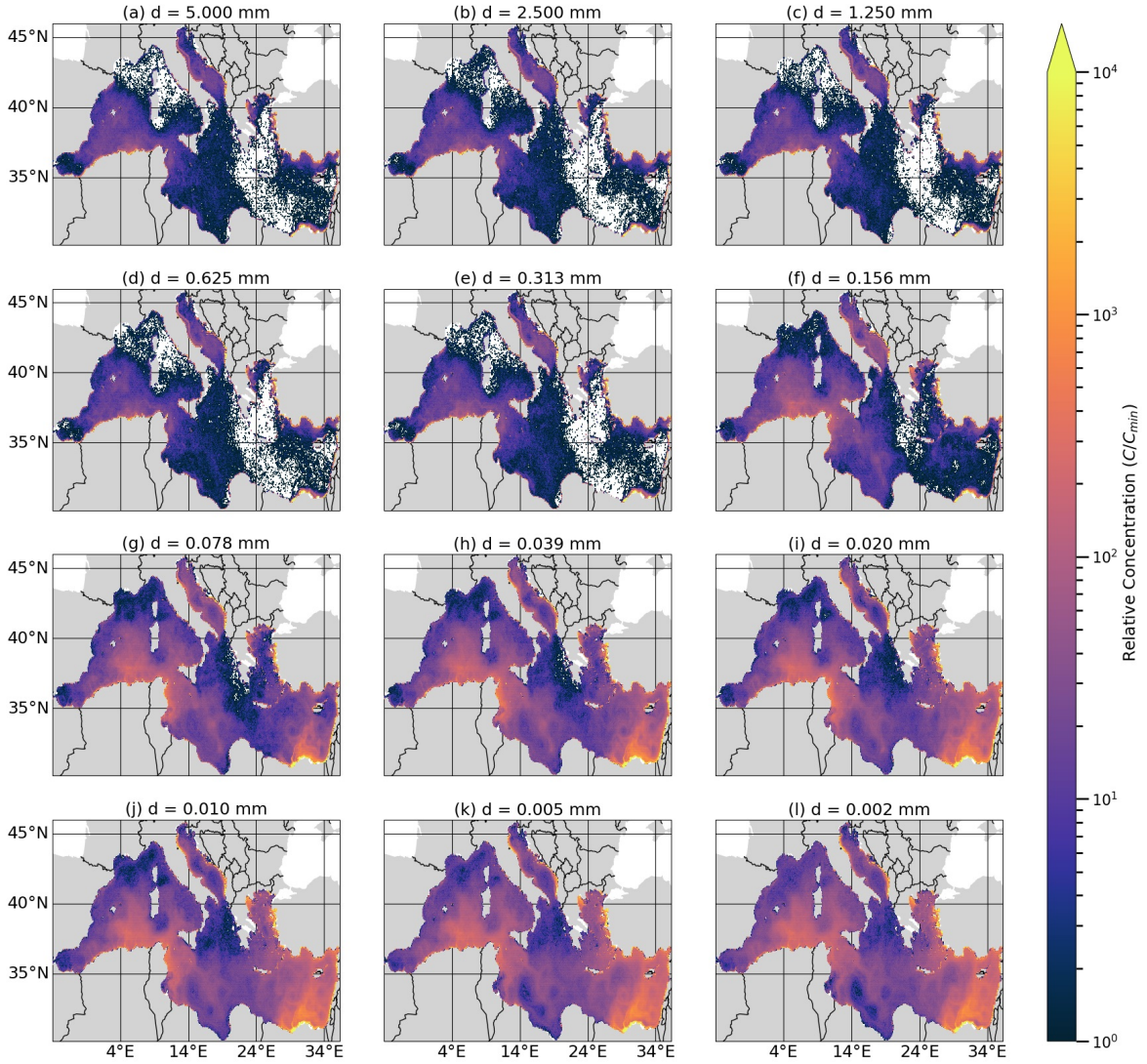

Figure 5.A.12: The column-integrated horizontal microplastic concentrations for $5.000 - 0.002$ mm particles. All concentrations are for the first year of the simulation with size-dependent resuspension and $\rho = 920$ kg m^{-3}.

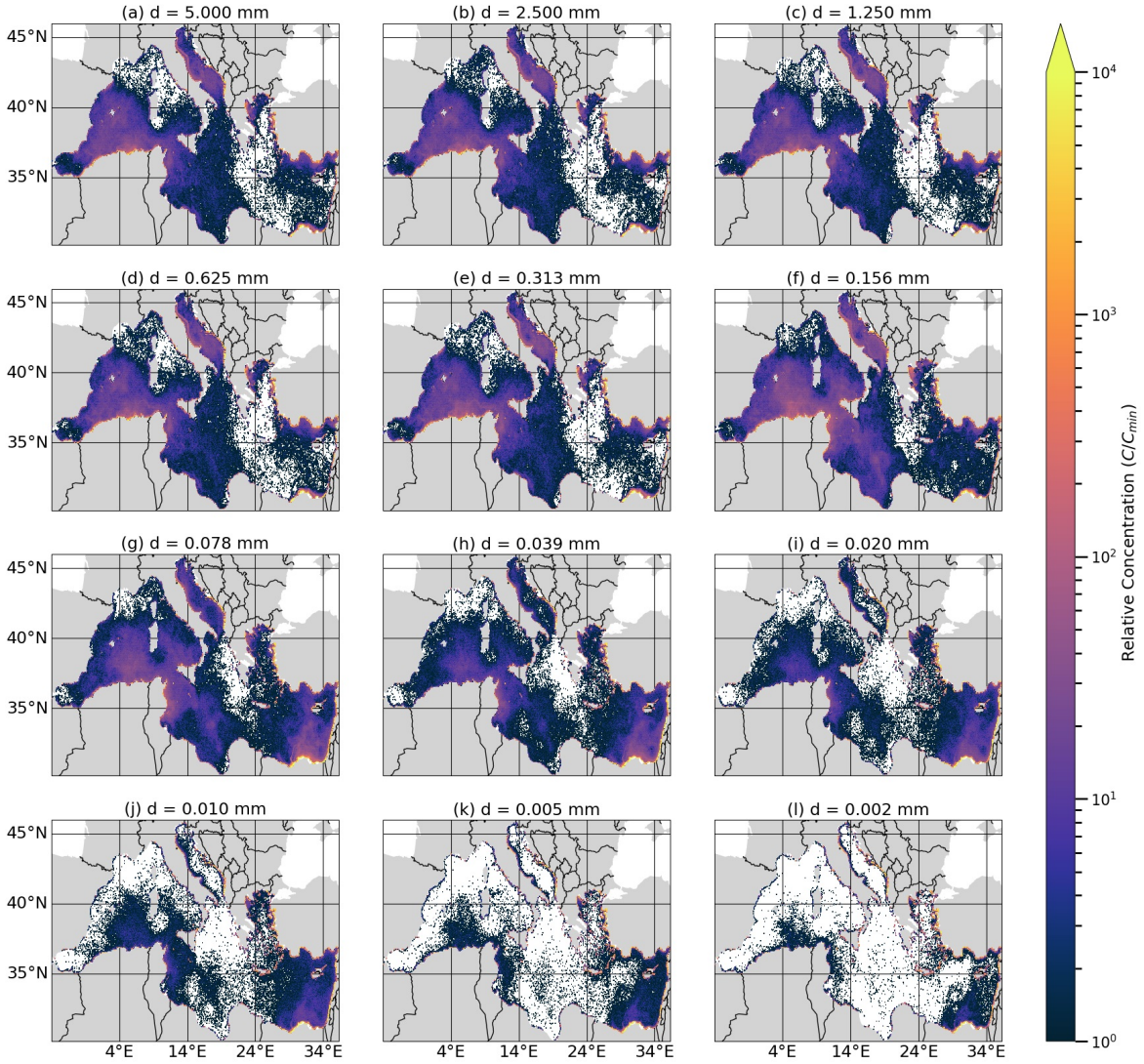

Figure 5.A.13: The $z < 1$ m horizontal microplastic concentrations for $5.000 - 0.002$ mm particles. All concentrations are for the first year of the simulation with size-dependent resuspension and $\rho = 920$ kg m^{-3}.

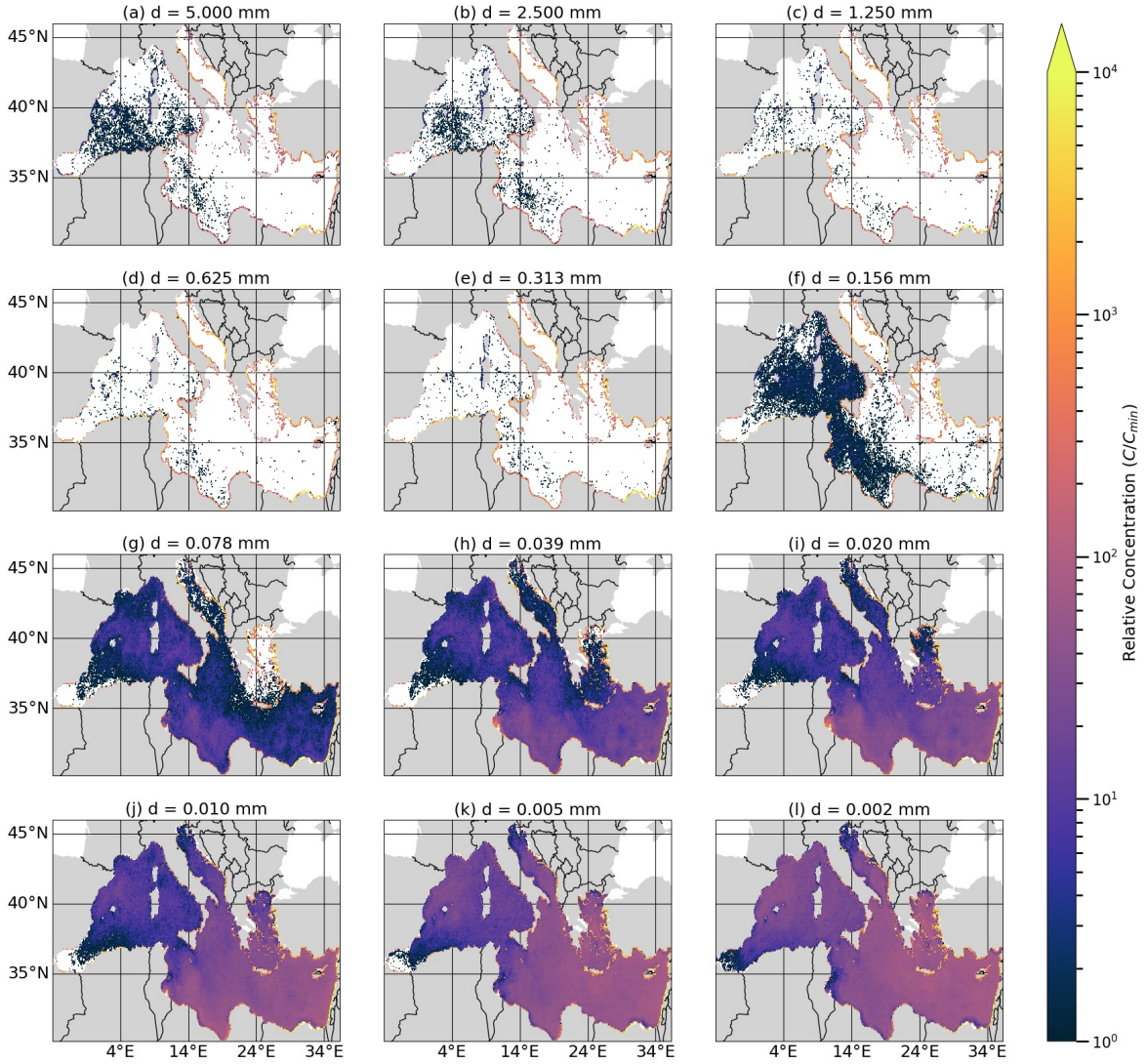

Figure 5.A.14: The column-integrated horizontal microplastic concentrations for $5.000 - 0.002$ mm particles. All concentrations are for the third year of the simulation with size-dependent resuspension and $\rho = 920$ kg m^{-3}.

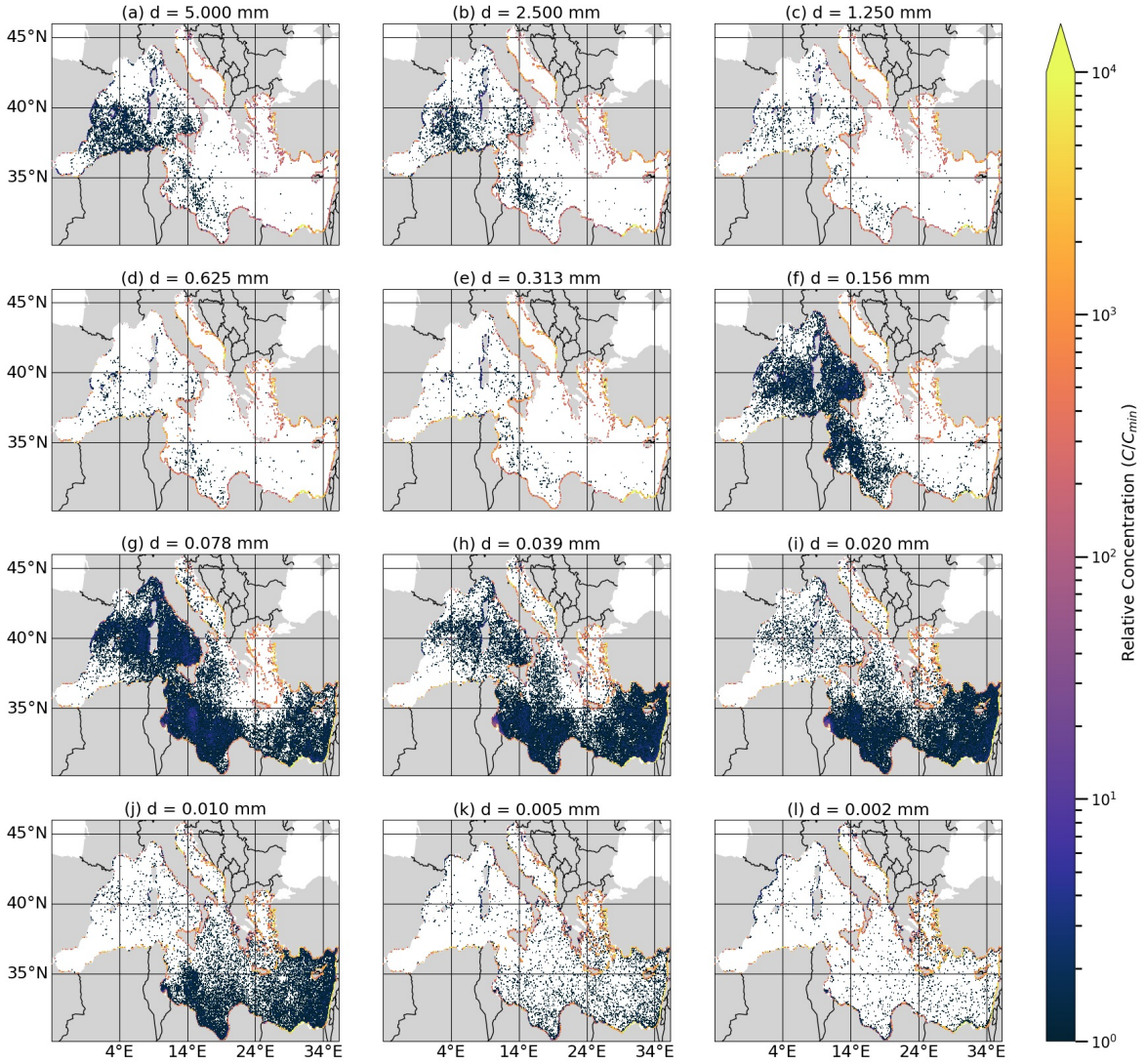

Figure 5.A.15: The $z < 1$ m horizontal microplastic concentrations for $5.000 - 0.002$ mm particles. All concentrations are for the third year of the simulation with size-dependent resuspension and $\rho = 920$ kg m^{-3}.

Bibliography

Alsina, J. M., Jongedijk, C. E., & van Sebille, E., 2020. Laboratory measurements of the wave-induced motion of plastic particles: Influence of wave period, plastic size and plastic density, *Journal of Geophysical Research: Oceans*, 125(12), e2020JC016294.

Andrady, A. L., 2017. The plastic in microplastics: A review, *Marine pollution bulletin*, 119(1), 12–22.

Ballance, A., Ryan, P., Turpie, J., et al., 2000. How much is a clean beach worth? the impact of litter on beach users in the cape peninsula, south africa, *South African Journal of Science*, 96(5), 210–230.

Ballent, A., Pando, S., Purser, A., Juliano, M., & Thomsen, L., 2013. Modelled transport of benthic marine microplastic pollution in the nazaré canyon, *Biogeosciences*, 10(12), 7957–7970.

Beaumont, N. J., Aanesen, M., Austen, M. C., Börger, T., Clark, J. R., Cole, M., Hooper, T., Lindeque, P. K., Pascoe, C., & Wyles, K. J., 2019. Global ecological, social and economic impacts of marine plastic, *Marine pollution bulletin*, 142, 189–195.

Bergmann, M., Wirzberger, V., Krumpen, T., Lorenz, C., Primpke, S., Tekman, M. B., & Gerdts, G., 2017. High quantities of microplastic in arctic deep-sea sediments from the hausgarten observatory, *Environmental science & technology*, 51(19), 11000–11010.

Boufadel, M., Liu, R., Zhao, L., Lu, Y., Özgökmen, T., Nedwed, T., & Lee, K., 2020. Transport of oil droplets in the upper ocean: impact of the eddy diffusivity, *Journal of Geophysical Research: Oceans*, 125(2), e2019JC015727.

Breivik, Ø., Bidlot, J.-R., & Janssen, P. A., 2016. A stokes drift approximation based on the phillips spectrum, *Ocean Modelling*, 100, 49–56.

Brignac, K. C., Jung, M. R., King, C., Royer, S.-J., Blickley, L., Lamson, M. R., Potemra, J. T., & Lynch, J. M., 2019. Marine debris polymers on main hawaiian island beaches, sea surface, and seafloor, *Environmental science & technology*, 53(21), 12218–12226.

Browne, M. A., Chapman, M. G., Thompson, R. C., Amaral Zettler, L. A., Jambeck, J., & Mallos, N. J., 2015. Spatial and temporal patterns of stranded intertidal marine debris: is there a picture of global change?, *Environmental Science & Technology*, 49(12), 7082–7094.

Carlson, D. F., Suaria, G., Aliani, S., Fredj, E., Fortibuoni, T., Griffa, A., Russo, A., & Melli, V., 2017. Combining litter observations with a regional ocean model to identify sources and sinks of floating debris in a semi-enclosed basin: the adriatic sea, *Frontiers in Marine Science*, 4, 78.

Carvajalino-Fernandez, M. A., Sævik, P. N., Johnsen, I. A., Albretsen, J., & Keeley, N. B., 2020. Simulating particle organic matter dispersal beneath atlantic salmon fish farms using different resuspension approaches, *Marine Pollution Bulletin*, 161, 111685.

Charalambous, C., 2014. On the evolution of particle fragmentation with applications to planetary surfaces.

Clark, L. K., DiBenedetto, M. H., Ouellette, N. T., & Koseff, J. R., 2020. Settling of inertial nonspherical particles in wavy flow, *Physical Review Fluids*, 5(12), 124301.

Cózar, A., Echevarría, F., González-Gordillo, J. I., Irigoien, X., Úbeda, B., Hernández-León, S., Palma, Á. T., Navarro, S., García-de Lomas, J., Ruiz, A., et al., 2014. Plastic debris in the open ocean, *Proceedings of the National Academy of Sciences*, 111(28), 10239–10244.

Cózar, A., Sanz-Martín, M., Martí, E., González-Gordillo, J. I., Ubeda, B., Gálvez, J. Á., Irigoien, X., & Duarte, C. M., 2015. Plastic accumulation in the mediterranean sea, *PloS one*, 10(4), e0121762.

Critchell, K., Grech, A., Schlaefer, J., Andutta, F., Lambrechts, J., Wolanski, E., & Hamann, M., 2015. Modelling the fate of marine debris along a complex shoreline: Lessons from the great barrier reef, *Estuarine, Coastal and Shelf Science*, 167, 414–426.

Daily, J., Onink, V., Jongedijk, C. E., Laufkötter, C., & Hoffman, M. J., 2021. Incorporating terrain specific beaching within a lagrangian transport plastics model for lake erie, *Microplastics and Nanoplastics*, 1(1), 1–13.

de Haan, W. P., Uviedo, O., Ballesteros, M., Canales, Í., Curto, X., Guart, M., Higueras, S., Molina, A., Sanchez-Vidal, A., et al., 2022. Floating microplastic loads in the nearshore revealed through citizen science, *Environmental Research Letters*, 17(4), 045018.

de Lavergne, C., Vic, C., Madec, G., Roquet, F., Waterhouse, A. F., Whalen, C., Cuypers, Y., Bouruet-Aubertot, P., Ferron, B., & Hibiya, T., 2020. A parameterization of local and remote tidal mixing, *Journal of Advances in Modeling Earth Systems*, 12(5), e2020MS002065.

Debrot, A. O., Tiel, A. B., & Bradshaw, J. E., 1999. Beach debris in curacao, *Marine Pollution Bulletin*, 38(9), 795–801.

Delandmeter, P. & Van Sebille, E., 2019. The parcels v2. 0 lagrangian framework: new field interpolation schemes, *Geoscientific Model Development*, 12(8), 3571–3584.

DiBenedetto, M. H., Ouellette, N. T., & Koseff, J. R., 2018. Transport of anisotropic particles under waves, *Journal of Fluid Mechanics*, 837, 320–340.

ECMWF, 2017. Ifs documentation cy46r1, part vii: Ecmwf wave model.

Egger, M., Sulu-Gambari, F., & Lebreton, L., 2020. First evidence of plastic fallout from the north pacific garbage patch, *Scientific reports*, 10(1), 1–10.

Enders, K., Lenz, R., Stedmon, C. A., & Nielsen, T. G., 2015. Abundance, size and polymer composition of marine microplastics ≤ 10 μm in the atlantic ocean and their modelled vertical distribution, *Marine pollution bulletin*, 100(1), 70–81.

Escudier, R., Clementi, E., Nigam, T., Pistoia, J., Grandi, A., & Aydogdu, A., 2021. Quality information document (cmems-med-quid-006-004).

Fazey, F. M. & Ryan, P. G., 2016. Biofouling on buoyant marine plastics: An experimental study into the effect of size on surface longevity, *Environmental Pollution*, 210, 354–360.

Fischer, R., Lobelle, D., Kooi, M., Koelmans, A., Onink, V., Laufkötter, C., Amaral-Zettler, L., Yool, A., & van Sebille, E., 2021. Modeling submerged biofouled microplastics and their vertical trajectories, *Biogeosciences Discussions*, pp. 1–29.

Gerritse, J., Leslie, H. A., de Tender, C. A., Devriese, L. I., & Vethaak, A. D., 2020. Fragmentation of plastic objects in a laboratory seawater microcosm, *Scientific reports*, 10(1), 1–16.

Gregory, M. R., 2009. Environmental implications of plastic debris in marine settings–entanglement, ingestion, smothering, hangers-on, hitch-hiking and alien invasions, *Philosophical Transactions of the Royal Society B: Biological Sciences*, 364(1526), 2013–2025.

Hardesty, B. D., Lawson, T., van der Velde, T., Lansdell, M., & Wilcox, C., 2017. Estimating quantities and sources of marine debris at a continental scale, *Frontiers in Ecology and the Environment*, 15(1), 18–25.

Hersbach, H., Bell, B., Berrisford, P., Hirahara, S., Horányi, A., Muñoz-Sabater, J., Nicolas, J., Peubey, C., Radu, R., Schepers, D., et al., 2020. The era5 global reanalysis, *Quarterly Journal of the Royal Meteorological Society*, 146(730), 1999–2049.

Hinata, H., Mori, K., Ohno, K., Miyao, Y., & Kataoka, T., 2017. An estimation of the average residence times and onshore-offshore diffusivities of beached microplastics based on the population decay of tagged meso-and macrolitter, *Marine pollution bulletin*, 122(1-2), 17–26.

Houpert, L., Testor, P., De Madron, X. D., Somot, S., D'ortenzio, F., Estournel, C., & Lavigne, H., 2015. Seasonal cycle of the mixed layer, the seasonal thermocline and the upper-ocean heat storage rate in the mediterranean sea derived from observations, *Progress in Oceanography*, 132, 333–352.

Kaandorp, M. L., Dijkstra, H. A., & van Sebille, E., 2020. Closing the mediterranean marine floating plastic mass budget: inverse modeling of sources and sinks, *Environmental science & technology*, 54(19), 11980–11989.

Kaandorp, M. L., Dijkstra, H. A., & van Sebille, E., 2021. Modelling size distributions of marine plastics under the influence of continuous cascading fragmentation, *Environmental Research Letters*, 16(5), 054075.

Kaandorp, M. L., Ypma, S. L., Boonstra, M., Dijkstra, H. A., & van Sebille, E., 2022. Using machine learning and beach cleanup data to explain litter quantities along the dutch north sea coast, *Ocean Science*, 18(1), 269–293.

Kerpen, N. B., Schlurmann, T., Schendel, A., Gundlach, J., Marquard, D., & Hüpgen, M., 2020. Wave-induced distribution of microplastic in the surf zone, *Frontiers in Marine Science*, p. 979.

Kooi, M., Reisser, J., Slat, B., Ferrari, F. F., Schmid, M. S., Cunsolo, S., Brambini, R., Noble, K., Sirks, L.-A., Linders, T. E., et al., 2016. The effect of particle properties on the depth profile of buoyant plastics in the ocean, *Scientific reports*, 6(1), 1–10.

Kooi, M., Nes, E. H. v., Scheffer, M., & Koelmans, A. A., 2017. Ups and downs in the ocean: effects of biofouling on vertical transport of microplastics, *Environmental science & technology*, 51(14), 7963–7971.

Korres, G., Ravdas, M., & Zacharioudaki, A., 2019. Mediterranean sea waves hindcast (cmems med-waves).

Kukulka, T., Proskurowski, G., Morét-Ferguson, S., Meyer, D., & Law, K., 2012. The effect of wind mixing on the vertical distribution of buoyant plastic debris, *Geophysical Research Letters*, 39(7).

Lacerda, A. L. d. F., Rodrigues, L. d. S., van Sebille, E., Rodrigues, F. L., Ribeiro, L., Secchi, E. R., Kessler, F., & Proietti, M. C., 2019. Plastics in sea surface waters around the antarctic peninsula, *Scientific reports*, 9(1), 3977.

Lange, M. & van Sebille, E., 2017. Parcels v0.9: Prototyping a lagrangian ocean analysis frameworkfor the petascale age, *Geoscientific Model Development Discussions*, 10, 4175–4186.

Large, W. G., McWilliams, J. C., & Doney, S. C., 1994. Oceanic vertical mixing: A review and a model with a nonlocal boundary layer parameterization, *Reviews of geophysics*, 32(4), 363–403.

Lebreton, L., Egger, M., & Slat, B., 2019. A global mass budget for positively buoyant macroplastic debris in the ocean, *Scientific reports*, 9(1), 1–10.

Lebreton, L. C., Van Der Zwet, J., Damsteeg, J.-W., Slat, B., Andrady, A., & Reisser, J., 2017. River plastic emissions to the world's oceans, *Nature communications*, 8, 15611.

Lebreton, L.-M., Greer, S., & Borrero, J. C., 2012. Numerical modelling of floating debris in the world's oceans, *Marine pollution bulletin*, 64(3), 653–661.

Liubartseva, S., Coppini, G., Lecci, R., & Clementi, E., 2018. Tracking plastics in the mediterranean: 2d lagrangian model, *Marine pollution bulletin*, 129(1), 151–162.

Madec, G., Bourdallé-Badie, R., Bouttier, P.-A., Bricaud, C., Bruciaferri, D., Calvert, D., Chanut, J., Clementi, E., Coward, A., Delrosso, D., et al., 2017. Nemo ocean engine.

Mascarenhas, R., Santos, R., & Zeppelini, D., 2004. Plastic debris ingestion by sea turtles in paraíba, brazil, *Marine pollution bulletin*, 49(4), 354–355.

McWilliams, J. C. & Sullivan, P. P., 2000. Vertical mixing by langmuir circulations, *Spill Science & Technology Bulletin*, 6(3-4), 225–237.

Merlino, S., Locritani, M., Bernardi, G., Como, C., Legnaioli, S., Palleschi, V., & Abbate, M., 2020. Spatial and temporal distribution of chemically characterized microplastics within the protected area of pelagos sanctuary (nw mediterranean sea): Focus on natural and urban beaches, *Water*, 12(12), 3389.

Molnar, J. L., Gamboa, R. L., Revenga, C., & Spalding, M. D., 2008. Assessing the global threat of invasive species to marine biodiversity, *Frontiers in Ecology and the Environment*, 6(9), 485–492.

Morales-Caselles, C., Viejo, J., Martí, E., González-Fernández, D., Pragnell-Raasch, H., González-Gordillo, J. I., Montero, E., Arroyo, G. M., Hanke, G., Salvo, V. S., et al., 2021. An inshore–offshore sorting system revealed from global classification of ocean litter, *Nature Sustainability*, 4(6), 484–493.

Mountford, A. & Morales Maqueda, M., 2019. Eulerian modeling of the three-dimensional distribution of seven popular microplastic types in the global ocean, *Journal of Geophysical Research: Oceans*, 124(12), 8558–8573.

O'Brine, T. & Thompson, R. C., 2010. Degradation of plastic carrier bags in the marine environment, *Marine pollution bulletin*, 60(12), 2279–2283.

Onink, V., Wichmann, D., Delandmeter, P., & van Sebille, E., 2019. The role of ekman currents, geostrophy, and stokes drift in the accumulation of floating microplastic, *Journal of Geophysical Research: Oceans*, 124(3), 1474–1490.

Onink, V., Jongedijk, C. E., Hoffman, M. J., van Sebille, E., & Laufkötter, C., 2021a. Global simulations of marine plastic transport show plastic trapping in coastal zones, *Environmental Research Letters*, 16(6), 064053.

Onink, V., van Sebille, E., & Laufkötter, C., 2021b. Empirical lagrangian parametrization for wind-driven mixing of buoyant particles at the ocean surface, *Geoscientific Model Development Discussions*, pp. 1–19.

Pabortsava, K. & Lampitt, R. S., 2020. High concentrations of plastic hidden beneath the surface of the atlantic ocean, *Nature communications*, 11(1), 1–11.

Pedrotti, M. L., Mazzocchi, M. G., Lombard, F., Galgani, F., Kerros, M. E., Henry, M., Elineau, A., Petit, S., Fernandez-de Puelles, M. L., Gasparini, S., et al., 2018. Tara mediterranean expedition: assessing the impact of microplastics on mediterranean ecosystem, in *Proceedings of the International Conference on Microplastic Pollution in the Mediterranean Sea*, pp. 25–29, Springer.

Pieper, C., Ventura, M. A., Martins, A., & Cunha, R. T., 2015. Beach debris in the azores (ne atlantic): Faial island as a first case study, *Marine pollution bulletin*, 101(2), 575–582.

Pieper, C., Martins, A., Zettler, E., Loureiro, C. M., Onink, V., Heikkilä, A., Epinoux, A., Edson, E., Donnarumma, V., Vogel, F. d., et al., 2019. Into the med: Searching for microplastics from space to deep-sea, in *International Conference on Microplastic Pollution in the Mediterranean Sea*, pp. 129–138, Springer.

Poulain, M., Mercier, M. J., Brach, L., Martignac, M., Routaboul, C., Perez, E., Desjean, M. C., & Ter Halle, A., 2018. Small microplastics as a main contributor to plastic mass balance in the north atlantic subtropical gyre, *Environmental science & technology*, 53(3), 1157–1164.

Ramon, J., Lledó, L., Torralba, V., Soret, A., & Doblas-Reyes, F. J., 2019. What global reanalysis best represents near-surface winds?, *Quarterly Journal of the Royal Meteorological Society*, 145(724), 3236–3251.

Resmerită, A.-M., Coroaba, A., Darie, R., Doroftei, F., Spiridon, I., Simionescu, B. C., & Navard, P., 2018. Erosion as a possible mechanism for the decrease of size of plastic pieces floating in oceans, *Marine pollution bulletin*, 127, 387–395.

Ruiz-Orejón, L. F., Sardá, R., & Ramis-Pujol, J., 2018. Now, you see me: High concentrations of floating plastic debris in the coastal waters of the balearic islands (spain), *Marine pollution bulletin*, 133, 636–646.

Ryan, P. G., Perold, V., Osborne, A., & Moloney, C. L., 2018. Consistent patterns of debris on south african beaches indicate that industrial pellets and other mesoplastic items mostly derive from local sources, *Environmental Pollution*, 238, 1008–1016.

Semcesen, P. O. & Wells, M. G., 2021. Biofilm growth on buoyant microplastics leads to changes in settling rates: Implications for microplastic retention in the great lakes, *Marine Pollution Bulletin*, 170, 112573.

Simon-Sánchez, L., Grelaud, M., Garcia-Orellana, J., & Ziveri, P., 2019. River deltas as hotspots of microplastic accumulation: The case study of the ebro river (nw mediterranean), *Science of the total environment*, 687, 1186–1196.

Song, Y. K., Hong, S. H., Jang, M., Han, G. M., Jung, S. W., & Shim, W. J., 2017. Combined effects of uv exposure duration and mechanical abrasion on microplastic fragmentation by polymer type, *Environmental science & technology*, 51(8), 4368–4376.

Tsiaras, K., Hatzonikolakis, Y., Kalaroni, S., Pollani, A., & Triantafyllou, G., 2021. Modeling the pathways and accumulation patterns of micro-and macro-plastics in the mediterranean, *Frontiers in Marine Science*, p. 1389.

Turcotte, D., 1986. Fractals and fragmentation, *Journal of Geophysical Research: Solid Earth*, 91(B2), 1921–1926.

Van Den Bremer, T. & Breivik, Ø., 2018. Stokes drift, *Philosophical Transactions of the Royal Society A: Mathematical, Physical and Engineering Sciences*, 376(2111), 20170104.

Van Franeker, J. A. & Law, K. L., 2015. Seabirds, gyres and global trends in plastic pollution, *Environmental pollution*, 203, 89–96.

van Sebille, E., Wilcox, C., Lebreton, L., Maximenko, N., Hardesty, B. D., Van Franeker, J. A., Eriksen, M., Siegel, D., Galgani, F., & Law, K. L., 2015. A global inventory of small floating plastic debris, *Environmental Research Letters*, 10(12), 1–11.

Van Sebille, E., Aliani, S., Law, K. L., Maximenko, N., Alsina, J. M., Bagaev, A., Bergmann, M., Chapron, B., Chubarenko, I., Cózar, A., et al., 2020. The physical oceanography of the transport of floating marine debris, *Environmental Research Letters*, 15(2), 023003.

Viršek, M. K., Lovšin, M. N., Koren, Š., Kržan, A., & Peterlin, M., 2017. Microplastics as a vector for the transport of the bacterial fish pathogen species aeromonas salmonicida, *Marine pollution bulletin*, 125(1-2), 301–309.

Waldschläger, K. & Schüttrumpf, H., 2019a. Effects of particle properties on the settling and rise velocities of microplastics in freshwater under laboratory conditions, *Environmental science & technology*, 53(4), 1958–1966.

Waldschläger, K. & Schüttrumpf, H., 2019b. Erosion behavior of different microplastic particles in comparison to natural sediments, *Environmental science & technology*, 53(22), 13219–13227.

Woodall, L. C., Sanchez-Vidal, A., Canals, M., Paterson, G. L., Coppock, R., Sleight, V., Calafat, A., Rogers, A. D., Narayanaswamy, B. E., & Thompson, R. C., 2014. The deep sea is a major sink for microplastic debris, *Royal Society open science*, 1(4), 140317.

Wright, S. L., Thompson, R. C., & Galloway, T. S., 2013. The physical impacts of microplastics on marine organisms: a review, *Environmental pollution*, 178, 483–492.

Zacharioudaki, A., Ravdas, M., Korres, G., & Lyubartsev, V., 2020. Quality information document (cmems-med-quid-006-012).

Zeri, C., Adamopoulou, A., Koutsikos, N., Lytras, E., Dimitriou, E., et al., 2021. Rivers and wastewater-treatment plants as microplastic pathways to eastern mediterranean waters: First records for the aegean sea, greece, *Sustainability*, 13(10), 5328.

Zhao, D. & Li, M., 2019. Dependence of wind stress across an air–sea interface on wave states, *Journal of Oceanography*, 75(3), 207–223.

Zhao, S., Zettler, E. R., Bos, R. P., Lin, P., Amaral-Zettler, L. A., Mincer, T. J., et al., 2022. Large quantities of small microplastics permeate the surface ocean to abyssal depths in the south atlantic gyre, *Global Change Biology*.

Zhu, L., Zhao, S., Bittar, T. B., Stubbins, A., & Li, D., 2020. Photochemical dissolution of buoyant microplastics to dissolved organic carbon: rates and microbial impacts, *Journal of hazardous materials*, 383, 121065.

Chapter 6

Discussion & outlook

The work within this thesis provides novel insights into the transport and transformation of plastic debris in the ocean. Chapter 3 investigated the role of plastic beaching and resuspension on a global scale, and indicated that coastal waters might play a more prominent role in the fate of plastic debris than previously suspected. However, the scope of the transport scenarios in chapter 3 was limited to floating plastic at the ocean surface, and did not consider vertical transport processes. Chapter 4 describes parametrizations that model wind-driven vertical turbulent mixing within the surface ocean mixed layer. Using this parametrization and the beaching parametrization from chapter 3, chapter 5 shows that the particle size and density can strongly influence the full three-dimensional transport of microplastics in the Mediterranean Sea. In addition, chapter 5 examined the influence of microplastic fragmentation, and demonstrated that it likely does not play a significant role in microplastic mass loss over short time periods (up to 3 years). From this body of work, various general conclusions can be drawn, which are discussed in section 6.1. Section 6.2 then discusses a number of limitations, and outlines future research perspectives based on this thesis.

6.1 Overview of the main results

6.1.1 The importance of coastal transport processes

Within this thesis plastic transport was considered on both a global and regional scale, and in both cases coastlines and coastal waters were found to play a critical role in the overall fate of plastic debris. On a global scale, at least 77% of plastic debris is expected to be within 10 km of the ocean coastlines, while for large microplastics particles (< 5 mm) in the Mediterranean Sea up to 94% of microplastic particles are within the coastal zone. With such a large fraction of the total plastic budget, nearshore transport processes likely play a crucial role in the fate of plastic debris in the ocean. While the importance of coastal transport processes on global plastic transport had been noted (Zhang, 2017), the influence of these coastal processes on plastic debris remains poorly understood and the ocean modeling community has largely focused on understanding transport in the open ocean (Kubota et al., 2005; Van Sebille, 2015; Lebreton et al., 2018; Onink et al., 2019). However, both chapter 3 and 5 underscore how crucial these coastal processes can be.

The underlying assumption of the beaching and resuspension parametrization described in chapter 3 is that the longer a particle is adrift close to shore or beached on the coastline, the more likely it is to at some point beach or be resuspended. While this assumption might not always be strictly true (floating plastic might sink due to biofouling (Fazey & Ryan, 2016) or beached plastic might be buried in sediment (Taïbi et al., 2021)), Hinata et al. (2017) and Pawlowicz (2021) suggest that to first order this assumption is valid. In addition, the stochastic

nature of the parametrizations acknowledges that sub-grid coastal processes play a crucial role in plastic beaching and resuspension. In contrast, a common form of parametrizing plastic beaching by tracking a particle until it sticks to the coastline (Lebreton et al., 2012; Liubartseva et al., 2018; Chenillat et al., 2021) is more an indication of the numerical difficulties in calculating particle trajectories near boundaries rather than being due to oceanographic processes (Lynch et al., 2014). To illustrate, open ocean currents might transport a particle towards a coastline in the physical world, but as it gets closer to land the currents would be more affected by coastal processes. For example, this could result in the particle moving parallel to the coastline if there was a predominantly nearshore along-shore current. However, none of these coastal currents would be resolved within the oceanic general circulation model (OGCM) output, and so the model would predict that the particle would immediately beach on the coastline. As such, making beaching a purely stochastic process acknowledges that the actual physical processes that result in particle beaching are not fully represented within the flow fields, whereas the artificial anti-beaching current described in chapter 2 prevents particle beaching due to the numerical advection.

Finally, the parametrizations are flexible, as beaching and resuspension timescales λ_B and λ_R can be defined to be functions of variables such as coastal geomorphology (Daily et al., 2021) or the particle size (Chapter 5). While coastal geomorphology can influence beached plastic concentrations on short spatial scales, it was not shown to strongly affect the distribution of beached plastic on a global scale (Chapter 3). This was also demonstrated by Daily et al. (2021), who applied the same beaching/resuspension parametrizations for Lake Erie with λ_B and λ_R both depending on local geomorphology. While geomorphology-dependent beaching and resuspension influenced local beached plastic concentrations, the overall distribution of beached plastic around the lake was not strongly affected (Daily et al., 2021). In contrast, size-dependent resuspension was shown to have a stronger influence on the relative amount of beached plastic, although this was more on the total amount of beached plastic than its horizontal distribution. Ultimately, the actual 'correct' values of λ_B and λ_R remain highly uncertain, and further field and modeling work will be required to constrain these parameters.

6.1.2 The influence of vertical transport processes

Chapter 5 highlights the importance of including vertical transport processes in modeling plastic debris transport, especially for smaller microplastic particles. modeling studies that focus just on positively buoyant plastic debris, such as described in chapter 3, assume that the positive buoyancy of the particle will keep it at the ocean surface. While this assumption might hold for large objects, positively buoyant microplastic particles have been sampled below the ocean surface due to turbulent vertical transport processes (Kukulka et al., 2012; Kooi et al., 2016; Pieper et al., 2019b). Given that including vertical transport strongly influences the large-scale transport and distribution of microplastic particles (Chapter 5), neglecting vertical transport processes leads to an incomplete understanding of the fate of plastic debris in the ocean. In addition, it also underscores the need for modeling studies to indicate the size and type of plastic items that are being considered within a study. For example, the beaching study described in chapter 3 does not explicitly specify the types of object being considered, as the virtual particles were assumed to represent the general category of positively buoyant marine plastic debris. Similar imprecise definitions are more common throughout the literature (Van Sebille, 2015; Liubartseva et al., 2018; Kaandorp et al., 2020; Suaria et al., 2020), but given the influence particle size and density have on the particle transport behavior it is an oversimplification to assume that the modelled transport will hold for all types of plastic objects.

Biofouling is a process that was consciously left out of the size-dependent transport and fragmentation scenarios, as the constantly changing particle densities would complicate isolating

the specific influence of the particle size on the particle transport. In addition, the influence biofouling might have on fragmentation rates is poorly understood. However, biofouling can play a crucial role in the long-term fate of plastic debris in the ocean, as the growth of biofilm on plastic surfaces can increase the object's density and decrease its buoyancy (Fazey & Ryan, 2016). Given that the rate of biofouling depends on the complex interplay between variables such as the object size, polymer type and the environmental conditions (Lobelle & Cunliffe, 2011; Fazey & Ryan, 2016), biofouling is a difficult process to study within a modeling setting. Fischer et al. (2022) examined the role of biofouling on particles with various sizes (0.01 - 1 mm) and within various ocean regions with distinct biological and physical properties. As was reported by Kooi et al. (2017), biofouling was found to lead to vertical oscillatory behavior, as biofilm would increase the particle density and cause it to sink. However, below the euphotic zone the lack of sunlight would cause a gradual decrease in the amount of biofilm, which in turn would decrease the particle density, increase the buoyancy and lead to the particle rising towards the surface again. While such oscillations have yet to be observed from field measurements, it would imply that plastic debris is distributed throughout the water column as has been shown with field measurements (Pieper et al., 2019b; Egger et al., 2020; Pabortsava & Lampitt, 2020).

Even when positively buoyant, the results described in chapter 5 and Fischer et al. (2022) demonstrate that microplastic particles can be mixed far below the ocean surface at depths of over 3000 m. As such, vertical transport processes are clearly essential in order to get a complete understanding of plastic debris dynamics in the ocean. This is especially the case considering that both chapter 5 and Fischer et al. (2022) likely underestimate the total vertical mixing in the ocean. As described in chapter 4, Langmuir circulation (LC) processes can increase the strength of near-surface mixing by a factor 3 - 4 (McWilliams & Sullivan, 2000). However, LC-driven mixing occurs on spatial scales of meters to tens of meters (McWilliams & Sullivan, 2000), and as such it is not resolved within OGCMs. It is not trivial to calculate the amplification of vertical mixing due to LC processes, and so while chapter 4 demonstrated the influence LC-driven mixing can have on the vertical distribution of microplastic particles, both chapter 5 and Fischer et al. (2022) applied the KPP mixing parametrization assuming negligible LC-driven turbulent mixing. Meanwhile, the scenarios in chapter 5 did not include the influence of biofouling, while Fischer et al. (2022) focused on biofouling within specific ocean regions and therefore did not include horizontal advection. Finally, while both chapter 5 and Fischer et al. (2022) used the de Lavergne et al. (2020) climatology to account for vertical mixing due to internal tides, other subsurface processes such as internal waves and current shear instabilities are not accounted for (Skyllingstad et al., 1996; Cuypers et al., 2013). Therefore, future work could integrate the biofouling and transport models described in chapter 5 and Fischer et al. (2022) to more fully study the 3D transport of plastic debris in the ocean.

6.1.3 The role of fragmentation

Plastic fragmentation in marine environments is a complex process, and the work in chapter 5 demonstrates that the importance of accounting for plastic fragmentation within a modeling framework depends on the research question being studied. Microplastic fragmentation is shown to be a slow process, with beach-based fragmentation not strongly influencing the size distribution of polyethylene and polypropylene microplastic particles within the Mediterranean Sea over a period of 3 years. Similarly, although fragmentation has been suggested as possible sink of plastic mass through the mass transfer to small micro-/nanoplastic particles (Lebreton et al., 2019), over a 3 year period at most 2.45% of plastic mass is transferred to fragments smaller than 0.156 mm. Ocean-based fragmentation can contribute to the generation of microplastic particles, but unless the ocean-based fragmentation occurs on similar timescales as beach-based fragmentation its influence is negligible. As such, most short-term modeling studies of polyethylene and

polypropylene plastic debris up to around 3 years in length can neglect fragmentation processes.

However, over longer timescales (years to decades), fragmentation can play an important role in the gradual transfer of plastic mass from coastal waters to the open ocean. The size-dependent transport scenarios in chapter 5 show that smaller particles are more likely to reach the open ocean, and fragmentation plays a critical role in reducing the size of plastic debris. While fragmentation might be slow, over the course of decades it could lead to the complete degradation of a plastic object into smaller fragments (Song et al., 2017; Gerritse et al., 2020), which in turn could result in the gradual offshore and subsurface transfer of plastic mass in the ocean. The fragmentation scenarios in chapter 5 are calibrated for polyethylene and polypropylene fragments, and for such polymers fragmentation can play a role in the large-scale particle transport over timescales of decades. However, other polymers such as polystyrene can fragment significantly faster (Song et al., 2017), which suggests that fragmentation could play a more important short-term role in modeling the transport of such plastic debris types.

6.1.4 The fate of plastic in the ocean

While a field measurement provides insight into the amount and type of plastic objects found at a given location at a given time, it is essentially just a snapshot with little to no information as to the origin of any specific plastic fragment. Models can track virtual plastic particles throughout the ocean, and based on work such as Van Sebille et al. (2012) and Onink et al. (2019) it has been assumed that over timescales of years to decades plastic debris accumulates in the subtropical ocean gyres. This is supported by the high concentrations in particularly the North Atlantic and North Pacific subtropical gyres (Law et al., 2010; Lebreton et al., 2018; Van Sebille, 2015), and also by presence of floating debris that is decades old (Lebreton et al., 2018). However, the total amount of plastic afloat at the ocean surface is estimated to be significantly less that the amount of plastic thought to enter the ocean in just a single year (Jambeck et al., 2015; Van Sebille et al., 2015), and processes such as biofouling and fragmentation can cause physical changes to plastic debris over the course of years instead of decades (Kaandorp et al., 2021; Fazey & Ryan, 2016; Gerritse et al., 2020). As such, while surface plastic debris concentrations might continue to increase within the subtropical gyres (Wilcox et al., 2019), this can not be the ultimate fate of all or even the majority of plastic debris in the ocean. The work described within this thesis is one of the first modeling efforts that accounts for beaching, nearshore- and offshore-transport and transformation processes. While the parametrizations are not perfect and not all transport mechanisms are fully accounted for, the work described in chapters 3 and 5 provides a general description of the fate of positively buoyant plastic when it enters the ocean from land-based sources.

The rise velocity is crucial to predicting the fate of plastic debris. Particles with higher rise velocities, which generally implies either larger and/or lighter objects, are unlikely to reach the open ocean. While the distribution of particles between the beach and coastal water reservoirs is dependent on the ratio of the beaching and resuspension timescales, the fraction of the total plastic input that reaches the open ocean remains relatively small with at most 23% of the total input globally reaching the open ocean without considering the particle size. In the Mediterranean Sea, this fraction is even lower for large microplastics ($d = 5.000$ mm), where on average at most 5.74% of plastic particles is further than 5 km from the coastline. However, as particles get smaller this nearshore trapping starts to decrease, with up to 25% of $d = 0.002$ mm microplastic particles reaching open waters. The existence of such a sorting mechanism based on plastic debris size and buoyancy has been hypothesized based on field observations (Morales-Caselles et al., 2021), and Stokes drift could at least partially account for this. Onink et al. (2019) demonstrated that Stokes drift plays an important role in the landward transport of plastic particles, but the strength of Stokes drift decreases exponentially with increasing depth

(Breivik et al., 2016). As particles get smaller, they are more easily mixed below the ocean surface (Chapters 4 and 5) and the weaker subsurface Stokes drift results in fewer particles remaining trapped near coastlines. Vertical transport processes therefore play a critical role in determining how easily a plastic object is able to escape to the open ocean.

A plastic object also changes physically and chemically the longer it spends adrift in the ocean and stranded on coastlines. Plastic objects undergo a constant cycle of beaching and resuspension (Chapter 3), and are exposed to UV radiation, temperature fluctuations and mechanical stresses (Andrady, 2017). This can lead to the oxidation and fracturing of the object's surface, where over time smaller plastic fragments can break off of the original parent object (Andrady, 2017). At the same time, microbes and larger marine organisms can settle on a plastic object, creating a biofilm and potentially also contributing to the fragmentation process (Yang et al., 2021). The fragments will undergo the same cycle of beaching and resuspension as the parent object, but as a fragment gets smaller it becomes more likely to escape into the open ocean. There a particle can continue to break into smaller fragments, but this likely occurs at a much slower rate due to lower temperatures, oxygen levels and partial blocking of UV radiation by sea water slowing down surface oxidation processes (Andrady, 2017). Continued biofouling can lead to the eventual sinking of a particle as it becomes more dense, where it might end up down on the sea floor or gradually oscillate in depth. Given enough time, a plastic object can completely degrade into a range of micro- and potentially nanoparticles (Kaandorp et al., 2021; Piccardo et al., 2020), but this is likely a slow process taking place over decades, depending on the object size, shape and polymer type.

In summary, it is an oversimplification to assume that plastic debris will simply end up floating at the ocean surface in the subtropical ocean gyres. While concentrations within the gyres are orders of magnitude higher compared to other regions of the ocean (such as at the equator), the model scenarios in chapter 3 and 5 indicate that almost all buoyant plastic remains trapped on or near coastlines. It is also an oversimplification that there is just one general 'fate' for plastic debris in the ocean, as transport processes are strongly affected by the particle size and buoyancy.

A number of processes were not considered within this thesis, and their influence on plastic debris in the ocean is generally not completely understood. For example, the plastic debris scenarios described within this thesis are relatively short, with the longest Lagrangian simulations spanning up to 5 years. It is uncertain what would happen with marine plastic over much longer timescales (decades to centuries). Plastic found afloat within the North Pacific gyre have been dated to be up to 50 years old (Lebreton et al., 2018), but it is unclear whether any plastic object will eventually be broken down into progressively smaller plastic fragments or perhaps even completely remineralize (Hoellein & Rochman, 2021). A plastic object might also end up buried within sediment, such as on a beach (Fauziah et al., 2015) or below the seafloor (Brignac et al., 2019), and it is unclear whether this would be a temporary or permanent sink (Martin et al., 2020; Okuku et al., 2022). Given that plastic transport is essentially carbon transport, it is even possible that plastic debris plays a role within the marine carbon cycle (Galgani & Loiselle, 2021; Smeaton, 2021), although the extent to which this is the case remains highly uncertain and speculative.

The role of the deep sea as a potential sink of plastic debris is also not fully understood, for while the scenarios in chapter 5 show that even positively buoyant plastic debris can be found thousands of meters below the ocean surface, it is unsure how much plastic remains there. Neither the size-dependent transport nor the fragmentation scenario included interactions with the sea floor as there was insufficient literature to develop and validate a parametrization

of such processes, and as such the role of deep ocean in the fate of plastic debris remains uncertain.

Finally, the interaction between marine wildlife and plastic debris remains complicated and poorly understood. While there is extensive evidence that plastic debris can harm marine wildlife on an individual level (Gregory, 2009), it is difficult to estimate the harm plastic debris can cause to a species as a whole. In turn, marine wildlife can also affect marine debris, such as via biofouling (Fazey & Ryan, 2016) or by contributing to the fragmentation of microplastic fragments (Dawson et al., 2018). While the work within this thesis contributes to the comprehension of how various physical processes affect the fate of plastic debris in the ocean, greater understanding plastic-ecosystem interactions will be crucial to evaluating the impact of plastic pollution on the ocean as a whole.

6.1.5 The global plastic mass budget: where is all the plastic?

Since Jambeck et al. (2015) estimated 4.8 - 12.7 million tons of plastic waste entered the ocean in 2010 alone, a lot of effort has gone towards constraining the amount of plastic debris in various marine habitat reservoirs to try and establish a closed global plastic mass budget. Based largely on microplastic measurements, the ocean surface was estimated to hold at most up to 236 000 tons (Van Sebille et al., 2015; Eriksen et al., 2014; Cózar et al., 2014). While this total might be 4 - 16 times higher when accounting for larger debris items (Lebreton et al., 2018), it still adds up to just a fraction of the total amount of plastic estimated to enter the ocean in just a single year. Part of this missing mass could actually be in the open ocean but just below the ocean surface, as Pabortsava & Lampitt (2020) reports subsurface microplastic count and mass concentrations in the North Atlantic that are higher than at the ocean surface. In contrast, Egger et al. (2020) reported an exponential drop in microplastic count and mass concentrations with depth in the North Pacific, but between 56 - 80% of the micro- and mesoplastic mass in the top 2000 m of the water column could still be below 5m from the ocean surface. Plastic debris can also settle on the seabed, and an estimated 8.4 million tons of microplastic mass lies on the seabed globally (Barrett et al., 2020). However, this estimate is likely conservative, as it doesn't account for plastic debris larger than 5 mm nor for higher plastic concentrations in coastal sediments (Barrett et al., 2020). Finally, coastlines can have plastic concentrations of up to 947 kg km^{-1} (Debrot et al., 2013) and can potentially hold a large fraction of the total plastic in the marine environment, but concrete numerical estimates remain challenging given the lack of standardized field measurements (Browne et al., 2015).

This thesis indicates that coastal systems could potentially hold over 77% of all positively buoyant plastic that enters the ocean, even if the exact distribution of plastic between beaches and adrift in coastal waters is strongly dependent on model parameters. The estimates of floating plastic mass by Van Sebille et al. (2015), Cózar et al. (2014) and Eriksen et al. (2014) were largely based on microplastic measurements collected in the open ocean, but both models (Chapter 3) and observations (Ruiz-Orejón et al., 2016; Pedrotti et al., 2016) suggest floating plastic concentrations are higher in nearshore areas. As such, the total amount of floating plastic debris might be significantly higher than previously assumed.

Assuming that 54% of the total plastic input into the ocean is at least initially positively buoyant (Geyer et al., 2017) and using the low-end estimate from Jambeck et al. (2015) that 4.7 million tons entered the ocean in 2010, beaches hold an estimated 0.72 - 2.06 million tons of plastic debris (Chapter 3). However, there are a number of reasons why this estimate is highly unreliable. First, there have been several indications that the Jambeck et al. (2015) plastic inputs are too high (Tramoy et al., 2019; Van Emmerik et al., 2019). Jambeck et al. (2015) made a number of assumptions regarding waste generation and mismanagement that rested in part on expert judge-

ment, which at the time was justified given the insufficient availability of waste (mis)management worldwide. This led to estimates such that 83% of Indonesian waste was mismanaged, and that 15 - 40 % of all plastic waste ended up in the ocean. However, Van Emmerik et al. (2019) estimated that just 3% of the mismanaged waste in Jakarta ended up in the ocean, and Tramoy et al. (2019) similarly concludes that the Jambeck et al. (2015) approach overestimates the amount of plastic entering the ocean from the Seine river. As such, the total amount of plastic entering the ocean could be overestimated, which in turn would affect the estimated amount of the beached plastic mass. There are other plastic input estimates from land-based sources such as rivers (Lebreton et al., 2017; Schmidt et al., 2017), but these are also in part based on the Jambeck et al. (2015) mismanaged waste estimates and therefore might similarly overestimate plastic inputs.

Secondly, the assumption that 54% of the plastic input is positively buoyant is highly uncertain, as it assumes that the polymer composition of plastic production is the same as for discarded waste. At the same time it also assumes that all negatively buoyant polymer objects will sink (e.g. a PET bottle with trapped air would float (Ryan, 2015)) and all positively buoyant polymers will float (polyethylene and polypropylene are found at the sea floor (Brignac et al., 2019)). Finally, the model scenarios in chapter 3 do not consider the plastic debris size, density or fragmentation processes, and it is shown in chapter 5 that this can significantly affect the amount of beached plastic. One possible approach to estimate the total amount of beached debris would be to follow the approach of Van Sebille et al. (2015), where relative model concentrations are combined with a standardized field observations. However, given the lack of standardization in measurement methodologies in collecting and reporting beached plastic concentrations (Browne et al., 2015), such an approach is currently not feasible. As such, the total amount of beached plastic remains highly uncertain.

Chapter 5 and Fischer et al. (2022) show that subsurface microplastic concentrations can have particle count concentrations on the same order as surface measurements, and field measurements have similarly shown high subsurface concentrations (Pieper et al., 2019b; Choy et al., 2019; Egger et al., 2020; Pabortsava & Lampitt, 2020). However, the number of field measurements is limited, and so while Pabortsava & Lampitt (2020) estimate the top 200m of the North & South Atlantic could hold up to 21.1 million tons of plastic debris, this is based on measurements collected at just 12 stations that are not necessarily representative of all Atlantic waters. Meanwhile, the results in chapter 5 indicate that it is predominantly small microparticles (< 0.1 mm) that get mixed below the ocean surface, while most of the plastic mass is found in larger particles (Lebreton et al., 2018). Macroplastic objects are found up to thousands of meters below the ocean surface (Pasquini et al., 2016; Spirkovski et al., 2019; Sogabe & Takatsuji, 2021; Song et al., 2021) and as such the subsurface ocean could hold a large mass of plastic debris, but the work within this thesis does not constrain the mass of subsurface plastic.

6.2 Limitations & future perspectives

6.2.1 Model validation with field measurements

Models are powerful at testing and evaluating various scenarios of plastic debris transport and transformation, but model validation with field measurements is crucial to evaluate how well a model represents and reproduces the physical world. While large standardized datasets of plastic measurements are not always readily available, where possible the results described in chapters 3, 4 and 5 were compared with field observations.

It is difficult to track plastic dynamics in coastal regions, but there have been a number

of field studies that agree with the model predictions that coastal waters have higher plastic concentrations than further offshore (Ryan, 2015; Ruiz-Orejón et al., 2016; Morales-Caselles et al., 2021). While this is not sufficient to conclude that coastal waters truly hold more total plastic mass than the open ocean, it is a promising indication that coastal processes could indeed trap the majority of plastic entering the ocean from land-based sources within the coastal zone, and that the particle size could play an important role in this (Morales-Caselles et al., 2021). Field experiment with gps trackers such as Pawlowicz (2021) could play a critical role in this, both to study particle dynamics during the final stages prior to beaching and to investigate how likely plastic debris is to reach the open ocean. Laboratory experiments could also play a role in studying particle dynamics in coastal environments, even though an experimental setup might not exactly reproduce coastal conditions. For example, flume and wave tank experiments such as Kerpen et al. (2020) and Alsina et al. (2020) can reproduce particle transport in a variety of wave conditions which would be challenging to study in a natural environment given the difficulty in tracking all the small microplastic particles.

Evaluating the performance of the beaching parametrizations in chapter 3 and 5 is difficult, as it is challenging to isolate the effects of various processes. On a global scale, the model scenarios overpredict the amount of beached plastic in comparison to field observations by up to three orders of magnitude. In contrast, the relative concentrations match reasonably well with the relative distributions in South Africa (Ryan et al., 2018), Australia (Hardesty et al., 2017) and parts of the United States (Ribic et al., 2010, 2012). The amount of beached plastic on islands appears to be underestimated (Barnes & Milner, 2005; Pieper et al., 2015), but this could be due to the input scenarios neglecting the maritime plastic inputs that have been shown to contribute significantly to beached plastic on islands (Lavers & Bond, 2017; Ryan et al., 2019; Pieper et al., 2019a). In general, given how strongly the input scenario affects the modelled distribution of beached plastic, it is unclear whether a comparison with field observations is actually evaluating the performance of the beaching parametrization or the accuracy of the input scenario. Ultimately both the input and beaching components are critical for the overall model performance and result in the final model output and predictions, but the difficulty in isolating these two effects makes model tuning challenging. In a case where a large field dataset is available, Bayesian machine learning techniques can be applied to simultaneously tune and constrain a range of model parameters. For example, Kaandorp et al. (2020) found that a beaching timescale $\lambda_B = 26$ days resulted in optimal model performance relative to field microplastic concentrations, but this was only possible given the relatively extensive sampling of microplastic concentrations in the Mediterranean Sea. Such an analysis would be difficult when accounting for both plastic beaching and resuspension on a global scale, and thus while chapter 3 describes an extensive model parameter sensitivity analysis, it does not strongly constrain the beaching and resuspension timescale parameter values.

Another difficulty in comparing field measurements and model predictions again comes back to questions of scale, both spatial and temporal. Plastic concentrations can be extremely variable on short spatial and temporal timescales both in the ocean (Lebreton et al., 2018) and on coastlines (Browne et al., 2015; Pieper et al., 2015; Kaandorp et al., 2022). A single measurement is therefore not necessarily indicative of plastic concentrations in general for a given region. To get a more complete understanding of plastic concentrations at a site repeated measurements have to be taken at preferably regular and frequent time intervals (Kaandorp et al., 2022). Similarly, in an ideal situation measurements would be taken at uniformly-spaced spatial intervals to study the spatial variability (Hardesty et al., 2017; Kaandorp et al., 2022). However, sites are frequently only sampled once or a limited number of times given time, economic and accessibility constraints (Browne et al., 2015). Ideally a model would be able to reproduce both the absolute concentrations and variability found at a given site in the physical world, but in part due to the limited

spatial and temporal resolution of the OGCM datasets used in this thesis this is not feasible. In conclusion, a model should always be compared relative to observations as a baseline for model performance. However, in order to develop true predictive models that will be able to reproduce both absolute plastic concentrations and the variability more high-resolution field datasets are required.

While it depends on the particular scope of a study, field plastic concentrations are not always reported with divisions for different particle sizes. As such, limited evaluation with field observations was possible for the size-dependent results described in chapters 4 and 5. This is particularly a problem for particles smaller than ≈ 0.33 mm, as manta trawl nets remain the most common sampling technique for microplastics adrift in the ocean. As these nets typically have a mesh size of $0.20 - 0.33$ mm, they undersample small particles. Alternative measurement systems that could sample small particles such as niskin bottles (Pieper et al., 2019b) or high-volume filtration systems (Zhao et al., 2022) are not yet widely used. Given these limitations, there is currently insufficient data to validate the relative distributions of different particle sizes in the Mediterranean, let alone distinguish between different particle densities. However, the agreement between model predictions and observations regarding the existence of size-dependent coastal trapping mechanisms (Morales-Caselles et al., 2021) is promising, as it indicates that the main physical processes governing large-scale particle transport are at least partially resolved.

Given the relatively large dataset of near-surface vertical concentration profiles, the wind mixing parametrizations described in chapter 4 can be evaluated over a relatively wide range of wind conditions. Ideally there would be sufficient data to subdivide the measured vertical profiles into particle size/buoyancy classes, vertical profiles would be measured at wind speeds higher than 9.3 m s^{-1} and there would be more extensive sampling of the vertical profiles below 5m from the ocean surface. However, with the currently available data at least model validation under various wind conditions is possible. Overall, the modelled vertical concentration profiles match reasonably well with the field measurements, but both the KPP and SWB parametrizations tend to underestimate the depth to which particles are mixed below the surface. With the KPP parametrization, this can be partially corrected for by including LC-driven turbulent mixing, suggesting that neglecting LC turbulence underestimates the vertical transport processes. Given that LC processes are not resolved within OGCMs and there has been limited work parametrizing this LC-driven vertical mixing amplification, both the work in chapter 5 and Fischer et al. (2022) applied the KPP wind mixing parametrizations assuming negligible LC turbulence. This could have implications on the large-scale particle transport, but this has yet to be investigated. The vertical concentration variability is much smaller with the modelled concentration profiles than in the field measurements, but in this particular model setup this is to be expected. The concentration profiles in chapter 4 were calculated assuming constant wind conditions over a period of 12 hours, whereas this does not occur in the physical world. In addition, the field measurements are sorted solely according to wind conditions at the time the samples were collected, and e.g. variable mixed layer depths (MLD) at the sample locations could influence the vertical concentration profiles and thus show higher variability when all these measurements are plotted within one panel. Given that the parametrizations can adapt to time-varying wind and MLD conditions (as shown in chapter 5 and Fischer et al. (2022)), the overall model performance of the wind mixing parametrizations is quite good.

In short, continued collaboration between scientists within the marine plastic research community collecting field measurements and developing numerical models is vital to advance the understanding of the fate of plastic debris in the ocean. From a modeling perspective, three specific advancements within the field measurement sector would help to advance model development. Firstly, there is an urgent need for increased standardization of field measurements. Especially for field campaigns sampling coastlines, the wide variety of sampling methodologies,

reporting standards and even the units used hinder inter-study comparisons and the validation of numerical models. For example, while there is general agreement that microplastics refer to particles smaller than 5 mm in size (Frias & Nash, 2019), there is no standardized lower limit for what microplastic particles are sampled within a field campaign. Given that smaller particles are numerically more common, this can have important implications when concentrations are only reported as microplastic counts per unit area or length (Smith & Turrell, 2021).

Secondly, providing more detailed information regarding the different concentrations and size distributions of plastic debris according to the polymer type and overall density could provide insight into how such variables affect the distribution of plastic debris in the ocean. By standardizing definitions and methodologies, it would be easier to compare concentrations reported by different studies at different times. Secondly, given the variability in plastic concentrations on short spatial and temporal scales, it is important to design field campaigns where sites are sampled at frequent and regular intervals. With these datasets more advanced statistical models could be developed that in the future could for example predict large-scale plastic beaching or resuspension events (Kaandorp et al., 2022). However, this is only possible with high resolution datasets. Finally, large regions of the global ocean are undersampled, particularly below the ocean surface, and it is vital that areas such as remote coastlines, islands, the deep sea and the water column are more extensively sampled to gain a better understanding of the distribution and behavior of plastic debris. While none of these suggestions are trivial to implement, it does provide a general overview of the types of field measurements that are necessary from a modeling perspective to advance the marine plastic field. In addition, while higher resolution datasets covering larger stretches of the global ocean are important, assuring such samples are collected using standardized methodologies is critical to ensure that all these additional measurements can actually be easily compared.

6.2.2 Future development

The work presented in this thesis is an advancement in the understanding of the transport and transformation of plastic debris when it enters the ocean, and various directions are available for future research.

The results in chapters 3 and 5 indicate that most plastic debris remains trapped near coastlines, but it is difficult to determine whether this trapping might not be due to the absence of nearshore transport processes in the circulation data. OGCM-based data products such as the HYCOM and CMEMS reanalyses poorly resolve nearshore ocean dynamics (Liu et al., 2014) due to a number of reasons. Large-scale OGCMs typically have spatial resolutions on the order of ≈ 10 km, whereas physical processes such as coastal currents, surface waves and wave breaking typically operate on relatively short spatial scales (0 - 100m) (Van Sebille et al., 2020). In addition, tidal currents can play an important role in nearshore circulation patterns (Lentz & Fewings, 2012) and the transport and beaching of plastic debris (Sterl et al., 2020; Kaandorp et al., 2022), but are not always included within OGCMs such as HYCOM (Zhang et al., 2020). Finally, coastal morphology and bathymetry play a large role in small-scale circulation patterns (Van Rijn et al., 2011), but the coastlines within OGCMs are coarse approximations of the true coastal geomorphology. Given these limitations, it is possible that the high degree of nearshore trapping is due to the poor representation of coastal circulation patterns.

There are a number of different approaches that could be taken to investigate this. One option is to develop OGCMs that either have variable grid resolution or utilize nested models so that the OGCMs have higher model resolutions near coastlines. This strategy is done with regional ocean models such as (Critchell et al., 2015), but it might not be computationally

feasible to attain sufficiently high model resolutions on a global scale. Another possibility is to identify a number of coastal regions such as Brazil, Peru or Western India that exhibit a high degree of coastal trapping, and use high-resolution regional ocean models to investigate plastic dynamics in these regions. If a high proportion of the plastic remains trapped near coastlines in this region, such as (Critchell et al., 2015) demonstrated for the northwestern Australian coast, this would give more confidence that the nearshore trapping of plastic debris is a result of physical processes and not just a numerical artifact. Given the wide variety of coastal systems globally within which coastal plastic transport is still poorly understood (Zhang, 2017), modeling studies examining plastic transport on a variety of spatial and temporal scales would be required to get a more comprehensive understanding of how coastal processes affect plastic debris transport on a global scale.

The beaching and resuspension parametrizations introduced in chapter 3 and expanded in chapter 5 and Daily et al. (2021) can be extended in various ways. While ideally nearshore and beaching processes would be resolved explicitly within OGCMs, this will likely remain computationally infeasible for the foreseeable future barring paradigm-shifting advancements in e.g. quantum computing (Frolov, 2017). The beaching parametrization described within this thesis is powerful in that the beaching and resuspension timescales are flexible parametrizations that can be readily adapted to account for variables such as coastal geomorphology (Daily et al., 2021) and particle size (Hinata et al., 2017). However, the absolute values of these timescales are poorly constrained, and future work could focus on constraining how the timescales depend on geomorphological and environmental conditions. This could be by means of high-resolution wave and beaching models (Alsina et al., 2020), but also by means of field experiments such as Hinata et al. (2017) and Pawlowicz (2021). By conducting field experiments using various drifter sizes tracked through GPS in different marine environments, the nearshore behavior of plastic debris in different marine environments can be studied.

While the wind-driven vertical turbulent mixing parametrizations described in chapter 4 are useful tools in representing vertical transport processes, they do come with a set of limitations. In general, it would be ideal if turbulent mixing fields were provided in OGCM reanalysis datasets, as this would allow the calculation of turbulent transport that is entirely consistent with other model fields. However, given storage requirements (a single year of OGCM output can already require terabytes of storage without turbulence fields), it is unsure whether this will always be feasible. Out of the KPP and SWB parametrizations, the KPP approach represents the most complete set of physics, but work is required to expand the underlying theoretical framework to account for mixing due to wave-breaking at the ocean surface. In addition, the influence of LC-driven mixing on large scale transport must be studied in more detail. In order to determine whether LC-driven mixing affects the large-scale transport, one possible approach would be to run size-dependent model scenarios such as in chapter 5 with different degree of LC-driven mixing amplification. Even then, ideally a parametrization would be developed that calculates the LC-driving mixing amplification based on large-scale oceanographic variables such as the Stokes drift and local wind conditions (McWilliams & Sullivan, 2000).

Finally, the exact definition of the MLD used in these model scenarios needs to be considered. In chapter 5, the MLD from the CMEMS Mediterranean Sea Physics Reanalysis is used, which defines the MLD based on density difference criteria relative to the density at 10 meters depth (Escudier et al., 2020). However, in periods with strong vertical density stratification, this leads to the MLD being fixed at almost 10 m throughout the entire Mediterranean basin, resulting in unphysical peaks in microplastic concentrations at the MLD. Given that this is likely a direct result of the MLD definition, future research could examine alternative methods of defining the MLD within the KPP parametrization or otherwise adapt the parametrization in

order to prevent similar numerical issues in the future.

While the model scenarios described in chapter 5 account for a large number of physical processes, there are still processes that are not incorporated. One obvious process is biofouling, and future research could combine the biofouling framework from (Fischer et al., 2022) with the size-dependent transport scenario to study the combined effect of biofouling with full 3D advection. There are also a number of other processes that are poorly understood that would be of interest for future model development. One example is deep sea processes, such as the settling and sedimentation of plastic debris on the sea bed. There have been a number of laboratory and modeling experiments examining the resuspension of debris that has settled on the sea floor (Ballent et al., 2013; Waldschläger & Schüttrumpf, 2019; Carvajalino-Fernandez et al., 2020), but in general there is a poor understanding of what happens with plastic debris when it reaches the ocean floor.

A second example is the interactions between plastic debris and marine wildlife, which are crucial to evaluate the impact plastic debris has on marine ecosystems. The nature of these interactions is likely strongly size dependent, as the size of plastic debris will impact what type of marine wildlife it will interact with (e.g. a zooplankton organism is unable to ingest a large fishing net). Fragmentation likely plays an important role in estimating the long-term impact of plastic pollution, given that the generation of plastic fragments implies that an object's size can change over time. For these simulations the Lagrangian framework might not be the most suitable, given that computational costs can limit the length and number of particles within a simulation. Instead, Eulerian or transition matrix models might be adapted. Alternatively, new frameworks for implementing particle fragmention within Lagrangian models would need to be developed.

Finally, one major point of uncertainty within any plastic modeling study is the input scenario. While the Jambeck et al. (2015) input estimates are still commonly cited and used as a basis for input scenarios, the growing evidence that these estimates might be too high highlights that future work needs to focus on gaining a better understanding of how plastic debris enters the ocean. This is vital for any efforts to establish a global marine plastic mass budget, but also for modeling efforts for e.g. the global distribution of beached plastic as in chapter 3. In addition, a better understanding of marine plastic inputs is vital. While e.g. shipping activity can be used as a proxy for plastic inputs (Lebreton et al., 2012; van Duinen et al., 2022), it does not indicate the absolute amounts entering the ocean via these sources. Given that maritime sources are important contributors for marine plastic beached on islands (Pieper et al., 2019a; Ryan et al., 2019) and that maritime plastic debris such as lost or discarded fishing nets can potentially cause significant harm via ghost fishing (Dabrowska et al., 2021), a better understanding of all marine plastic inputs, both land- and ocean-based, is vital for envisioning the fate and impact of plastic debris in the ocean.

This thesis has focused on the marine plastic pollution from a scientific perspective, specifically how various physical processes affect the large-scale distribution of plastic debris in the ocean. While the specifics of developing and implementing the various parametrizations might not be immediately relevant for a general audience, the results within this thesis can have important implications for policy makers and society as a whole. For example, given the high amounts of plastic debris on beaches, beach cleanups can be a particularly important component in any campaign to reduce plastic pollution in the environment. In addition, the results in chapter 3 indicate regions such as the US east coast and the Argentinian coastline are particularly vulnerable to having plastic debris escaping to the open ocean. Given the technological challenges in removing plastic debris from open ocean environments, it is critical to identify particularly vulnerable regions to focus cleanup efforts before plastic debris reaches the open ocean. Particularly

the work on fragmentation highlights the long persistence of plastic debris in the ocean. While transport processes such as from coastlines to the subtropical gyres might require a couple of years, the slow fragmentation rate implies that it will take decades to possibly centuries for plastic debris to degrade within marine environments. As such, it is important that society as a whole takes measures to drastically reduce the input of plastic into the ocean given that it will persist there for decades to come.

Bibliography

Alsina, J. M., Jongedijk, C. E., & van Sebille, E., 2020. Laboratory measurements of the wave-induced motion of plastic particles: Influence of wave period, plastic size and plastic density, *Journal of Geophysical Research: Oceans*, 125(12), e2020JC016294.

Andrady, A. L., 2017. The plastic in microplastics: A review, *Marine pollution bulletin*, 119(1), 12–22.

Ballent, A., Pando, S., Purser, A., Juliano, M., & Thomsen, L., 2013. Modelled transport of benthic marine microplastic pollution in the nazaré canyon, *Biogeosciences*, 10(12), 7957–7970.

Barnes, D. K. & Milner, P., 2005. Drifting plastic and its consequences for sessile organism dispersal in the atlantic ocean, *Marine Biology*, 146(4), 815–825.

Barrett, J., Chase, Z., Zhang, J., Holl, M. M. B., Willis, K., Williams, A., Hardesty, B. D., & Wilcox, C., 2020. Microplastic pollution in deep-sea sediments from the great australian bight, *Frontiers in Marine Science*, p. 808.

Breivik, Ø., Bidlot, J.-R., & Janssen, P. A., 2016. A stokes drift approximation based on the phillips spectrum, *Ocean Modelling*, 100, 49–56.

Brignac, K. C., Jung, M. R., King, C., Royer, S.-J., Blickley, L., Lamson, M. R., Potemra, J. T., & Lynch, J. M., 2019. Marine debris polymers on main hawaiian island beaches, sea surface, and seafloor, *Environmental science & technology*, 53(21), 12218–12226.

Browne, M. A., Chapman, M. G., Thompson, R. C., Amaral Zettler, L. A., Jambeck, J., & Mallos, N. J., 2015. Spatial and temporal patterns of stranded intertidal marine debris: is there a picture of global change?, *Environmental Science & Technology*, 49(12), 7082–7094.

Carvajalino-Fernandez, M. A., Sævik, P. N., Johnsen, I. A., Albretsen, J., & Keeley, N. B., 2020. Simulating particle organic matter dispersal beneath atlantic salmon fish farms using different resuspension approaches, *Marine Pollution Bulletin*, 161, 111685.

Chenillat, F., Huck, T., Maes, C., Grima, N., & Blanke, B., 2021. Fate of floating plastic debris released along the coasts in a global ocean model, *Marine Pollution Bulletin*, 165, 112116.

Cózar, A., Echevarría, F., González-Gordillo, J. I., Irigoien, X., Úbeda, B., Hernández-León, S., Palma, Á. T., Navarro, S., García-de Lomas, J., Ruiz, A., et al., 2014. Plastic debris in the open ocean, *Proceedings of the National Academy of Sciences*, 111(28), 10239–10244.

Critchell, K., Grech, A., Schlaefer, J., Andutta, F., Lambrechts, J., Wolanski, E., & Hamann, M., 2015. Modelling the fate of marine debris along a complex shoreline: Lessons from the great barrier reef, *Estuarine, Coastal and Shelf Science*, 167, 414–426.

Cuypers, Y., Le Vaillant, X., Bouruet-Aubertot, P., Vialard, J., & Mcphaden, M. J., 2013. Tropical storm-induced near-inertial internal waves during the cirene experiment: Energy fluxes and impact on vertical mixing, *Journal of Geophysical Research: Oceans*, 118(1), 358–380.

Dabrowska, A., Lopata, I., & Osial, M., 2021. The ghost nets phenomena from the chemical perspective, *Pure and Applied Chemistry*, 93(4), 479–496.

Daily, J., Onink, V., Jongedijk, C. E., Laufkötter, C., & Hoffman, M. J., 2021. Incorporating terrain specific beaching within a lagrangian transport plastics model for lake erie, *Microplastics and Nanoplastics*, 1(1), 1–13.

Dawson, A. L., Kawaguchi, S., King, C. K., Townsend, K. A., King, R., Huston, W. M., & Bengtson Nash, S. M., 2018. Turning microplastics into nanoplastics through digestive fragmentation by antarctic krill, *Nature communications*, 9(1), 1–8.

de Lavergne, C., Vic, C., Madec, G., Roquet, F., Waterhouse, A. F., Whalen, C., Cuypers, Y., Bouruet-Aubertot, P., Ferron, B., & Hibiya, T., 2020. A parameterization of local and remote tidal mixing, *Journal of Advances in Modeling Earth Systems*, 12(5), e2020MS002065.

Debrot, A. O., van Rijn, J., Bron, P. S., & de León, R., 2013. A baseline assessment of beach debris and tar contamination in bonaire, southeastern caribbean, *Marine Pollution Bulletin*, 71(1-2), 325–329.

Egger, M., Sulu-Gambari, F., & Lebreton, L., 2020. First evidence of plastic fallout from the north pacific garbage patch, *Scientific reports*, 10(1), 1–10.

Eriksen, M., Lebreton, L. C., Carson, H. S., Thiel, M., Moore, C. J., Borerro, J. C., Galgani, F., Ryan, P. G., & Reisser, J., 2014. Plastic pollution in the world's oceans: more than 5 trillion plastic pieces weighing over 250,000 tons afloat at sea, *PloS one*, 9(12), e111913.

Escudier, R., Clementi, E., Omar, M., Cipollone, A., Pistoia, J., Aydogdu, A., Drudi, M., Grandi, A., Lyubartsev, V., Lecci, R., CretÃ, S., Masina, S., Coppini, G., & Pinardi, N., 2020. Mediterranean sea physical reanalysis (cmems med-currents, e3r1 system).

Fauziah, S. H., Liyana, I., & Agamuthu, P., 2015. Plastic debris in the coastal environment: The invincible threat? abundance of buried plastic debris on malaysian beaches, *Waste Management & Research*, 33(9), 812–821.

Fazey, F. M. & Ryan, P. G., 2016. Biofouling on buoyant marine plastics: An experimental study into the effect of size on surface longevity, *Environmental pollution*, 210, 354–360.

Fischer, R., Lobelle, D., Kooi, M., Koelmans, A., Onink, V., Laufkötter, C., Amaral-Zettler, L., Yool, A., & van Sebille, E., 2022. Modeling submerged biofouled microplastics and their vertical trajectories, *Biogeosciences*, pp. 1–29.

Frias, J. & Nash, R., 2019. Microplastics: finding a consensus on the definition, *Marine pollution bulletin*, 138, 145–147.

Frolov, A., 2017. Can a quantum computer be applied for numerical weather prediction?, *Russian meteorology and hydrology*, 42(9), 545–553.

Galgani, L. & Loiselle, S. A., 2021. Plastic pollution impacts on marine carbon biogeochemistry, *Environmental Pollution*, 268, 115598.

Gerritse, J., Leslie, H. A., de Tender, C. A., Devriese, L. I., & Vethaak, A. D., 2020. Fragmentation of plastic objects in a laboratory seawater microcosm, *Scientific reports*, 10(1), 1–16.

Geyer, R., Jambeck, J. R., & Law, K. L., 2017. Production, use, and fate of all plastics ever made, *Science advances*, 3(7), e1700782.

Gregory, M. R., 2009. Environmental implications of plastic debris in marine settings - entanglement, ingestion, smothering, hangers-on, hitch-hiking and alien invasions, *Philosophical Transactions of the Royal Society B: Biological Sciences*, 364(1526), 2013–2025.

Hardesty, B. D., Lawson, T., van der Velde, T., Lansdell, M., & Wilcox, C., 2017. Estimating quantities and sources of marine debris at a continental scale, *Frontiers in Ecology and the Environment*, 15(1), 18–25.

Hinata, H., Mori, K., Ohno, K., Miyao, Y., & Kataoka, T., 2017. An estimation of the average residence times and onshore-offshore diffusivities of beached microplastics based on the population decay of tagged meso-and macrolitter, *Marine pollution bulletin*, 122(1-2), 17–26.

Hoellein, T. J. & Rochman, C. M., 2021. The "plastic cycle": a watershed-scale model of plastic pools and fluxes, *Frontiers in Ecology and the Environment*, 19(3), 176–183.

Jambeck, J. R., Geyer, R., Wilcox, C., Siegler, T. R., Perryman, M., Andrady, A., Narayan, R., & Law, K. L., 2015. Plastic waste inputs from land into the ocean, *Science*, 347(6223), 768–771.

Kaandorp, M. L., Dijkstra, H. A., & van Sebille, E., 2020. Closing the mediterranean marine floating plastic mass budget: inverse modeling of sources and sinks, *Environmental science & technology*, 54(19), 11980–11989.

Kaandorp, M. L., Dijkstra, H. A., & van Sebille, E., 2021. Modelling size distributions of marine plastics under the influence of continuous cascading fragmentation, *Environmental Research Letters*, 16(5), 054075.

Kaandorp, M. L., Ypma, S. L., Boonstra, M., Dijkstra, H. A., & van Sebille, E., 2022. Using machine learning and beach cleanup data to explain litter quantities along the dutch north sea coast, *Ocean Science*, 18(1), 269–293.

Kerpen, N. B., Schlurmann, T., Schendel, A., Gundlach, J., Marquard, D., & Hüpgen, M., 2020. Wave-induced distribution of microplastic in the surf zone, *Frontiers in Marine Science*, p. 979.

Kooi, M., Reisser, J., Slat, B., Ferrari, F. F., Schmid, M. S., Cunsolo, S., Brambini, R., Noble, K., Sirks, L.-A., Linders, T. E., et al., 2016. The effect of particle properties on the depth profile of buoyant plastics in the ocean, *Scientific reports*, 6(1), 1–10.

Kooi, M., Nes, E. H. v., Scheffer, M., & Koelmans, A. A., 2017. Ups and downs in the ocean: effects of biofouling on vertical transport of microplastics, *Environmental science & technology*, 51(14), 7963–7971.

Kubota, M., Takayama, K., & Namimoto, D., 2005. Pleading for the use of biodegradable polymers in favor of marine environments and to avoid an asbestos-like problem for the future, *Applied Microbiology and Biotechnology*, 67(4), 469–476.

Kukulka, T., Proskurowski, G., Morét-Ferguson, S., Meyer, D. W., & Law, K. L., 2012. The effect of wind mixing on the vertical distribution of buoyant plastic debris, *Geophysical Research Letters*, 39(7).

Lavers, J. L. & Bond, A. L., 2017. Exceptional and rapid accumulation of anthropogenic debris on one of the world's most remote and pristine islands, *Proceedings of the National Academy of Sciences*, 114(23), 6052–6055.

Law, K. L., Morét-Ferguson, S., Maximenko, N. A., Proskurowski, G., Peacock, E. E., Hafner, J., & Reddy, C. M., 2010. Plastic accumulation in the north atlantic subtropical gyre, *Science*, 329(5996), 1185–1188.

Lebreton, L., Van Der Zwet, J., Damsteeg, J.-W., Slat, B., Andrady, A., & Reisser, J., 2017. River plastic emissions to the world's oceans, *Nature communications*, 8(1), 1–10.

Lebreton, L., Slat, B., Ferrari, F., Sainte-Rose, B., Aitken, J., Marthouse, R., Hajbane, S., Cunsolo, S., Schwarz, A., Levivier, A., et al., 2018. Evidence that the great pacific garbage patch is rapidly accumulating plastic, *Scientific reports*, 8(1), 1–15.

Lebreton, L., Egger, M., & Slat, B., 2019. A global mass budget for positively buoyant macroplastic debris in the ocean, *Scientific reports*, 9(1), 1–10.

Lebreton, L.-M., Greer, S., & Borrero, J. C., 2012. Numerical modelling of floating debris in the world's oceans, *Marine pollution bulletin*, 64(3), 653–661.

Lentz, S. J. & Fewings, M. R., 2012. The wind-and wave-driven inner-shelf circulation, *Annual review of marine science*, 4, 317–343.

Liu, Y., Weisberg, R. H., Vignudelli, S., & Mitchum, G. T., 2014. Evaluation of altimetry-derived surface current products using lagrangian drifter trajectories in the eastern gulf of mexico, *Journal of Geophysical Research: Oceans*, 119(5), 2827–2842.

Liubartseva, S., Coppini, G., Lecci, R., & Clementi, E., 2018. Tracking plastics in the mediterranean: 2d lagrangian model, *Marine pollution bulletin*, 129(1), 151–162.

Lobelle, D. & Cunliffe, M., 2011. Early microbial biofilm formation on marine plastic debris, *Marine pollution bulletin*, 62(1), 197–200.

Lynch, D. R., Greenberg, D. A., Bilgili, A., McGillicuddy Jr, D. J., Manning, J. P., & Aretxabaleta, A. L., 2014. *Particles in the coastal ocean: Theory and applications*, Cambridge University Press.

Martin, C., Baalkhuyur, F., Valluzzi, L., Saderne, V., Cusack, M., Almahasheer, H., Krishnakumar, P., Rabaoui, L., Qurban, M., Arias-Ortiz, A., et al., 2020. Exponential increase of plastic burial in mangrove sediments as a major plastic sink, *Science advances*, 6(44), eaaz5593.

McWilliams, J. C. & Sullivan, P. P., 2000. Vertical mixing by langmuir circulations, *Spill Science & Technology Bulletin*, 6(3-4), 225–237.

Morales-Caselles, C., Viejo, J., Martí, E., González-Fernández, D., Pragnell-Raasch, H., González-Gordillo, J. I., Montero, E., Arroyo, G. M., Hanke, G., Salvo, V. S., et al., 2021. An inshore–offshore sorting system revealed from global classification of ocean litter, *Nature Sustainability*, 4(6), 484–493.

Okuku, E., Owato, G., Kiteresi, L. I., Otieno, K., Kombo, M., Wanjeri, V., Mbuche, M., Gwada, B., Chepkemboi, P., Achieng, Q., et al., 2022. Are tropical estuaries a source of or a sink for marine litter? evidence from sabaki estuary, kenya, *Marine Pollution Bulletin*, 176, 113397.

Onink, V., Wichmann, D., Delandmeter, P., & van Sebille, E., 2019. The role of ekman currents, geostrophy, and stokes drift in the accumulation of floating microplastic, *Journal of Geophysical Research: Oceans*, 124(3), 1474–1490.

Pabortsava, K. & Lampitt, R. S., 2020. High concentrations of plastic hidden beneath the surface of the atlantic ocean, *Nature communications*, 11(1), 1–11.

Pasquini, G., Ronchi, F., Strafella, P., Scarcella, G., & Fortibuoni, T., 2016. Seabed litter composition, distribution and sources in the northern and central adriatic sea (mediterranean), *Waste management*, 58, 41–51.

Pawlowicz, R., 2021. The grounding of floating objects in a marginal sea, *Journal of Physical Oceanography*, 51(2), 537–551.

Pedrotti, M. L., Petit, S., Elineau, A., Bruzaud, S., Crebassa, J.-C., Dumontet, B., Martí, E., Gorsky, G., & Cózar, A., 2016. Changes in the floating plastic pollution of the mediterranean sea in relation to the distance to land, *PloS one*, 11(8), e0161581.

Piccardo, M., Renzi, M., & Terlizzi, A., 2020. Nanoplastics in the oceans: Theory, experimental evidence and real world, *Marine Pollution Bulletin*, 157, 111317.

Pieper, C., Ventura, M. A., Martins, A., & Cunha, R. T., 2015. Beach debris in the azores (ne atlantic): Faial island as a first case study, *Marine pollution bulletin*, 101(2), 575–582.

Pieper, C., Amaral-Zettler, L., Law, K. L., Loureiro, C. M., & Martins, A., 2019a. Application of matrix scoring techniques to evaluate marine debris sources in the remote islands of the azores archipelago, *Environmental Pollution*, 249, 666–675.

Pieper, C., Martins, A., Zettler, E., Loureiro, C. M., Onink, V., Heikkilä, A., Epinoux, A., Edson, E., Donnarumma, V., Vogel, F. d., et al., 2019b. Into the med: Searching for microplastics from space to deep-sea, in *International Conference on Microplastic Pollution in the Mediterranean Sea*, pp. 129–138, Springer.

Ribic, C. A., Sheavly, S. B., Rugg, D. J., & Erdmann, E. S., 2010. Trends and drivers of marine debris on the atlantic coast of the united states 1997–2007, *Marine pollution bulletin*, 60(8), 1231–1242.

Ribic, C. A., Sheavly, S. B., Rugg, D. J., & Erdmann, E. S., 2012. Trends in marine debris along the us pacific coast and hawai'i 1998–2007, *Marine Pollution Bulletin*, 64(5), 994–1004.

Ruiz-Orejón, L. F., Sardá, R., & Ramis-Pujol, J., 2016. Floating plastic debris in the central and western mediterranean sea, *Marine Environmental Research*, 120, 136–144.

Ryan, P. G., 2015. Does size and buoyancy affect the long-distance transport of floating debris?, *Environmental Research Letters*, 10(8), 084019.

Ryan, P. G., Perold, V., Osborne, A., & Moloney, C. L., 2018. Consistent patterns of debris on south african beaches indicate that industrial pellets and other mesoplastic items mostly derive from local sources, *Environmental Pollution*, 238, 1008–1016.

Ryan, P. G., Dilley, B. J., Ronconi, R. A., & Connan, M., 2019. Rapid increase in asian bottles in the south atlantic ocean indicates major debris inputs from ships, *Proceedings of the National Academy of Sciences*, 116(42), 20892–20897.

Schmidt, C., Krauth, T., & Wagner, S., 2017. Export of plastic debris by rivers into the sea, *Environmental science & technology*, 51(21), 12246–12253.

Skyllingstad, E. D., Paluszkiewicz, T., Denbo, D. W., & Smyth, W. D., 1996. Nonlinear vertical mixing processes in the ocean: modeling and parameterization, *Physica D: Nonlinear Phenomena*, 98(2-4), 574–593.

Smeaton, C., 2021. Augmentation of global marine sedimentary carbon storage in the age of plastic, *Limnology and Oceanography Letters*, 6(3), 113–118.

Smith, L. & Turrell, W. R., 2021. Monitoring plastic beach litter by number or by weight: The implications of fragmentation, *Frontiers in Marine Science*, p. 1359.

Sogabe, A. & Takatsuji, K., 2021. Marine-dumped waste tyres cause the ghost fishing of hermit crabs, *Royal Society open science*, 8(10), 210166.

Song, X., Lyu, M., Zhang, X., Ruthensteiner, B., Ahn, I.-Y., Pastorino, G., Wang, Y., Gu, Y., Ta, K., Sun, J., et al., 2021. Large plastic debris dumps: New biodiversity hot spots emerging on the deep-sea floor, *Environmental Science & Technology Letters*, 8(2), 148–154.

Song, Y. K., Hong, S. H., Jang, M., Han, G. M., Jung, S. W., & Shim, W. J., 2017. Combined effects of uv exposure duration and mechanical abrasion on microplastic fragmentation by polymer type, *Environmental science & technology*, 51(8), 4368–4376.

Spirkovski, Z., Ilik-Boeva, D., Ritterbusch, D., Peveling, R., & Pietrock, M., 2019. Ghost net removal in ancient lake ohrid: A pilot study, *Fisheries Research*, 211, 46–50.

Sterl, M. F., Delandmeter, P., & van Sebille, E., 2020. Influence of barotropic tidal currents on transport and accumulation of floating microplastics in the global open ocean, *Journal of Geophysical Research: Oceans*, 125(2), e2019JC015583.

Suaria, G., Perold, V., Lee, J. R., Lebouard, F., Aliani, S., & Ryan, P. G., 2020. Floating macro-and microplastics around the southern ocean: Results from the antarctic circumnavigation expedition, *Environment International*, 136, 105494.

Taïbi, N.-E., Bentaallah, M. E. A., Alomar, C., Compa, M., & Deudero, S., 2021. Micro-and macro-plastics in beach sediment of the algerian western coast: First data on distribution, characterization, and source, *Marine Pollution Bulletin*, 165, 112168.

Tramoy, R., Gasperi, J., Dris, R., Colasse, L., Fisson, C., Sananes, S., Rocher, V., & Tassin, B., 2019. Assessment of the plastic inputs from the seine basin to the sea using statistical and field approaches, *Frontiers in Marine Science*, 6, 151.

van Duinen, B., Kaandorp, M. L., & van Sebille, E., 2022. Identifying marine sources of beached plastics through a bayesian framework: Application to southwest netherlands, *Geophysical Research Letters*, p. e2021GL097214.

Van Emmerik, T., Loozen, M., Van Oeveren, K., Buschman, F., & Prinsen, G., 2019. Riverine plastic emission from jakarta into the ocean, *Environmental Research Letters*, 14(8), 084033.

Van Rijn, L. C. et al., 2011. *Principles of fluid flow and surface waves in rivers, estuaries, seas and oceans*, vol. 1, Aqua Publications Amsterdam, The Netherlands.

Van Sebille, E., 2015. The oceans' accumulating plastic garbage, *Physics Today*, 68, 60–61.

Van Sebille, E., England, M. H., & Froyland, G., 2012. Origin, dynamics and evolution of ocean garbage patches from observed surface drifters, *Environmental Research Letters*, 7(4), 044040.

Van Sebille, E., Wilcox, C., Lebreton, L., Maximenko, N., Hardesty, B. D., Van Franeker, J. A., Eriksen, M., Siegel, D., Galgani, F., & Law, K. L., 2015. A global inventory of small floating plastic debris, *Environmental Research Letters*, 10(12), 124006.

Van Sebille, E., Aliani, S., Law, K. L., Maximenko, N., Alsina, J. M., Bagaev, A., Bergmann, M., Chapron, B., Chubarenko, I., Cózar, A., et al., 2020. The physical oceanography of the transport of floating marine debris, *Environmental Research Letters*, 15(2), 023003.

Waldschläger, K. & Schüttrumpf, H., 2019. Erosion behavior of different microplastic particles in comparison to natural sediments, *Environmental science & technology*, 53(22), 13219–13227.

Wilcox, C., Hardesty, B. D., & Law, K. L., 2019. Abundance of floating plastic particles is increasing in the western north atlantic ocean, *Environmental Science & Technology*, 54(2), 790–796.

Yang, H., Chen, G., & Wang, J., 2021. Microplastics in the marine environment: sources, fates, impacts and microbial degradation, *Toxics*, 9(2), 41.

Zhang, H., 2017. Transport of microplastics in coastal seas, *Estuarine, Coastal and Shelf Science*, 199, 74–86.

Zhang, Z., Wu, H., Peng, G., Xu, P., & Li, D., 2020. Coastal ocean dynamics reduce the export of microplastics to the open ocean, *Science of the Total Environment*, 713, 136634.

Zhao, S., Zettler, E. R., Bos, R. P., Lin, P., Amaral-Zettler, L. A., Mincer, T. J., et al., 2022. Large quantities of small microplastics permeate the surface ocean to abyssal depths in the south atlantic gyre, *Global Change Biology*.

Acknowledgements

Charlotte, this PhD would not have been possible without you. You were was always available with input and advice, and our many long discussions have now culminated in this thesis. Despite the fact that we spent significantly less time in the same country than either of initially anticipated, everything generally went smoothly and I really appreciate that from the very beginning this was very much a project we did together, including everything from coming up with new research directions to the final writing process. But perhaps even more importantly, you've always been supportive and considerate with all the logistical and personal challenges that come with completing a PhD, and I could not thank you enough for all her support, guidance and insight over these past four years.

Erik, you've now helped supervise my work in one form or another over the last 5 years and I'd like to thank you for all the help you've given me. Ever since my master I've learned a lot about the entire research process from you, and thank you for always forwarding me different opportunities (such as the job opening for this very PhD position). Also, I really appreciate how I was welcomed back into the IMAU Parcels community when I relocated back to Utrecht, and I wish you all the best in bringing Parcels to the masses over the coming years.

Dr. Miguel Morales Maqueda, thank you for taking to the time to evaluate this thesis as my external reviewer, and for your patience and understanding in scheduling the date of the PhD defence.

This PhD started with me working in Bern, and I would first like to thank Fortunat Joos for your help and experience in helping to solve the various scientific and organizational issues that popped over the years. Thomas Stocker, thank you for being the chair of my defence and your insight into the M-1 modeling component of chapter 4. Doris Rätz, Claudia Maschke and Bettina Schüpbach, thank you for all your help with any administrative matters, particularly when I was working from the Netherlands. Gunnar Jansen, thank you for all the technical support and for the many saved hours that I would have otherwise spent hunting down some obscure bug. Matthew Hoffman, I really enjoyed our work together on the beaching project, and I'm proud of how the paper turned out. Thank you to Thomas Frölicher and all of the ocean modeling group for adopting me into the group. Friedrich, Emmanuele and Lars, I had a lot of fun with the Kupsky Kings and I hope we find some time to play together again soon. Woonmi, Santi and Ashley, thank you for our weekly squash games and the wholly deserved sushi lunches afterwards. Jan-Dirk, bedankt voor de gezelligheid, steun en speciaalbiertjes, en ik heb onze lunches gemist deze laatste twee jaar.

In Utrecht, I'd like to thank everyone I got to meet and work with in the Parcels group over the years. I had a lot of fun and learned a lot of about all the different ways particle tracking can be applied in ocean research. Philippe, thank you for all Parcels assistance during in my masters and early PhD years, and I had a great time together on the Pelagia and afterwards in Cape Town. Christian, thank you as well for all the help with Parcels, and for taking to the time to answer all my computer science-related questions. Cleo, I really enjoyed our talks, and without you the beaching/resuspension parametrizations from chapter 3 would never have taken

shape the way they did. Mikael, I've enjoyed our chats and I'm glad we got to work together on the fragmentation scenarios in chapter 5. Daan, thanks for your help on all diffusion and Markov-1 related matters, it was a great help with the wind-mixing parametrizations in chapter 4. Delphine, I've had a great time work on various projects with you over the last two years, and best of luck to you and everyone else from the Particle Trackers in the further development of Sea Clearly! Finally, thank you to Linda Amaral - Zettler, Erik Zettler and everyone else from the PE442 and PE448 research cruises for giving the opportunity to experience some real-world physical oceanography, and for so many card games that I finally learned how to properly shuffle.

Thank you to Carla, Sebas, Deirde, Jonne, Madi, Leanne and Ali for all the fun times here in Utrecht outside of the PhD work, without all of you these 4 years would've been a lot more difficult. Carla, thank you as well for all your help proofreading my thesis. Inger, thank you for your crash course in Data Science/Engineering that both saved me a ton of time in streamlining the model setups and showed me an interesting future career path. Finally, thank you to Sam and Tony for your constant canine company and your prompt warnings whenever someone walked past the house.

Ik kan heel mijn familie niet genoeg bedanken voor al hun advies, hulp en gezelligheid tijdens mijn hele leven, laat staan alleen tijdens mijn PhD. Carin en Marcel, zonder jullie zou ik niet zijn wie ik nu was, en jullie waren er altijd wanneer ik jullie nodig had. Een groot deel van de scriptie is uiteindelijk ook gewoon bij jullie thuis gedaan, en zijn we met z'n allen zo door de eerste lockdown gekomen. Hugo, ik kan me geen beter broertje wensen, en ik ben de tel kwijt geraakt hoe vaak je niet heen en weer naar Bern bent gekomen voor skiën, verhuizingen of gewoon voor de gezelligheid. Janny, Willy, Piet and Aaldert, ook jullie wil ik voor alles bedanken, en het betekend veel voor mij dat jullie er allemaal bij zijn nu ik mijn PhD ook echt afmaak.

Finally, I cannot give enough thanks to Pau, for all your patience, love and support over all the years, including before I even started my PhD. It has not always been easy, but I could not have finished this without you, while at the same time seeing what is most important to me. I don't know how to best put it into words, but thank you for absolutely everything.

Publications

Published:

Onink, V., Wichmann, D., Delandmeter, P., & van Sebille, E. (2019). The role of Ekman currents, geostrophy, and stokes drift in the accumulation of floating microplastic. *Journal of Geophysical Research: Oceans*, 124(3), 1474–1490.

Onink, V., Jongedijk, C. E., Hoffman, M. J., van Sebille, E., & Laufkötter, C. (2021). Global simulations of marine plastic transport show plastic trapping in coastal zones. *Environmental Research Letters*, 16(6), 064053.

Daily, J., Onink, V., Jongedijk, C. E., Laufkötter, C., & Hoffman, M. J. (2021). Incorporating terrain specific beaching within a lagrangian transport plastics model for Lake Erie. *Microplastics and Nanoplastics*, 1(1), 1–13.

Onink, V., van Sebille, E., & Laufkötter, C. (2022). Empirical Lagrangian parametrization for wind-driven mixing of buoyant particles at the ocean surface. *Geoscientific Model Development*, 15(5), 1995–2012.

Fischer, R., Lobelle, D., Kooi, M., Koelmans, A., Onink, V., Laufkötter, C., Amaral-Zettler, L., Yool, A. & van Sebille, E. (2022). Modeling submerged biofouled microplastics and their vertical trajectories. *Biogeosciences*, 19(8), 2211–2234.

In preparation:

Onink, V., Kaandorp, M. L. A., van Sebille, E., & Laufkötter, C. (*in preparation*). The influence of particle size and fragmentation on large-scale microplastic transport in the Mediterranean Sea.

Erklärung

gemäss Art. 18 PromR Phil.-nat. 2019

Name, Vorname:	Onink, Victor
Matrikelnummer:	18-125-799
Studiengang:	Climate Sciences
	Bachelor ☐ Master ☐ Dissertation ☒
Titel der Arbeit:	From coastlines to the deep sea: modeling plastic transport in the global ocean
Leiter der Arbeit:	Dr. Charlotte Laufkötter

Ich erkläre hiermit, dass ich diese Arbeit selbständig verfasst und keine anderen als die angegebenen Quellen benutzt habe. Alle Stellen, die wörtlich oder sinngemäss aus Quellen entnommen wurden, habe ich als solche gekennzeichnet. Mir ist bekannt, dass andernfalls der Senat gemäss Artikel 36 Absatz 1 Buchstabe r des Gesetzes über die Universität vom 5. September 1996 und Artikel 69 des Universitätsstatuts vom 7. Juni 2011 zum Entzug des Doktortitels berechtigt ist. Für die Zwecke der Begutachtung und der Überprüfung der Einhaltung der Selbständigkeitserklärung bzw. der Reglemente betreffend Plagiate erteile ich der Universität Bern das Recht, die dazu erforderlichen Personendaten zu bearbeiten und Nutzungshandlungen vorzunehmen, insbesondere die Doktorarbeit zu vervielfältigen und dauerhaft in einer Datenbank zu speichern sowie diese zur Überprüfung von Arbeiten Dritter zu verwenden oder hierzu zur Verfügung zu stellen.

Bern, 27/06/2022

Unterschrift